UNIVERSIDAD MICHOACANA DE SAN NICOLÁS DE HIDALGO

INSTITUTO DE INVESTIGACIÓN EN METALURGIA Y MATERIALES

Consolidation of Mine Tailings and Immobilization of Heavy Metals through Geopolymerization Reactions

Tesis para obtener Doctorado en ciencias en metalurgia y ciencias de los materiales

PRESENTA:
M.C. Qian Wan

ASESOR:
Dr. Feng Rao Wu

COASESOR:
Dr. Shaoxian Song Hu

Morelia, Michoacán, México, Febrero 2018

Acknowledgement

The financial supports from the Consejo Nacional de Ciencia y Tecnología (CONACyT) of Mexico under the grant No. 270186 and the National Natural Science Foundation of China (NSFC) under the project No. 51474167 are gratefully acknowledged. I would also like to thank the CONACyT for a scholarship under the grant No. 635638 during my Ph.D. studying. I appreciate Universidad Michoacana de San Nicolás de Hidalgo (UMSNH) and the Instituto de Investigacion en Metalurgia y Materials (IIMM) who provide an enjoyable working environment.

Next, I would like to express my sincere gratitude to Dr. Feng Rao Wu as my wonderful supervisor. Dr. Rao always gives me great encouragement and guidance in my research. Without his support and push, I would not be what I am today. In addition, I want to give my thanks to Dr. Rao and his wife, Fenfang Zhu, as friends and families. It is them who gave me the endless help and warmth in a foreign country. After that, I want to give my great gratitude to my co-supervisor, Dr. Shaoxian Song. His fund of knowledge and serious attitude in work are worthy of my learning. And He also gives me great help in my experiment and research.

Furthermore, I want to thank my parents for their unconditional love and support in all my life. I would not concentrate on my research, without their support and encouragement. I also want to thank my lovely wife, Mengmei Yao, for her never-ending support and give for studying my Ph. D. degree.

And I would like to express my sincere gratitude to Dr. Ramiro Escudero, Dr. Carlos León, Dr. Diana Cholico and Dr. Ricardo Morales for their invaluable advice in my work. I also want to thank all my friends in IIMM, M.C. Carlos Arreola, Ing. Alma Gallegos, M.C. Zhili Li, M.C. Xing Li. Thanks for your help and support in my work and life. Thanks to all my friends at Wuhan University of Technology.

Qian Wan

Contents

Index of Figures

Index of Tables

Abstract

In this work, mine tailings are consolidated through geopolymerization reactions to be of a satisfactory mechanical property and the toxic substances in mine tailings are immobilized. To approach the geopolymerization of mine tailings without calcination, the features of mine tailings were first simulated in the syntheses of metakaolin geopolymers, which were of high Si/Al ratios, high content of quartz sand and no calcination. Then, geothermal clay, which was of the intermediate reactivity between metakaolin and mine tailings in geopolymerization reactions, was studied in geopolymer formation. After that, mine tailings have been consolidated directly. Microstructures of the mine tailings-based geopolymers were studied and the immobilization forms of heavy metals were quantitatively calculated.

In a typical experiment for studying the variables (e.g., Si/Al ratio) in geopolymer formation, aluminosilicates (metakaolin, geothermal clay or mine tailings) were activated by alkali solutions, then, the consolidated products were characterized for their mechanical property and microstructure. This data was used to illustrate how the variables affect the geopolymerization reactions. In a typical synthesis, raw aluminosilicates were mixed with alkali solution (e.g. NaOH and Na_2SiO_3). Then the mixture was poured into a cubic steel mold (50 mm×50 mm×50 mm) and vibrated on a vibration table for 3 min to liberate the air bubbles. After that, the mold was sealed for the curing process, in which it was first cured at 60 °C for 6 h and continued at room temperature for 7 days. The products were characterized by scanning electron microscopy (SEM), x-ray diffraction (XRD), Fourier transform infrared spectroscopy (FTIR), X-ray photoelectron spectroscopy (XPS) for morphology and microstructures, and mechanical tester for compressive strength. ^{29}Si nuclear magnetic resonance (NMR) spectra were used to study the microstructure of products, the short-range ordering and the molecular structure. Gaussian peak deconvolution was employed to separate and quantify the $Q^n(mAl)$ species ($0 \leq m \leq n \leq 4$, m, n=integer) in geopolymer gel.

Through synthesizing metakaolin-based geopolymers with stimulated features from mine tailings, it is found that 1) geopolymers could be formed at high Si/Al ratio (e.g., 5:1), 2) inert minerals like quartz could be associated with geopolymer gel as filler materials in the formation of geopolymers, 3) calcination increased the reactivity of metakaolin greatly at 650-850 ºC. Then, through investigating the synthesis of geopolymer with geothermal clay without calcination, it is shown that Na_2SiO_3 and NaOH tended to play the roles of geopolymeric gel formation and aluminosilicate dissolution, and high water content leaded to porous structure and low compressive strength in geothermal clay-based geopolymers. After that, mine tailings-based geopolymers were formed with compressive strength from 1.2 MPa to 17.3 MPa. And lead were mainly immobilized in the forms of $PbO•7SiO_2$, $PbO•4SiO_2$ and incorporating with the network of binders in mine tailings-based geopolymers.

Keywords: Geopolymer; Geopolymerization; Metakaolin; Si/Al ratio; Quartz sand; Calcination; Geothermal clay; Mine tailings; Alkali-activated binder; Lead immobilization.

Resumen

En el presente trabajo, desechos mineros son consolidados a través del proceso de reacciones de geopolimerización para ser de propiedades mecánicas satisfactorias mientras que las sustancias toxicas en los desechos mineros son inmovilizadas. Para tratar la geopolimerización de deshechos mineros sin calcinación, las características de los desechos mineros fueron simuladas primeramente en la síntesis de geopolímero de metacaolín con altas relaciones Si/Al, alto contenido de arena de cuarzo y sin calcinación. Después, arcilla geotérmica, la cual fue de reactividad intermedia entre el metacaolín y los desechos mineros en las reacciones de geopolimerización, fue estudiada en la formación del geopolimero. Posteriormente, los desechos mineros se consolidaron directamente. Microestructuras de los geopolímeros hechos de los desechos mineros fueron estudiados y las formas de inmovilización de metales pesados fueron calculadas cuantitativamente.

Un experimento típico para estudiar las variables (e.g. relacion Si/Al) en la formación de geopolimeros, aluminosilicatos (metacaolín, arcilla geotérmica o desechos mineros) fueron activados por medio de soluciones alcalinas, después, los productos consolidados fueron caracterizados para conocer sus propiedades mecánicas y microestructura. Esta información fue usada para ilustrar como las variables afectan las raciones de geopolimerización. En una síntesis típica, aluminosilicatos en bruto fueron mezclados con una solución alcalina (NaOH and Na_2SiO_3)). Después, la mezcla fue vertida dentro de un recipiente cubico de acero (50 mm×50 mm×50 mm) y sometida a vibración por 3 min para liberar las burbujas de aire. Posteriormente, el molde fue sellado para el proceso del curado y se inició el proceso de curado 60 ºC por 6 h y después a temperatura ambiente por 7 días. Los geopolimeros fueron caracterizados por microscopía electrónica de barrido (MEB), difracción de rayos-x (DRX), espectroscopia de infrarrojo por transformada de Fourier (EITF) y espectroscopia de fotoelectrones de rayos-x (EFRX) para morfología y microestructuras. Para analizar la resistencia a la compresión se utilizó una máquina universal. Los espectros de resonancia magnética nuclear (RMN) fueron utilizados para estudiar la microestructura de los productos., el orden de corto alcance y la estructura molecular. El método de deconvolución de picos Gaussiana fue empleada para separar y cuantificar las especies $Q^n(mAl)$ ($0 \leq m \leq n \leq 4$, m, n=entero) en el gel del geopolímero.

Mediante la síntesis de geopolimeros de metacaolín con características simuladas de deshechos mineros se encontró que: 1) los geopolimeros se pueden formar a altas relaciones Si/Al (e.g., 5:1), 2) materiales inertes como el cuarzo puedes usarse a los como material de relleno durante la formación de los geopolimeros, 3) la calcinación incremento significativamente la reactividad del metacaolín a temperaturas entre 650-850 ºC. Posteriormente, mediante la investigación de la síntesis de geopolímeros con arcillas geotérmicas sin calcinación se demostró que tanto NaOH como Na_2SiO_3 tomaron un papel importante en la formación del gel geopolimérico y la disolución de los aluminosilicatos. Por otro lado, un alto contenido de agua condujo a una estructura porosa y a bajo esfuerzo de compresión en geopolímeros hechos a base de arcillas geotérmicas. Finalmente, los geopolimeros hechos a base de deshechos mineros fueron formados mostrando esfuerzos de compresión de 1.2 MPa a 17.3 MPa. El plomo fue principalmente inmovilizado en la forma de $PbO•7SiO_2$, $PbO•4SiO_2$ e incorporado a la red de ligantes en los geopolímeros hechos a base de deshechos mineros.

Introduction

Mine tailings are waste materials that contain process water, fine gangue minerals, heavy metals and any toxic substances used in the ore dressing (Rao and Liu, 2015). A huge amount of mine tailings is generated each year in the exploitation of resources. With estimates of contemporary mine tailings production is in a range between 5 to 7 billion tons per year worldwide (Lu and Wang, 2012; Mudd and Boger, 2013).

Geopolymers are aluminosilicate materials with three-dimensional (3D) amorphous micro-structures. They are formed by geopolymerization processes in which the oxides of silicon and aluminum minerals or aluminosilicate minerals are activated by alkalis to form 3D polymeric networks. Although some ancient structures, like the Pyramids in Egypt, are believed to be products of geopolymerization, the terms "geopolymer" and "geopolymerization" were first coined by Davidovits in the 1980s (Barsoum et al., 2006). Table 1 presents a summary of the major historical references and milestones in the development of geopolymers. The raw materials for synthesizing geopolymers have also been widened from metakaolin and fly ash to various aluminosilicate minerals, clays, solid wastes, and their mixtures.

Table 1. Summary of geopolymer development with highlights of the applications in treating mine tailings

Author	Year	Description	Significance
Davidovits	1982	A new technical language for the transfer of basic scientific information	The term "geopolymer" was coined
Wastiels et al.	1993	Mineral polymer based on fly ash	First report of geopolymers by alkaline activation of fly ash
Xu and van Deventer	2000, 2002	Geopolymerization of multiple minerals	Geopolymerization of aluminosilicate wastes, extending precursors from metakaolin and fly ash
Duxson et al.	2007	The review paper "Geopolymer technology: the current state of the art"	Extensively reviewed the developments of geopolymers
Wan et al.	2017	Consolidation of Mine Tailings and Heavy Metal Retention by Alkaline Activation: Part I and Part II	Demonstrate the mechanism of heavy metals immobilization

At the first, geopolymer was used as fire-resistant materials. Due to the excellent performances (e.g. rapid development of mechanical strength, dimensional stability, acid resistance and excellent adherence to aggregates), in the past thirty years, the applications of geopolymer have been expanded to alternative construction materials, impermeable materials and adsorbing materials, etc. Up to the present, the main research direction about geopolymer is the use as a substitute of Portland cement.

In this thesis work, we will add appropriate reagents such as alkalis to the mine tailings sludge to activate geopolymerization reactions of the aluminosilicate minerals. The network structure of the clays resulting from the geopolymerization reactions could strengthen the tailings sludge.

Justification

Mine tailings are usually disposed of into tailing ponds in slurry form, which is a permanent environmental liability. Their components (e.g. heavy metals) permeate and contaminate the soil and underground water resources. The failure of steep-sided tailing dams can happen due to earthquakes, blasting vibration and extreme weather (Wills and Napier-Munn, 2006). Therefore, it is a huge potential security hazard to the local flora, fauna and people. Some methods like using hydrocyclone and flocculants have been investigated to solve this problem. However, these technologies either added costly or poisonous reagents or required thickening machines of high-energy consumption.

Some researchers also pointed out that geopolymer could be used to consolidate mineral processing tailings. Consolidation of mine tailings through geopolymerization has following advantages: first, mine tailings consist of clay, quartz, and other gangue minerals which rich in Si and Al. These are excellent raw materials for geopolymerization. In addition, the slurries of mine tailings are of an alkaline condition, which is favorable for inducing an alkali activation reaction. Furthermore, the compressive strength requirement for tailings sludge and the period to reach the compressive strength, i.e., 5kPa within the first year after deposition of the tailings, and 10 kPa after 5 years, are significantly lower than those geopolymers used in other areas (5-100 MPa).

Hypothesis

In this thesis work, I hypothesize that adding appropriate reagents such as alkalis to the mine tailings sludge could activate geopolymerization reactions of the aluminosilicate minerals (clays). The network structure of the clays resulting from the geopolymerization reactions could strengthen the tailings sludge. Simultaneously, the toxic ions such as heavy metals can be attracted by the formed tailings geopolymers. The water remaining in the tailings sludge is confined in the treated sludge through mineral hydration by small additions of cementitious materials. The formation of geopolymer gel and the mechanism of metal ions immobilization are studied.

General Objective

I attempted to graft the geopolymerization technology on the consolidation of mine tailings and synthesize geopolymers with satisfactory compressive strength and durability, as well as to immobilize the heavy metals in the mine tailings.

Goals

1) To synthesize geopolymers by using metakaolin and systematically study the synthesizing conditions.
2) To synthesize geopolymers with quartz sand and study the influence of quartz in geopolymerization.
3) To synthesize geopolymer with metakaolin that calcined at different temperature and to study how the activity of raw materials effect the geopolymerization.
4) To synthesize geopolymer with geothermal clay which endured geothermal activity possesses and has a higher reactivity than usual clay.
5) To consolidate mine tailings through geopolymerization and study the effect of heavy metal on the microstructures and mechanical properties of the alkali activated binders.

6) To study the immobilization mechanism of heavy metals in alkali activated binders.

CHAPTER 1

Literature Review

1.1. Parameters for geopolymerization reactions and geopolymer syntheses

1.1.1. Raw materials

Metakaolin was initially used as the raw material and has become a model compound in geopolymerization. It was usually used to compare with other precursor materials, for instance fly ash. A number of other raw materials, including natural minerals, metallurgical wastes and their mixtures, were exploited to synthesize geopolymers in recent years. Diaz-Loya et al. (2011) studied the mechanical properties of 25 fly ash-based geopolymers from different sources. They reported that the mechanical behavior of these geopolymer cements were similar to that of ordinary Portland cement (OPC) concrete. Xu and van Deventer (2000) used 16 natural minerals, which were classified into four crystal structure groups (ortho-, di- and ring- silicates, chain silicates, sheet silicates, and framework silicates) and six mineral groups (garnet, mica, feldspar, clay, sodalite, and zeolite), to synthesize geopolymers. They found that natural aluminosilicate minerals could be a source material for geopolymers, and the aluminosilicate frameworks show a higher extent of dissolution in alkaline solution, thus a higher compressive strength was obtained after geopolymerization, than the chain, sheet and ring structure aluminosilicates.

As reported in the literature, the raw aluminosilicate materials in geopolymerization can be broadly divided into two groups: 1) calcined materials such as fly ash, metakaolinite, slag, construction residues and pozzolanic wastes; 2) noncalcined materials such as kaolinite, feldspar, clays, and mineral processing tailings. Geopolymerization of calcined raw materials generally has faster dissolution and gelation rate that results in geopolymers, which show higher early compressive strength than non-calcined materials. This phenomenon was attributed to the fact that calcination improves the reactivity of the raw materials by changing the crystalline structure into an amorphous structure that is easier to leach. However, geopolymers synthesized from non-calcined raw materials display a higher increase in the compressive strength in the later stage of the geopolymerization reaction. And geopolymers synthesized from a mixture of calcined and non-calcined materials benefit from the interaction between the raw materials that could activate each other and enhance the extent of the reaction to generate a high compressive strength products (Xu and van Deventer, 2002). Figure 1.1 shows a series of SEM images of geopolymers (together with their compressive strength) synthesized from three types of raw materials: namely fly ash, fly ash and kaolinite, fly ash, kaolinite and albite, at optimal mass ratios. A thicker gel phase can be observed from geopolymers synthesized with fly ash and kaolinite than those synthesized from fly ash alone. With the addition of albite, more fly ash particles were transferred to the gel phase, so that fewer large fly ash particles are observed in the image. The final compressive strength of the three geopolymers follows the order: $GP_{\text{fly ash}} < GP_{\text{flyash+kaolinite}} < GP_{\text{flyash+kaolinite+albite}}$.

1.1.2. Si/Al ratio

The two main structural elements of geopolymers (Si and Al) and their ratio in raw materials play a critical role in geopolymerization, and have been studied extensively. Davidovits proposed geopolymer structure as asialate (silicon-oxo-aluminate) network consisting of SiO_4 and AlO_4 tetrahedrons linked alternately by sharing all oxygen atoms. Cations such as Na^+, K^+ and Ca^{2+} are present in the framework cavities to balance the negative charge of AlO_4. Their empirical formula is $M_n(-(SiO_2)_z-AlO_2)_n \bullet wH_2O$, where M is the alkaline element, *z* is 1,2, or 3 representing the structures of polysialate (-Si-O-Al-O-), polysialate-siloxo (Si-

O-Al-O-Si-O) and polysialate-disiloxo (Si-O-Al-O-Si-O-Si-O), respectively, and n is the degree of geopolymerization (Singh et al., 2005). Table 1.1 presents some typical geopolymers synthesized with various SiO_2/Al_2O_3 ratios. It is easily noticed that geopolymers are usually synthesized by using a relatively narrow range of Si/Al ratios (from 0.8 to 2.5).

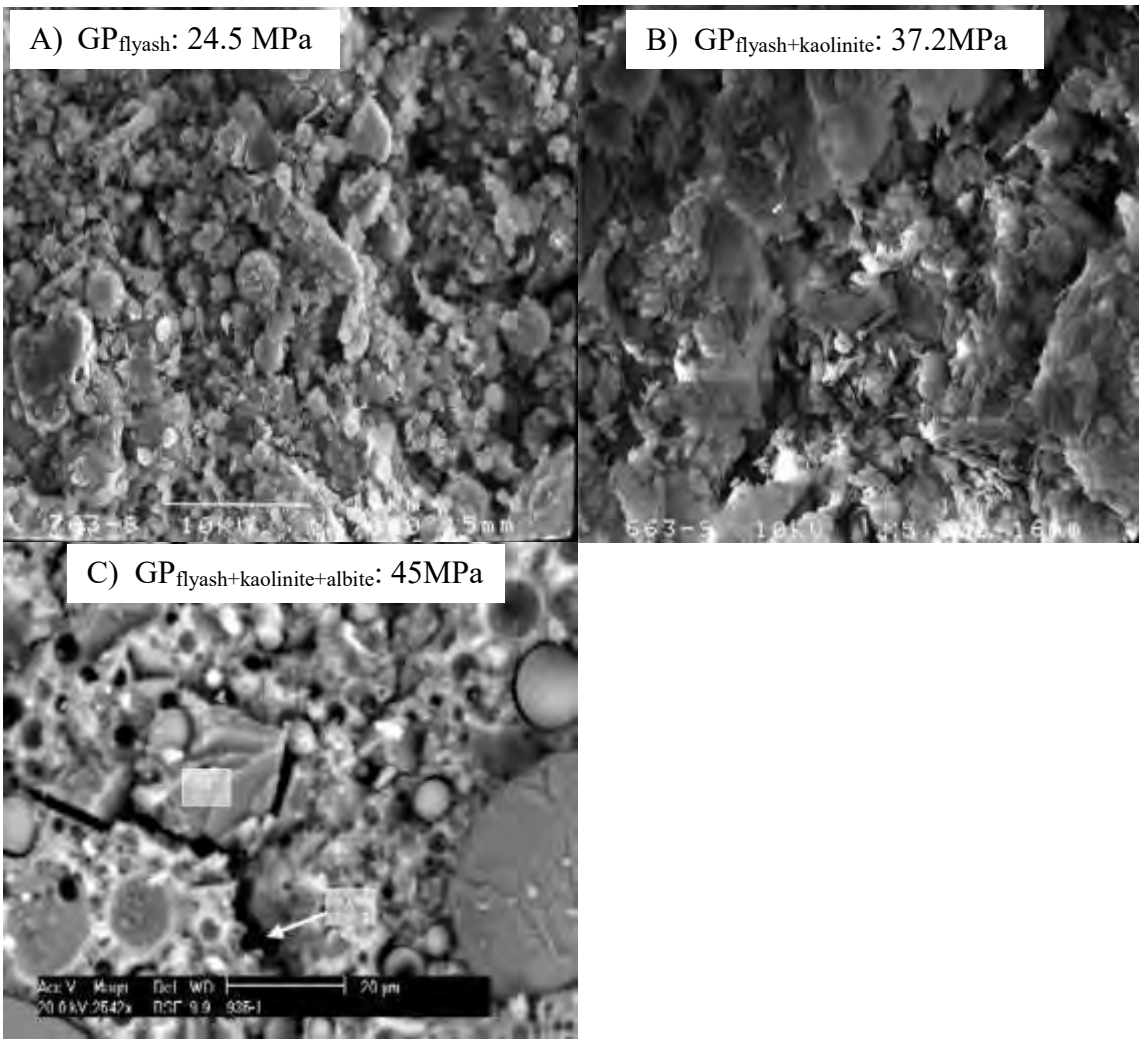

Figure 1.1. Geopolymers synthesized from A) fly ash, B) kaolinite and fly ash, C) albite, kaolinite and fly ash (Xu and van Deventer, 2002)

However, it is inevitable to encounter geopolymers formed at a Si/Al ratio higher than 2.5 due to broad raw aluminosilicates with high Si content are involved and silicates are employed as alkaline activators (Khale and Chaudhary, 2007; Zhang et al., 2010). Recently, geopolymerization has been suggested as a potential technology to consolidate mine tailings and oil sands tailings (Rao and Liu, 2015); which are mainly unpredictable aluminosilicate minerals covering a great range of Si/Al ratios. Further, Ahmari and Zhang (2012) have used copper mine tailings to produce eco-friendly bricks for construction, which contains 64.8 wt% SiO_2 and 7.08 wt% Al_2O_3 (Si/Al ratio is around 8:1). In addition, different Si/Al ratios have been reported to reach the maximum compressive strength of synthesized geopolymers. For instance, Duxson et al. (2007) reported a maximum strength at Si/Al ratio of 1.9 from

metakaolin based geopolymers, however, Silva et al. (2007) stated that the most favorable Si/Al molar ratio for strength development in metakaolin-based geopolymer was 1.7. And Rowles and O' Connor (2003) even reported the maximum strength was 64 ± 3 MPa at a Si/Al/Na ratio of 2.5:1:1.3 in the synthesis of a metakaolin based geopolymer with sodium silicate as activator. This controversy is acceptable because different studies were different in other synthesizing conditions such as alkali types, curing time and temperature, etc. However, the reaction nature of silicate precursor on sodium aluminosilicate hydrate (NA-S-H) gel formation and geopolymer's strength was not consistent in literature either. Many researchers reported that the structural stability of geopolymers increased with the addition of silicates, due to the formation of long chain silicate oligomers and Al-O-Si complexes in the geopolymers (Lee and van Deventer, 2002; McCormick et al., 1989). While some studies stated that the addition of soluble silicates could not induce fundamental changes in the structure of geopolymers (Duxson et al., 2005; Khale and Chaudhary, 2007; Provis et al., 2005). A very high silicate concentration promotes the formation of Si-rich gels with a high percentage of bridge bonds that results in a more amorphous geopolymer with a lower strength (Criado et al., 2007), and excess silicate could hinder water evaporation, thus impede geopolymer structure formation (Cheng and Chiu, 2003).

Table 1.1. Typical geopolymers synthesized with different Si/Al ratios

Reference	SiO_2/ Al_2O_3	Alkali Metal	Curing in Oven		Main raw material	Additives (mass %)	Compressive strength (MPa)
			Temp (°C)	Time (h)			
van Jaarsveld et al., 2002	1.75	K	30	24	Fly ash	Kaolinite (15%)	51.4
Phair et al., 2004	1.67	Na	23	—	Fly ash	Kaolinite (14%)	32.7
Phair et al., 2001	1.64	Na	45	24	Fly ash	Cement (12%)	50
Xu and van Deventer, 2003	2.10	K	40	24	Kaolinite, fly ash and albite	—	45
Xu and van Deventer, 2003	2.30	K&Na	40	24	Kaolinite and albite	—	24.4
Cheng and Chiu, 2003	3.13	K	60	3	Blast furnace slag	Metakaolin	79
Rowles and O´Connor, 2003	2.6	Na	75	24	Metakaolinite	—	15
Puertas et al., 2000	3.33	Na	65	1.25	Kaolinite	—	54
Silva et al., 2007	3.81	Na	40	24	Metakaolinite	—	23
Silva et al., 2007	5.01	Na	40	8	Metakaolinite	—	18

1.1.3. Alkali activator

Alkali activator significantly affects the geopolymerization on leaching silicon and aluminum from raw materials and on the formation of aluminosilicate glassy gel, as well as on the condensation process. The alkali activators can be divided into two categories, viz. alkalis such as NaOH, KOH, Na_2CO_3 and K_2CO_3 and silicate additives such as Na_2SiO_3 and K_2SiO_3 (Duxson et al., 2007; Fernández-Jiménez et al., 2013; Xiong et al., 2004). Table 1.2 summarizes some experiences for controlling alkali activators from various research groups. Although different designs were reported, it can be concluded that alkali activators usually consists a very high alkali concentration and an optimal silicate additive. In most studies, the high alkali concentrations were expressed as weight ratio with respect to the raw materials,

e.g. metakaolinite and fly ash, or as stoichiometric concentration in the precursor solutions. For instance, Wang et al. (2005) reported that the flexural strength, compressive strength and apparent density of metakaolinite geopolymer increased with increasing NaOH concentration from 4 mol/L to 14 mol/L. They attributed this increase to the enhanced dissolution of the metakaolinite particulates at high alkali concentrations. The effect of pH of the precursor slurry on the mechanical properties of synthesized geopolymers has also been reported. Phair and van Deventer (2001) synthesized waste-based geopolymers and stated that the compressive strength at pH 14 was 50 times higher than that at pH 12. They observed that the geopolymer precursors remained viscous and behaved like cement at lower pH, and attained a more fluid gel composition at higher pH, which was less viscous and more workable. They found that more small silicate oligomers and monomers were formed at higher slurry pH. In general, researchers agreed that a higher alkali concentration prompted the geopolymerization reactions, and thus resulted in better mechanical properties of the geopolymers (Figure 1.2). However, Fernández-Jiménez et al. (2006) reported from an alkali activation of a fly ash geopolymer that increasing Na_2O from 14.1wt% to 14.9 wt% led to a reduction of the mechanical properties. The similar result also reported when beyond the rate at Na/Al of 0.63, the further increases in NaOH content give a reduced rate of geopolymer formation. It could be that the newly formed geopolymer gel re-dissolves in a highly alkaline system, leading to a slower effective rate of gel growth and gel crystallinity (Rees et al., 2007). The effect of alkali concentration on the geopolymer´s mechanical properties and the leaching or catalytic mechanism is still an interesting area that should be studied further. However, this effect should be studied together with the cation and anion type of the alkalis and the addition of silicate. For instance, carbonate ion can form sodium bicarbonate that decreases the degree of geopolymerization when carbonate alkalis are utilized.

Table 1.2.Typical experiments on designing alkali activators

Reference	Raw materials	Activating solution	Optimal activator	Curing detail
Rahier et al., 1997	Metakaolinite: 85% Non-reactive minerals: 15%	SiO_2/Na_2O: Constant at 1.4 H_2O/ Na_2O: 8.9-13.9 Sodium silicate/metakaolinite: 0.8-1.7	SiO_2/Na_2O: 1.4 H_2O/ Na_2O: 11.9 Sodiumsilicate/metakaolinite: 1.0	60°C for 24 hours
Liew et al., 2012	Metakaolin SiO_2: 54% Al_2O_3: 31.7%	NaOH: 6-10 mol/L SiO_2/NaOH: 0.16-0.28	NaOH: 8 mol/L SiO_2/NaOH: 0.2	80°C for 7 days
Wang et al., 2005	Metakaolinite Si: 42.39% Al: 29.86% O: 26.17%	NaOH: 4-12 mol/L NaOH/Na_2SiO_3: 4.15:1	NaOH: 12 mol/L NaOH/Na_2SiO_3: 4.15:1	65°C for 10 hours
Phair and van Deventer, 2001	Metakaolin Slag Fly ash	pH: 12-14 Al_2O_3/ SiO_2: 6.1-6.4	pH: 14 K-silicate and KOH	45°C for 24 hours
Fernández-Jiménez and Palomo, 2006b	Fly ash SiO_2: 53.1% Al_2O_3: 24.8%	Na_2O: 5%-15% [a] SiO_2: 0-9.52% [a]	Na_2O: 14.09% [a] SiO_2/Na_2O: 0.118	85°C for 20 hours
Ma et al., 2012	Fly ash SiO_2: 48.4% Al_2O_3: 31.4%	Na_2O: 1%-1.5%[a] SiO_2: 0-1.5% [a]	Na_2O: 1.5% [a] SiO_2: 1% [a]	40°C for 28 days
Bakharev, 2005	Fly ash SiO_2: 50%	Na_2O: 2-8%	Na_2O: 8% SiO_2/Na_2O: 2.02	75°C for 28 days

	Al_2O_3: 28%	SiO_2/Na_2O: Constante at 2.02		
Rattanasak and Chindaprasirt, 2009	Fly ash SiO_2: 39.5 Al_2O_3: 19.5%	NaOH: 5-15 mol/L SiO_2/NaOH: 0.5-2	NaOH: 15 mol/L SiO_2/NaOH: 1	65°C for 48 hours Separate mixing of NaOH and SiO_2.

[a]Weight percent in the fly ash and alkali activator mixtures

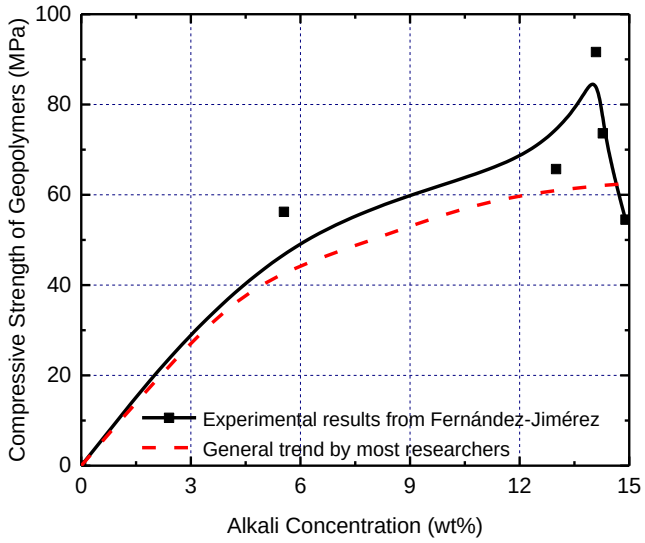

Figure 1.2. A comparison of the reported effects of alkali concentrations on the compressive strength (Phair and van Deventer, 2001)

1.1.4. Water amount

Water also plays an important role in geopolymerization. Water takes part in the dissolution, polymerization and condensation reactions during geopolymer synthesis (Sagoe-Crentsil and Weng, 2007). As the medium for the dissolution of raw materials, the transfer of various ions and polymerization of aluminate and silicate tetrahedron, water has great effects on the geopolymer formation and the properties of the binders. In general, researchers agreed that the mechanical property of geopolymer decreases as the ratio of water to solid by mass increases. Xie and Kayali (2014) synthesized fly ash-based geopolymers with the molar ratio of H_2O/Na_2O changing from 11 to 13. It is shown that reducing water content in the synthesis of geopolymer are beneficial and lead to extra strength gain in the final product. However, little research focuses on synthesizing geopolymer with a high water content that is common condition in mine tailings.

1.1.5. Calcination

In geopolymerization, the dissolution of raw materials plays an important role because it forms the precursors for polymerization and condensation. Generally, calcination in the pre-treatment or choosing by-products after calcination is employed to obtain raw materials with high reactivity for the dissolution. For instance, metakaolin obtained through heating kaolinite in the temperature range among 500–900 °C was studied as exemplary material in geopolymer synthesis (Rahier et al., 1996). Similarly, ore-dressing tailings of bauxite heated at 800 °C for 1h has been synthesized into geopolymer of 40 MPa in compressive strength (Ye et al., 2014). But Xu and van Deventer (2002) reported a different result, when

synthesized geopolymer with calcined and non-calcined materials. It was found that the geopolymer manufactured from calcined material obtained higher early strength, while it formed from non-calcined materials possessed higher increase in strength during the later stages of curing. In addition, the calcination temperature and time of metakaolin are greatly different in literature. For instance, Rahier et al. (1996) applied heating at 700 °C for one hour in their pioneering studies of the synthesis, structure and properties of metakaolin geopolymers. Sagoe-Crentsil and Weng (2007) employed heating at 850 °C for 5 h in studying the dissolution processes, hydrolysis and condensation reactions in metakaolin geopolymer preparation. Zhang et al. (2010) used heating at 700 °C for 12 h in studying the composition design and microstructure of metakaolin geopolymer. It is generally accepted that metakaolin obtained through heating possesses an amorphous structure, in which the SiO_4 sheets persist but in a distorted form, while the octahedral aluminum sheets are profoundly altered, although some short-range structure is preserved (Wan et al., 2017). In the heating process, Al coordination first changes from octahedral (Al^{VI}) to pentahedral (Al^{V}) and tetrahedral (Al^{IV}), with Al^{V} and Al^{IV} developing simultaneously. Then, Al^{VI} reappears when new phases begin to crystallize, some Al^{IV} persists, but A^{IV} disappears (Bergaya and Lagaly, 2006). The transition of Al coordination has been used in the elucidation of the zeolite yield in its synthesis and compressive strength of metakaolin and $Ca(OH)_2$ mixture, and it is accepted that the reactivity of metakaolin was at a maximum when the content of Al^{VI} was at a minimum (Rocha and Klinowski, 1990). But Kuenzel et al. (2002) studied coordination of $Al^{(IV,\ V\ and\ VI)}$ atoms in three types of metakaolin, and the properties of geopolymers formed from them. They stated that no clear correlation was found between the $Al^{(IV,\ V\ and\ VI)}$ content in metakaolin samples and setting time, heat output or strength development of geopolymer.

1.2. Consolidation of mine tailing through geopolymerization reactions

1.2.1. Mine tailing and its harm

Mine tailings are the materials left after the process of separating the valuable fraction of the uneconomic fraction of an ore. Millions tons of mineral tailings are produced each year, and billions tons are already stored globally. For instance, 87% of the gross reserves of vanadium metal are in stone coal in China, from with the extraction of 1ton of V_2O_5 produces 120-150 tons of mine tailings. Because mine tailings include the residual reagent for mineral processing and many heavy metals, stockpiling of them can result in the contamination of the soil and underground water resources, and this practice has been linked to the deformities and deaths of local flora and fauna (Gentes et al., 2006; Lee and Correa, 2005; Renault et al., 2000). In addition, mine tailings are usually disposed into natural or engineered depressions, surrounded by dams. The failure of tailing dam can happen due to earthquakes, blasting vibration and extreme weather. As the public grows increasingly aware of these environmental issues and disasters related to mineral tailings, mining projects are facing greater levels of scrutiny from government agencies in terms of sustainability and social responsibility. The familiar practice of containing mineral tailings slurry by conventional dam and dykes is no longer considered acceptable in many countries (Zhang and Stana, 2010).

1.2.2. Traditional methods

Some methods have been investigated to solve the problem posed by mine tailings. The main methods are shown as follows: 1) Hydrocyclone, as an inexpensive device for particle

classification and concentration purposes, is widely used in the mineral processing industry (Ortega-Rivas, 2007). In Collahuasi copper mine in Chile, the use of hydrocyclones for increasing recovery of concentrate and decreasing the amount of water in tailing has been applied (Mining-Technology, 2014) 2) Flocculants are widely used in solid/liquid separation, which can improve the settling rate of the solids and clarity of the liquid phase obviously. Yachin (1996) has studied to use a flocculants-assisted hydrocyclones in a copper tailings disposal. They reported that under suitable conditions, flocculation could significantly enhance solid-liquid separation in hydrocyclones, producing an underflow with over 98% solids recovery as compared to the recovery of less than 53% with conventional hydrocyclone. 3) Thickener is also a common solid-liquid separation device based on gravity sedimentation. It is widely used in mine tailings treatment. In 1985, Alcoa built three high density super thickeners at the Pinjarra refinery for tailings disposal (Cooling and Clenister, 1992). The largest of these operations consists of a thickener having a diameter of 90 m and a 10-m-deep compression zone, which has a capacity of 450 tons/h and can produce a 50 wt% solids underflow. 4) Filtration equipment is common for dewatering coal tailings and red mud, through various mechanical, physical or biological operations mine tailing is separated (Bethell, 2012; Power et al., 2011). Pressure filtration has been used in Meishan Iron Mine, China. With the pressure of 0.5 to 0.55 MPa, the filter cake was molded and the water content was lower than 20%. However, these technologies either added costly reagents or required thickening machines of high energy consumption.

Therefore, to strengthen and reuse mine tailings such as backfill materials and construction bricks have been studied. Traditionally, the use of mine tailings as backfill materials in mining tunnels after blending OPC is the most attractive approach to tailings management. The Brunswick mine, in New Brunswick, Canada, used plant tailings to prepare pastefill (Jung and Clark, 1995). The Portland cement is the only binder used for the strength requirement of the fill. The cement percentage varied from 2-7% was used for filling secondary stopes and 5-7% cement was used for stope plugs. It helped the mine to achieve a tighter filling of the stopes, improvement in delivery system reliability and a quicker turn-around time of stopping. Brackebusch (1995) also reported that relatively small amounts of cement (3% to 5%) was used with mine tailings to produce stiff backfill material with the compressive strength between 1.5 to 3.5 MPa. Consolidation of mine tailing with cement can reduce mine dewatering, save labor and materials and reduce tailing impoundment requirements. However, these binders showed the low resistance and weak immobilization of toxic components to the acidic conditions, which are common in the natural environment (Kesimal et al. 2005).

1.2.3. Consolidate mine tailings through geopolymerization

Geopolymers are aluminosilicate materials with the high compressive strength and show superior capacity in the immobilization of heavy metals. In addition, mine tailings are usually rich in calcium and aluminosilicate minerals, as well as the slurries, are of an alkaline condition, which are the advantages for inducing an alkali activation reaction. Davidovits (1996) first pointed out that geopolymer cement could be used to stabilize mineral processing tailings. Sand, mineral processing tailings and geopolymers in the ratio of 20:13:7 were blended to produce solidified tailings. Tailings from four different types of mines, base metal, potash, coal and uranium mines, respectively, were tested. After casting, setting and curing at ambient temperatures, the solidified products were tested for resistance to leaching. It is

concluded that the geopolymer-stabilized-and-solidified mineral processing tailings had archaeological long term stability. Ahmari and Zhang (2012) prepared copper mine tailings-based bricks through alkali activation and indicated that the heavy metals were effectively immobilized in the bricks, but compression was applied in the preparation. Similarly, iron mine tailings-based bricks were synthesized with a compressive strength of 50.53 MPa by adding sodium silicate to the tailings in powder form (Kuranchie et al., 2016). Panias and Giannopoulou (2007) used fly ash and copper flotation tailings in the alkali activation processes. They stated that the products were of compressive strength around 10 MPa and of high immobilization ability on Cu, Ni, Pb, Zn, Mn and Al. However, these studies only reported the consolidation phenomenon of mine tailings by alkali activation, namely compressive strength and morphology of the synthesized products. And they are lack of investigation on the activation reaction and microstructure of the products. In these products, usually both the calcium silicate hydrate (C-S-H) and geopolymer gel formed because calcium minerals (e.g., calcite) and aluminosilicate minerals coexist in most mine tailings, but it was rarely distinguished them by previous studies. Furthermore, the effect of heavy metals in mine tailings on the microstructure of alkali activated products is still vague and controversial. Lee et al. (2016) prepared fly ash-based geopolymer for the immobilization of lead, and they showed that the addition of lead decreased the compressive strength of formed geopolymers. While Nikolić et al. (2014) reported a small increase in the compressive strength of fly ash-based geopolymer with the addition of 0.5% lead by mass.

1.3. Immobilization of heavy metals through geopolymerization

1.3.1. Heavy metals pollution

Mineral resources represent an important role in the socio-economic development, thus the exploitation and utilization of mineral resources are essential in the world. Nonetheless, mineral extraction, especially tailings disposal, has inflicted serious environmental damage, especially in the realm of heavy metal pollution (Acosta et al., 2011). Rashed (2010) reported that the tailings from a gold mine, at Allaqi Aswan, Egypt, lead to a heavy metal pollution to the environment. The results showed that the soil and plants near the gold mine tailing were highly toxic, and the plants and soil can't be used for grazing and agriculture. Zhao et al. (2007) investigated the soil heavy metal pollution around the Dabaoshan Mine, China. Significantly high levels of Cu, Zn, Cd and Pb were found in the paddy soils near the mine, which were 567, 1140, 2.48 and 191 mg/kg, respectively. These metals were continuously dispersed downstream from the tailings and wastewater. In summary, this kind of pollution not only degrades the quality of the waterbodies and crops, but also threatens the health of animals and human beings by way of the food chain (Dong et al., 2011).

1.3.2. Immobilization of heavy metals

Alkali activated products such as geopolymer and C-S-H phases form raw materials into consolidated binders that immobilize heavy metals. For example, alkali-activated blast furnace slag binders with the main hydration product of C-S-H phase at a low Ca/Si ratio were found to immobilize exceeded 99.9% of Zn, Cd, Pb and 98.8% of Cr in them. In OPC composites with additions of siliceous fly ash, fluidized bed combustion ash and slag, heavy metals of Pb^{2+}, Cu^{2+}, Zn^{2+}, Cd^{2+}, Mn^{2+} were found to be immobilized higher than 99.82% (Giergiczny and Król, 2008). In geopolymer phase, van Jaarsveld et al. first proposed the heavy metals immobilization mechanism as physical encapsulation, adsorption and bonding

of the ions into the geopolymer gel (van Jaarsveld et al., 1997). Then, geopolymers were synthesized with slag and metakaolin in the presence of Pb and Cu ions in the range of 0.1-0.3 wt%, into which higher than 98.5% of the heavy metals were immobilized. And the immobilization of Pb was higher than that of Cu when high dosages of heavy metals were applied (Zhang et al., 2007). And in metakaolin-based geopolymers, 1wt% of Pb was found to be immobilized with the Pb release was less than 5 ppm (Perera et al., 2005). Fly ash-based geopolymers activated by sodium silicate were studied for the immobilization of Cr^{6+}, Cd^{2+} and Pb^{2+} (Zhang et al., 2008). After static leaching the geopolymers with H_2SO_4, $MgSO_4$, Na_2CO_3 and deionized water for 2000 h, it was found that lead was effectively immobilized in geopolymers, as was cadmium except the most acidic leaching environments, but the immobilization of chromium was problematic.

1.3.3. Mechanism

Even though the phenomenon of heavy metal immobilization in alkali-activated products has been extensively reported with good agreements, the mechanism has been studied obliquely and differently, which is still inconsistent. For instance, fly ash-based geopolymers were crushed into various size fractions before applying kinetic leaching analyses, of which the release of heavy metals qualitatively proceeded along the combination of pore and boundary distributions in the geopolymers. Thus it was stated that the immobilization of heavy metals in geopolymers was governed by a combination of physical encapsulation, chemical bonding and adsorption (Zhang et al., 2008). Phair et al. (2004) examined the effect of Al source and alkali activator on Pb and Cu immobilization in fly ash-based geopolymer. The immobilization efficiency in the geopolymers synthesized with NaOH was much better than that with Na-silicate or mixture of Na-silicate and NaOH. Therefore, they considered the immobilization of Pb and Cu required reaction with species dissolved from the starting materials in order to form a new aluminosilicate phase. And in another alkali-activated fly ash-based binder, it was stated that lead compound was immobilized through the formation of Pb_3SiO_5 because it was indicated in XRD characterizations (Palacios and Palomo, 2004). However, Nikolic et al. (2014) reported that no evidence could identify the formation of a new Pb-phase through XRD. Guo et al. (2017) used three types of Pb compounds, namely PbO, $PbSO_4$ and PbS, to study the Pb immobilization into alkali activated fly ash-based binders. Through XRD and backscattered electron (BSE) SEM measurements, they observed isolated PbS particles in the final binders, but no isolated PbO and $PbSO_4$ compounds. Then through XPS, they found the chemical environment of Si and Al was not affected by adding any of the Pb compounds. They stated that the Pb is converted to an amorphous form and participated in the geopolymer network when Pb compounds were added in soluble forms; On the contrary, the Pb was physically encapsulated when it was added in inert form. El-Eswed et al. (2015) used 0.1 mol/L HCl, 0.1 mol/L NaOH, 0.1 mol/L NaCl and 1.0 mol/L NaCl solutions to leach Pb from kaolin/zeolite-based geopolymers. They found that the most aggressive solution in leaching was the 1 mol/L NaCl, and the more heavy metals immobilized, the more exchangeable ions (Na^+ and K^+) released into the leachate. Thus, they speculated that Pb immobilization was due to charge balance in geopolymers. Lee et al. (2016) employed a sequential extraction procedure to study the immobilization of lead in aluminate-activated fly ash-based binder and classified the immobilized Pb as exchangeable, acid-soluble, reducible, oxidizing and residual. They considered that the binders with a Si:Al ratio

of 2 were more suitable for immobilizing lead, because almost all (99%) of the extracted lead existed in the oxidizing and residual fractions in these binders.

Based on these studies, four types of immobilization forms of heavy metals in alkali-activated binders are summarized as follows. They are 1) heavy metal ions are encapsulated physically in binder´s porous structures, 2) heavy metals are formed into the binder network chemically, 3) heavy metal ions are bound to the binders through charge balance and 4) precipitates containing heavy metals are formed and encapsulated physically. However, no research revealed directly the immobilization form of heavy metals in either C-S-H phase or geopolymer phase.

CHAPTER 2

Experimental

2.1. Research line

Research line of the work is presented schematically in Figure 2-1. As it shows, the Chapters 1 to 3.3 are the preparation chapters. In Chapter 1, the literature about the synthesis of geopolymers and the mechanism of geopolymerization reactions were reviewed. Chapter 2 is the experimental of the thesis work. In Chapter 3.1, the effect of Si/Al ratios on the geopolymer gel formation in metakaolin-based geopolymer was investigated. It provides fundamentals for the synthesis of geopolymers with mine tailings that might possess extensive Si/Al ratios, because silicate minerals are the main components in mine tailings. In Chapter 3.2, the incorporation of quartz sand in the reinforcement of metakaolin geopolymers has been investigated. It indicates the formation of a combination by several micrometers around quartz particles, which associates them to the geopolymeric gel as filler materials in metakaolin geopolymers. This work not only fills the gap of incorporation of quartz sand in geopolymers, but also gives a clue on using non-calcined aluminosilicates (e.g., mine tailings) in the synthesis of geopolymers. In Chapter 3.3, the effect of calcining temperature to the reactivity of raw materials was studied. It provides a further understanding of the reactivity of mine tailing. Chapter 3.4 is the transitional work, in which geopolymers were synthesized with geothermal clays. Geothermal clays are considered as raw aluminosilicate materials with the reactivity between metakaolin and mine tailings. The results show that geothermal clay can be used to produce geopolymer with a satisfactory mechanical property. This work gives guidance for synthesizing geopolymer by using mine tailings directly. In Chapter 3.5 and 3.6, the consolidation of mine tailings through alkali activation was studied, and the mechanism of heavy metals immobilization in alkali-activated binders was investigated.

2.2. Materials

Kaolinite from Hubei Chemicals in China was used to prepare metakaolin through calcination at 800℃ in air for 5h. The chemical composition of metakaolin measured by X-ray Fluorescence (XRF) is given in Table 2-1. The mass ratios of SiO_2 and Al_2O_3 are close to 1:1 which is the ratio in pure metakaolin. Sodium hydroxide (NaOH) and sodium silicate (Na_2SiO_3) of analytical reagents of the American Chemical Society (ACS) reagent grade were purchased from Sinopharm Chemical Reagent, China and used as alkaline activator in the synthesis of geopolymers. Silica fume (SiO_2) from Jingfeng Material, China was used as soluble silica additive to maintain Si/Al ratio in the syntheses. The silica fume should react completely with the sodium hydroxide into silicate as the literature reported previously.

Quartz sand collected from Michoacán, Mexico was used as silica filler additive. The quartz sand was milled and classified into 6 size ranges of >180 μm, 180-105 μm, 105-75 μm, 75-32 μm, 32-12 μm and <12 μm. Rutile sand (TiO_2>98%) collected from Hainan, China of size range 75-48 mm was used a comparing filler additive.

In the preparation of geopolymers with metakaolin heated at various temperatures, kaolinite with a particle size of 50% ≤4 μm was collected from Hubei province, China. It was heated at 550 °C, 600 °C, 650 °C, 700 °C, 750 °C, 800 °C, 850 °C, 900 °C and 950 °C in air for 6 h, respectively.

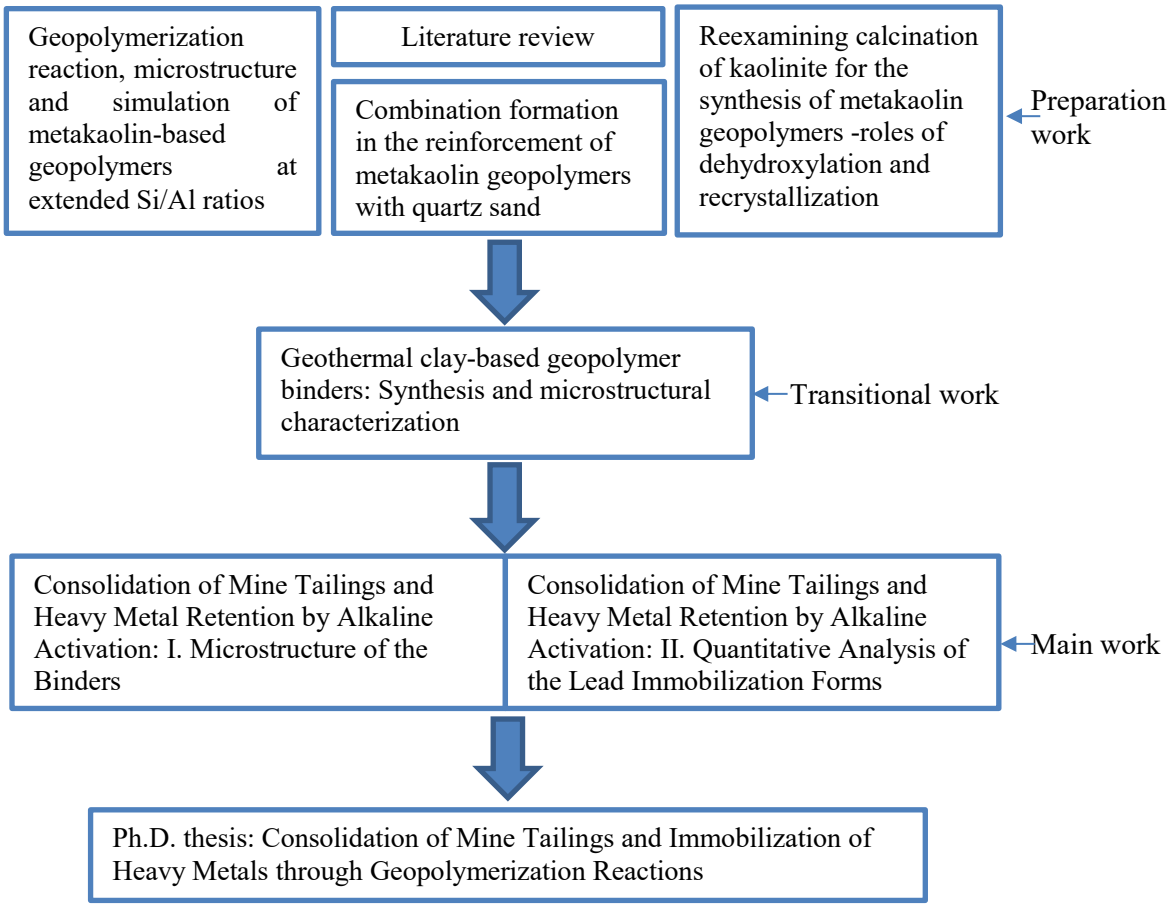

Figure 2.1. Schematic presentation of the research line

Table 2.1. Chemical composition of the metakaolin

Component	SiO_2	Al_2O_3	K_2O	Fe_2O_3	TiO_2	MgO
wt%	52.8	43.7	1.2	0.6	0.5	0.2

Geothermal clay rock was collected from the Los Azufres geothermal field, Mexico at the depth of 250 m where the temperature exceeds 150 °C. It was measured the particle size at 50% and 85% of cumulative undersize of 26.9 μm and 36.3 μm, respectively from a Shimadzu SALD-1100 laser diffraction analyzer. Table 2-2 gave the chemical analysis of the whole geothermal clay rock measured by X-ray fluorescence (XRF, PANalytical Axios), in which SiO_2 and Al_2O_3 are the main components with Si/Al ratio around 3.5:1. Figure 2-2 showed the X-ray diffraction (XRD, Bruker D8) patter of the geothermal clay, which gave the 47.44 % kaolinite and 49.85 % cristobalite in mass. Although other clay minerals (e.g., montmorillonite or illite) were not identified in the XRD pattern of the geothermal clay, they were presumably included according to the components of Table 2-2.

Table 2.2. Chemical analysis of the whole geothermal clay rock

Components	SiO_2	Al_2O_3	SO_3	K_2O	Na_2O	MgO
Mass %	71.30	17.11	1.80	0.37	0.07	0.03

	Fe_2O_3	P_2O_5	CaO	TiO_2	ZrO_2	LOI
	0.08	0.002	0.031	0.055	0.017	9.089

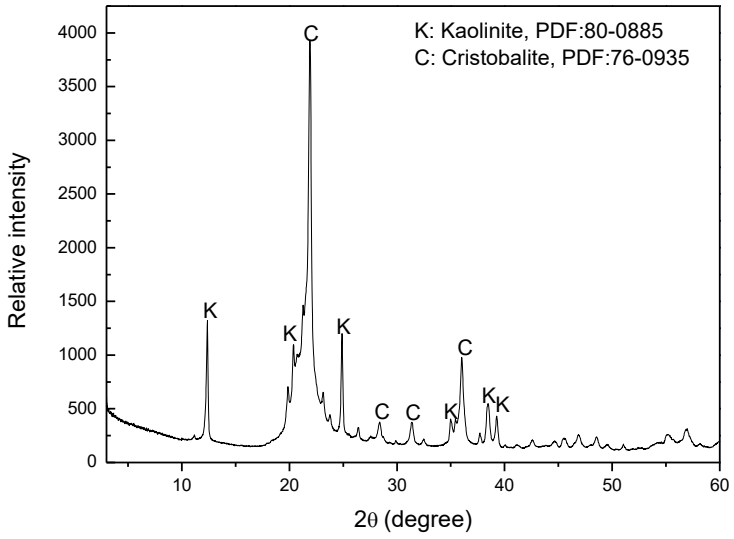

Figure 2.2. XRD pattern of the geothermal clay rock

The mine tailings of sphalerite flotation were collected from the Dulong mill in Yunnan, China. It was measured the particle size at 50% and 85% of cumulative undersize of 20 μm and 46.7 μm, respectively from a Shimadzu SALD-1100 laser diffraction analyzer. Table 2-3 gave the chemical analysis of the whole tailing sample measured by X-ray fluorescence (XRF, PANalytical Axios), in which CaO, MgO, SiO_2 and Al_2O_3 were the main components. Figure 2-3 showed the X-ray diffraction (XRD, Brucker D8) pattern of the mine tailing with main dolomite and calcite, while a small quantity of kaolinite and quartz. Quantitative calculation based on the XRF and XRD results gave 45.72% dolomite, 35.26% calcite, 5.22% kaolinite and 3.69% Quartz in the mine tailing. Lead nitrate ($Pb(NO_3)_2$, ACS reagent grade) were used to adjust the lead content in mine tailings. Acetic acid (CH_3COOH, ACS reagent grade) and deionized water were used in the leaching process. Sodium hydroxide (NaOH, ACS reagent grade), hydrochloride acid (HCl, ACS reagent grade) and potassium chloride (KCl) were used in the zeta potential measurements.

Table 2.3. Chemical composition of the mine tailing

Component	CaO	Fe_2O_3	MgO	ZnO	SiO_2	SO_3	K_2O
wt%	33.66	0.19	9.94	1.77	6.20	1.46	0.24
	Na_2O	Al_2O_3	PbO	BaO	P_2O_5	TiO_2	LOI
	0.30	2.06	0.15	0.31	0.27	0.09	43.35

2.3. Geopolymer synthesis

In a typical synthesis, alkaline solution was first prepared and then mixed with the raw materials. The mixture was poured into a cubic steel mold (50 mm×50 mm×50 mm) and vibrated on a vibration table for 3 min to liberate the air bubbles. After that, the mold was

sealed for the curing process, in which it was first cured at 60 °C for 6 hours and continued at room temperature for 7 days.

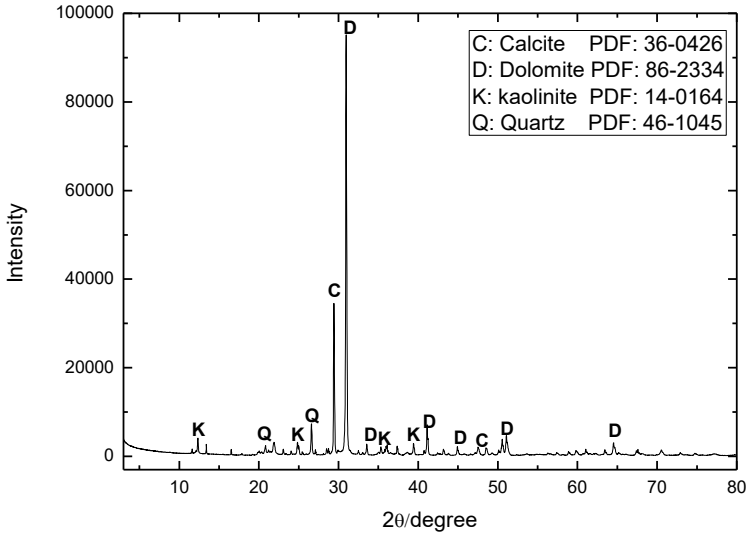

Figure 2.3. XRD pattern of the mine tailing

In the preparation of geopolymers at Si/Al ratios of 1:1, 1.5:1, 2:1, 3:1, 4:1 and 5:1, 0.5 mol metakaolin, 5.5 mol H_2O, 1 mol NaOH were used, while silica fume (silica corrector) of 0, 0.5, 1, 2, 3 and 4 mol was used, respectively. In all the six syntheses, the molar ratios of Na_2O/Al_2O_3 and Na_2O/H_2O were 1:1 and 1:12, the ratio of solid/liquid (S/L) was 1.12:1 g/ml.

For investigating the effect of quartz sand in metakaolin-based geopolymers, all syntheses were conducted by keeping Na_2O/Al_2O_3 and Na_2O/H_2O ratios of 1:1 and 1:12, only the additives are variable. The specimens No. 1-6 were synthesized with additives of 5 mol/L silica fume and 5 mol/L quartz sand with size ranges of 240-180 μm (No. 1), 180-105 μm (No. 2), 105-75 μm (No. 3), 75-32 μm (No. 4), 32-12 μm (No. 5) and 12-6 μm (No. 6). The specimens No. 7-12 were synthesized with additive of only quartz sand at 10 mol/L, corresponding to the 6 size ranges of descending order. The specimens No. 13-14 were synthesized with only silica fume additive of 10 mol/L and 5 mol/L, respectively. The specimen No. 15 was synthesized with rutile sand (75-48 μm) and silica fume additives of both 5 mol/L.

In the preparation of geopolymers with metakaolin heated at various temperatures, 1 mol metakaolin (222 g), 1mol Na_2SiO_3 (122 g) and 12 mol H_2O (216 mL) were used, with the molar ratios of Na_2O/Al_2O_3 and Na_2O/H_2O were 1:1 and 1:12, and the solid/liquid (S/L) was 1.03:1 g/mL.

In the preparation of geopolymers synthesized with geothermal clay, for preparations No. 1-8, geothermal clay sample (222 g) without and with calcination at 200, 400, 450, 500, 550, 600 and 800 °C were used as raw aluminosilicates. The alkaline activator solutions were synthesized consistently with 0.5mol Na_2SiO_3, 0.5mol NaOH and 9 mol H_2O, making the

solid to liquid and Na/Al ratios in geopolymers as 1.37:1 and 2.01:1, respectively. For preparations No. 8-14, raw aluminosilicates were of geothermal clay (222 g) heated at 800 °C, while the alkaline activator solutions were different in the Na_2SiO_3 to NaOH ratios. For preparations No. 15-17, geothermal clay samples (222 g) were heated at 800 °C and alkaline activator solutions were of 0.5 mol Na_2SiO_3 and 0.5 mol NaOH. The variable was the water dosage, of which 10 mol, 11 mol and 12 mol were used respectively.

In the preparation of mine tailing-based geopolymers, the variables were the mine tailing to metakaolin ratio and the added amount of lead in the raw materials. For syntheses No. 1-6, the ratios of mine tailing to metakaolin were 1:1, 3:2, 7:3, 4:1, 9:1 and without metakaolin, respectively. For syntheses No. 7-16, $Pb(NO_3)_2$ was added from 1-10% to the total mass of raw materials (444 g). The $Pb(NO_3)_2$ was added in solid and mixed with raw materials for 5 min. The alkaline activator solutions were prepared consistently with 1 mol Na_2SiO_3 and 12 mol H_2O, making the solid to liquid ratio in each synthesis as 2.05.

2.4. Characterization

The binders were characterized by scanning electron microscopy (SEM, JEOL JSM-5610LV), Fourier transform infrared spectroscopy (FTIR, Nexus JSM-5610) and X-ray diffraction (XRD, Bruker D8) for morphology and microstructures, and mechanical tester (Hangzhou Xingo Technology, EHC-1300) for compressive strength. In the measurements of compressive strength, three specimens were tested and the average value was used. The chemical states of lead, aluminum and sodium compounds in the binders were measured on an X-ray photoelectron spectroscopy (XPS, Thermo Fisher Scientific ESCALAB 250Xi) with Al Kα radiation (hv=1486.6 eV). The testing conditions were set as source power of 400 W, pass energy of 37.25 eV, energy resolution of 0.44 eV and sensitivity of 3.28 Mcps. Binding energies were corrected with respect to the C 1s peak at 284.8 eV. To prepare samples for XPS analysis, the binders were milled to powders with a particle size less than 32 μm and dried in a vacuum desiccator before the analysis. ^{29}Si nuclear magnetic resonance (NMR) spectra of geopolymers were obtained by using a NMR spectroscopy (Bruker AVANCE III) at 79.49 MHz. Powdered geopolymer specimens were packed into 7 mm ZrO_2 rotors. Spectra were acquired at spinning speeds of 12 kHz with peak positions referenced to an external standard of tetramethylsilane (TMS) and recorded with 1s delay time. The lack of spectral resolution for silicon in geopolymers has been overcome by adopting Gaussian peak deconvolution to separate and quantify $Q^n(mAl)$ species ($0 \leq m \leq n \leq 4$) as previously reported. NMR studies have shown that all silicon and aluminum sites are in tetrahedral coordination in geopolymers, thus $n \leq 4$. And the resonance of a $Q^4(mAl)$ center with the replacement of each aluminum by silicon is an approximate ≤5 ppm shift, with $Q^4(4Al)$, $Q^4(3Al)$, $Q^4(2Al)$, $Q^4(1Al)$, $Q^4(0Al)$ resonating at approximately -84, -89, -93, -99 and -107 ppm, respectively. ^{27}Al nuclear magnetic resonance (NMR) spectra of metakaolin and geopolymer were determined with NMR spectroscopy (Bruker AVANCE III) at 104.3 MHz. Powdered specimens were packed into 4 mm ZrO_2 rotors. Spectra were acquired at spinning speeds of 10 kHz with peak positions referenced to aluminum nitrate ($Al(NO_3)_3$) and recorded with 2 s delay time. The coordination of $Al^{(VI, V \text{ and } IV)}$ in metakaolin was obtained by applying Seasolve PeakFit™ software and Gaussian peak deconvolution as reported elsewhere.

The Al and Si dissolution, N-A-S-H gel and geopolymer of extended Si/Al ratios were characterized, in order to understand the chemical reactions in geopolymerizations. First, using the same dosages of metakaolin, silica fume (SiO_2), NaOH and H_2O as those used in geopolymer syntheses, the dissolved Si and Al concentrations were measured in separated tests. The alkaline activator (with silica fume) and metakaolin were mixed and agitated for a particular reaction time, namely 5, 10, 20 or 60 min, respectively. Then, 1.9 L water was added into the mixture and the suspension was agitated for 30 s. After that, the slurry was further diluted to avoid undesirable precipitation, filtered and analyzed for dissolved Al and Si compounds by atomic absorption spectroscopy (AAS, GBC Avanta M). The dissolved Si concentrations were abstained from the measured concentrations minus added silica fume concentrations, while the dissolved Al concentrations were the measured ones. By using the same synthesizing conditions, N-A-S-H gels and geopolymers at extended Si/Al ratios were synthesized parallelly. Before curing, the N-A-S-H gels were freeze-dried and vacuum evaporated to prepare specimens for FTIR measurements, in which they were milled and molded with potassium bromide (KBr).

Modelling and simulation were applied to geopolymer oligomers for the calculation of binding energies relative to silica atoms, and to geopolymers for the total energy. Si, Al, O and H atoms are modeled, and each Si or Al atom had 4 bonded neighbors (Q^4, either O or OH). The models were geometry optimized with density functional theory (DFT) calculations as reported elsewhere. In energy calculation, double numerical basis sets and polarization function as adopted in DMOL3 of Materials Studio were used. Electrons were included in the calculation with a basis set cutoff of 0.42 nm. The geometries were assumed to converge if the energies and forces on the atoms were smaller than 0.001 kcal/mol and 0.5 kcal/mol/Å, respectively. The binding energy relative to Si atoms was calculated as following:

$$E_{Si} = E_{oligomer-Si} + E_{atomSi} - E_{oligomer} \quad (1)$$

where $E_{oligomer}$ was the total energy of the oligomer, $E_{oligomer\text{-}Si}$ was the total energy of the oligomer when one Si atom was removed, E_{atomSi} was the intrinsic energy of a single Si atom and E_{Si} was the binding energy relative to one Si atom. The geopolymer structure in a pure cube with the periodic boundary condition of a density 1.04 g/cm^3 was built from the modeled geopolymer oligomers through the Amorphous Cell module in Materials Studio software. The MD simulations were performed with the NPT ensemble (constant number of particles, constant pressure 0.1 MPa and temperature 298 K) for 200Ps to equilibrate the system, then with the NVT ensemble (constant number of particles, constant volume and temperature 298 K) for 1 ns. The Coulomb force was calculated using the Ewald summation scheme. A time step of 1fs and a cut-off distance of 1.5 nm were adopted in simulation.

Differential scanning calorimetry (DSC) and thermogravimetric analysis (TGA) were performed using a STA 449F3 DSC-TG test machine (Netzsch, Germany) to characterize the nature of kaolinite at heating rate of 10 °C/min in nitrogen atmosphere from 0 to 1100 °C. The isothermal heat revolution in the first 48 h of geopolymerization reactions, such as dissolution, polymerization and condensation, were characterized by a C80 micro-calorimeter from Setaram, France, with the external temperature maintained at 25 ± 0.001 °C.

Toxicity characteristic leaching procedure (TCLP) tests were conducted to analyze the leaching of lead from the mine tailings-based binders. The extraction liquid was prepared by

dissolving 5.7 mL acetic acid in 1 L deionized water. The binders were crushed into powders with a size less than 48 μm . In a polyethylene container, the extraction liquid and binder powder were mixed at a liquid to solid ratio of 20:1, followed by a stirring for 20 h. Then, the leachate was separated by centrifugation and filtration. And lead concentration in the leachate was determined by AAS. The ratio of leached lead to the total lead in the binders and lead concentration in the leachate were given for the immobilization efficiency. According to United States Environmental Protection Agency (USEPA) regulatory levels, samples with lead concentration in the TCLP leachate less than 5 ppm can be considered to be non-hazardous (Alter, 2005).

CHAPTER 3

Results and Discussion

3.1. Geopolymerization reaction, microstructure and simulation of metakaolin-based geopolymers at extended Si/Al ratios

3.1.1 Al, Si dissolution and N-A-S-H gel formation

In geopolymerizations, Al and Si dissolution is critical because it is the first stage that releases aluminate and silicate monomers by alkali attack on raw aluminosilicates. Figure 3.1.1 gives the dissolution rates of Al and Si compounds at various Si/Al ratios of reaction time from 5 to 60 minutes. The dissolution rates of Al increases sharply in the first 5 minutes, and then increased slightly (Figure 3.1.1a). At 60 minutes of reaction time, the number of dissolved Al/initial Al is less than 6% and the highest concentration of dissolved Al compounds is around 26 mmol/L, which is much lower than the solubility of $Al_2O_4^{2-}$ (0.72 mol/L). It corresponds well with the reported phenomenon of geopolymerization process that 1) the dissolving and polymerizing reactions take place simultaneously; 2) a long time is required for the dissolution and diffusion of aluminate and silicate monomers from raw aluminosilicates. For a particular reaction time (e.g., 20 minutes), the dissolution rate of Al increases as increasing Si/Al ratio from 1:1 to 2:1, and then keeps a constant as increasing this ratio to 3:1. As the used alkali is a constant, this increase indicates that soluble silicates accelerate the polymerization of aluminate monomers, so as to the dissolution of Al from raw aluminosilicate (metakaolin), however the acceleration of polymerization or condensation reach a balance at Si/Al=2:1.

As noted in Figure 3.1.1 (b), the dissolution rate of Si is in consistent with that of Al at Si/Al ratios of 1:1, 1.5:1, and 2:1, suggesting the simultaneity of alkaline dissolution of Si and Al from metakaolin. However, for initial 5 minutes of Si/Al ratios of 1:1, and 1.5:1, the dissolution rates of Si are lower than those of Al. The initial stage of dissolving aluminosilicate minerals in alkaline solution displays preferential release of aluminum, because the Al-O bonds are weaker than Si-O bonds, and dissolved Al species adsorb on metakaolin reducing the dissolution of Si species. But this effect is weakened with increasing the reaction time because the polymerization of Si-O-Al monomers and oligomers consuming the dissolved Al compounds. For Si/Al ratio of 3:1, the dissolution rates of Si at a particular time are higher than those of Si/Al ratio of 2:1, which might be resulted from the interference of high concentration of soluble silicates (2 mol/L). The Al and Si dissolution at Si/Al ratios of 1:1, 1.5:1, 2:1 and 3:1 suggests that soluble silicate promotes Al dissolution, but reaches a balance with polymerization at Si/Al ratio of 2:1.

Figure 3.1.2 presents the FTIR spectra of N-A-S-H gels formed at various Si/Al ratios. The absorption peaks around 3440 cm^{-1} and 1651 cm^{-1} are OH^- stretching vibrations and H-OH bonds, corresponding to structure hydroxyl (OH^-) and adsorbed water in the gels, respectively. In metakaolin, these two peaks indicate the calcination of kaolinite is not complete, and a low content of free water is adsorbed during measurements. The peak around 1440 cm^{-1} is due to the asymmetric stretching mode of O-C-O bonds in CO_3^{2-} groups. It appears in N-A-S-H gels but not in metakaolin, indicating that carbonation takes place on N-A-S-H gels during syntheses. The peaks at 781 cm^{-1} and 475 cm^{-1} in metakaolin spectrum are attributed to amorphous Al-O stretching vibration and O-Si-O vibration in kaolinite. The intensity of these two peaks reduces in the spectra of N-A-S-H gels, indicating the reaction of metakaolin into N-A-S-H gels. The band around 1000 cm^{-1} is the overlaps of bonds of Si-O-Si (1123 cm^{-1}) in silicate derivatives, Si-O-Al (1078 cm^{-1}) in

residual metakaolin and Si-O-T (T is tetrahedral Si or Al) asymmetric stretching band (980 cm^{-1}) in N-A-S-H gels. The peak of Si-O-Al vibration in metakaolin at 1078 cm^{-1} shifts to a lower wavenumber of 980 cm^{-1} in N-A-S-H gels, because the Si-O-T linkages are of high non-bridging oxygen and Al substitutions. The intensity of Si-O-T peak of Si/Al ratios 1.5:1 and 2:1 is higher than that of 1:1 and 3:1, suggesting more geopolymeric linkages are formed. It is in good agreement with the dissolution results of Al (Figure 3.1.1a), and alumina dissolution is decisive in the formation of N-A-S-H gels when silicate is employed as alkaline activator.

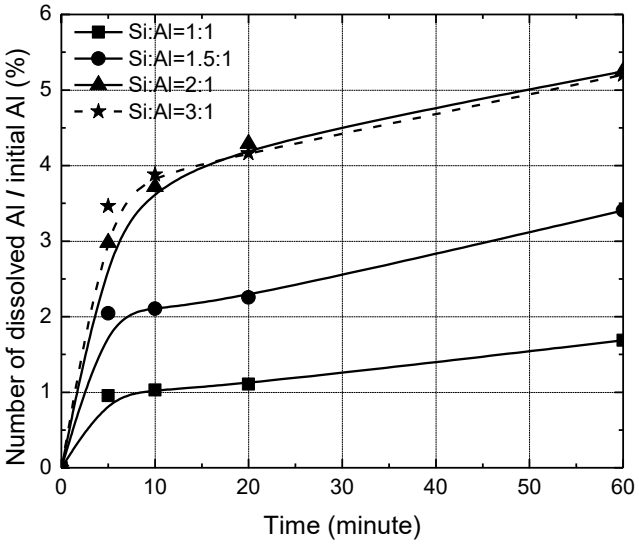

(a)

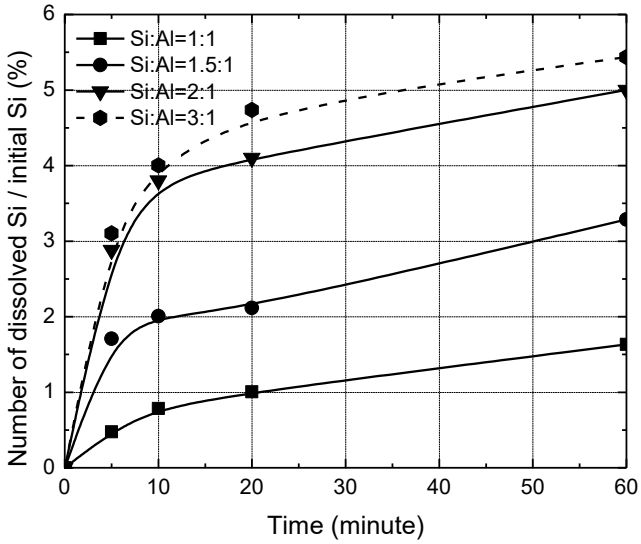

(b)

Figure 3.1.1. Dissolution rates of Al (a) and Si (b) compounds from metakaolin

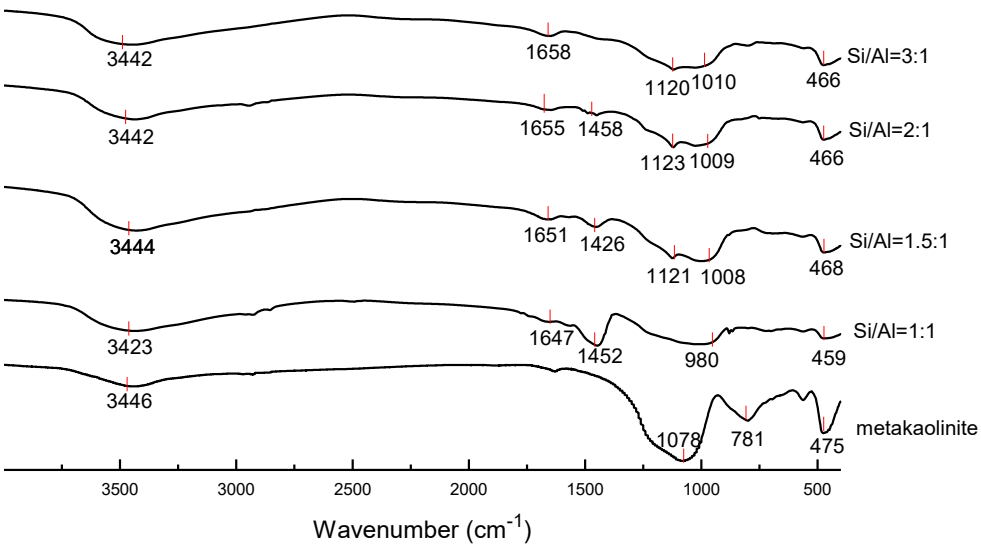

Figure 3.1.2. FTIR spectra of the N-A-S-H gels as a function of Si/Al ratios

3.1.2 Mechanical Property and microstructure of geopolymers

Figure 3.1.3 presents the compressive strength of geopolymers as a function of Si/Al ratios. The compressive strength increases sharply from 2.1 MPa to 31.2 MPa as changing the Si/Al ratios from 1:1 (no silicate) to 1.5:1 (0.5 mol/L silicate), indicating that soluble silicate promotes the formation of geopolymer at low concentrations. And the compressive strength increases to the maximum (36.8 MPa) with raising the Si/Al ratio to 2:1. However, with increasing the Si/Al ratios continually to 3:1, 4:1 and 5:1, the compressive strength decreases to 14.5, 11.2 and 5.5 MPa, respectively. It is in a good agreement with the study that excessive soluble silicate weakens geopolymers´ strength.

Figure 3.1.4 gives the ^{29}Si NMR spectra and their deconvolution of geopolymers synthesized at Si/Al ratios of 1:1, 1.5:1, 2:1 and 4:1, respectively, as well as the deconvoluted fractions of silicon tetrahedron sites present as $Q^4(4Al)$, $Q^4(3Al)$, $Q^4(2Al)$, $Q^4(1Al)$ and $Q^4(0Al)$. The dotted NMR spectrum of Si/Al ratio 1:1 (Figure 3.1.4a) possesses a sharp peak, indicating high contents of crystalline phase are formed, which are zeolite nuclei as evidenced in the XRD measurements (Figure 3.1.5). However, the NMR spectra of Si/Al ratios 1.5:1, 2:1 and 4:1 (Figure 3.1.4b, 3.1.4c and 3.1.4d) show broad band, suggesting the amorphous structure in these geopolymers. As increasing the Si/Al ratios, peak and/or band in NMR spectra shift to right side (lower frequency), indicating less aluminum tetrahedrons are coordinated to silicon tetrahedrons. In the deconvoluted fractions, $Q^4(4Al)$ is the main compound in geopolymer of Si/Al ratio 1:1, in which a trace amount of $Q^4(3Al)$ and $Q^4(2Al)$ compounds are present. Interestingly, $Q^2(1Al)$ is found due to the high concentration of aluminate monomers. As increasing the Si/Al ratios from 1.5:1 to 2:1 and 4:1, the fractions of $Q^4(4Al)$ and $Q^4(3Al)$ decrease, while the fractions of $Q^4(1Al)$ and $Q^4(0Al)$ increase, but the fraction of $Q^4(2Al)$ shows the maximum at Si/Al ratio of 2:1.

Together with mechanical properties of geopolymers at various Si/Al ratios, geopolymers with high compressive strength possess high fractions (> 80%) of Q^4(3Al), Q^4(2Al) and Q^4(1Al), which might be N-A-S-H gels, and low fractions of Q^4(4Al) and Q^4(0Al), which might be zeolite nuclei and silicate derivatives, respectively.

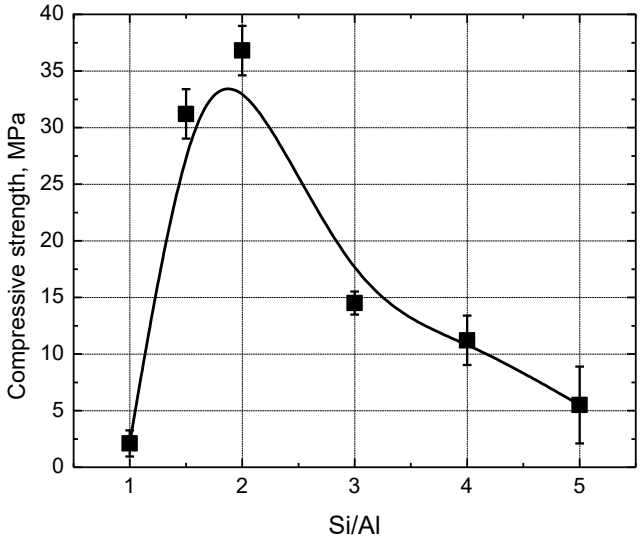

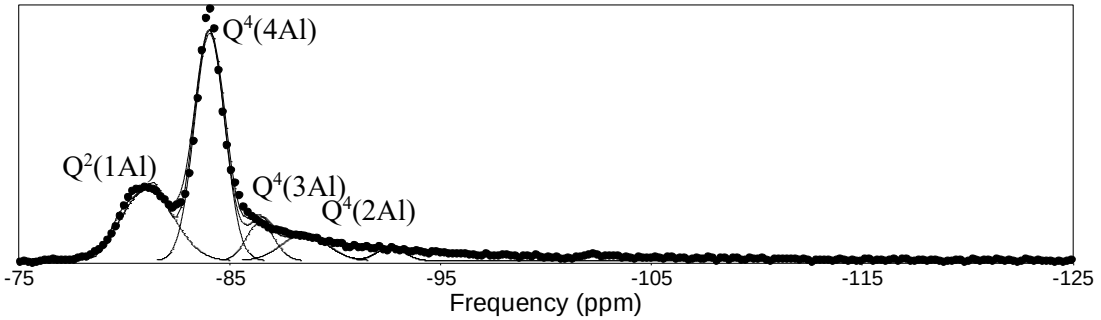

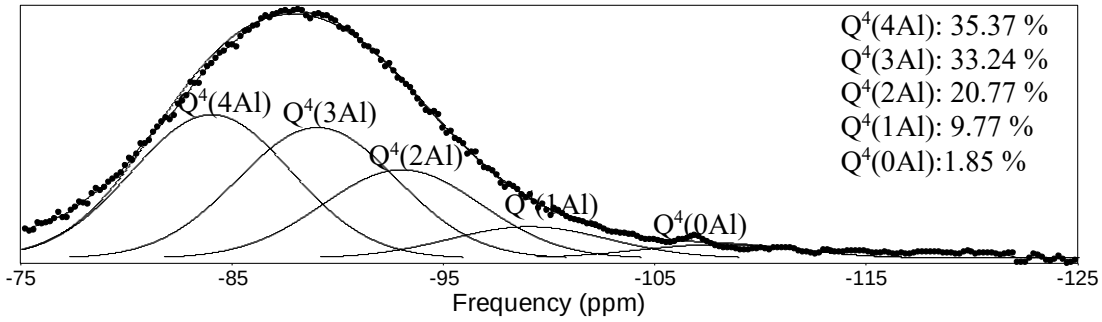

(b)

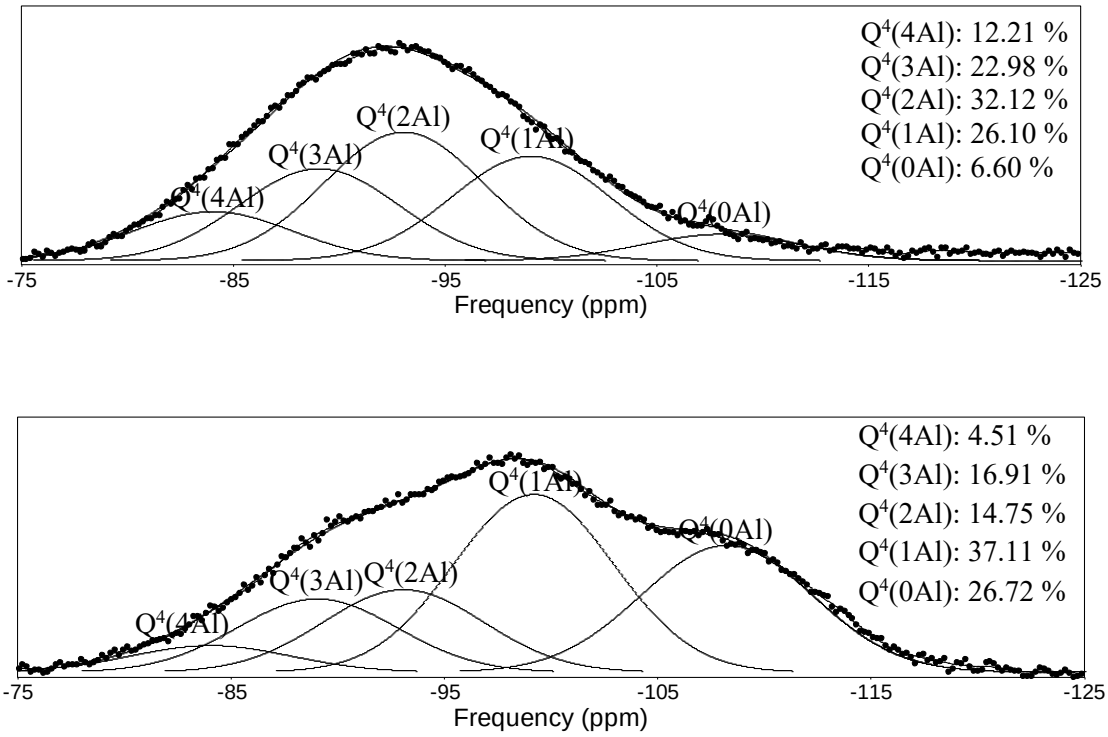

(d)

Figure 3.1.4. ^{29}Si NMR spectra (dotted line) and their deconvolutions (solid line) of geopolymers synthesized at Si/Al ratios of 1:1 (a), 1.5:1 (b), 2:1 (c) and 4:1 (d)

The XRD patterns of metakaolin and geopolymers synthesized at various Si/Al ratios (Figure 3.1.5a) evidence the evolution of aluminosilicates obtained in NMR measurements. The metakaolin shows semi-crystalline to amorphous pattern with some kaolinite peaks, implying the calcination of kaolinite was not complete. The geopolymers synthesized at Si/Al ratios from 1.5:1 to 4:1 shows featureless amorphous XRD patterns with one hump centered at approximately 27-29° 2θ, which is in a good agreement with the reported XRD patterns of geopolymers. However, the geopolymer synthesized at Si/Al ratio of 1:1 presents characteristic peaks of zeolite A, indicating a high content of crystalline zeolitic nuclei was formed in it.

Figure 3.1.5b shows the XRD patterns of geopolymers synthesized at Si/Al ratios of 1:1 and 2:1 after curing at room temperature for 12 months. The geopolymers give analogous XRD patterns after 12 months, namely zeolite A is identified in geopolymer of Si/Al ratio of 1:1 and quartz still exists in the 2:1 Si/Al ratio geopolymer. However, the intensities of XRD peaks become lower, which might be due to the geopolymerization reaction. Together with the NMR spectra, it can be summarized for the evolution of aluminosilicates in synthesizing geopolymers at various Si/Al ratios as following. 1) At Si/Al ratio of 1:1, relatively high concentration of aluminate monomers are dissolved by alkali, thus zeolitic nuclei of high aluminum (Q^4(4Al), Q^2(1Al)) are formed, but porous zeolite products are not formed because of the low reaction temperature and high solid concentration. 2) At Si/Al ratio around 2:1, the concentrations of aluminate and silicate monomers are proper to develop N-A-S-H gels in the microstructural forms of Q^4(3Al) and Q^4(2Al). 3) At high

Si/Al ratios (e.g., 4:1), dissolved aluminate monomers are insufficient thus species of low aluminum (Q^4(1Al)) and nesosilicates or silicic acid (Q^4(0Al)) are mainly formed.

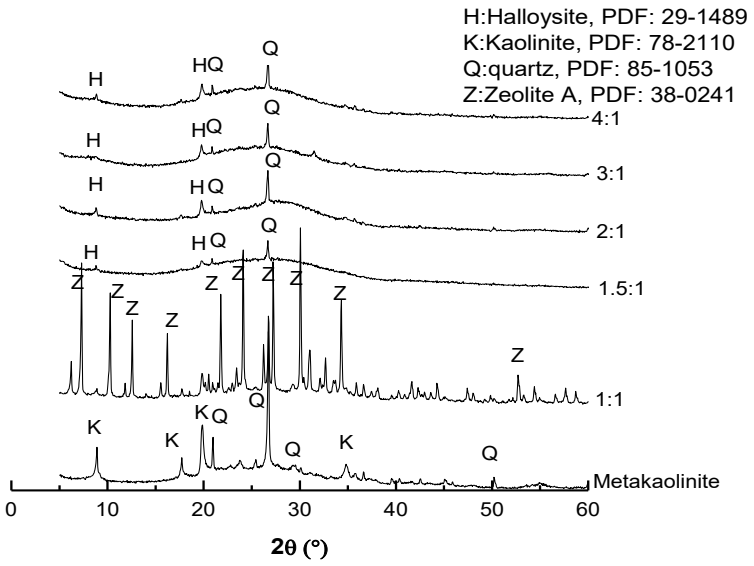

(a)

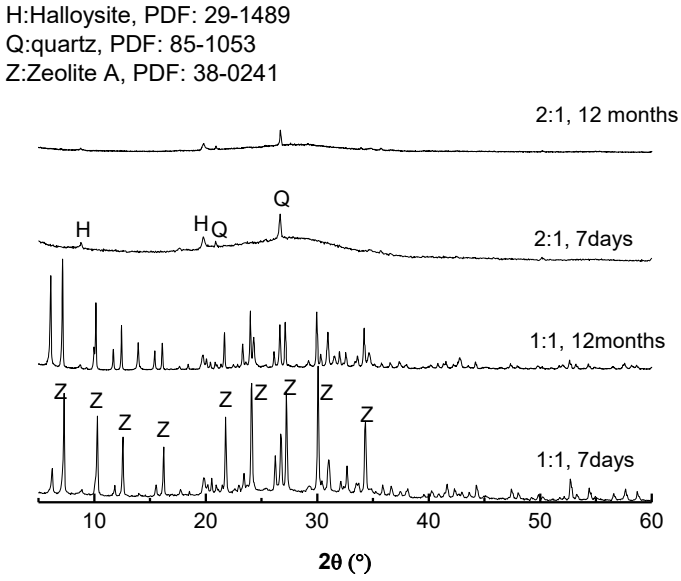

(b)

Figure 3.1.5. XRD patterns of geopolymers synthesized at various Si/Al ratios (a) and after 12 months curing

Figure 3.1.6 gives the SEM images of geopolymers synthesized at various Si/Al ratios. At Si/Al ratio of 1:1, a little geopolymer binder and a number of zeolitic nuclei are observed. And most of these nuclei are not dispersed in the geopolymer binders, thus macrospores are formed. It is in a good agreement with the NMR result and XRD pattern that geopolymers synthesized at Si/Al ratio of 1:1 possess high contents of crystalline phase. At Si/Al ratio of 2:1, a homogeneous geopolymer binder is formed. At Si/Al ratio of 3:1, derivatives of soluble silicate (e.g., nesosilicates and silicic acid) are observed on the geopolymer binder. At Si/Al ratio of 4:1, the geopolymer binder is not found, and plenty of micropores or mesopores are formed. Together with the compressive strengths at various Si/Al ratios (Figure 3.1.3), it can be noted that the formation of geopolymer binder is the main effect in controlling geopolymers´ strength.

3.1.3 Simulation

Table 3.1.1 gives the binding energy relative to one Si atom and the total energy of kaolinite-based geopolymers at various Si/Al ratios, based on the optimized structures of oligomers and molecular dynamic orientation of geopolymers. The geopolymers of Si/Al ratios 2:1 and 3:1 have higher binding energies to one Si atom compared to geopolymers at Si/Al ratios of 1:1, 4:1 and 5:1, verifying geopolymers with high compressive strength could be formed at Si/Al ratios of 2:1 and 3:1. However, the total energy of geopolymers decreases with increasing the Si/Al ratios from 1:1 to 5:1, suggesting that geopolymers at Si/Al ratio of 1:1 have the most stable molecular orientation. Obviously, this energy is not in agreement with the mechanical properties of geopolymers.

Table 3.1.1 Binding energy relative to one Si atom and total energy of geopolymers

Si/Al ratio	Binding energy relative to one Si atom	Total energy of geopolymers
1:1	0.66 Ha	-23701.47Kcal/mol
2:1	0.79 Ha	-21456.38 Kcal/mol
3:1	0.79 Ha	-20686.83Kcal/mol
4:1	0.77 Ha	-20786.16Kcal/mol
5:1	0.76 Ha	-19935.66 Kcal/mol

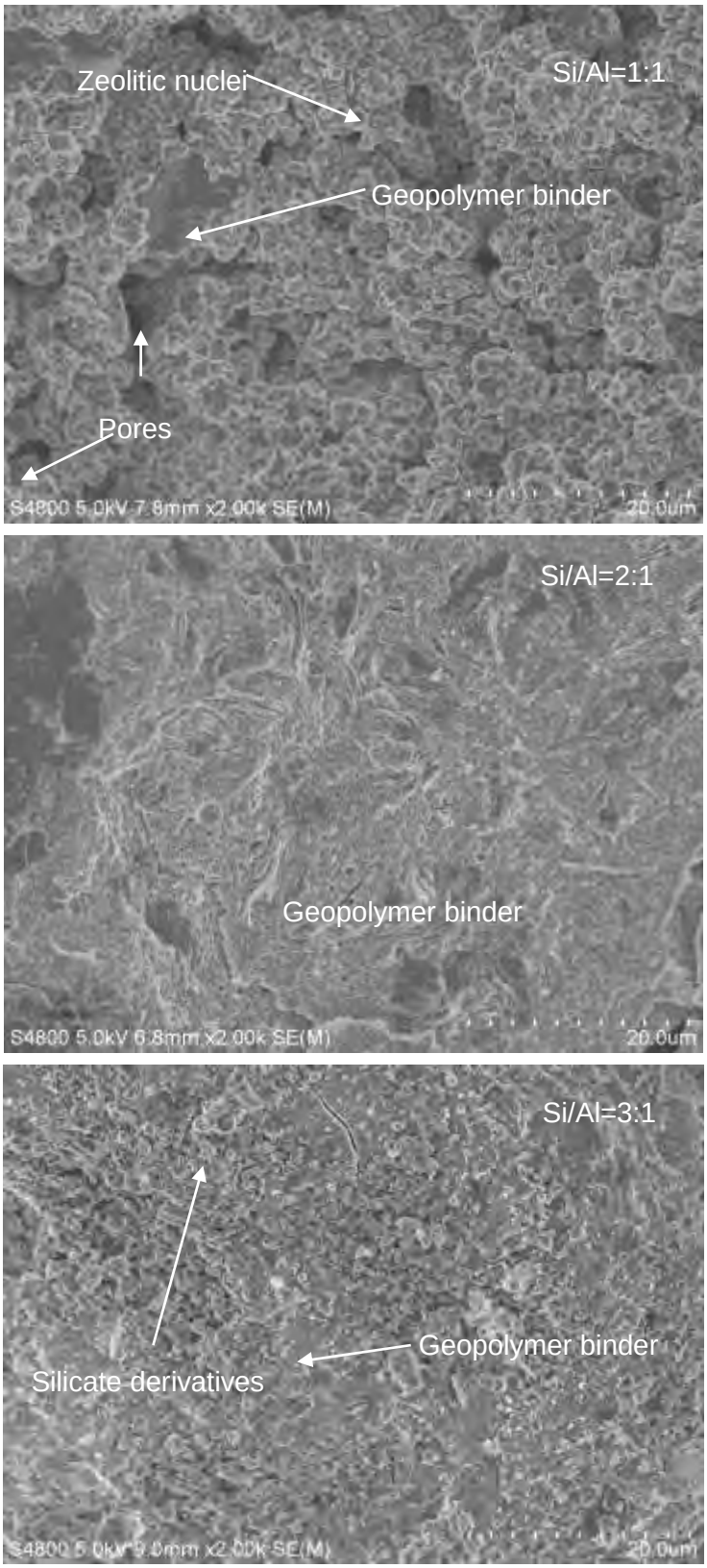
Zeolitic nuclei
Si/Al=1:1
Geopolymer binder
Pores
S4800 5.0kV 7.8mm x2.00k SE(M)
20.0um
Si/Al=2:1
Geopolymer binder
S4800 5.0kV 6.8mm x2.00k SE(M)
20.0um
Si/Al=3:1
Geopolymer binder
Silicate derivatives
S4800 5.0kV 9.8mm x2.00k SE(M)
20.0um

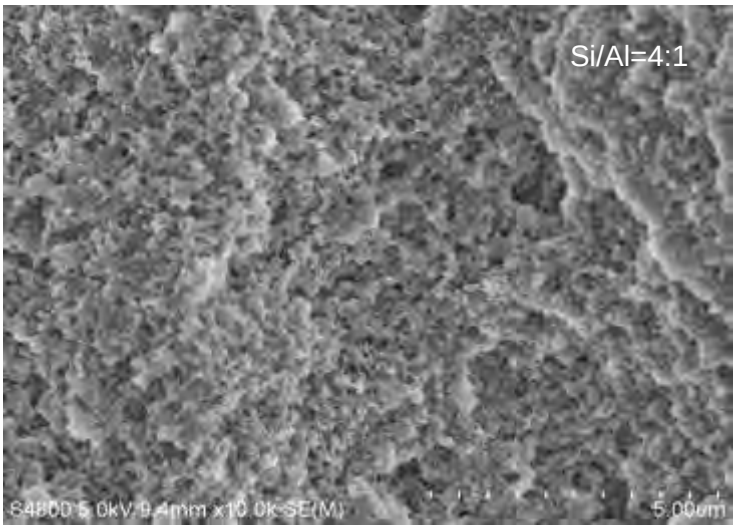

Figure 3.1.6. SEM images of geopolymers synthesized at various Si/Al ratios

3.2. Combination formation in the reinforcement of metakaolin geopolymers with quartz sand

3.2.1 Reinforcement of metakaolin geopolymer by quartz fillers

Figure 3.2.1 shows the SEM images of metakaolin geopolymers synthesized with additives of only quartz sand of 10 mol/L (No. 12), quartz sand and silica fume of both 5 mol/L (No. 6), rutile sand and silica fume of both 5 mol/L (No. 15), and only silica fume of 10 mol/L and 5 mol/L (No. 13 and 14), as well as the compressive strength data. As increasing the dosage of silica fume additive (No. 12, No. 6, No. 13), more silicate is generated, the morphology of geopolymers shows an increasing degree of homogeneity. The geopolymer synthesized without silica fume shows a porous structure and a much lower compressive strength than others. It corresponds well with the report that silicate promotes the formation of silicate oligomers and geopolymeric gel, which results in homogenous structures and increases mechanical properties of geopolymer products to some extent. However, the compressive strength of geopolymer synthesized with additives of both quartz sand and silica fume (No. 6) is much higher than the geopolymers (No. 13) synthesized without quartz sand, even though more homogenous structure is produce in geopolymer No. 13. It indicates the quartz sand reinforces mechanical strength of geopolymer, which functions as inert filler material.

Some studies state that excessive soluble silicate forms "Si-" bridge bonds and hinders water evaporation in the syntheses of geopolymers, which develops amorphous structure and lowers the compressive strength of fly ash and slag geopolymers. Therefore, geopolymer with only 5 mol/L silica fume additive (No. 14) has been synthesized for a comparison. Compared with the geopolymer No. 6, the geopolymer synthesized with equal soluble silicate shows similar homogeneous structure but a decreased compressive strength by 21 MPa. This result excludes the possibility that excessive silicate leads the reduction of compressive strength from geopolymers No. 6 to No. 13. In addition, compared with

another filler material, namely rutile sand (No. 15), the geopolymer (No. 6) synthesized with quartz sand as filler material shows a resembling homogeneous structure, but a higher compressive strength by 10.7 MPa.

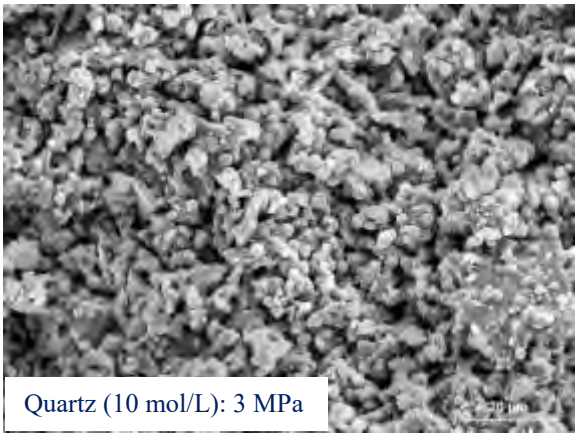

No. 12

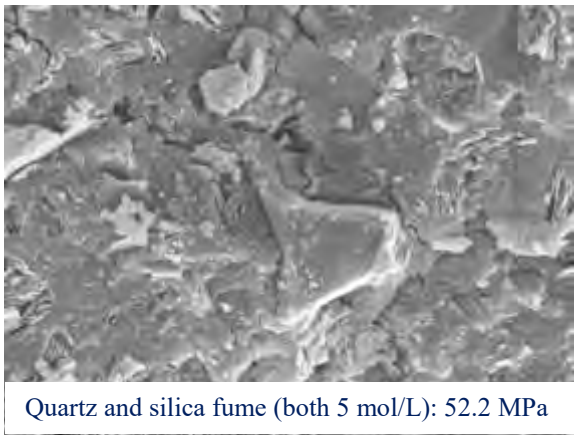

No. 6

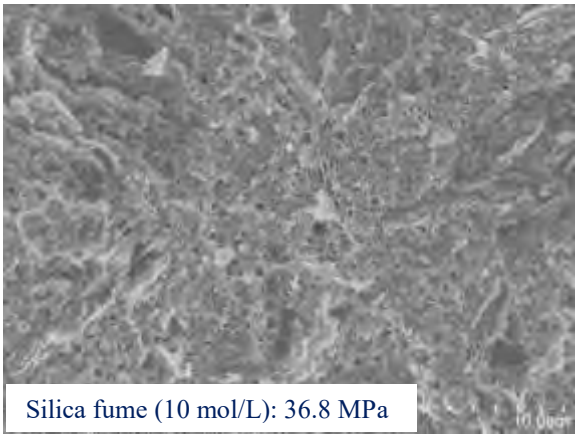

No. 13

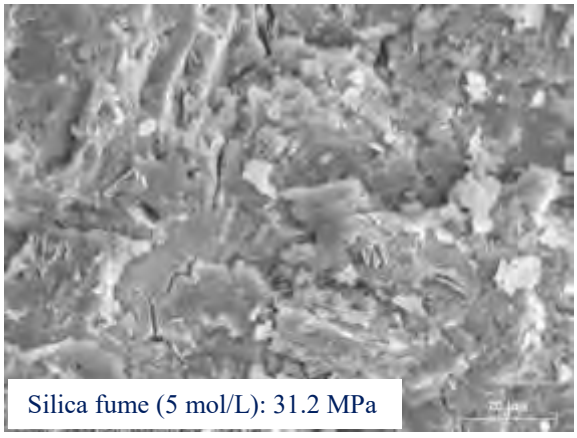

No. 14

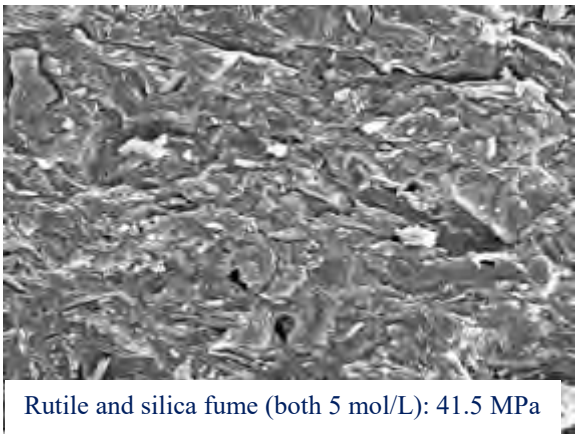

No. 15

Figure 3.2.1. SEM images and compressive strength data of metakaolin geopolymers synthesized with various additive regimes

3.2.2 Combination associates quartz fillers in geopolymer gel

It has been reported that quartz sand as filler materials interacts with Portland cement, decreases the large pores in concrete, and strengths concrete paste. However, a few studies investigated on the microstructural aspect of the interaction between quartz sand and geopolymeric gel. Thus FTIR measurements and SEM image analysis are employed to study the combination formation of quartz fillers in geopolymer gel. Figure 3.2.2 shows the FTIR spectra of geopolymers synthesized with quartz and silica fume (No. 6), only silica fume (No.14) and rutile plus silica fume (No. 15). The absorption peaks at 3440 cm^{-1}, 1651 cm^{-1} and 1440 cm^{-1} are OH^- stretching vibrations, H-OH bonds of free water and asymmetric stretching of O-C-O bonds in CO_3^{2-} groups, corresponding to adsorbed H_2O and carbonation during the curing of geopolymers. They are identical peaks in both spectra of geopolymers with quartz and silica fume (No. 6) and with only silica fume (No. 14). However, the peak at 695 cm^{-1} that represents the bond of quartz only appears in geopolymer with quartz and silica fume, indicating the insolubility of quartz particles during geopolymerization. The peaks at 557 cm^{-1} and 475 cm^{-1} correspond to zeolite framework in the geopolymer structure, which are of higher transmittance in geopolymer with only silica fume (No. 14). It suggests that more zeolite frameworks are formed during the reactions in geopolymer No. 14. The band at 980 cm^{-1} represents the Si-O-T bonds (T is tetrahedral Si or Al) in geopolymeric gel, which shifted left in the spectrum of geopolymer with quartz and silica fume compared with the spectrum of geopolymer with only with silica fume, indicating more Si-O-Si bonds have formed by adding quartz sand in geopolymerization. It suggests that quartz sand might be partly dissolved to form "Si-" combinations with geopolymeric gel that incorporates the quartz particles. In addition, the spectrum of geopolymer synthesized with rutile sand and silica fume (No. 15) shows similar peaks as the geopolymer with quartz sand and silica fume (No. 6), because rutile sand and quartz sand are of similar characteristic peaks in FTIR spectra. While, its broad band at 980 cm^{-1} might be a result of the overlying of Ti-O bonds and Si-O-T vibrations.

The energy dispersive X-ray (EDX) mapping of Si, O, and Al was carried out in geopolymer (No. 5) synthesized with silica fume and quartz sand of 32~12 μm. As shown in Figure 3.2.3 around quartz particle, the relative Si/Al ratios of points I, II, III, IV, and V are 12:1, 5:1, 5:1, 2:1 and 1.5:1, respectively. At point I, the Si content is much higher than Al, indicating the insolubility of quartz particle in geopolymerization reactions. At points II and III of the combination connecting quartz particles and geopolymeric gel, the Si/Al ratios decrease equally from point I. And the Si/Al ratio decreases with increasing the distance from quartz particle to pints IV and V. At point V, the Si/Al ratio is 1.5:1, which is equal to the Si/Al ratio of raw materials (metakaolin, silica fume and quartz) if assuming no dissolution of quartz particles. This result indicates the formation of a transitional combination in several micrometers that emerges the quartz particles into geopolymeric gel. In studying interactions between quartz sand and sodium silicate, it is reported that both reactions of quartz dissolution and precipitation of saturated silicate species such as $SiO(OH)_3^-$ and $SiO_2(OH)_2^{2-}$ take place in the formation of combination on quartz sand particle surface. So this combination is mainly composed of polysiloxo (-Si-O-). It corresponds well with the hypothesis of the formation of specific zirconia-associated, three-dimensional polysialate species in the incorporation of zirconia into fly ash geopolymers However, it is interesting to note that the metakaolin geopolymer synthesized with rutile

sand as filler possesses a lower compressive strength than that with quartz sand as filler (Figure 3.2.1). It might be resulted from the fact that the dissolution, precipitation and formation of titanium-polysiloxo combination in rutile metakaolin geopolymer are distinguished from those in quartz metakaolin geopolymer.

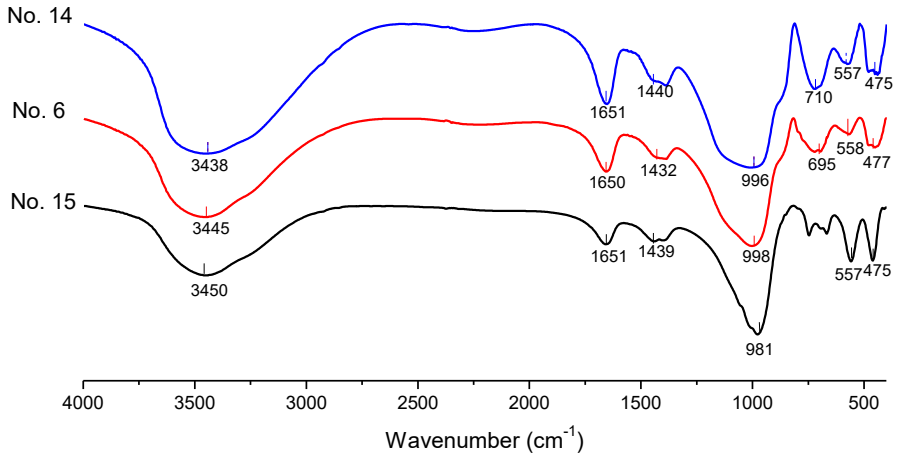

Figure 3.2.2. FTIR spectra of geopolymers synthesized with quartz and silica fume (No. 6), only silica fume (No.14) and rutile plus silica fume (No. 15)

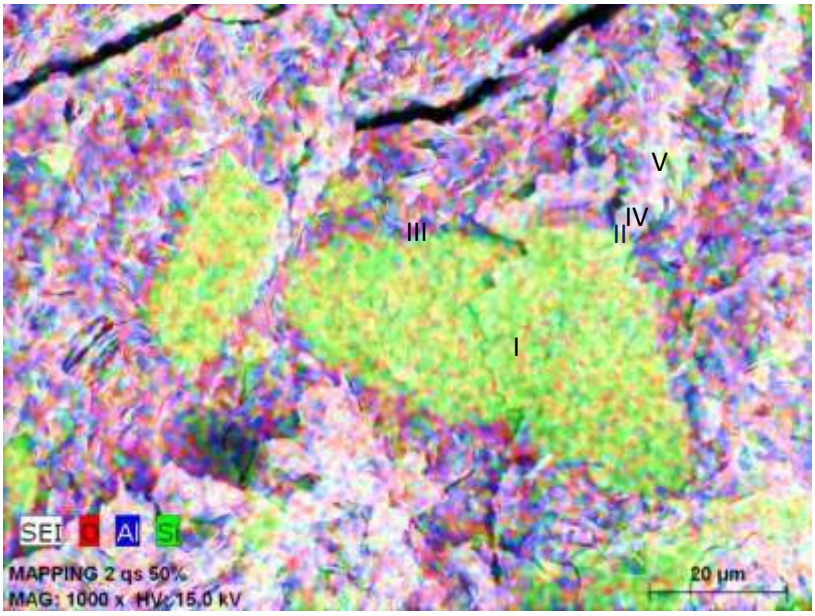

Figure 3.2.3 Energy dispersive X-ray (EDX) mapping of Si, O, and Al in geopolymer (No. 5) synthesized with quartz sand and silica fume

3.2.3 Size of quartz sand in combination formation

Figure 3.2.4 presents the compressive strength data of geopolymers synthesized with silica fume and quartz sand of various size ranges (No. 1-6), with only quartz sand of various size ranges (No. 7-12), and without quartz sand. The geopolymers synthesized with quartz sand and silica fume show high compressive strengths (Figure 3.2.4a). The maximum strength is obtained at the size range of 75~32 μm. A slight reduction in compressive strength is observed as decreasing the particle size to 32~12 μm and 12~6 μm, suggesting the reduction of reinforcement on metakaolin geopolymers by filler material of extremely fine size. And a decrease of strength by 10 MPa is observed as increasing the particle size from 75~32 μm to 180~105 μm, further by 31 MPa as increasing the particle size to 240~180 μm. It suggests that quartz particles of big size are difficult to be combined into geopolymeric gel. The geopolymers (No. 7-12) synthesized without silica fume lost the homogeneous geopolymeric gel structure (Figure 3.2.1), resulting in porous products of strength lower than 5 MPa (Figure 3.2.4b). As summarized and compared in Figure 3.2.4c, the geopolymer synthesized with silica fume and quartz sand of optimal size range possesses a much higher compressive strength (>10 MPa) than those without quartz sand or with rutile sand.

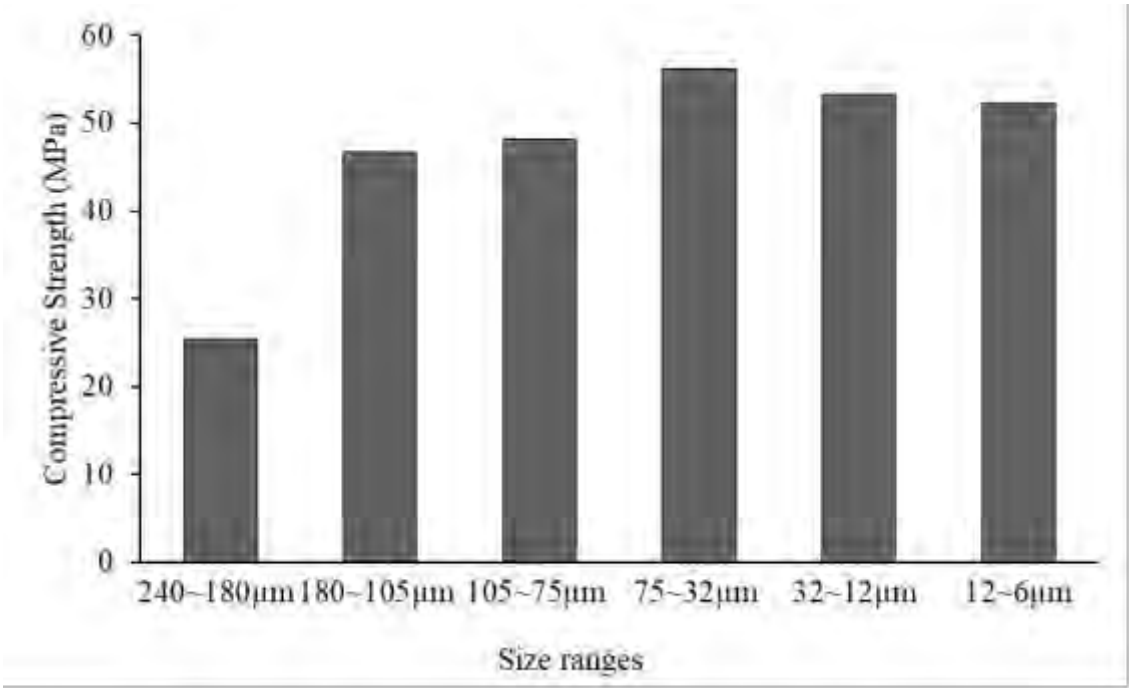

(a)

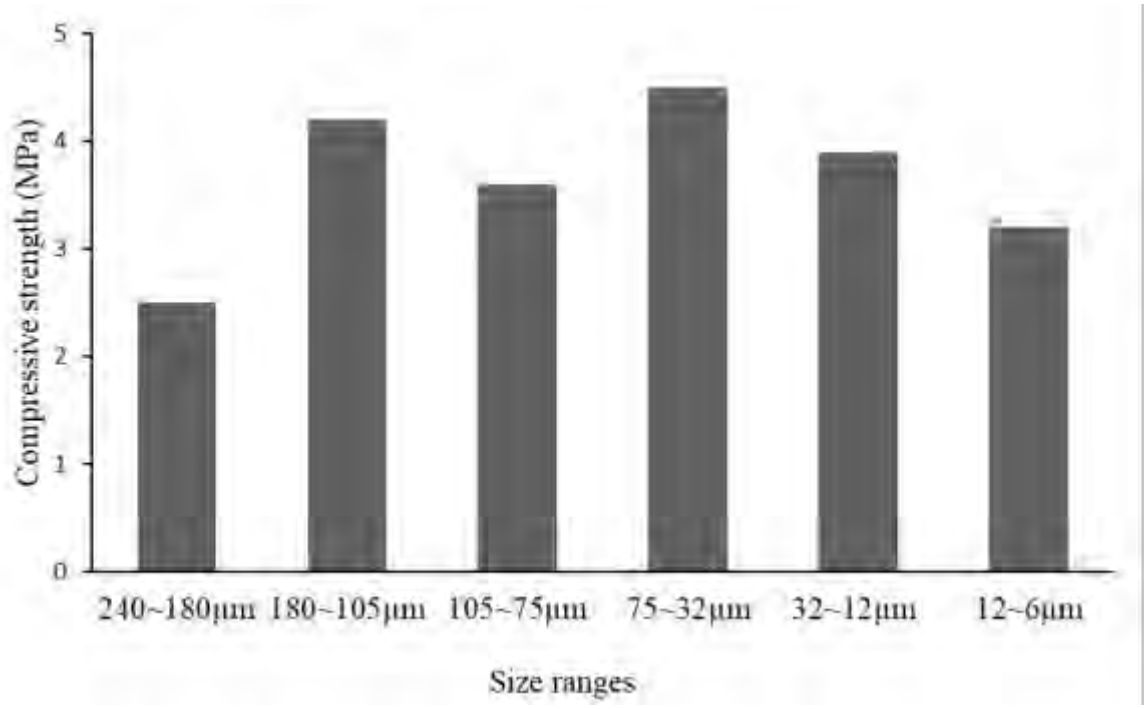

(b)

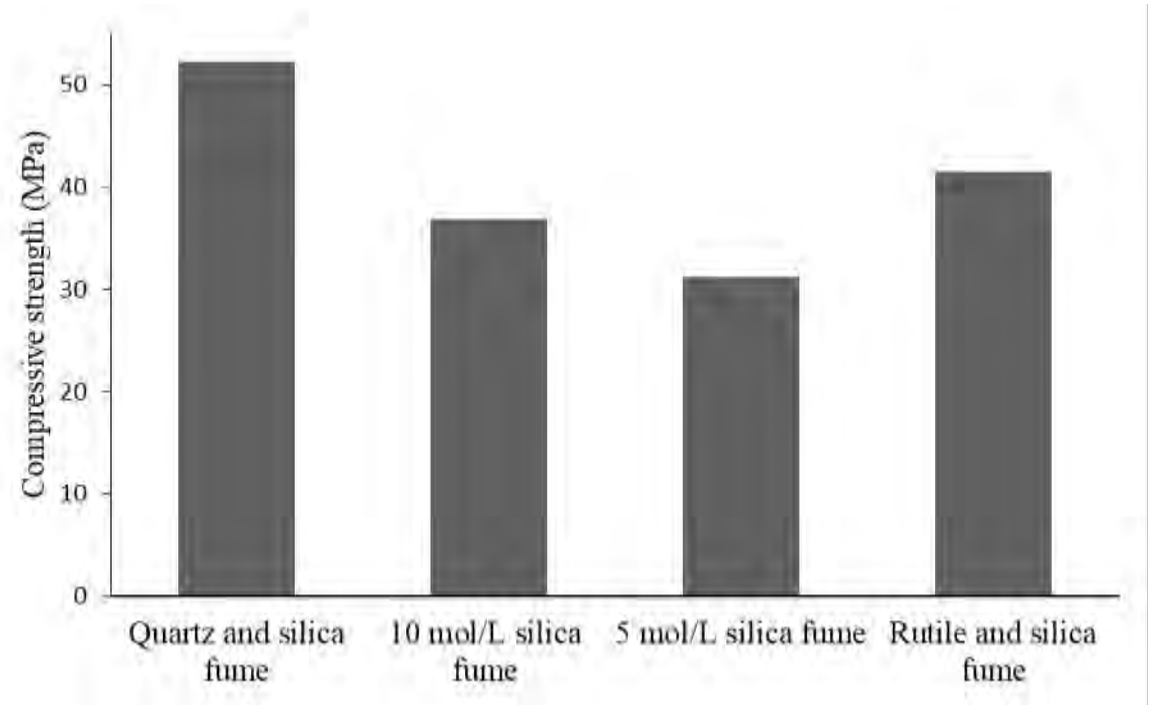

(c)

Figure 3.2.4. Compressive strength data of geopolymers synthesized with silica fume and quartz sand (a), with only quartz sand (b) and without quartz sand (c)

The combination should be positively correlated with the surface area of quartz particles, because they are formed by dissolution and precipitation of hydrolyzed silica species only on the surface of particles. The smaller is the particle size, the more combination forms. Figure 3.2.5 shows the XRD patterns of geopolymers (No. 2, 3 and 4) synthesized with silica fume and quartz sand of size ranges 180~105 μm, 105~75 μm, and 75~32 μm, respectively, and of geopolymer (No. 14) with only silica fume. The four spectra show the amorphous structure of geopolymers with trace peak of quartz, which is more noticeable in the spectra of geopolymers with quartz sand. It confirms the insolubility of quartz sand in geopolymerization reactions. It is interesting to note that the peak intensity of amorphous Si-O-Si chains in geopolymeric gel at 2θ of 13° increases as decreasing the quartz particle size, indicating the formation of more Si-O-Si chains in the combination as decreasing particle size.

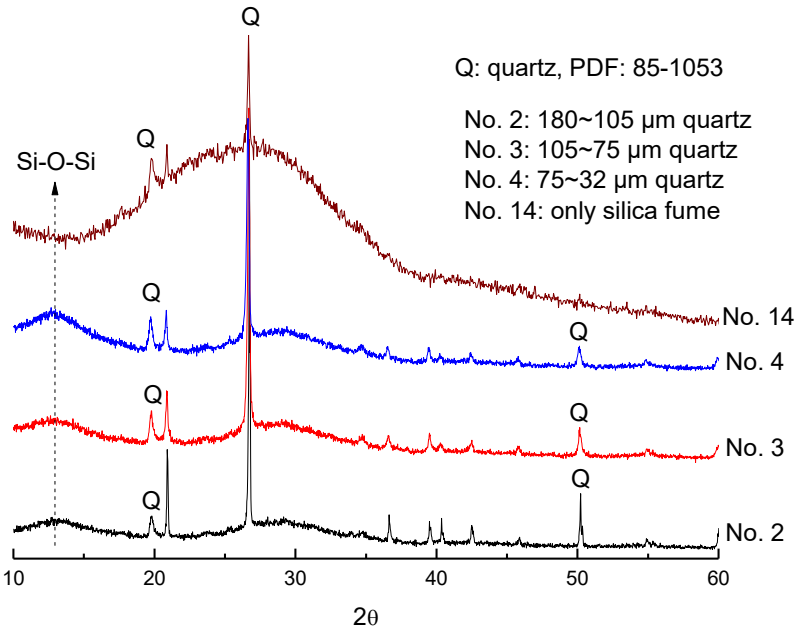

Figure 3.2.5. XRD spectra of geopolymers No. 2, 3, 4 and 14

The short-range ordering and molecular structure of geopolymers have been investigated with great success using NMR spectroscopy. The lack of spectral resolution for silicon in geopolymers has been overcome by adopting Gaussian peak deconvolution to separate and quantify $Q^n(mAl)$ species ($0 \le m \le n \le 4$). It is reported from other NMR studies that all silicon and aluminum sites are in tetrahedral coordination in geopolymers, thus $n=4$. And the resonance of a $Q^4(mAl)$ center with the replacement of each aluminum by silicon is an approximate -5 ppm shift, with $Q^4(4Al)$, $Q^4(3Al)$, $Q^4(2Al)$, $Q^4(1Al)$, $Q^4(0Al)$ resonating at approximately -84, -89, -93, -99 and -107 pmm, respectively. Figure 3.2.6 shows the ^{29}Si NMR spectra and their deconvolution of geopolymers (No. 2, 3, and 4) synthesized with silica fume and quartz sand of various size ranges 180~105 μm, 105~75 μm, and 75~32 μm, respectively, and of geopolymer (No. 14) with only silica fume. The spectra of geopolymers synthesized with silica fume and quartz show typical broad resonance

centered at -85 to -93 ppm, which is in accordance with previous studies. The peak at -107 ppm in the spectra of geopolymers (No. 2, 3, and 4) with quartz sand represents the residual quartz particles, of which the intensity increases as increasing the particles size. It verifies the dissolution and formation of combination is positively correlated with the surface area of quartz particles. The lager is the particle size, the smaller is the specific surface area, the more residual quartz remains. The spectrum of the geopolymer (No. 14) synthesized with only silica fume is different from those with quartz sand and silica fume, which shows very low intensity at the peak of quartz and two sharp peaks at -84 and -90 ppm. It suggests the main micro-structures in geopolymer No. 14 is zeolite framework, showing good agreement with the FTIR results (Figure 3.2.2).

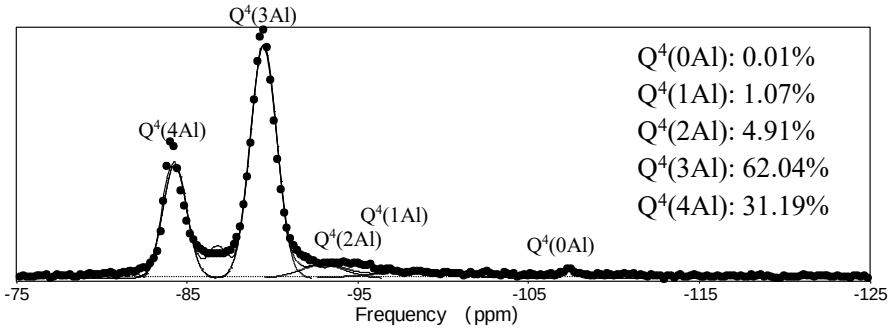

No. 14

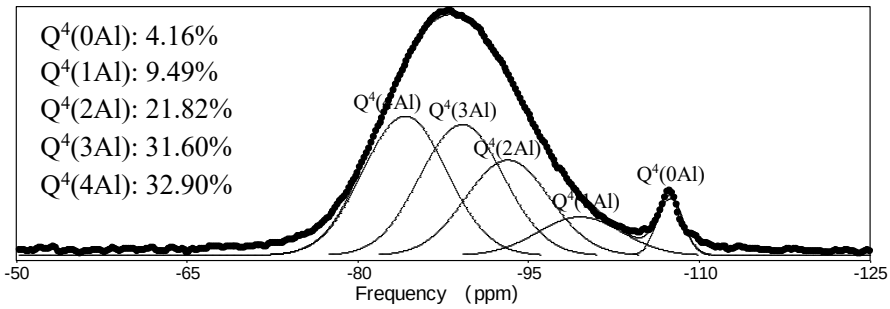

No. 4

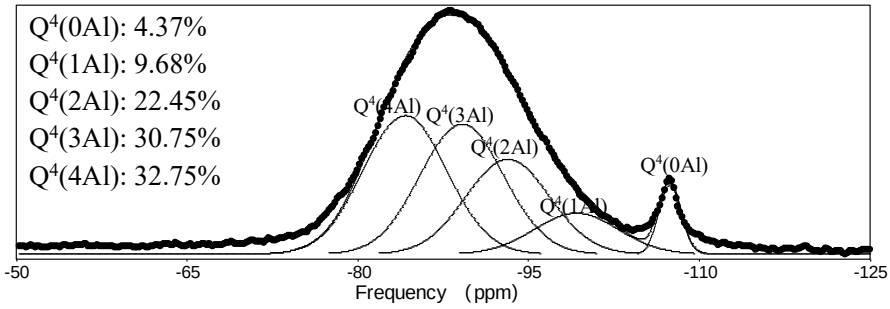

No. 3

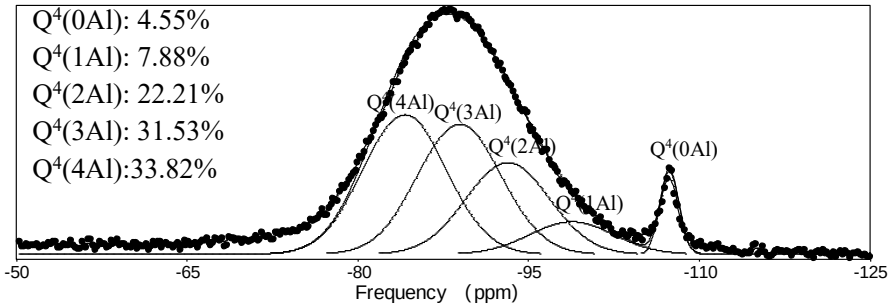

No. 2

Figure 3.2.6. ^{29}Si NMR spectra (left side) and their deconvolution (right size) of geopolymers synthesized with silica fume and quartz sand of various size ranges, and of geopolymer with only silica fume

Deconvolution of ^{29}Si NMR spectra gives the fractions of silicon tetrahedron sites present as $Q^4(4Al)$, $Q^4(3Al)$, $Q^4(2Al)$, $Q^4(1Al)$ and $Q^4(0Al)$. In the geopolymer (No. 14) with only silica fume, $Q^4(0Al)$ is not observed, which obeys Loewenstein´s Rule in geopolymeric gel that every aluminum ion forms $Al(OSi)_4$. The fraction $Q^4(4Al)$ is equal of 30% in the four geopolymers, indicating the $Q^4(4Al)$ sites are resulted from geopolymeric gel and not affected by the formation of combinations on quartz particles. Interestingly, the fraction $Q^4(3Al)$ is higher in geopolymer (No. 14) with only silica fume than in geopolymers (No. 2, 3 and 4) with quartz sand and silica fume, but the fractions $Q^4(2Al)$ and $Q^4(1Al)$ behave the opposite. It suggests the lack of paring aluminum tetrahedrons or the excess of silicon tetrahedrons in geopolymers with quartz sand. In comparison with geopolymer No. 14, the addition of quartz sand is the only difference in synthesizing parameters of geopolymer No. 2, 3 and 4. Therefore, incorporation of quartz sand into metakaolin geopolymers affects the ratio of silicon to aluminum tetrahedrons by either production of silicate species or competition of alkalis with metakaolin in the dissolution of quartz particles. As the particle size of quartz sand decreases in geopolymers 2, 3 and 4, more surface of quartz is involved in the dissolution, thus a higher ratio of silicon to aluminum tetrahedrons is produced and higher fractions of $Q^4(2Al)$ and $Q^4(1Al)$ are observed in the deconvolution of NMR spectra.

Figure 3.2.7 presents the SEM images of metakaolin geopolymers with silica fume and quartz sand of size ranges in 180~105 μm (No. 2), 105~75 μm (No. 3), and 75~32 μm (No. 4). Cracks are easily observed in the geopolymer with quartz sand of 180~105 μm. While both crack and combination are observed as decreasing the size range of quartz sand to 105~75 μm. However, combination is mainly observed around quartz particles in the size range of 75~32 μm. It is in a good agreement with the previous results that more combination is formed around quartz particles of smaller size range, because they are of higher surface area.

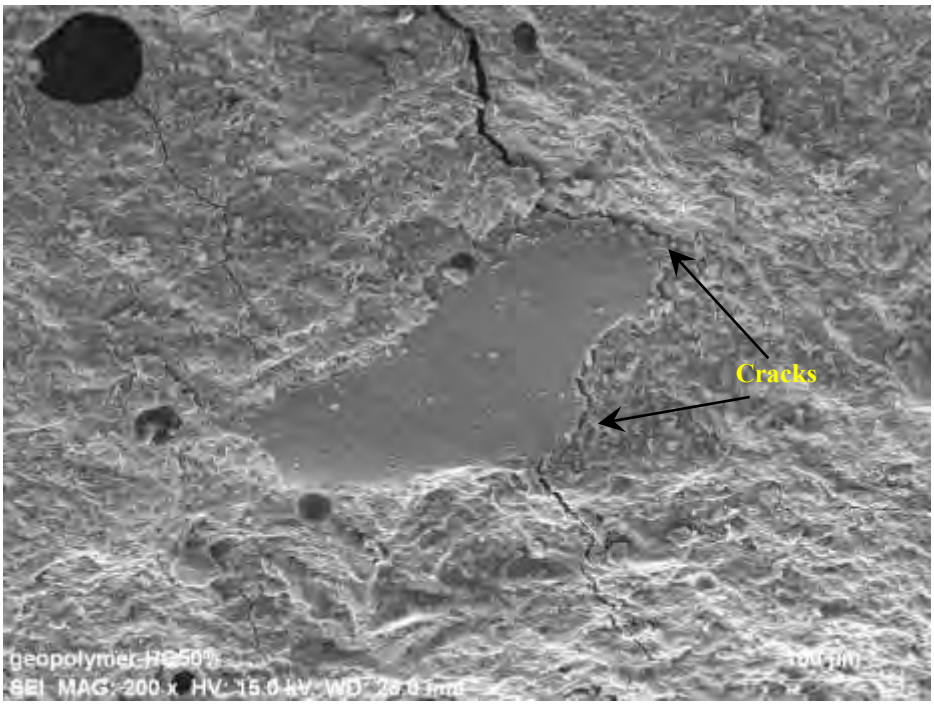
Cracks
geopolymer-HG50%
SEI MAG: 200 x HV: 15.0 kV WD: 25.0 mm

No. 2

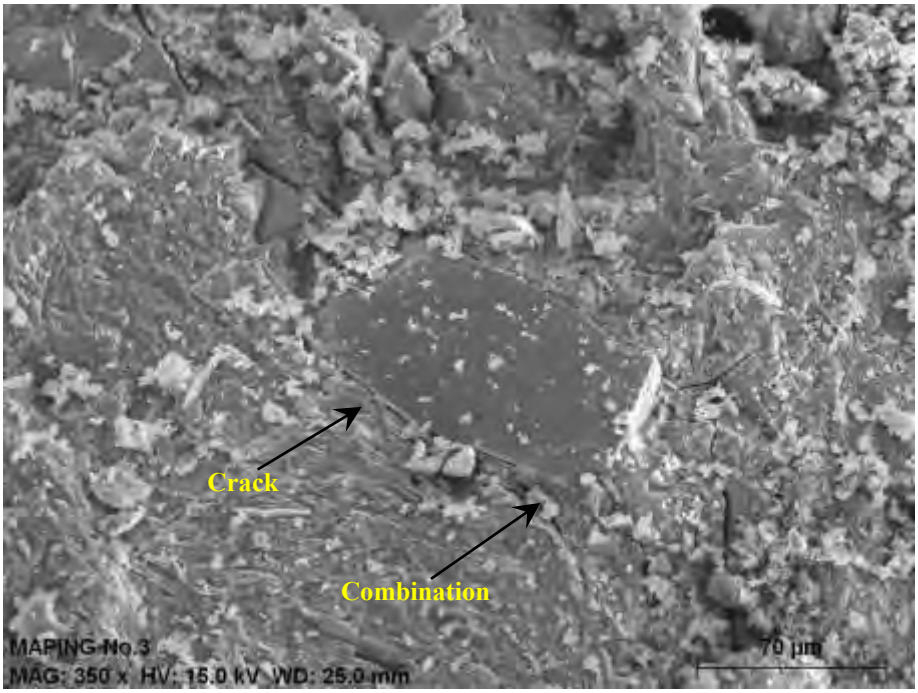
Crack
Combination
MAPING-No.3
MAG: 350 x HV: 15.0 kV WD: 25.0 mm
70 µm

No. 3

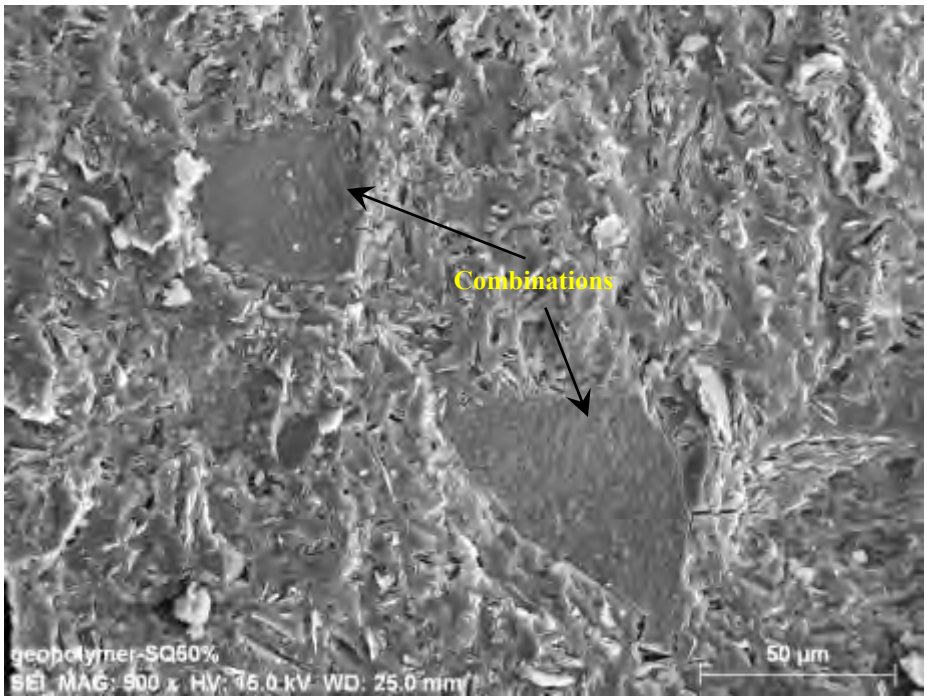

No. 4

Figure 3.2.7. SEM images of metakaolin geopolymers with silica fume and quartz sand of various size ranges

3.3. Reexamining calcination of kaolinite for the synthesis of metakaolin geopolymers - roles of dehydroxylation and recrystallization

3.3.1 Results

Figure 3.3.1 gives the ^{27}Al NMR spectra and their deconvolution of kaolin heated at various temperatures, as well as the fractions of aluminum coordination, namely Al^{VI}, Al^{V} and Al^{IV}, are summarized in Figure 3.3.2. The NMR spectrum of kaolin possesses only a sharp peak, indicating high contents of crystalline phase (octahedral Al sheet). The NMR spectra of metakaolin heated at various temperatures show broad band and several peaks, suggesting the formation of amorphous phase and the transformation of aluminum coordination. According to reported Al coordination in phyllosilicates by NMR spectroscopy, the frequencies around 0, 25, and 55 ppm correspond to Al^{VI}, Al^{V} and Al^{IV}, respectively. In metakaolin heated at different temperatures, these frequencies might change trivially because of the different status of tetrahedral Si linked to Al. For instance, Al^{VI} is characterized at 0.2 ppm and 2.3 ppm in kaolin and metakaolin heated at 800 °C, indicating AlO_6 links to tetrahedral $Si(Q^3)$ or $Si(Q^2)$ after dehydroxylation at 800 °C. As noted in Figure 3.3.2, only Al^{VI} is identified in kaolin at room temperature, Al^{VI}, Al^{V} and Al^{IV} are identified at heating temperatures between 550 to 900 °C, while Al^{VI} and Al^{IV} are shown at heating temperature of 950 °C. The fractions of Al^{VI} decrease as increasing heating temperature to 800 °C, with Al^{V} and Al^{IV} increase simultaneously, then the fractions of

Al^{VI} re-increase as increasing heating temperature to 950 °C, simultaneously Al^{V} decreases to zero.

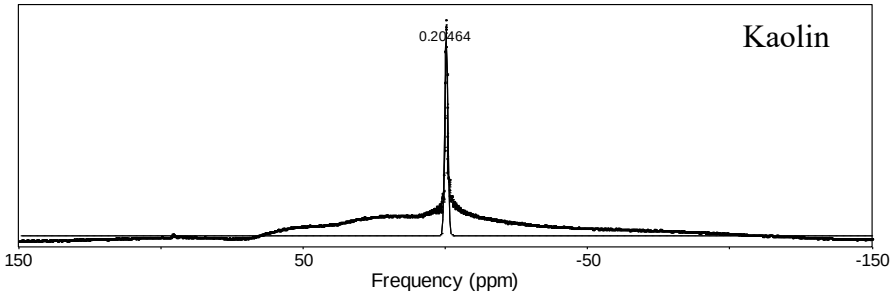

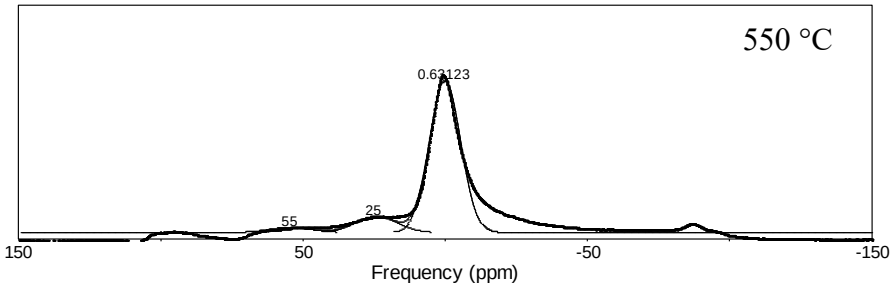

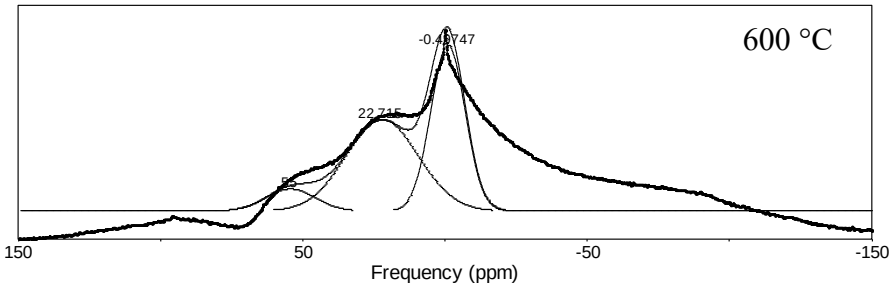

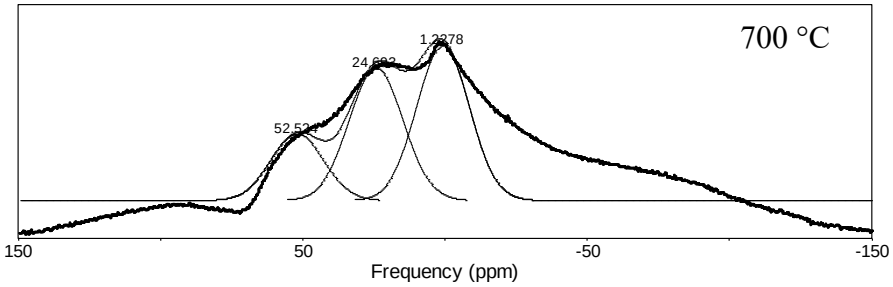

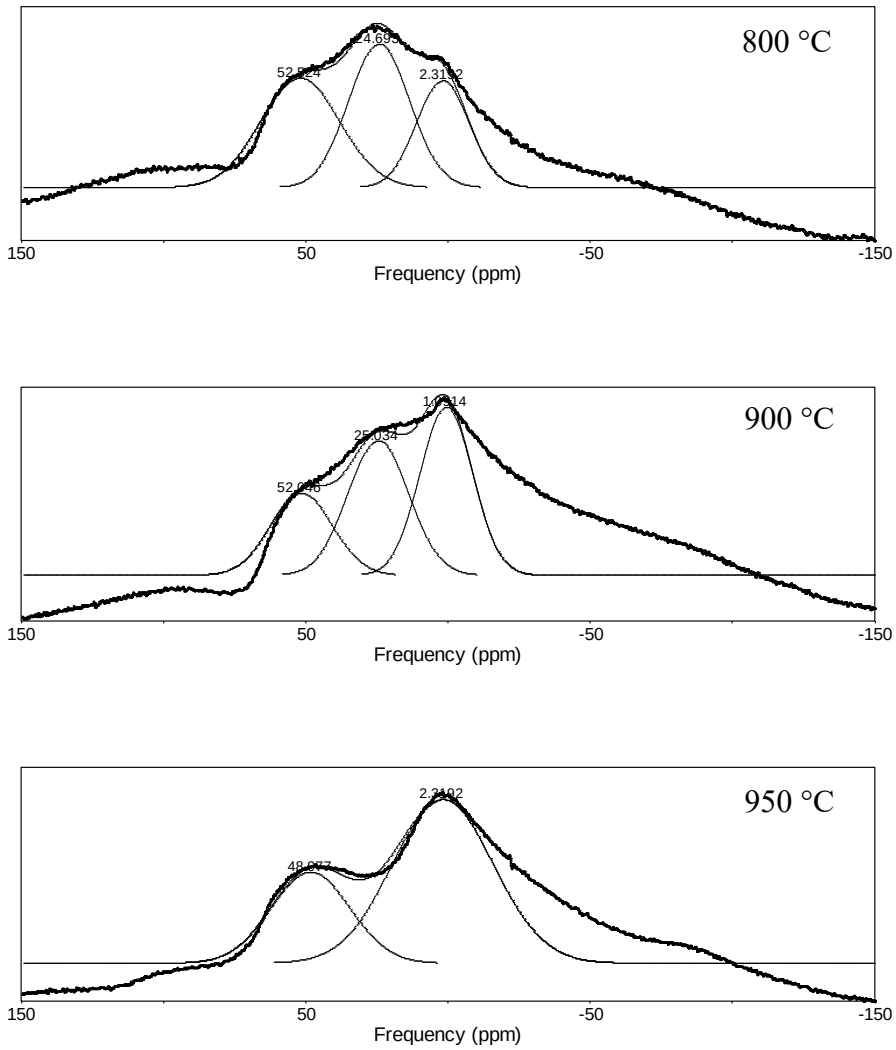

Figure 3.3.1. ^{27}Al NMR spectra (dotted line) and their deconvolution (solid line) of metakaolin heated at various temperatures

Figure 3.3.3 shows the DSC and TGA curves of the kaolin sample, in which three temperature regions have been classified. In region I from 40 to 400 °C, the weight loss increases gradually (TGA), and the first endothermic peak around 100 °C in DSC curve corresponds to the dehydration of adsorbed water. In region II from 400 to 780 °C, the weight loss increases sharply, and the second endothermic peak at 500 °C in DSC curve is related to dehydroxylation of the kaolin sample. In regions III from 780 to 1100 °C, the weight loss increases slightly, and the exothermic peak at 990 °C suggests the recrystallization of metakaolin. In the upper temperature regions, dehydration and dehydroxylation may overlap, as well as dehydroxylation and recrystallization. These results correspond well with the reported thermal analysis of kaolinite, the differences on temperatures for endothermic and exothermic peaks might be resulted from the properties of kaolinite samples from different origins.

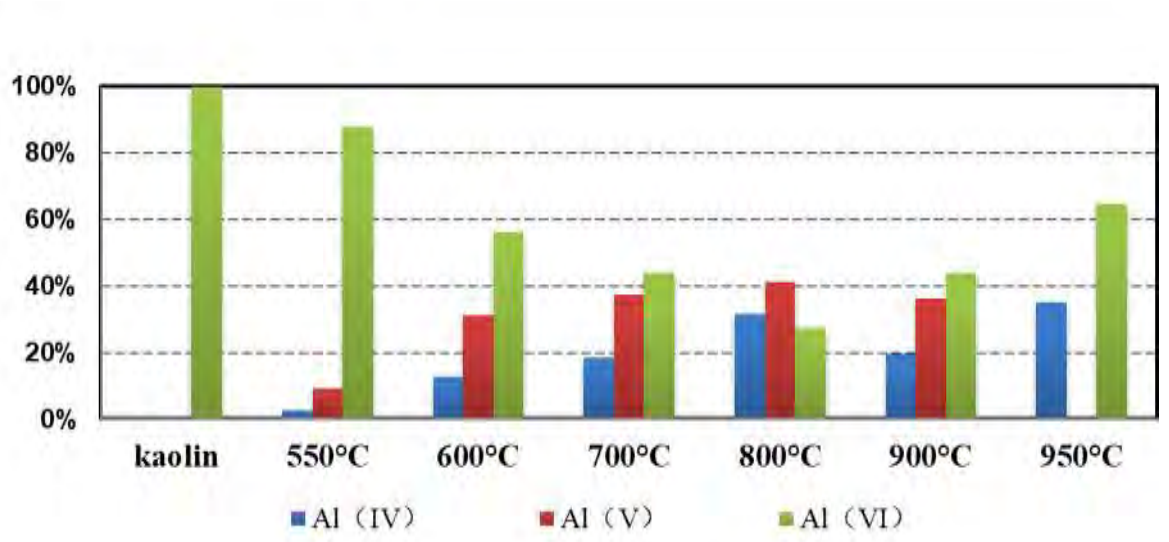

Figure 3.3.2. Fractions of Al^{VI}, Al^{V} and Al^{IV} coordination in metakaolin heated at various temperatures

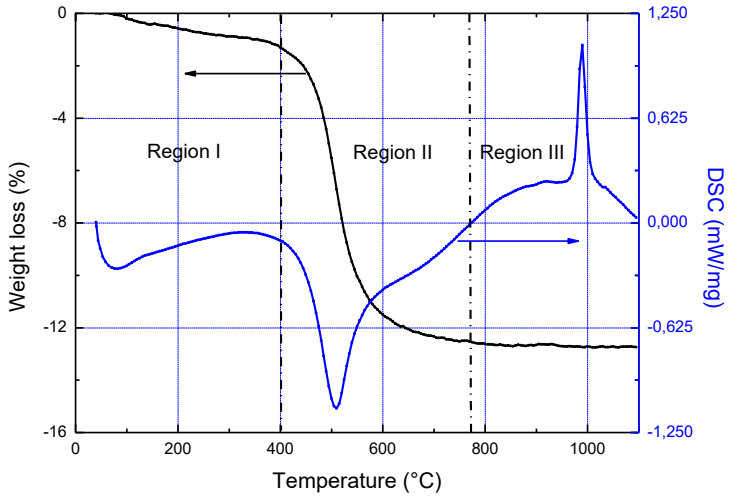

Figure 3.3.3. Thermal analysis curves of the kaolin sample

Figure 3.3.4 presents the XRD spectra of metakaolin samples heated at temperatures from 550-950 °C. The spectra of 600 to 900 °C show amorphous pattern with trace crystalline peak of quartz, implying the amorphous structure of metakaolin. At 550 °C, the spectrum shows amorphous structure with crystalline peaks of kaolinite and quartz, suggesting the incompletion of dehydroxylation. At 950 °C, the spectrum shows amorphous structure with crystalline peaks of spinel-type γAl_2O_3 and mullite, indicating recrystallization of the metakaolin. These results are in a good agreement with the NMR results and thermal analysis that different degrees of dehydroxylation and recrystallization take place through calcination with temperatures from 550 to 950 °C.

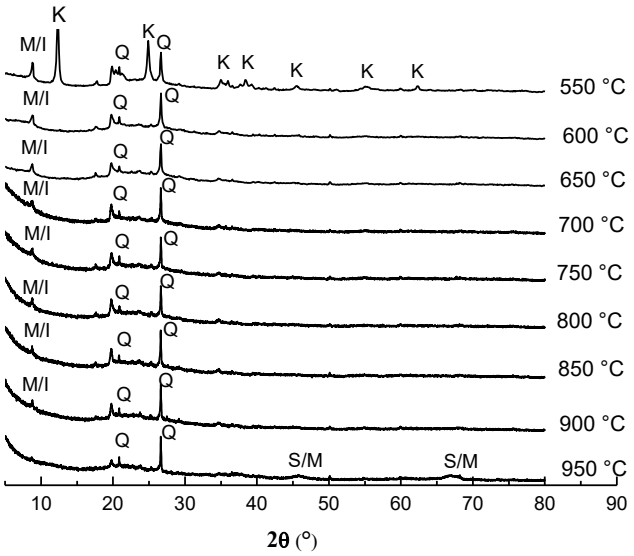

Figure 3.3.4. XRD patterns of metakaolin heated at 550-950 °C (K: kaolinite PDF: 78-2110; M/I: mica/illite PDF: 46-0741; Q: quartz PDF: 79-1906; S/M: spinel-type γAl_2O_3/mullite PDF: 87-0345)

In geopolymerization, Al and Si dissolution is critical because it is the first stage that releases aluminate and silicate monomers by alkali attack on raw aluminosilicates, followed by polymerization of the monomers and condensation into three-dimensional aluminosilicate network. In order to characterize dissolution rates of metakaolin heated at various temperatures, the rates of Al release at 60 minutes with the same amounts of metakaolin, sodium silicate and water has been measured in separated tests, of which the results are present in Figure 3.3.5. With metakaolin heated from 550 to 700 °C, the rates of Al release are high and increases slightly. Then, the rates of Al release decrease sharply as increasing heating temperature from 700 to 950 °C.

Heat revolution of geopolymerization reactions with metakaolin heated at 600, 800 and 900 °C in the first 48 hours has been studied and present in Figure 3.3.6. The exothermic peak I, which is sharp and appears immediately after mixing, implies the wetting of metakaolin particles and dissolution reactions. The time required for this process is less than 15 minutes. For peak I, the heat output of geopolymerization decreases as increasing calcination temperatures, indicating calcination reduces wettability of metakaolin. The exothermic peak II, which takes place around 3 hours, indicates reactions of continue dissolution and polymerization that oligomers combine to form geopolymer network. The heat output of geopolymerization in this process is equal of both metakaolins heated at 600 and 800 °C, which is much higher than that at 900 °C. It suggests that the intensity of dissolution and polymerization reactions with metakaolin heated at 900 °C is much lower than those at 600 and 800 °C.

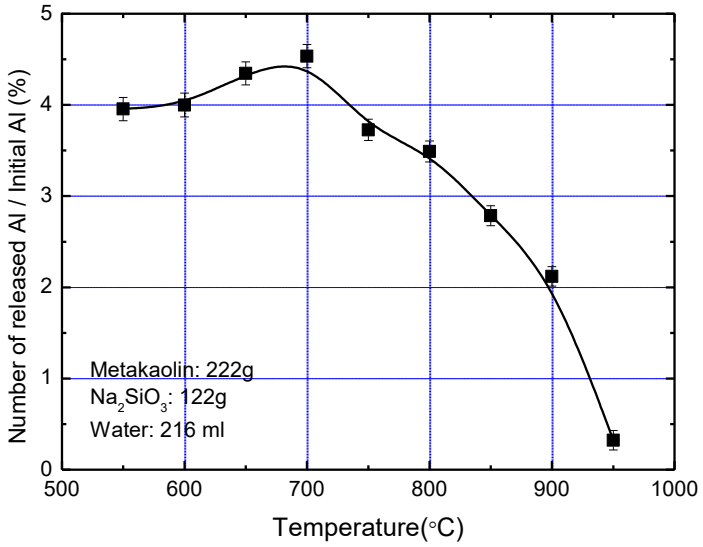

Figure 3.3.5. Dissolution rates of Al compounds with metakaolin heated at various temperatures

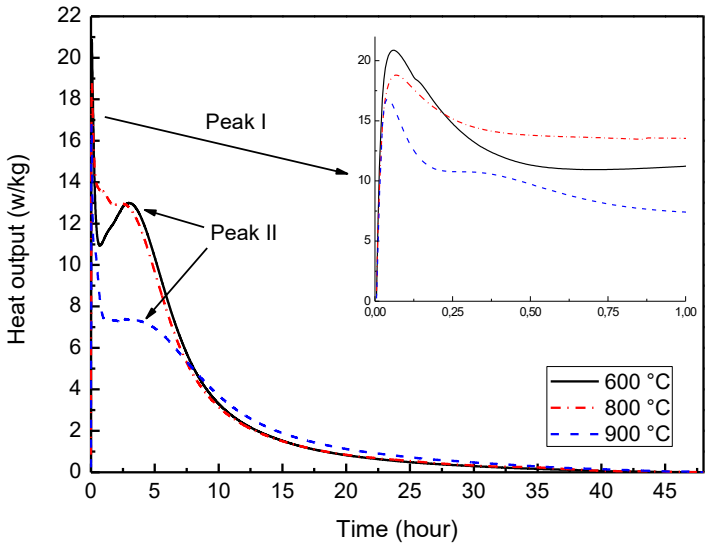

Figure 3.3.6. Heat evolution of geopolymerization reactions with metakaolin heated at various temperatures

Figure 3.3.7 gives the compressive strength of geopolymers with metakaolin heated at various temperatures. The compressive strength increases sharply from 9.4 to 35.6 MPa as changing the metakaolin calcination temperature from 550 to 650 °C. Then, the

compressive strength keeps a plateau (> 30 MPa) as increasing metakaolin calcination temperature from 650 to 850 °C. However, with increasing the metakaolin calcination temperature continually to 900 and 950 °C, the compressive strength reduces to 23.8 and 2.2 MPa, respectively.

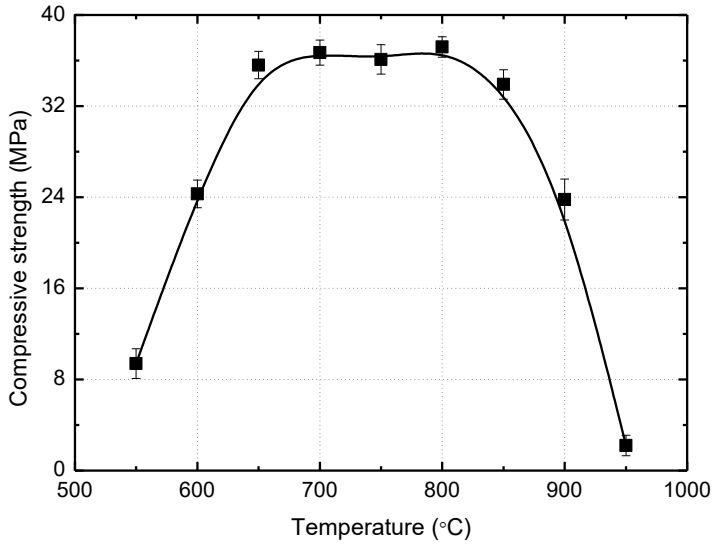

Figure 3.3.7. Compressive strength of geopolymer synthesized with metakaolin samples heated from 550°C to 950°C

Figure 3.3.8 shows the ^{27}Al NMR spectra and their deconvolution of geopolymers synthesized with metakaolins heated at 600, 800 and 900°C. The spectra possess a dominant sharp peak at frequency around 57 ppm, which represents Al^{IV} and implies the formation of geopolymer gel in the geopolymers. Except for the main product peak of geopolymer gel, the small peak suggests residual Al^{VI} in the geopolymers. The location of this peak is at frequency of 0.57 ppm for 600 °C and 2.32 ppm for 800 and 900 °C, which differentiates that Al^{VI} in the precursor metakaolins are of residual kaolinite and of recrystallization, respectively. Interestingly, the Al^{V}, which appears in raw metakaolins, is transformed into Al^{IV} in the geopolymerization reactions.

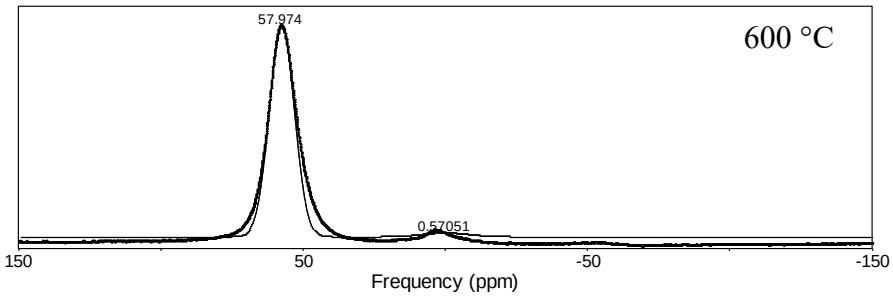

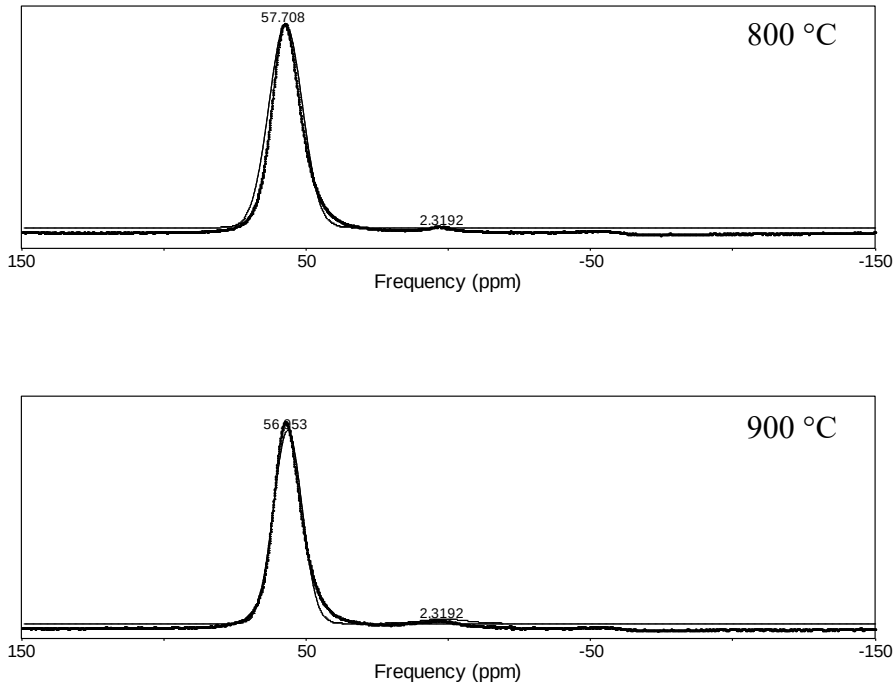

Figure 3.3.8. ^{27}Al NMR spectra of geopolymers synthesized with metakaolins heated at various temperatures

Figure 3.3.9 shows the SEM images of geopolymers synthesized with metakaolin heated at various temperatures. In geopolymer with metakaolin heated at 550 °C, a part of crystalline grains appears, indicating residual kaolinite in the geopolymer. However, the crystalline grains become less and disappear as increasing the calcination temperature of metakaolin. And the geopolymers with metakaolin heated at 800 and 900 °C show extremely homogeneous geopolymer binder in microstructure.

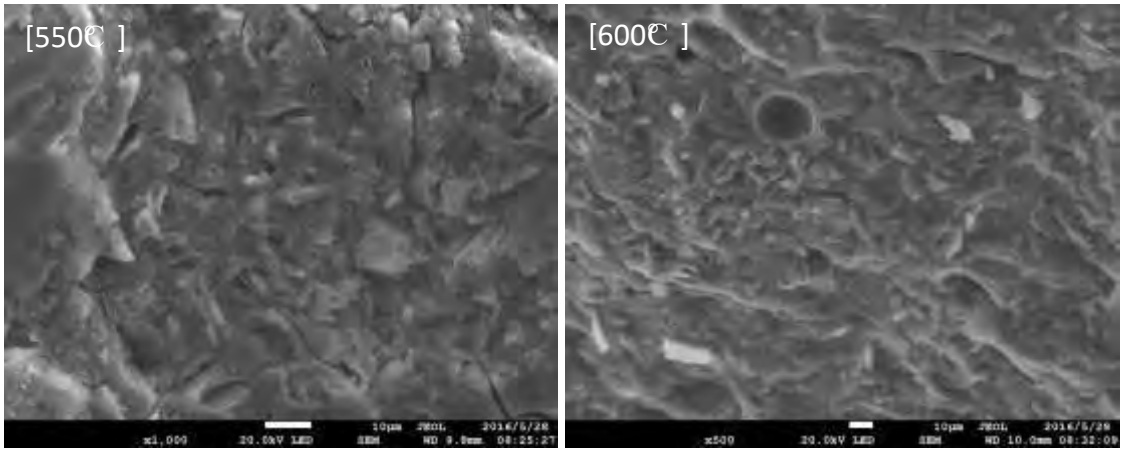

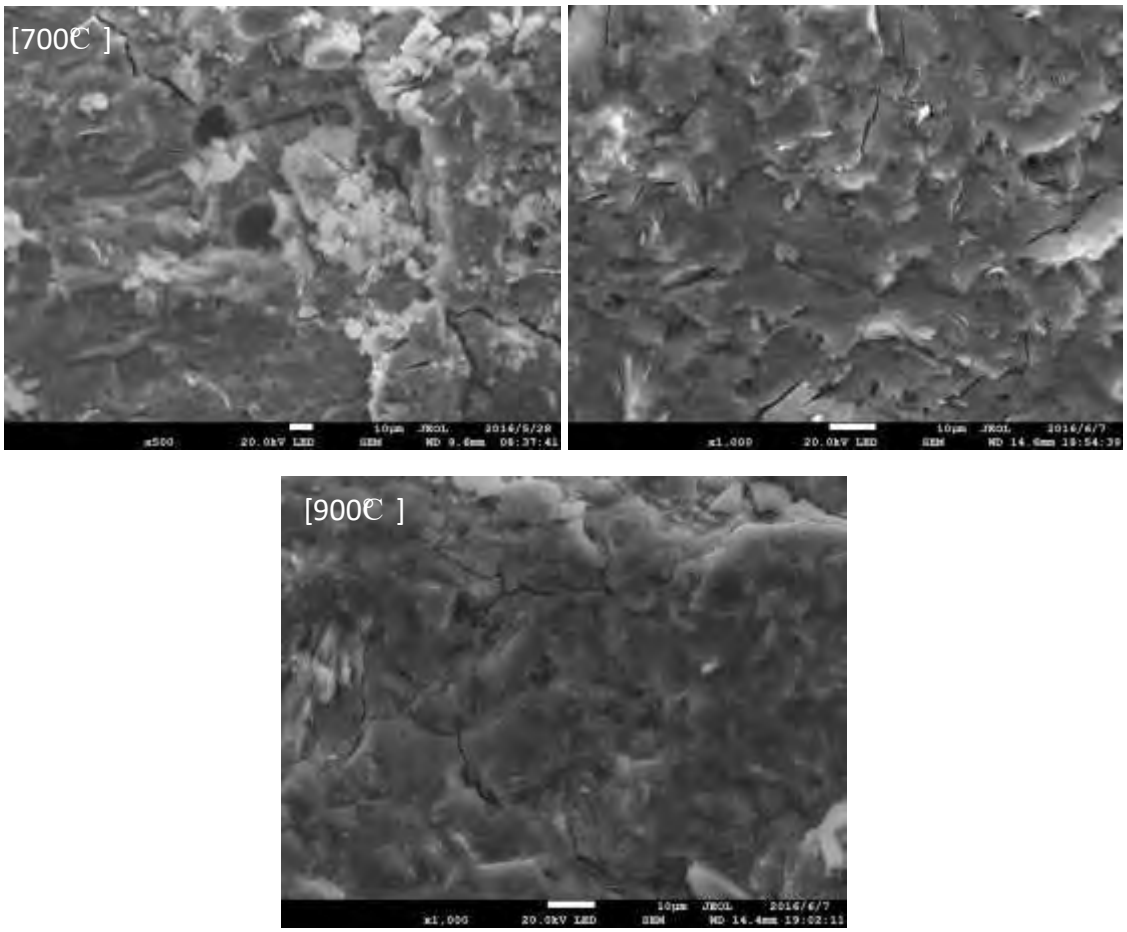

Figure 3.3.9. SEM images of geopolymer synthesized with metakaolin heated at various temperatures

3.3.2 Discussion

Kaolinite goes through dehydroxylation and/or recrystallization in typical calcination regimes in the syntheses of metakaolin geopolymers. The octahedral Al sheets are destroyed, and then transformed to a spinel-type phase or Si-containing γAl_2O_3 together with amorphous silica, after that, mullite and cristobalite are recrystallized on further heating. With calcination time of 6 hours and changing calcination temperature, the results of thermal analysis, NMR measurements and XRD patterns show a good agreement on the calcination rate of the metakaolin samples. As increasing the calcination temperature from 550 to 800 °C, endothermic dehydroxylation takes place mainly; fraction of Al^{VI} decreases constantly; kaolinite only appears in the XRD spectrum of 550 °C. While as increasing it from 800 to 950 °C, the kaolinite samples pass through both dehydroxylation and recrystallization (exothermic); fraction of Al^{VI} increases again; spinel-type γAl_2O_3 and mullite appears in the XRD spectrum of 950 °C. The calcination rate of metakaolin determines the geopolymerization reactions and mechanical property of geopolymers when other parameters are the same in the syntheses of geopolymers.

For the beginning of geopolymerization reaction, metakaolin heated at 600 °C possesses higher reaction rate than that at 800 °C, as indicated from the higher heat output in the first

15 minutes and higher Al dissolution rate in the first hour. This result is opposite of the fact that metakaolin heated at 600 °C has lower calcination rate (dehydroxylation) than that heated at 800 °C. However, recrystallization becomes important at 800 °C as this temperature is in region III and the overlap of dehydroxylation and recrystallization in the calcination process (Figure 3.3.3), even though it is not the main reaction. Thus recrystallization is highly detrimental to beginning geopolymerization reaction. And if the recrystallization degree is high enough (e.g., metakaolin heated at 900 °C), this effect lasts for more hours. However, geopolymerization is an integrated process involving dissolution, polymerization, condensation and consolidation, of which these reactions overlap and last as long as months. The long reaction time gives the possibility to form geopolymers with optimal mechanical property, even though the beginning of geopolymerization reactions might be different. Thus a plateau of high compressive strength is obtained in the range of heating temperature from 650 to 850 °C, but Al dissolution turns to decrease at 700 °C. And it is consistent with reported studies that diverse heating regimes were supposed to be optimal and applied. The statement of only one temperature as the optimal heating temperature of metakaolin in the synthesis of geopolymers is dubious.

Sufficient degree of dehydroxylation and low recrystallization might be the two boundary conditions in the formation of geopolymers with high compressive strength. In this study, with heating temperature lower than 650 °C, the reduction of compressive strength is resulted from insufficient dehydroxylation. With heating temperature higher than 850 °C, the reduction of compressive strength is due to recrystallization in metakaolins. It is different from zeolite formation that metakaolin was found to have maximum reactivity when it had minimum Al^{VI}, because zeolite formation is a short time reaction compared to geopolymerization. Furthermore, the fractions of Al coordination, which has been used as criteria of metakaolin reactivity in zeolite formation and mechanical property of metakaolin and $Ca(OH)_2$ mixture, is not a convenient criteria of metakaolin in the synthesis of geopolymer. For example, the fractions of Al^{VI}, Al^{V} and Al^{VI} of metakaolin heated at 700 °C are almost equal to those of metakaolin heated at 900 °C (Figure 3.3.2), but the compressive strength of geopolymers synthesized by these metakaolins are greatly different (Figure 3.3.7). In metakaolin heated at 900 °C, recrystallization increases the fraction of Al^{VI} and decreases the fractions of Al^{V} and Al^{IV} to make them equal to those of metakaolin heated at 700 °C. And it is understandable that controversial statements have been present in studies when using Al coordination as criteria of metakaolin reactivity in the synthesis of geopolymers. In addition, microstructure of geopolymers studied by NMR and SEM measurements show some characteristics of metakaolin heated at various temperatures, but not reveal the detrimental recrystallization effect in geopolymerization.

3.4. Geothermal clay-based geopolymer binders: Synthesis and microstructural characterization

3.4.1 Heat-treated geothermal clay

The thermal analysis of the geothermal clay was performed to elucidate its reactivity in geopolymerization. Figure 3.4.1 presented the TG-DSC curves of the geothermal clay sample, which gave the collective thermal nature of its main components, namely kaolinite

and cristobalite. First, they are analogous to the TG-DSC curves of kaolinite. The endothermic peaks at around 100 and 550 ℃ in the DSC curve might be attributed to the moisture or absorbed water in hydrous clay minerals (e.g., illite and montmorillonite) (Liu et al., 2010) and dehydroxylation in kaolinite, corresponding to gradual and sharp mass losses in the TG curve, respectively. The "exothermic" peak at 1010 °C, which showed in status of less endothermic because of the interference from cristobalite, suggests the recrystallization of metakaolin, corresponding to a slightly mass loss. Secondly, cristobalite, which is a high-temperature polymorph of silica, confirmed its stability in mass loss (TGA) but endothermic (DSC) nature in the temperature range of 40-1100 °C. Thirdly, the endothermic peak at 750 °C, which corresponded to a sharp mass loss of around 1 %, might be due to the gasification of aluminum sulfate (Johnson and Gallagher, 1971). As noted before, the mass percentage of SO_3 is 1.8%. Obviously, calcination at 550°C induces the dehydroxylation of kaolinite in the geothermal clay sample and greatly increases its dissolution activity, so as to offer a high reactivity in geopolymerization.

The XRD patterns of geothermal clay heated at various temperatures (Figure 3.4.2) were consistent with the results of thermal analysis. In the XRD patterns of 200 and 400 ℃ , kaolinite, cristobalite and trace amount of tridymite were observed, corresponding to that of geothermal clay without calcination (Figure 3.4.1). However, in the XRD patterns of 600 and 800 °C, kaolinite was not observed. And it is interesting to note that the trace amount of tridymite was not observed at heating temperatures of 600 and 800 °C.

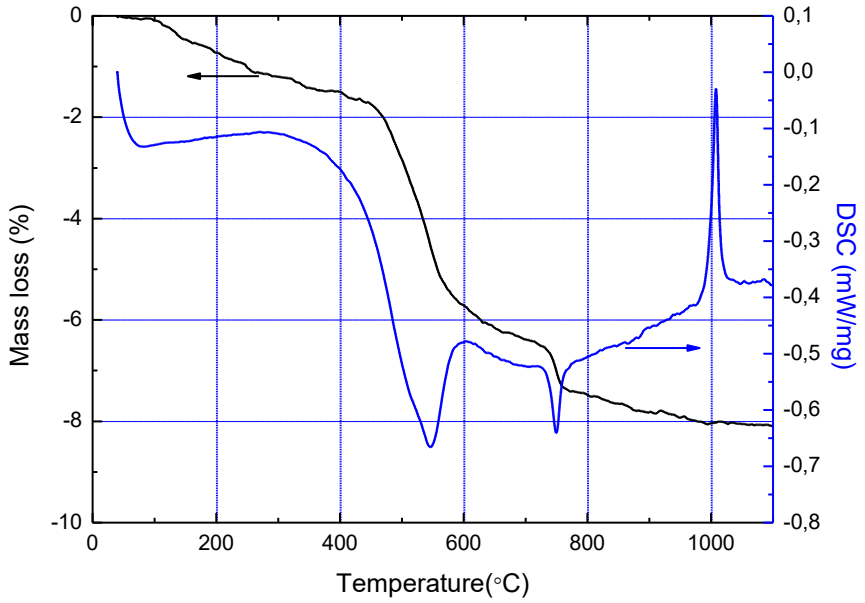

Figure 3.4.1. Thermal analysis curves of the geothermal clay sample

3.4.2 Geopolymer and microstructure

Figure 3.4.3 presented the compressive strength of geopolymers synthesized with geothermal clay samples heated at various temperatures. Of geothermal clay without calcination, geopolymer was hardly formed, of which possessed a low compressive strength around 1 MPa. It verifies the hypothesis that geothermal clay possesses higher dissolution

activity than normal clays because it is able to form geopolymer without calcination. With heating temperatures of 200-550 °C, the compressive strength of geopolymers increased slightly to 4.5 MPa. However, as increasing the heating temperature continually (600-800 °C), compressive strength of geopolymers increased sharply to more than triple times and then kept a plateau. The sharp increase in the compressive strength of geopolymers as changing heating temperature from 550 to 600 ℃ is in good agreement with the thermal analysis of the geothermal clay, in which 550 °C is a critical temperature for inducing dehydroxylation of kaolinite.

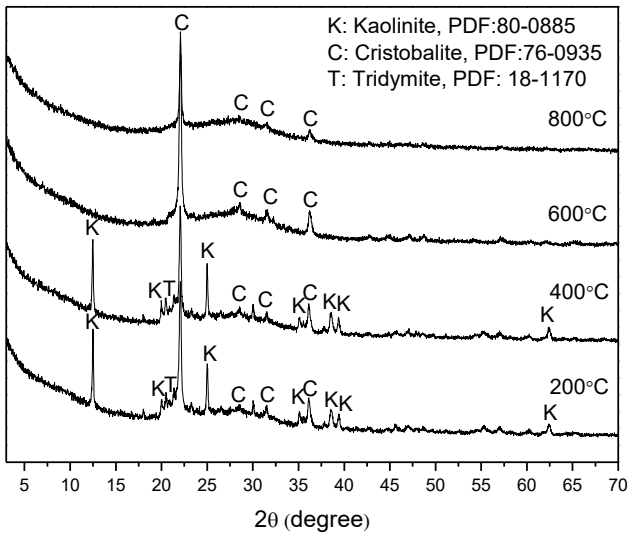

Figure 3.4.2. XRD patterns of geotherm clay samples heated at various temperatures

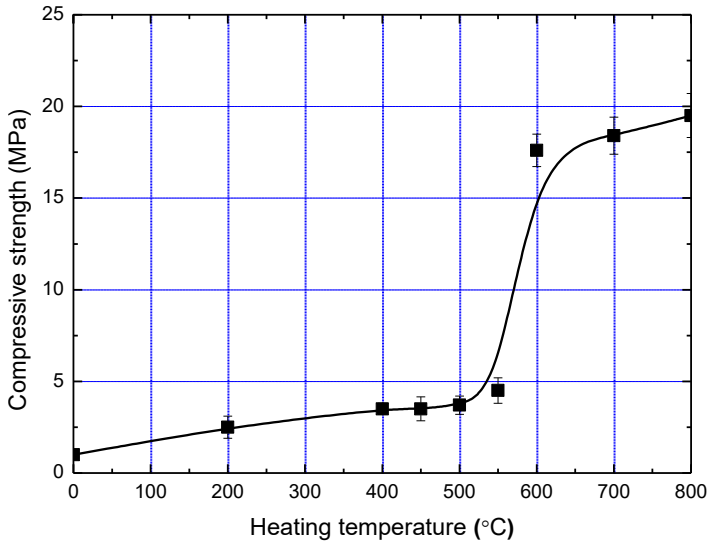

Figure 3.4.3. Compressive strength of geopolymers synthesized with geothermal clay samples heated at various temperatures (No. 1-8)

The microstructure of geopolymers corresponds well with the increase in compressive strength. In studying microstructure of geopolymers, short-range ordering and molecular structure have been investigated with great success using NMR spectroscopy. The lack of spectral resolution for silicon in geopolymers has been overcome by adopting Gaussian peak deconvolution to separate and quantify $Q^n(mAl)$ species ($0 \le m \le n \le 4$, m, n=integer). It has been reported that all silicon and aluminum sites are in tetrahedral coordination in geopolymers, thus n=4. And the resonance of a $Q^4(mAl)$ center with the replacement of each aluminum by silicon is an approximate -5 ppm chemical shift, with $Q^4(4Al)$, $Q^4(3Al)$, $Q^4(2Al)$, $Q^4(1Al)$, $Q^4(0Al)$ resonating at approximately -84, -89, -93, -99 and -108 ppm, respectively. Figure 3.4.4 showed the ^{29}Si NMR spectra and their deconvolution of geopolymers synthesized with geothermal clay heated at various temperatures. At heating temperature of 500 °C, the spectrum of geopolymer showed sharp peaks, indicating high contents of crystalline phase in it. While the spectra of geopolymers synthesized with geothermal clay heated at 600 and 800 °C showed broad band, suggesting the formation of amorphous geopolymeric gel. Because Si/Al ratio in the precursors is 4.2, $Q^4(2Al)$ and $Q^4(1Al)$ should be mainly formed in the geopolymeric gel. Thus in the spectra of 600 and 800 °C, the percentages of $Q^4(2Al)$ and $Q^4(1Al)$ were of 62 % and 57 %, respectively, but they were of 38 % in the spectrum of 500 °C. It verifies the formation of high contents of geopolymeric gel in geopolymers synthesized with geothermal clay heated at 600 and 800 °C. In geopolymer of 500 °C, the high contents of $Q^4(4Al)$and $Q^4(3Al)$ indicates dehydroxylation of kaolinite is incomplete (Wan et al., 2017), and the high content of $Q^4(0Al)$ might suggest the formation of sodium silicate glasses from the unreacted Na_2SiO_3

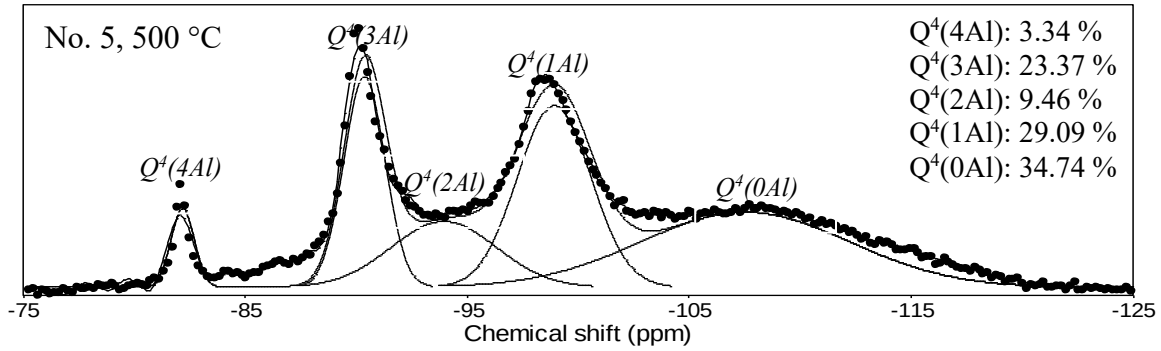

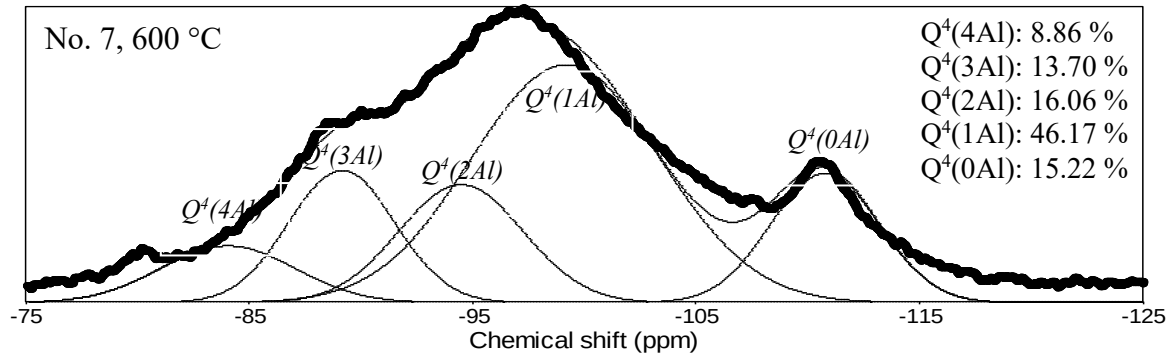

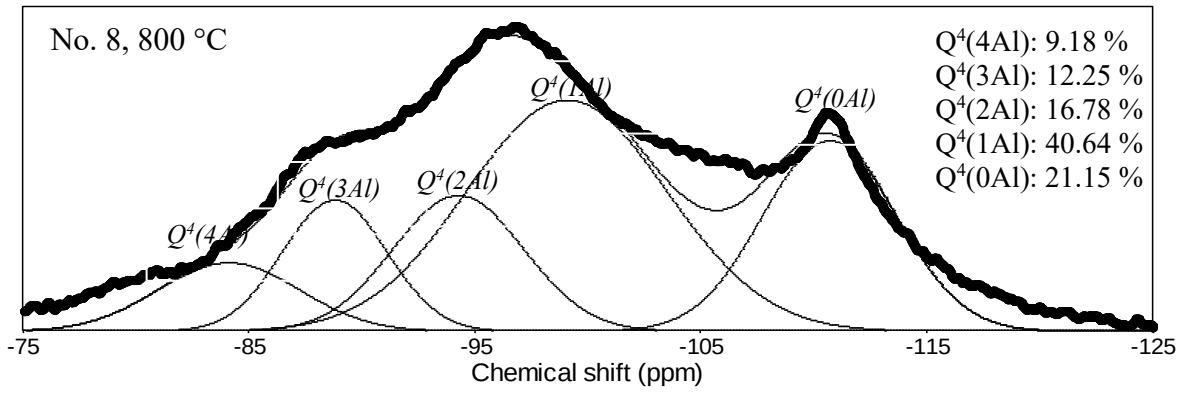

(c)

Figure 3.4.4. ^{29}Si NMR spectra and their deconvolution of geopolymers synthesized with geothermal clay heated at 500 (a), 600 (b) and 800 ℃ (c)

Figure 3.4.5 gave the XRD patterns and SEM images of geopolymers synthesized with geothermal clay heated at various temperatures. With geothermal clay heated at 550, 600 and 800 °C, the XRD patterns of geopolymers showed similar amorphous phase in geopolymeric gel and undissolved silica (cristobalite and trace amount of tridymite). However, the SEM images showed different morphology. At 550 °C, a plenty of granular particles dispersed and covered on the geopolymeric gel, indicating insufficient dissolution and some components are not involved in the geopolymerization reaction. The geopolymers synthesized with geothermal clay heated at 600 and 800 °C showed more homogeneous binder structure with less unreacted particles, indicating higher dissolution degree of raw aluminosilicates. Based on the facts that kaolinite and cristobalite are two main components in the geothermal clay and cristobalite remains after geopolymerization, it can be assert that the kaolinite (metakaolin after heating) and critobalite play the roles of geopolymeric gel formation and unreacted particles, respectively.

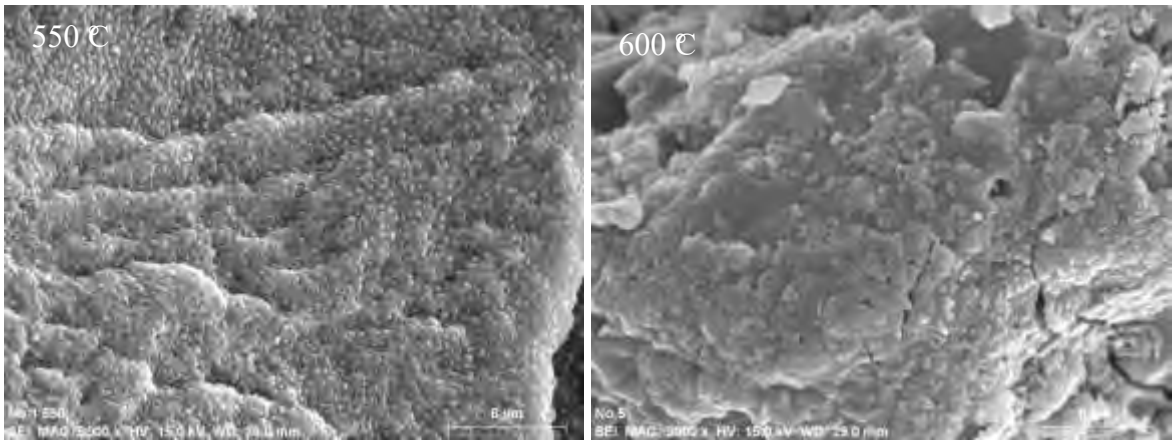

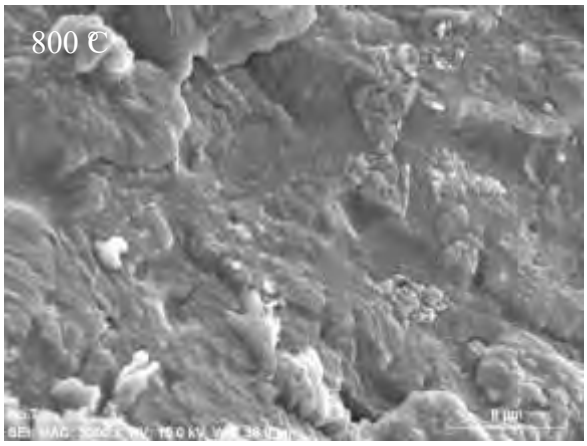

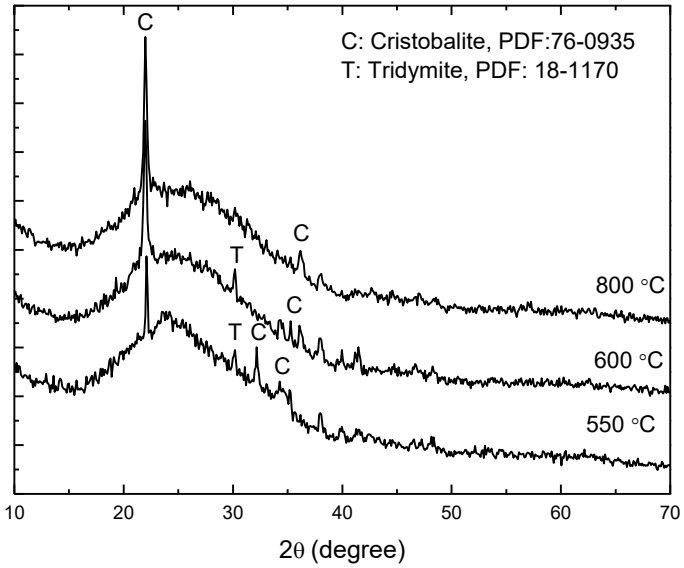

Figure 3.4.5. XRD patterns and SEM images of geopolymers synthesized with geothermal clay heated at various temperatures

Figure 3.4.6 presented the compressive strength of geopolymers synthesized with different combinations of Na_2SiO_3 and NaOH in activating geothermal clay heated at 800 °C. With only 1 mol Na_2SiO_3 or NaOH, low compressive strength of geopolymers at 9 and 2 MPa was obtained respectively, suggesting the irreplaceable role of Na_2SiO_3 and NaOH in the alkaline activator. At 0.5 mol Na_2SiO_3, the compressive strength of geopolymers increased as increasing the NaOH dosage to 0.5 mol, but reduced greatly as increasing NaOH dosage continually to 1 mol. It is consistent with the report that a high content of NaOH decreases the strength of geopolymers.

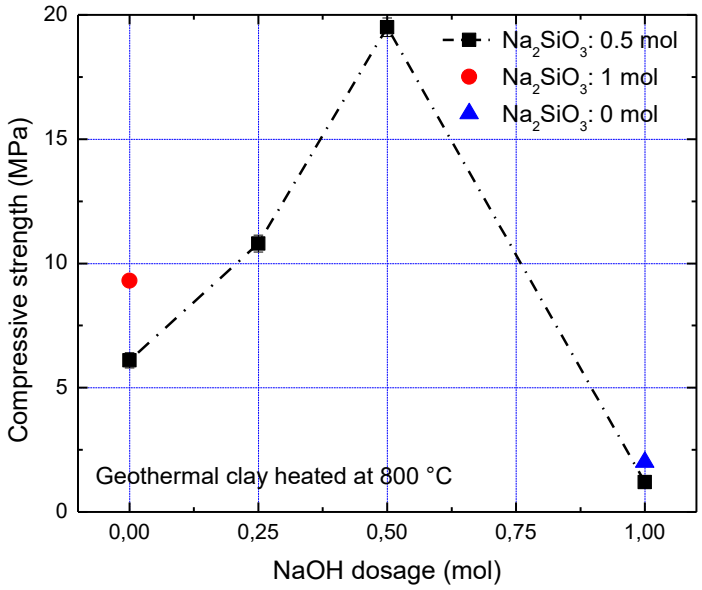

Figure 3.4.6. Compressive strength of geopolymers activated with various combinations of Na_2SiO_3 and NaOH (No. 9-14)

Figure 3.4.7 gave the SEM images of geopolymers synthesized with only 1 mol NaOH or Na_2SiO_3. The platy kaolinite and granular critobalite particles were observed in agglomeration at alkaline activator of 1 mol NaOH, which suggests no formation of geopolymeric gel and results in low compressive strength. With 1 mol Na_2SiO_3 as activator, geopolymeric binder was observed but with cracks, and undissolved kaolinite or critobalite particles were observed on geopolymeric gel, suggesting NaOH plays the role in the dissolution raw aluminosilicate. Compared with the geopolymer synthesized with 0.5 mol Na_2SiO_3 and 0.5 mol NaOH as activator (Figure 3.4.5), it is found that Na_2SiO_3 and NaOH tend to play the roles of geopolymeric gel formation and aluminosilicate dissolution, respectively, in activating geothermal clay.

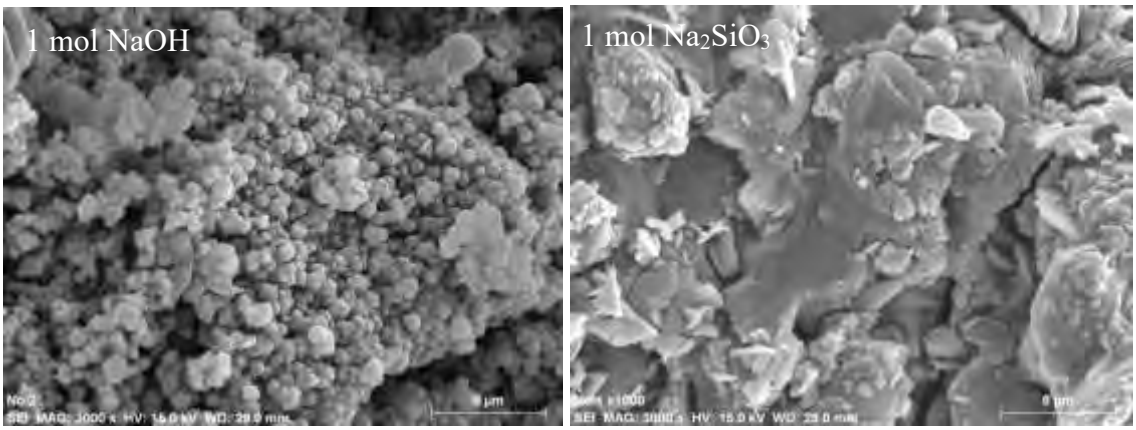

Figure 3.4.7. SEM images of the geopolymers activated with only 1 mol NaOH or Na_2SiO_3

Compressive strength of geopolymers synthesized with different water content was presented in Figure 3.4.8. The minimum water content for inducing sufficient mixing

during synthesis was 9 mol. As increasing the water content, the compressive strength of geopolymers decreased steadily. And geopolymer could not be formed at the water content of 12 mol.

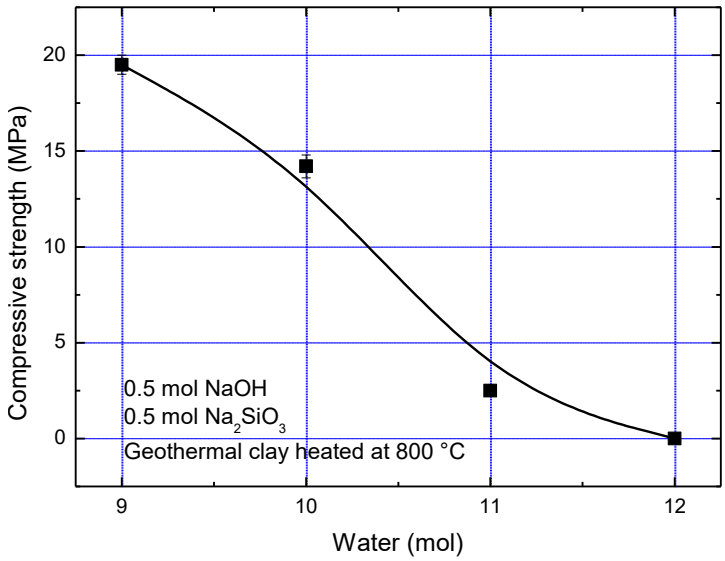

Figure 3.4.8. Compressive strength of geopolymers synthesized at different water contents (No. 8, 15-17)

Figure 3.4.9 gave the SEM images of geopolymers synthesized with water contents of 9 and 10 mol. A homogenous geopolymeric gel was observed at water content of 9 mol, but pores were observed at water content of 10 mol, which might be attributed to the evaporation of residual water. Thus the increase of water content is detrimental to geopolymer formation with geothermal clay, because it leads to the formation of porous structure and lowers the compressive strength. It is in good agreement with the report that excessive water hinders polycondensation in geopolymer formation and lowers the compressive strength.

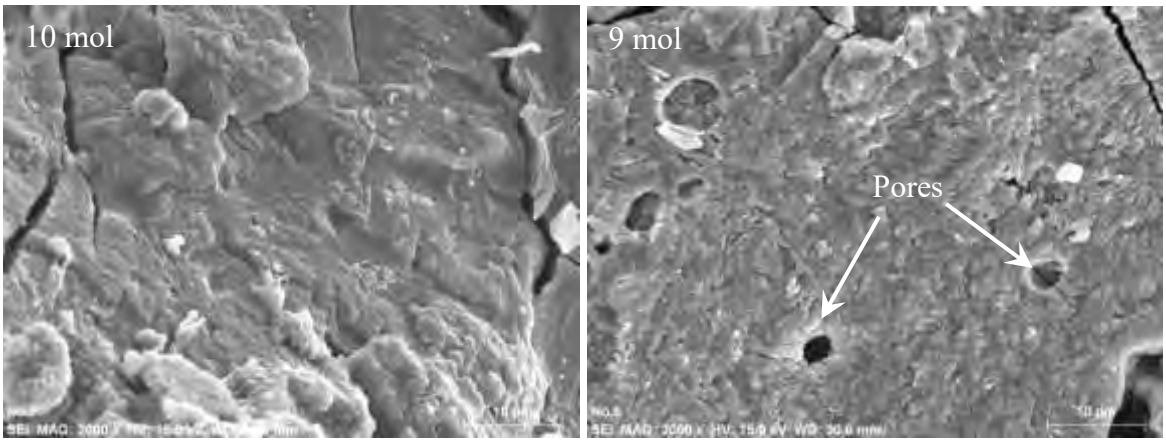

Figure 3.4.9. SEM images of geopolymers synthesized with different water contents

3.5. Consolidation of Mine Tailings and Heavy Metal Retention by Alkaline Activation: I. Microstructure of the Binders

3.5.1 Mechanical properties of the alkali-activated mine tailing-based binders

Figure 3.5.1 gave the compressive strength of the binders synthesized at various contents of mine tailings and $Pb(NO_3)_2$. Without metakaolin, the 100% mine tailing-based binder was formed with a compressive strength around 2 MPa. It verifies the hypothesis that mine tailings rich in calcium and aluminosilicate minerals are able to be activated by alkalis and form consolidated structures. Then, as adding metakaolin into the raw materials, compressive strength of the binders increased steadily, which achieved 15.5 MPa at the mine tailing to metakaolin ratio of 1:1. As metakaolin has been extensively used in the synthesis of geopolymers, these results suggest that the formation of geopolymer gel during alkali activation of mine tailings enhances the mechanical properties of the binders. As noted in Figure 3.5.1, at mine tailing to metakaolin ratio of 1:1, the compressive strength of the binders showed a three-stepped decrease as increasing the addition of $Pb(NO_3)_2$, of which the three steps were at $Pb(NO_3)_2$ additions of 0-2%, 3-6% and 9-10%. At the $Pb(NO_3)_2$ addition of 0-2%, compressive strength of the binders increased slightly from 15.5 to 17.3 MPa, which is consistent with the reported positive effect of Pb^{2+} on the strength of geopolymer gel. Then, it decreased sharply as increasing $Pb(NO_3)_2$ from 2 to 3%, and kept a plateau at the $Pb(NO_3)_2$ addition of 3-6%. After that, compressive strength of the binders decreased roughly again as increasing the $Pb(NO_3)_2$ amount to 9%, and kept a plateau at $Pb(NO_3)_2$ addition of 9-10%. These results indicate the addition of $Pb(NO_3)_2$ decreases the mechanical strength of alkali-activated binders generally, although it enhances the strength at a low content.

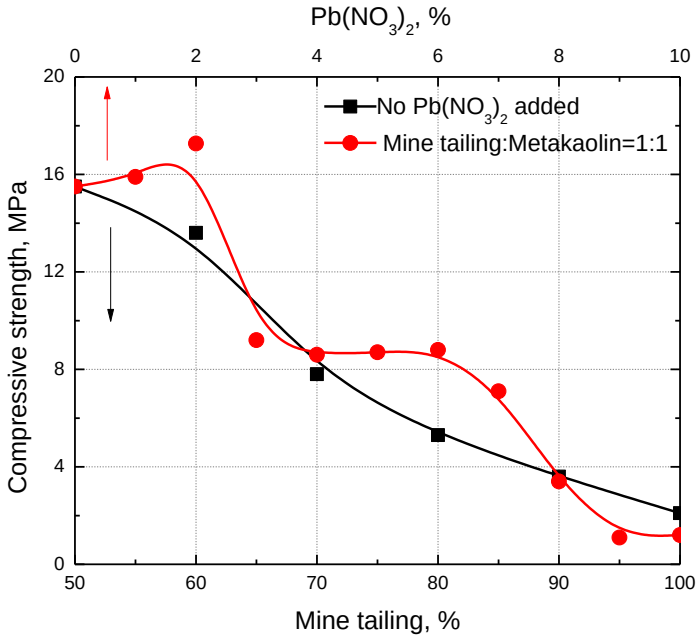

Figure 3.5.1. Compressive strength of geopolymers as a function of mine tailing to metakaolin ratio and $Pb(NO_3)_2$ addition

3.5.2 Effect of mine tailings to metakaolin ratio on microstructure of the binders

The geopolymer gel formation as the addition of metakaolin into the mine tailings can be observed from the microstructures of the binders. Figure 3.5.2 presented the SEM images of alkali-activated binders synthesized with mine tailing to metakaolin ratios of 1:1, 7:3 and 100% mine tailing. At mine tailing to metakaolin of 1:1, the product showed a homogeneous structure, indicating a high degree of binder formation. At the ratio of 7:3, more mineral particles were associated in the binder, and more cracks were observed. At 100% mine tailing, mineral particles, the C-S-H and/or geopolymer gel formed a heterogeneous and porous structure in the binder. Thus the addition of metakaolin raises the homogeneity of the binders, so as to increase the compressive strength of the binders (Figure 3.5.1).

Figure 3.5.3 gave the FTIR spectra of the binders synthesized at various mine tailing to metakaolin ratios. The absorption peaks around 3441 cm^{-1} and 1642 cm^{-1} were OH^- stretching vibrations and H-OH bonds, corresponding to structure hydroxyl (OH^-) and adsorbed water in the binders, respectively. The peak around 1450 cm^{-1} was due to the asymmetric stretching mode of O-C-O bonds in CO_3^{2-} groups, and the absorption peaks at 727 cm^{-1} and 870 cm^{-1} were the stretching vibration for Ca-C and Mg-C bonds in dolomite, respectively. These peaks suggested that dolomite was not completely reacted in the alkaline activation process. The adsorption peak at 468 cm^{-1} was the stretching vibration of O-Si-O bonds in kaolinite, which disappeared in the binders No. 5 and 6 with low addition of metakaolin. The band around 1000 cm^{-1} was the overlaps of Si-O-Si bonds (1123 cm^{-1}) in silicate derivatives, Si-O-Al (1078 cm^{-1}) in residual metakaolin, Si-O-T (T is tetrahedral Si or Al) asymmetric stretching band (980 cm^{-1}) in geopolymer gels and Si-O stretching vibration (970 cm^{-1}) in C-S-H gel. As reducing metakaolin content from samples No. 1 (50% metakaolin) to No. 6 (no metakaolin), the intensity of Si-O-T band decreased, indicating metakaolin stimulated the formation of geopolymer gel, meanwhile, this band became broader, suggesting the formation of more silicate derivatives and/or C-S-H gel. These results present roughly the evolution of geopolymeric and C-S-H gel in alkali-activated mine tailing-based binders as a function of metakaolin content. And NMR results confirm this evolution on the quantitative and molecular perspectives.

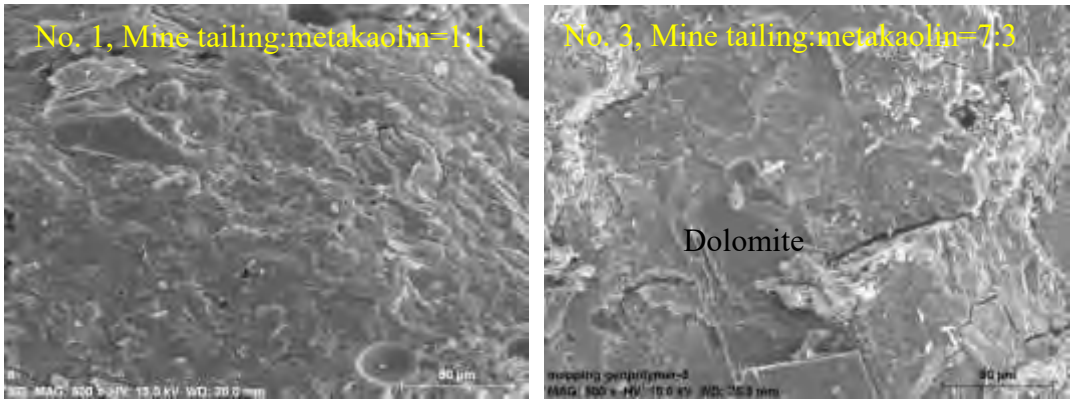

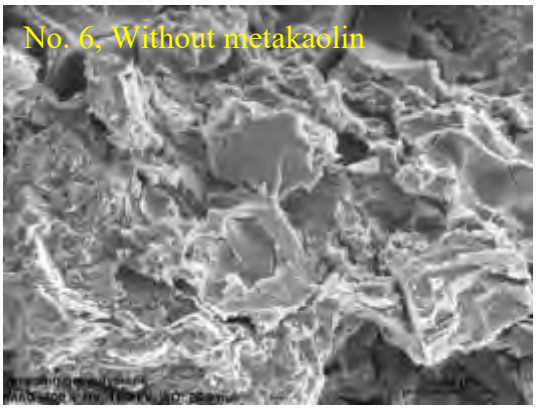

Figure 3.5.2. SEM images of alkali-activated binders synthesized at various mine tailing to metakaolin ratios

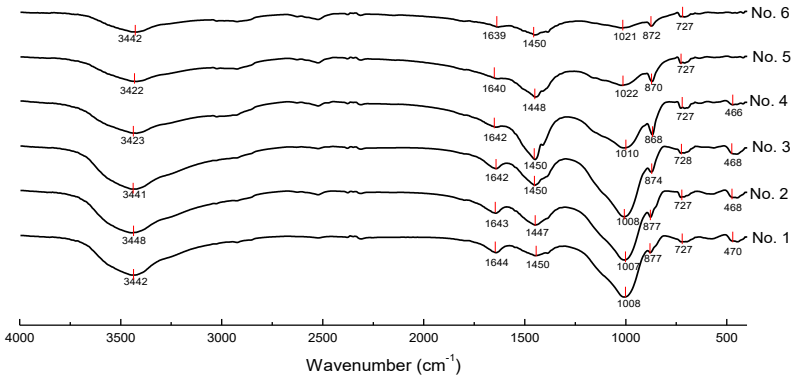

Figure 3.5.3. FTIR spectra of binders synthesized at various mine tailing to metakaolin

In studying microstructure of alkali-activated binders, short-range ordering and molecular structure have been investigated with great success using NMR spectroscopy. The lack of spectral resolution for silicon in these binders has been overcome by adopting Gaussian peak deconvolution to separate and quantify $Q^n(mAl)$ species ($0 \le m \le n \le 4$, m, n=integer). In geopolymer gel, it has been reported that all silicon and aluminum sites are in tetrahedral coordination in geopolymers, thus n=4. And the resonance of a $Q^4(mAl)$ center with the replacement of each aluminum by silicon is an approximate -5 ppm chemical shift, with $Q^4(4Al)$, $Q^4(3Al)$, $Q^4(2Al)$, $Q^4(1Al)$, $Q^4(0Al)$ resonating at approximately -84, -89, -93, -99 and -108 ppm, respectively. In C-S-H gel, ^{29}Si NMR spectra provide quantitative information Q^n ($0 \le n \le 2$), where Q is a silicate tetrahedron and n is the number of oxygens which bridge to adjacent tetrahedra. The peak at -71.3 ppm is due to the formation of belite (Q^0), the broader peaks at -79 and -85 ppm are due to end- (Q^1) and middle-chain (Q^2) groups present in the C-S-H respectively, and the peak at -82 ppm represents the $Q^2(1Al)$ when Al is involved. Figure 3.5.4 gave the ^{29}Si NMR spectra and their deconvolution of the binders synthesized at various mine tailing to metakaolin ratios, in which the NMR spectra were dotted lines. As increasing the mine tailing content from binders No. 1 to 3 and 6, the percentage of tetrahedral Si coordination in geopolymer gel ($Q^4(mAl)$, $0 \le m \le 4$) decreased from 79.45% to 68.23% and 33.92%, respectively. It is in good agreement with the FTIR

results that more geopolymer gel is formed with addition of metakaolin into the raw materials. And this decrease was mainly in the species of $Q^4(4Al)$, $Q^4(3Al)$ and $Q^4(2Al)$ rather than in $Q^4(1Al)$, which shows the important role of reactive aluminum in geopolymer gel formation. The three binders possessed the consistent percentage in belite (Q^0) of around 4%, while the percentages of Q^1, $Q^2(1Al)$ and Q^2 increased from 15.58% to 28.10% and 62.17% as changing the binders from No. 1 to 3 and 6 (50%, 70% and 100% mine tailings), respectively. It shows clearly the formation of Si sites in C-S-H gel when a high content of mine tailing is involved in the alkali activation process.

ratios

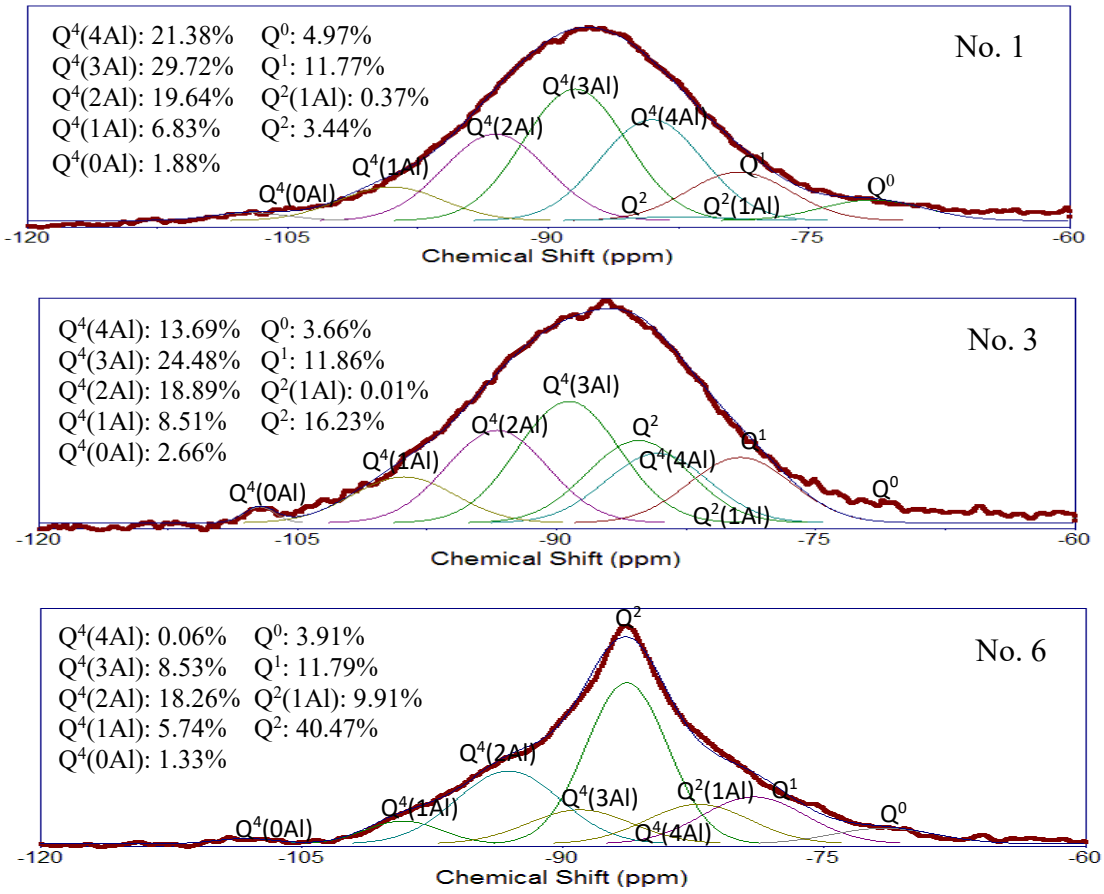

Figure 3.5.4. ^{29}Si NMR spectra and their deconvolution of the binders synthesized at mine tailing to metakaolin ratio of 1:1 (No. 1), 7:3 (No. 3) and no metakaolin (No. 6)

On the basis of previous results, the evolution of the microstructure of alkali-activated mine tailing-based binders were schematically presented in Figure 3.5.5. At 100% mine tailing (No. 6), C-S-H gel was mainly formed with a small percentage of geopolymer gel. As increasing metakaolin to 30% (No. 3), 68.23% geopolymer gel was formed in the binder. Then, at mine tailing to metakaolin ratio of 1:1 (50% metakaolin, No. 1), geopolymer gel was mainly formed in the binder. In the three binders, belite was formed at a small percentage (4%).

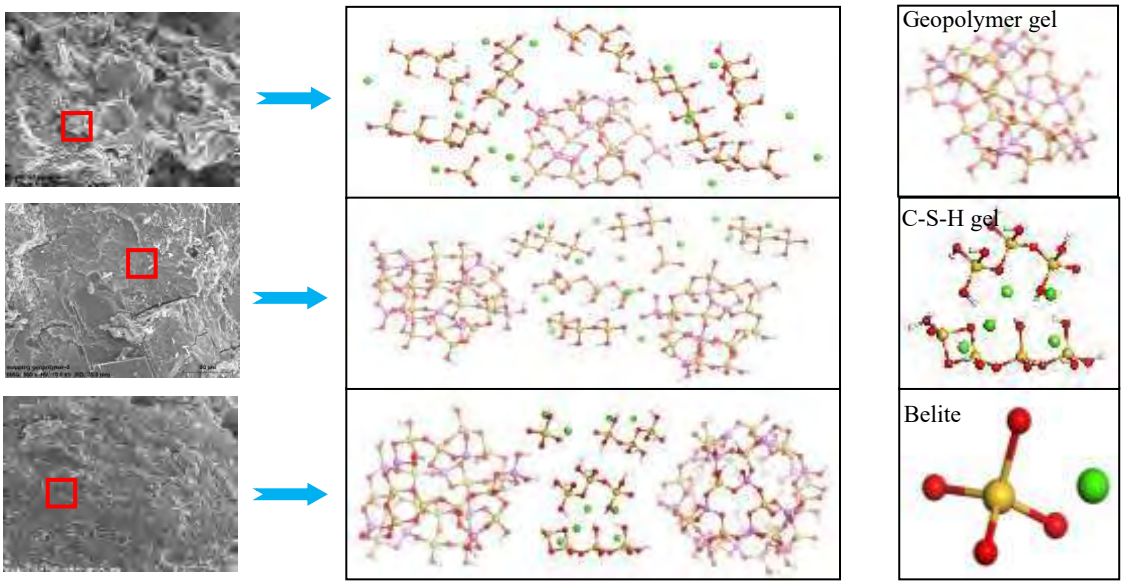

Figure 3.5.5. Schematic diagram of the evolution of alkali-activated mine tailing-based binders´ microstructures as a function of metakaolin addition

3.5.3 Effect of $Pb(NO_3)_2$ addition on the microstructure of the binder

Figure 3.5.6 showed the SEM images of alkali-activated mine tailing-based binders synthesized with $Pb(NO_3)_2$ additions of 1% (No. 7), 5% (No. 11) and 9% (No. 15), respectively. With $Pb(NO_3)_2$ addition of 1%, the binder showed a homogeneous structure resembling to that without $Pb(NO_3)_2$ addition (No. 1). With $Pb(NO_3)_2$ addition of 5%, gel was formed but not enough to develop a compact structure with the mineral particles. With $Pb(NO_3)_2$ addition of 9%, minerals particles and gel formed a porous and loose structure. These three $Pb(NO_3)_2$ percentages were in the three steps of the decrease in compressive strength (Figure 3.5.1), which gave the morphological observation on its decrease as increasing $Pb(NO_3)_2$ addition in the binders.

Figure 3.5.7 gave the FTIR spectra of alkali-activated mine tailing-based binders synthesized with various $Pb(NO_3)_2$ additions. Similarly, the absorption peaks of 3441 cm^{-1}, 1642 cm^{-1}, 1450 cm^{-1}, 727 cm^{-1}, 870 cm^{-1} and 468 cm^{-1} corresponded to the OH^- stretching vibrations, H-OH, O-C-O, Ca-C, Mg-C and O-Si-O bonds, respectively. The narrow peak at 1385 cm^{-1} was the vibration of NO_3^-, of which the intensity increased as increasing the $Pb(NO_3)_2$ addition. The band around 1000 cm^{-1} was the overlaps of Si-O-Si bonds (1123 cm^{-1}) in silicate derivatives, Si-O-Al (1078 cm^{-1}) in residual metakaolin, Si-O-T (T is tetrahedral Si or Al) asymmetric stretching band (980 cm^{-1}) in geopolymer gels and Si-O stretching vibration (970 cm^{-1}) in C-S-H gel. As discussed previously (Figure 3.5.4 and 3.5.5), geopolymer gel was the main species formed at mine tailing to metakaolin ratio of 1:1, thus this band was mainly due to geopolymer gel in the binder with 1% $Pb(NO_3)_2$ addition (No. 7). Its intensity kept the same as changing $Pb(NO_3)_2$ additions from 1% to 6% (No. 7-12), indicating the increase of $Pb(NO_3)_2$ content to 6% hardly affects the geopolymer gel formation in the binders. However, the binders with $Pb(NO_3)_2$ additions of 8% and 10% (No 14 and 16) showed the band of much lower intensity but broader, suggesting the reduction of geopolymer gel but more other species formation when the

$Pb(NO_3)_2$ content was high enough. These results corresponded well with the second and third steps of deceasing compressive strength in the binders as a function of $Pb(NO_3)_2$ addition (Figure 3.5.1), of which $Pb(NO_3)_2$ addition of 6% was the critical point.

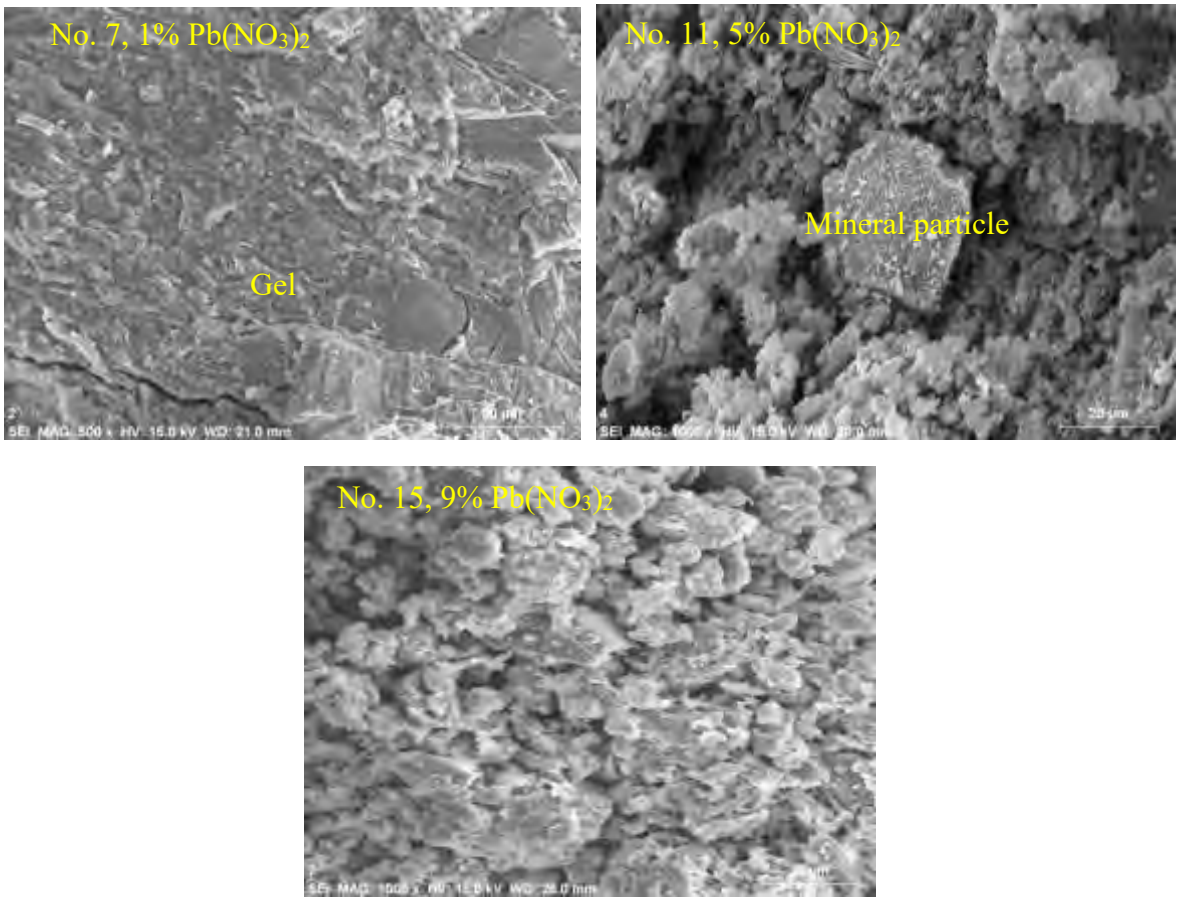

Figure 3.5.6. SEM images of alkali-activated mine tailing-based binders with various $Pb(NO_3)_2$ additions

The NMR results elucidated further the change in compressive strength of the binders as a function of $Pb(NO_3)_2$ addition to 6%. Figure 3.5.8 presented the ^{29}Si NMR spectra and their deconvolution of alkali-activated mine tailing-based binders synthesized at various $Pb(NO_3)_2$ additions, in which the dotted lines were the NMR spectra. Beside the $Q^n(mAl)$ species in geopolymer and C-S-H gels, the deconvoluted peaks at -97.4 ppm and -109.2 ppm are attributed to the Q^4 and Q^3 in lead silicate glass ($PbO{\bullet}nSiO_2$) when $Pb(NO_3)_2$ is added. As adding $Pb(NO_3)_2$ from 0 (No. 1, Figure 3.5.4) to 2%, 3% and 6% in the syntheses of the binders, tetrahedral Si coordination in geopolymer gel kept nearly the same from 79.45% to 79.22%, 79.54%, and 78.15%, respectively, confirming with the FTIR results (Figure 3.5.7) that geopolymer gel hardly changed as increasing $Pb(NO_3)_2$ to 6%. For the overall Si sites from 0 to 6% of $Pb(NO_3)_2$ additions, Si sites decreased from 20.55% (No. 1) to 11.3% (No. 12) in C-S-H gel, while increased from 0 to 10.51% in lead silicate glass. However, the arrangement of the tetrahedral Si coordination in geopolymer gel was changed with the addition of $Pb(NO_3)_2$, of which the amount of $Q^4(4Al)$, $Q^4(3Al)$ and $Q^4(2Al)$ decreased and that of $Q^4(1Al)$ and $Q^4(0Al)$ increased as summarized in Table 3.5.1.

It suggested the replacement of tetrahedral Al by lead silicate glass in the linkage of tetrahedral Si. And as noted in Figure 3.5.1, this linkage enhanced the compressive strength of the binders at a low amount (e.g., 2% $Pb(NO_3)_2$), but weakened it at a high amount (e.g., 6% $Pb(NO_3)_2$).

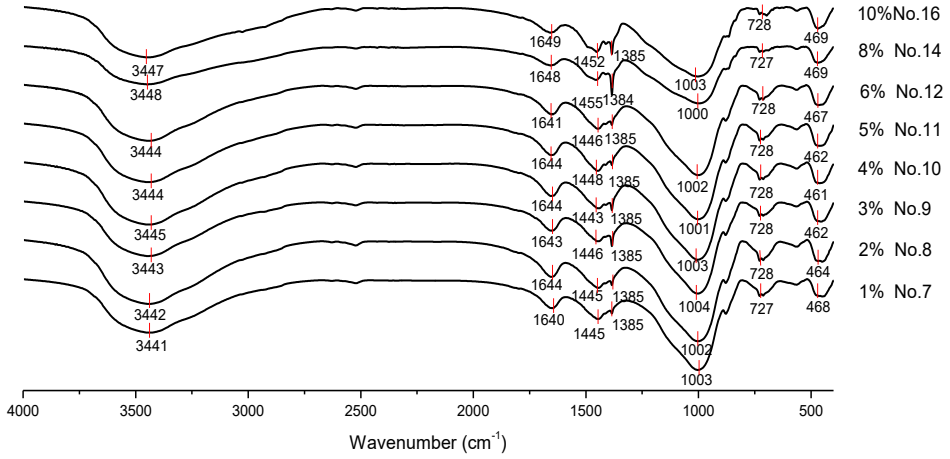

Figure 3.5.7. FTIR spectra of the alkali-activated mine tailing-based binders synthesized with $Pb(NO_3)_2$ additions of 1-10% (No.7-16)

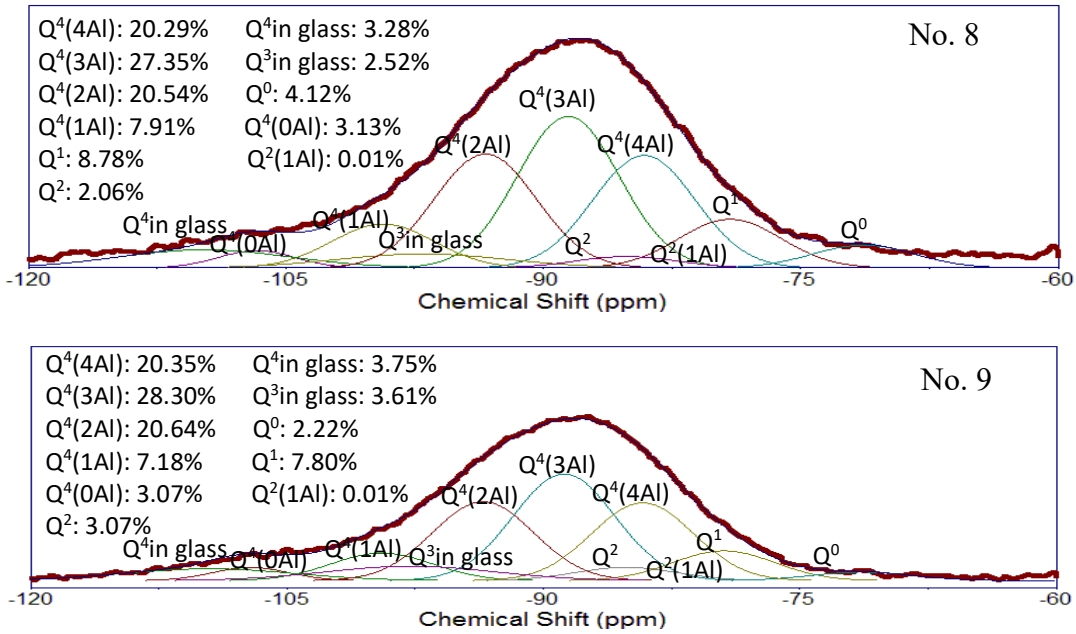

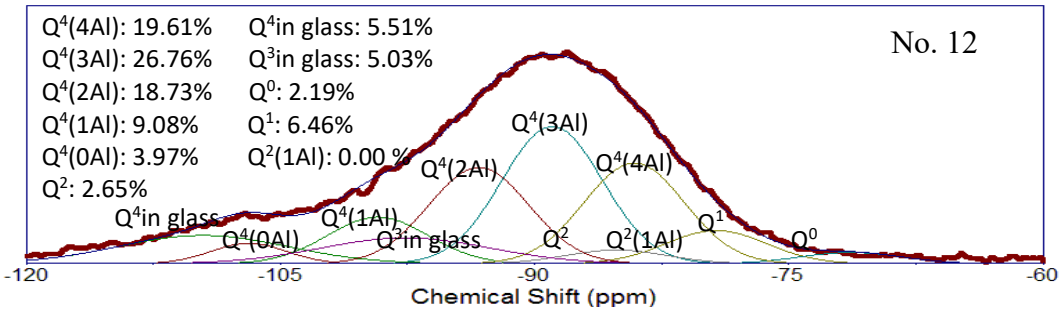

Figure 3.5.8. ^{29}Si NMR spectra and their deconvolution of alkali-activated mine tailing-based binders synthesized at $Pb(NO_3)_2$ additions of 2% (No. 8), 3% (No. 9) and 6% (No. 12)

Table 3.5.1. The change of tetrahedral Si coordination in geopolymer gel at various $Pb(NO_3)_2$ additions

No	$Pb(NO_3)_2$	*$Q^4(4Al)$*, *$Q^4(3Al)$* and *$Q^4(2Al)$*	*$Q^4(1Al)$* and *$Q^4(0Al)$*
1	0%	70.74%	8.71%
8	2%	68.18%	11.04%
9	3%	69.29%	10.25%
12	6%	65.10%	13.05%

3.6. Consolidation of Mine Tailings and Heavy Metal Retention by Alkaline Activation: II. Quantitative Analysis of the Lead Immobilization Forms

3.6.1 Immobilization of heavy metals

Figure 3.6.1 gave the results of TCLP tests of Pb for the mine tailings-based binders synthesized with various $Pb(NO_3)_2$ additions. Both the Pb concentration in the leachate and the percentage of leached Pb to total Pb increased in a similar trend as increasing the $Pb(NO_3)_2$ additions in the raw materials. At an extended $Pb(NO_3)_2$ addition of 10% (namely 6.2% of Pb), they were 37.6 ppm and 2.1%, respectively, indicating the lead was effectively immobilized in the mine tailings-based binders. At the $Pb(NO_3)_2$ additions less than 5%, the Pb concentration in the leachate was lower than 5 ppm, indicating the mine tailings-based binders can be considered as non- hazardous material according to the USEPA regulatory levels. In addition, both the Pb concentration in the leachate and the percentage of leached Pb to total Pb increased slightly at the $Pb(NO_3)_2$ addition less than 5%, but increased sharply at that higher than 5%. It suggests that the immobilization forms of lead ions in alkali-activated mine tailings-based binders might be different as increasing lead concentrations.

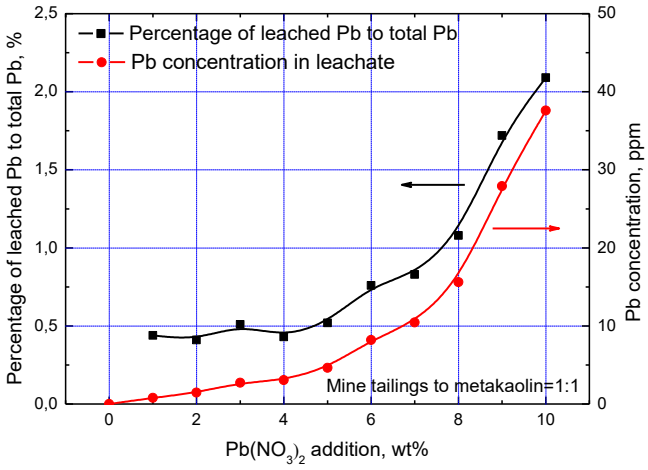

Figure 3.6.1. TCLP tests of Pb for the binders synthesized with various $Pb(NO_3)_2$ additions

Figure 3.6.2 showed the TCLP tests of lead for the binders synthesized with different percentages of mine tailings in the raw materials of mine tailings and metakaolin, in which the $Pb(NO_3)_2$ addition was 2%. The Pb concentration in the leachate was lower than 2 ppm, and not correlated with the contents of mine tailings. As reported in Part I, the difference in percentages of mine tailings in the raw materials, namely from 100% to 50%, resulted in various combinations of geopolymer gel, belite, lead silicate glass and CSH gel in the formed binders. However, these variations hardly affected the Pb immobilization efficiency, suggesting the multiple immobilization forms of lead. Furthermore, according to the Pb concentration in the leachate, it can be calculated that the leached Pb was less than 0.5% to the total Pb involved. It corresponds well with the previous TCLP tests that lead was successfully immobilized in the binders.

3.6.2 Mechanism of Immobilization

Figure 3.6.3 presented the ^{29}Si NMR spectra of the mine tailings-based binders synthesized with various $Pb(NO_3)_2$ additions. The spectra showed a broad band with the peak located around -88 ppm of chemical shift, indicating geopolymer and CSH gel are main components in the binders. As reported in literature of the NMR spectra, lead silicate crystals show sharp and narrow peaks, which are -84.2, -86.5 and -94.4 ppm in chemical shift for $PbSiO_3$, -94.3 and -96.6 ppm in chemical shift for H- and M-Pb_2SiO_4, and -77.5, -94.3 and -96 ppm in chemical shift for Pb_3SiO_7. Compared with the spectrum of binder with no $Pb(NO_3)_2$ addition, in the spectra of binders with $Pb(NO_3)_2$ additions of 2%, 3% and 6%, no sharp peak rose in the chemical shift range between -77.5 ppm to -96.6 ppm, which is characteristic for lead silicate crystals. Therefore, lead silicate crystal is hardly formed in the alkali-activated mine tailings-based binders. And compared with the spectrum of binder with no $Pb(NO_3)_2$ addition, the spectra of binders with $Pb(NO_3)_2$ additions showed a left shift, particularly in the chemical shift range between -94 and -115 ppm. As increasing the $Pb(NO_3)_2$ addition, the higher shift of the spectra was observed. It indicates the formation of lead silicate glass compounds of high silicate ($PbO•nSiO_2$, n>3), which possess characteristic peaks in this chemical shift range. For example, the lead silicate glass of $PbO•3SiO_2$ and $PbO•6SiO_2$ have the peaks at -95 ppm, -106 ppm and -95

ppm, -107 ppm, respectively. In addition, lead silicate glass compounds of low silicate ($PbO•nSiO_2$, n<1) usually show characteristic peaks in the chemical shift range of -94 ppm and -75 ppm, in which no difference is observed among the spectra with and without $Pb(NO_3)_2$ additions. It suggests that lead silicate glass compounds of low silicate were not formed in the alkali-activated mine tailings-based binders, which might be due to the excessive dosage of Na_2SiO_3 when reacting with $Pb(NO_3)_2$ in the synthesizing process.

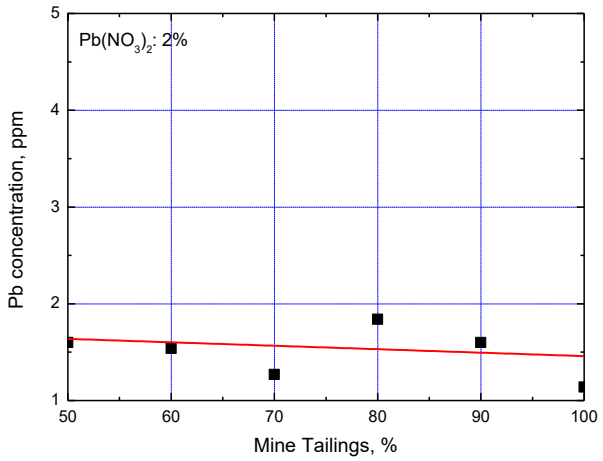

Figure 3.6.2. TCLP tests of lead for the binders synthesized with different contents of mine tailings

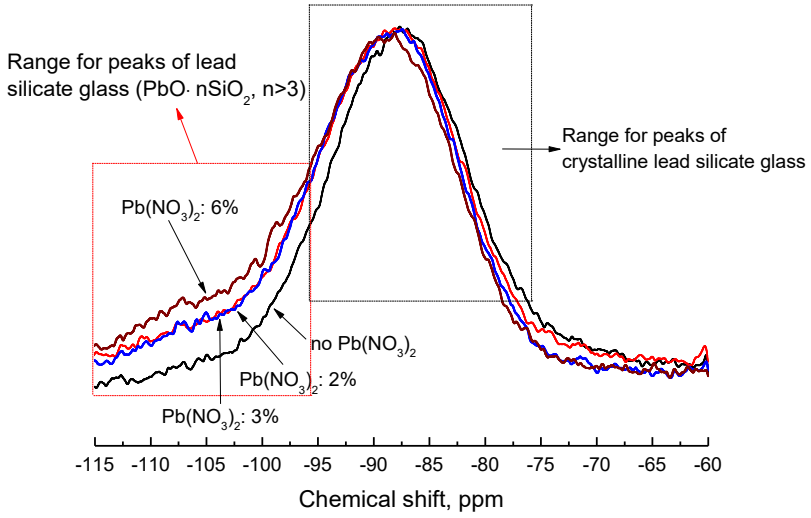

Figure 3.6.3. NMR spectra of geopolymer with different content of $Pb(NO_3)_2$

However, the ^{29}Si NMR spectra reflect the Pb coordination from the analysis of silicate species, rather than the Pb compounds directly. Thus the Pb 4f XPS spectra of mine tailings-based binders synthesized with 2% and 6% of $Pb(NO_3)_2$ additions (mine tailings to

metakaolin=1:1), and 2% of $Pb(NO_3)_2$ addition without metakaolin were presented in Figure 3.6.4. As reported in the formation of lead silicate compounds, for high lead content (mol_{Pb}:mol_{Si}>31%), lead covalently bonds to oxygen to form PbO_n pyramidal units with silicate, which is named lead in network. For low lead content, silicates form a three-dimensional silicon structure, while *PbO* mainly plays the role of modifier in the silicate glass. And for lead in silicate glass, the peaks at different binding energies indicate the different ratios of *PbO* to SiO_2. In Figure 3.6.4, the binding energies of Pb $4f^{7/2}$ and Pb $4f^{5/2}$ fitted peaks at 138.2 eV and 143.2 eV for lead in network, 138.6 eV and 143.6 eV for lead in silicate glass with the form of $PbO•4SiO_2$, as well as 139 eV and 144 eV for lead in silicate glass with the form of $PbO•7SiO_2$. The spectra of binders synthesized with metakaolin and mine tailings (2% and 6% of $Pb(NO_3)_2$) showed resembling peaks for lead in network and lead silicate glass of $PbO•4SiO_2$, and the intensities were higher at 6% of $Pb(NO_3)_2$. And the spectrum of the binder synthesized with only mine tailings (2% $Pb(NO_3)_2$) showed peaks mainly for lead silicate glass of $PbO•7SiO_2$.

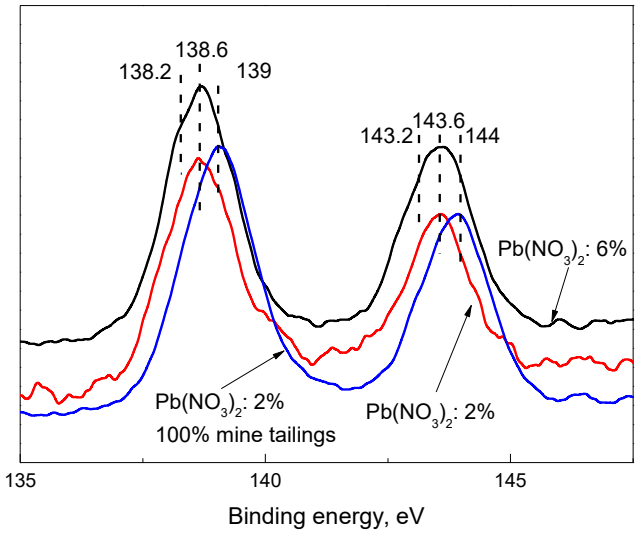

Figure 3.6.4. XPS spectra of different alkali-activated binders

After deconvolution of the Pb 4f XPS spectra of mine tailings-based binders, the fractions of lead in network and lead in silicate glass were obtained and given in Table 3.6.1. The fraction of lead in network in the binder synthesized with only mine tailings was 7.3%, which is much lower than those synthesized with mine tailings and metakaolin mixtures. As discussed in part I, CSH gel was the main phase in the binder synthesized with only mine tailings, while geopolymer gel was the main one in the binders synthesized with mine tailings and metakaolin mixtures. And ratio of lead in network increased with increasing the geopolymer gel phase, thus geopolymer gel induced the formation of lead in network, even though the lead content was very low. In the binder synthesized with mine tailings to metakaolin=1:1 and 2% of $Pb(NO_3)_2$, the fractions of lead in network, $PbO•4SiO_2$ and $PbO•7SiO_2$ were 41.75%, 3.89% and 54.37%, respectively. While in the binder of 6% of $Pb(NO_3)_2$, the fraction of $PbO•4SiO_2$ increased to 41.01%, and the fractions of lead in network and $PbO•7SiO_2$ decreased to 33.03% and 25.96%, respectively, which should be

attributed to the decrease of geopolymer gel phase and the increase of *PbO* to SiO_2 ratio. In the binder synthesized with only mine tailings and 2% $Pb(NO_3)_2$, the fraction of $PbO•7SiO_2$ was as high as 92.26%, confirming that SiO_2 in the alkaline activation process was excessive and a low amount of geopolymer gel was formed in this binder. If correlated the fractions of lead immobilization forms to the results of TCLP tests (Figure 3.6.1 and 3.6.2), it can be noted that 1) lead was immobilized well at low content and 2) the immobilization efficiency was higher when lead in network. Therefore, the leached lead was low at the synthesizing conditions of 2% $Pb(NO_3)_2$ addition and various mine tailings to metakaolin ratios. And the leached lead increased as increasing the $Pb(NO_3)_2$ additions, because more lead in silicate glass were formed.

Figure 3.6.5 showed the SEM and X-ray microanalytical mapping images for Pb, Ca and Si elements of the binder synthesized with metakaolin to mine tailings=1:1 and 6% of $Pb(NO_3)_2$ addition. In this binder, phases of geopolymer gel and CSH gel are the main components. The Pb was generally dispersed throughout the binder, but concentrated in areas that were full of Si and lack of Ca. It suggests the formation of Pb compounds with geopolymer gel and silicate glass, rather than with CSH gel, which is in good agreement with the NMR and XPS analysis.

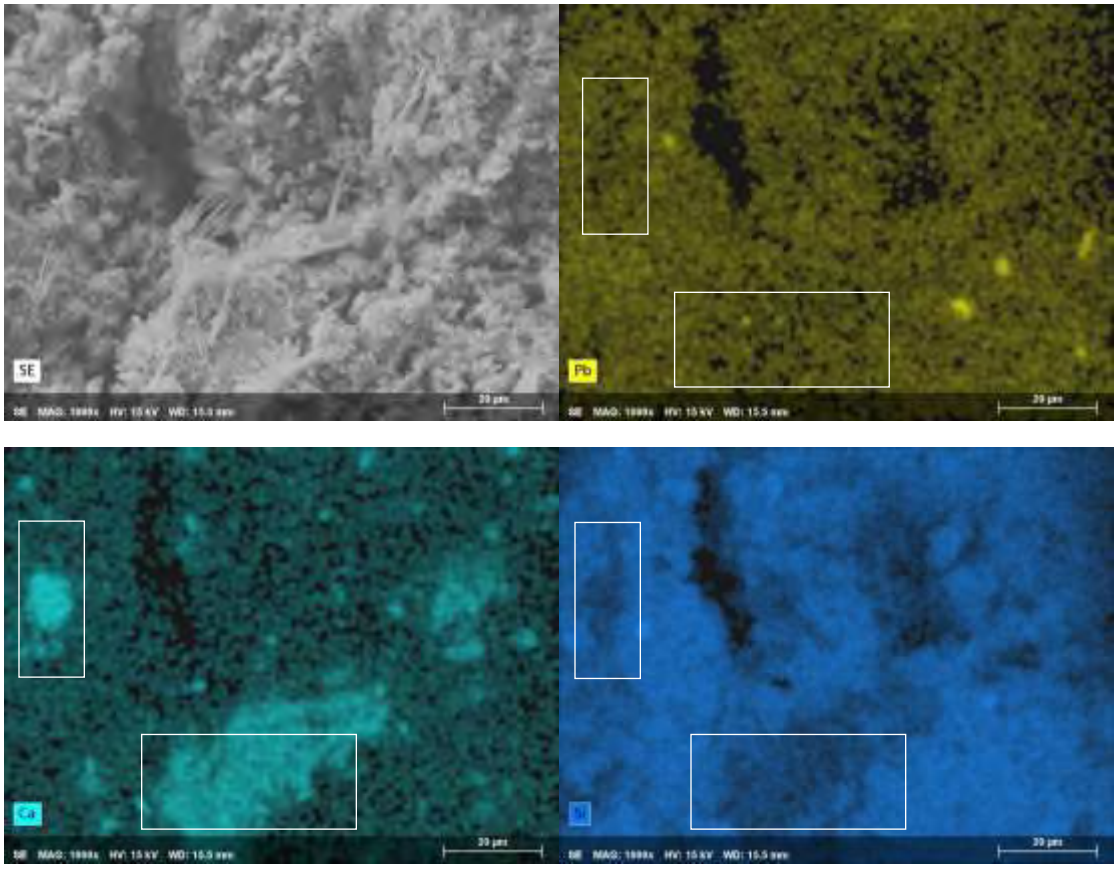

Figure 3.6.5. SEM and X-ray microanalytical mapping images for Pb, Ca and Si elements

Table 3.6.1. Deconvolution of Pb 4f XPS spectra of mine tailings-based binders

Binders	Lead in network	Lead in silicate glass	
		$PbO•4SiO_2$	$PbO•7SiO_2$
Metakaolin to mine tailings=1:1, 2% $Pb(NO_3)_2$	41.75%	3.89%	54.37%
Metakaolin to mine tailings=1:1, 6% $Pb(NO_3)_2$	33.03%	41.01%	25.96%
Only mine tailings, 2% $Pb(NO_3)_2$	7.30%	0.44%	92.26%

Some studies used zeta potential measurements to characterize the structure of alkali-activated products. For example, geopolymer gel was reported to be charged negatively when using geopolymers as adsorbents for ammonium and heavy metal ions. And for OPC, the more involvement of oxides (e.g., SiO_2), the more negative charge was. Figure 3.6.6 gave the zeta potential of alkali-activated mine tailings-based binders as a function of pH. Zeta potentials of the binders followed the behavior of oxides, in which decreased as increasing the pH, due to the protonation or deprotonation of surface groups as shown in equations (1) and (2). And as increasing the addition of $Pb(NO_3)_2$, the zeta potentials became more negative, particularly at a pH higher than 6. For the binders without $Pb(NO_3)_2$ to that of 2%, 4% and 6% additions, the point of zero charge (PZC) decreased from pH 7.2 to pH 6.5, pH 5.9 and pH 4.9, respectively. It suggests that the formation of PbO_n in both network and silicate glass results in more negative charge of the binders. If correlate the zeta potential results with the results of TCLP tests for binders synthesized with various $Pb(NO_3)_2$ additions (Figure 3.6.1), no increase of lead immobilization was observed for more negatively charged binders. Thus the immobilization form of charge balance was not observed.

$$M - OH + OH^- \rightarrow M - O^- + H_2O \quad (1)$$

$$M - OH + H^+ \rightarrow M - OH_2^+ \quad (2)$$

Figure 3.6.7 gave the Al 2p XPS spectra for the binders synthesized with various $Pb(NO_3)_2$ additions. Compared with the binder without $Pb(NO_3)_2$, the peaks in the spectra shifted right from 73.88 eV to 74.03 eV and 74.21 eV, respectively, in the binders synthesized with 2% and 6% $Pb(NO_3)_2$ additions. This shift is so little that it indicates the distribution of electronic-charge cloud was influenced by the addition of $Pb(NO_3)_2$, rather than suggests the change of Al valence. And the right shift for the spectra in binders at higher $Pb(NO_3)_2$ additions indicates the network of *PbO* to aluminum oxide tetrahedrals. It confirms with the Pb 4f XPS results that part of Pb was immobilized in the form of lead in network.

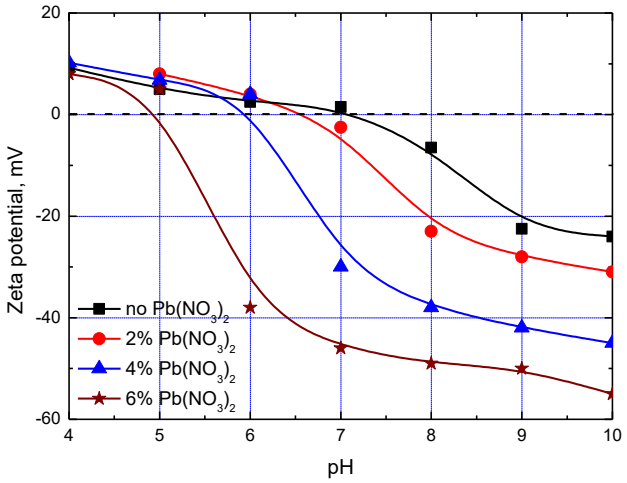

Figure 3.6.6. Zeta potential of mine tailings-based binders at various $Pb(NO_3)_2$ additions

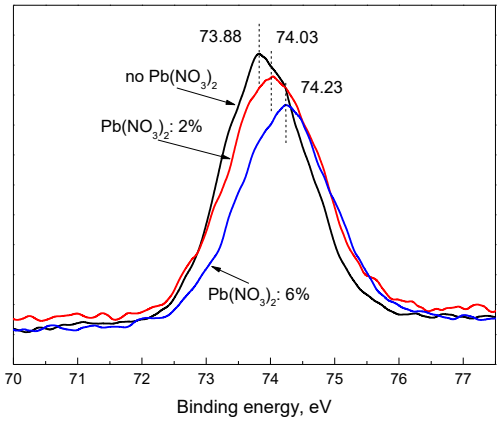

Figure 3.6.7. Al 2p XPS spectra of the binders synthesized with various $Pb(NO_3)_2$ additions

CHAPTER 4

Conclusions

Conclusions

1) Metakaolin-based geopolymers can been synthesized at Si/Al ratios from 1:1 to 5:1, and the satisfactory compressive strength was obtained. High contents of crystalline zeolitic nuclei ($Q^4(4Al)$) are formed at Si/Al ratio of 1:1, and high contents of silicate derivatives are formed at Si/Al ratios higher than 3:1.

2) Quartz sand can form combination by several micrometers around quartz particle, which associates them to geopolymeric gel as filler materials in metakaolin geopolymer. In metakaolin geopolymers synthesized with quartz sand of various size ranges, the smaller is the particle size, the higher is the particle surface involved in the formation of combination, thus higher fractions of $Q^4(2Al)$ and $Q^4(1Al)$ are observed in their micro-structures.

3) Dehydroxylation and recrystallization take place in heating kaolinite at moderate temperature (550-800 °C) and high temperature (850-950 °C), respectively. The joint effects of dehydroxylation and recrystallization determine the reactivity of metakaolin in geopolymerization reactions and mechanical properties of geopolymers, rather than the only Al^{VI} content.

4) Geothermal clay can be used to prepare geopolymer without calcination. In activating geothermal clay to synthesize geopolymers, Na_2SiO_3 and NaOH tend to play the roles of geopolymeric gel formation and aluminosilicate dissolution, respectively. High water content leads to porous structure and low compressive strength in geothermal clay-based geopolymers

5) Mine tailings rich in dolomite, calcite, kaolinite and quartz are consolidated into binders of compressive strength from 1.2 MPa to 17.3 MPa through alkaline activation. In the alkaline activation process, geopolymer gel, belite, lead silicate glass and calcium silicate hydrate (C-S-H) gel are formed. These species convert among each other as the addition of metakaolin or $Pb(NO_3)_2$ into the syntheses.

6) By mixing metakaolin into the mine tailings from 0 to 50%, tetrahedral Si coordination of geopolymer gel in the binders increases from 33.92% to 79.45%. Thus the binder is formed with more homogeneous structure and higher compressive strength. With the addition of $Pb(NO_3)_2$, compressive strength of the binders shows the three steps change at $Pb(NO_3)_2$ amounts of 0-2%, 3-6% and 9-10%. When the $Pb(NO_3)_2$ addition is less than 6%, the formed lead silicate glass enhances the compressive strength of the binders at its low quantity (e.g., 2%), but weakens that at its high quantity. When the $Pb(NO_3)_2$ addition is higher than 6%, the amount of geopolymer gel in the binders reduces, so that their compressive strength decreases.

7) Through synthesizing alkali-activated mine tailings-based binders, lead ions are well immobilized. At low $Pb(NO_3)_2$ additions (<5%), 99.5% of lead is immobilized in the binders, and they are non-hazardous materials because the concentration of lead in the leachate is less than 5 ppm. At extended $Pb(NO_3)_2$ additions (e.g. 10%), higher than 97.9% of lead is immobilized in the binders. This immobilization is independent of the geopolymer and C-S-H phases in the mine tailings-based binders.

8) In binders synthesized with only mine tailings and 2% $Pb(NO_3)_2$ addition, 92.26% immobilized lead is in the form of lead in silicate glass of $PbO•7SiO_2$, because of the low formation of geopolymer gel phase and the excessive content of Na_2SiO_3. With mine tailings to metakaolin=1:1 in the raw aluminosilicates and 2% $Pb(NO_3)_2$ addition, lead is immobilized in the forms of lead in network (41.75%), lead in silicate of $PbO•4SiO_2$ (3.89%) and $PbO•7SiO_2$ (54.37%), respectively. With increasing the $Pb(NO_3)_2$ addition to 6%, more $PbO•4SiO_2$ is formed, while the fractions of lead in network and $PbO•7SiO_2$ decrease, due to that a lower geopolymer gel phase is formed and more PbO is involved in the alkaline activation process.

9) SEM and X-ray microanalytical mapping images verify the concentration of immobilized lead with Si, rather than Ca. Zeta potential measurements of the binders synthesized with various $Pb(NO_3)_2$ additions suggest the formation of PbO_n in both network and silicate glass results in a more negative charge of them.

Recommendations for future work

In the thesis work, the mechanisms of the consolidation of mine tailings and immobilization of heavy metals were studied fundamentally. In the future work, we recommend encountering one trial tailing pond from mineral processing industries (e.g., flotation) for the application of this technology. The dosages of alkalis, curing condition, economical calculation and environmental estimation are recommended to test for this application.

Reference

Acosta, J.A., Faz, A., Martínez-Martínez, S., Zornoza, R., Carmona, D.M., Kabas, S., 2011. Multivariate statistical and GIS-based approach to evaluate heavy metals behavior in mine sites for future reclamation. J. Geochemical Explor. 109, 8-17.

Ahmari, S., Zhang, L., 2012. Production of eco-friendly bricks from copper mine tailings through geopolymerization. Constr. Build. Mater. 29, 323-331.

Barsoum, M.W., Ganguly, A., Hug, G., 2006. Microstructural evidence of reconstituted limestone blocks in the Great Pyramids of Egypt. J. Am. Ceram. Soc. 89, 3788-3796.

Bergaya, F., Lagaly, G., 2006. General introductions: Clays, clay minerals and clay science, Handbook of clay science. Elsevier, Amsterdam

Bethell, P.J., 2012. Dealing with the challenges facing global fine coal processing. Challenges Fine Coal Process. Dewatering, Dispos. 33-45.

Cheng, T.W., Chiu, J.P., 2003. Fire-resistant geopolymer produce by granulated blast furnace slag. Miner. Eng. 16, 205-210.

Cooling, D.J., Clenister, D.J., 1992. Practical aspects of dry residue disposal, Light Metals. 1992, 25-31.

Criado, M., Fernández-Jiménez, a., Palomo, a., 2007. Alkali activation of fly ash: Effect of the SiO_2/Na_2O ratio Part I: FTIR study. Microporous Mesoporous Mater. 106, 180-191.

Davidovits, J., 1996. Method for obtaining a geopolymeric binder allowing to stabilize, solidify and consolidate toxic or waste materials. Washington. U.S. Patent No. 5,539, 140.

Dong, J., Yang, Q., Sun, L., Zeng, Q., Liu, S., Pan, J., Liu, X., 2011. Assessing the concentration and potential dietary risk of heavy metals in vegetables at a Pb/Zn mine site, China. Environ. Earth Sci. 64, 1317-1321.

Duxson, P., Fernández-Jiménez, A., Provis, J.L., Lukey, G.C., Palomo, A., van Deventer, J.S.J., 2007. Geopolymer technology: the current state of the art. J. Mater. Sci. 42, 2917-2933.

Duxson, P., Mallicoat, S.W., Lukey, G.C., Kriven, W.M., van Deventer, J.S.J., 2007. The effect of alkali and Si/Al ratio on the development of mechanical properties of metakaolin-based geopolymers. Colloids Surfaces A Physicochem. Eng. Asp. 292, 8-20.

Duxson, P., Provis, J.L., Lukey, G.C., Separovic, F., van Deventer, J.S.J., 2005. ^{29}Si NMR study of structural ordering in aluminosilicate geopolymer gels. Langmuir 21, 3028-3036.

El-Eswed, B.I., Yousef, R.I., Alshaaer, M., Hamadneh, I., Al-Gharabli, S.I., Khalili, F., 2015. Stabilization/solidification of heavy metals in kaolin/zeolite based geopolymers. Int. J. Miner. Process. 137, 34-42.

Fernández-Jiménez, A., Palomo, A., Criado, M., 2006. Alkali activated fly ash binders. A comparative study between sodium and potassium activators. Mater. Construcción 56, 51-65.

Fernández-Jiménez, A., Zibouche, F., Boudissa, N., García-Lodeiro, I., Abadlia, M.T., Palomo, A., 2013. "Metakaolin-Slag-Clinker Blends." The Role of Na^+ or K^+ as Alkaline Activators of Theses Ternary Blends. J. Am. Ceram. Soc. 96, 1991-1998.

Gentes, M.L., Waldner, C., Papp, Z., Smits, J.E.G., 2006. Effects of oil sands tailings compounds and harsh weather on mortality rates, growth and detoxification efforts in nestling tree swallows (Tachycineta bicolor). Environ. Pollut. 142, 24-33.

Giergiczny, Z., Król, A., 2008. Immobilization of heavy metals (Pb, Cu, Cr, Zn, Cd, Mn) in the mineral additions containing concrete composites. J. Hazard. Mater. 160, 247-255.

Guo, B., Pan, D., Liu, B., Volinsky, A.A., Fincan, M., Du, J., Zhang, S., 2017. Immobilization mechanism of Pb in fly ash-based geopolymer. Constr. Build. Mater. 134, 123-130.

Ivan Diaz-Loya, E., Allouche, E.N., Vaidya, S., 2011. Mechanical Properties of Fly-Ash-Based Geopolymer Concrete. ACI Mater. J. 108, 300-306.

Jung, S.J., Clark, C.C., 1995. Experimental determination of rheologic properties of high-density paste fill. Trans. Min. Metall. Explor. Inc. 298, 1892-1896.

Khale, D., Chaudhary, R., 2007. Mechanism of geopolymerization and factors influencing its development: A review. J. Mater. Sci. 42, 729-746.

Kuenzel, C., Neville, T.P., Donatello. S., Vandeperre, L., Boccaccini, A.R., Chesseman, C.R., 2013. Influence of metakaolin characteristics on the mechanical properties of geopolymers. Appl. Clay Sci. 83, 308-314.

Kuranchie, F.A., Shukla, S.K., Habibi, D., 2016. Utilisation of iron ore mine tailings for the production of geopolymer bricks. Int. J. Mining, Reclam. Environ. 30, 92-114.

Lee, M.R., Correa, J.A., 2005. Effects of copper mine tailings disposal on littoral meiofaunal assemblages in the Atacama region of northern Chile. Mar. Environ. Res. 59, 1-18.

Lee, S., Van Riessen, A., Chon, C.M., Kang, N.H., Jou, H.T., Kim, Y.J., 2016. Impact of activator type on the immobilisation of lead in fly ash-based geopolymer. J. Hazard. Mater. 305, 59-66.

Lee, W.K.W., van Deventer, J.S.J., 2002. Structural reorganisation of class F fly ash in alkaline silicate solutions. Colloids Surfaces A Physicochem. Eng. Asp. 211, 49-66.

McCormick, A. V., Bell, A.T., Radke, C.J., 1989. Multinuclear NMR investigation of the formation of aluminosilicate anions. J. Phys. Chem. 93, 1741-1744.

Nikolić, V., Komljenović, M., Marjanović, N., Baščarević, Z., Petrović, R., 2014. Lead immobilization by geopolymers based on mechanically activated fly ash. Ceram. Int. 40, 8479-8488.

Ortega-Rivas, E., 2007. Hydrocyclones, Ullmann's Encyclopedia of Industrial Chemistry. Wiley Online Library.

Palacios, M., Palomo, A., 2004. Alkali-activated fly ash matrices for lead immobilisation: a comparison of different leaching tests. Adv. Cem. Res. 16, 137-144.

Panias, D., Giannopoulou, I., 2007. The geopolymerization technology for the utilization of mining and metallurgical solid wastes, in: Proceedings of European Metallurgical Conference, Dusseldorf, Germany. pp. 625-640.

Perera, D.S., Aly, Z., Vance, E.R., Mizumo, M., 2005. Immobilization of Pb in a geopolymer matrix. J. Am. Ceram. Soc. 88, 2586-2588.

Phair, J.W., van Deventer, J.S.J., 2001. Effect of silicate activator pH on the leaching and material characteristics of waste-based inorganic polymers. Miner. Eng. 14, 289-304.

Phair, J.W., van Deventer, J.S.J., Smith, J.D., 2004. Effect of Al source and alkali activation on Pb and Cu immobilisation in fly-ash based "geopolymers." Appl. Geochemistry 19, 423-434.

Power, G., Gräfe, M., Klauber, C., 2011. Bauxite residue issues: I. Current management, disposal and storage practices. Hydrometallurgy 108, 33-45.

Provis, J.L., Lukey, G.C., van Deventer, J.S.J., 2005. Do geopolymers actually contain nanocrystalline zeolites? a reexamination of existing results. Chem. Mater. 17, 3075-3085.

Rahier, H., Van Mele, B., Biesemans, M., Wastiels, J., Wu, X., 1996. Low-temperature synthesized aluminosilicate glasses. J. Mater. Sci. 31, 71-79.

Rao, F., Liu, Q., 2015. Geopolymerization and its potential application in mine tailings consolidation: a review. Miner. Process. Extr. Metall. Rev. 36, 399-409.

Rashed, M.N., 2010. Monitoring of contaminated toxic and heavy metals, from mine tailings through age accumulation, in soil and some wild plants at Southeast Egypt. J. Hazard. Mater. 178, 739-746.

Rees, C.A., Provis, J.L., Lukey, G.C., van Deventer, J.S.J., 2007. In situ ATR-FTIR study of the early stages of fly ash geopolymer gel formation. Langmuir 23, 9076-9082.

Renault, S., Zwiazek, J.J., Fung, M., Tuttle, S., 2000. Germination, growth and gas exchange of selected boreal forest seedlings in soil containing oil sands tailings. Environ. Pollut. 107, 357-365.

Rocha, J., Klinowski, J., 1990. ^{29}Si and ^{27}Al magic-angle-spinning NMR studies of the thermal transformation of kaolinite. Phys. Chem. Miner. 17, 179-186.

Rowles, M., O'connor, B., 2003. Chemical optimisation of the compressive strength of aluminosilicate geopolymers synthesised by sodium silicate activation of metakaolinite. J. Mater. Chem. 13, 1161-1165.

Sagoe-Crentsil, K., Weng, L., 2007. Dissolution processes, hydrolysis and condensation reactions during geopolymer synthesis: Part II. High Si/Al ratio systems. J. Mater. Sci. 42, 3007-3014.

Silva, P. De, Sagoe-Crenstil, K., Sirivivatnanon, V., 2007. Kinetics of geopolymerization: Role of Al_2O_3 and SiO_2. Cem. Concr. Res. 37, 512-518.

Singh, P.S., Bastow, T., Trigg, M., 2005. Structural studies of geopolymers by ^{29}Si and ^{27}Al MAS-NMR. J. Mater. Sci. 40, 3951-3961.

van Jaarsveld, J.G.S., van Deventer, J.S.J., Lorenzen, L., 1997. The potential use of geopolymeric materials to immobilise toxic metals: Part I. Theory and applications. Miner. Eng. 10, 659-669.

Wan, Q., Rao, F., Song, S., 2017. Reexamining calcination of kaolinite for the synthesis of metakaolin geopolymers-roles of dehydroxylation and recrystallization. J. Non. Cryst. Solids 460, 74-80.

Wang, H., Li, H., Yan, F., 2005. Synthesis and mechanical properties of metakaolinite-based geopolymer. Colloids Surfaces A Physicochem. Eng. Asp. 268, 1-6.

White, C.E., Provis, J.L., Proffen, T., van Deventer, J.S.J., 2010. The effects of temperature on the local structure of metakaolin-based geopolymer binder: A neutron pair distribution function investigation. J. Am. Ceram. Soc. 93, 3486-3492.

Wills, B.A., Napier-Munn, T., 2006. Mineral processing technology: An introduction to the practical aspects of ore treatment and mineral. Maryl. Height. MO Elsevier Sci. Technol. Books.

Xie, J., Kayali, O., 2014. Effect of initial water content and curing moisture conditions on the development of fly ash-based geopolymers in heat and ambient temperature. Constr. Build. Mater. 67, 20-28.

Xiong, C.J., Ban, C.H., Pei, X., Fang, Z., 2004. 'International workshop on sustainable development and concrete technology. China Build. Mater. Acad. PRC 309-317.

Xu, H., van Deventer, J.S.J., 2002. Geopolymerisation of multiple minerals. Miner. Eng. 15, 1131-1139.

Xu, H., van Deventer, J.S.J., 2000. The geopolymerisation of alumino-silicate minerals. Int. J. Miner. Process. 59, 247-266.

Yalcin, T., 1996. Tailings disposal using flocculant-assisted hydrocyclones. CIM Bull. 89, 98-100.

Ye, J., Zhang, W., Shi, D., 2014. Effect of elevated temperature on the properties of geopolymer synthesized from calcined ore-dressing tailing of bauxite and ground-granulated blast furnace slag. Constr. Build. Mater. 69, 41-48.

Zhang, J., Provis, J.L., Feng, D., van Deventer, J.S.J., 2008. Geopolymers for immobilization of Cr^{6+}, Cd^{2+}, and Pb^{2+}. J. Hazard. Mater. 157, 587-598.

Zhang, P., Stana, R., 2010. Phosphogypsum management and utilization: a review of research and industry practice, in: Conference Paper, AFA Int.'l Tehnical Conference & Exhibition, Tunisia.

Zhang, Y., Sun, W., C, Q., Lin, C., 2007. Synthesis and heavy metal immobilization behaviors of slag based geopolymer. J. Hazard. Mater. 143, 206-213.

Zhang, Y., Sun W., Li, Z., 2010. Composition design and microstructural characterization of calcined kaolin-based geopolymer cement. Appl. Clay Sci. 47, 271-275.

Zhou, J., Dang, Z., Cai, M., Liu. C., Soil heavy metal pollution around the Dabaoshan mine, Guangdong province, China. Pedosphere 17, 588-594.

APPENDIX I

List of Articles published and Submitted during the Ph.D. Studying

1. Articles published in international journals during the Ph. D. studying

1) **Wan Q.**, Rao F., Song S., Escudero R., Morales R., León-Patiño A.C., Zhang Y. Geopolymerization reaction, microstructure and simulation of metakaolin-based geopolymers at extended Si/Al ratios. Cement and Concrete Composites, 2017, 79: 45-52.

2) **Wan Q.**, Rao F., Song S., Cholico-González D.F., Ortiz N. Combination formation in the reinforcement of metakaolin geopolymers with quartz sand. Cement and Concrete Composites, 2017, 80: 115-122.

3) **Wan Q.**, Rao F., Song S., León-Patiño C.A. Geothermal clay-based geopolymer binders: Synthesis and microstructural characterization. Applied Clay Science, 2017, 146: 223-229.

4) **Wan Q.**, Rao F., Song S. Reexamining calcination of kaolinite for the synthesis of metakaolin geopolymers-roles of dehydroxylation and recrystallization. Journal of Non-Crystalline Solids, 2017, 460: 74-80.

2. Articles submitted to international journals during the Ph. D. studying

1) **Wan Q.**, Rao F., Song S., Xie X., Tong X. Consolidation of Mine Tailings and Heavy Metal Retention by Alkali Activation I. Microstructure of the Binders. Journal of Hazardous Materials, 2017.

2) **Wan Q.**, Rao F., Song S., Xie X., Tong X. Consolidation of Mine Tailings and Heavy Metal Retention by Geopolymerization II. Quantitative Analysis of the Immobilization Forms. Journal of Hazardous Materials, 2017.

APPENDIX II

Articles Published on Other Subjects

Articles Published on Other Subjects:

Jia F., Yang B., **Wan Q.**, Song S. Variation of interlayer binding energy of muscovite in its swelling. Computational Materials Science, 2017, 132: 74-80.

Cement and Concrete Composites 79 (2017) 45–52

Contents lists available at ScienceDirect

Cement and Concrete Composites

journal homepage: www.elsevier.com/locate/cemconcomp

Geopolymerization reaction, microstructure and simulation of metakaolin-based geopolymers at extended Si/Al ratios

Qian Wan [a, b], Feng Rao [a, *], Shaoxian Song [b, **], Ramiro E. García [a], Ricardo M. Estrella [a], Carlos L. Patiño [a], Yimin Zhang [b]

[a] Instituto de Investigación en Metalurgia y Materiales, Universidad Michoacana de San Nicolás de Hidalgo, Ed. "U", Ciudad Universitaria, Morelia, Michoacán, 58030, Mexico
[b] School of Resources and Environmental Engineering, Wuhan University of Technology, Luoshi Road 122, Wuhan, Hubei, 430070, China

ARTICLE INFO

Article history:
Received 21 January 2016
Received in revised form
31 December 2016
Accepted 26 January 2017
Available online 1 February 2017

Keywords:
Geopolymer
Si/Al ratios
Silica fume
N-A-S-H gel
Mine tailings

ABSTRACT

Metakaolin-based geopolymers were synthesized at Si/Al ratios of 1:1, 1.5:1, 2:1, 3:1, 4:1, and 5:1 by using silica fume as silica corrector to alter Si ratios. The microstructure and strength of these geopolymers were characterized through XRD, SEM, NMR and compressive strength measurements. The dissolving rates of Al and Si species in geopolymerization were measured, and freeze-dried N-A-S-H gel was characterized by FTIR spectra. Modelling and simulation were employed to calculate the binding energy of one Si atom and the total energy of geopolymers formed at various Si/Al ratios. At Si/Al ratio of 2:1, high concentrations of Si and Al species are dissolved from precursors, high contents of Si-O-T linkages are formed and the geopolymer is of high compressive strength. The mechanical strength of geopolymers at various Si/Al ratios is dependent on the formation of N-A-S-H gel, rather than the zeolitic nuclei or silicate derivatives. This study might provide fundamentals for the geopolymerization of mine tailings, which usually possess high Si/Al ratios.

1. Introduction

In the 1970s, Davidovits coined the term geopolymer to describe alkaline- or alkali-silicate- activated aluminosilicate binders with three-dimensional (3D) amorphous micro-structures of composition $M_2O{\bullet}mAl_2O_3{\bullet}nSiO_2$, where M represents alkali metals, $m \approx 1$ and $2 \leq n \leq 6$ [1]. Geopolymerization is an integrated process for the synthesis of geopolymers, which involves the reactions between two parts of raw materials: aluminosilicates and alkali activators. Researchers addressed studies in synthesizing geopolymers about 1) types of raw aluminosilicate materials and alkali activators; 2) mechanical properties and micro-structures of final geopolymer products; 3) curing conditions such as temperature, time, relative humidity, and in applying geopolymers about 4) the replacement for Portland cement; 5) special applications such as anti-corrosive cement and fireproof materials [2]. Almost all these studies concerned either the geopolymerization reactions or the geopolymer characteristics. However, as pointed out by recent reviews, the intrinsic chemical reactions in geopolymerization or the thermochemical nature of sodium-alumino-silicate-hydrate (N-A-S-H, geopolymer gel phase) and geopolymers are still being questioned [3-5]. The problems in studying this issue might come from the coexist of reacted and non-reacted raw aluminosilicates in geopolymers, the amorphous structure of geopolymers, and the simultaneous occurrence of various phase transformations such as dissolution, N-A-S-H gel formation and condensation in geopolymer formation. Further, a few of studies simulated the energy status of geopolymers on molecular level. [6] employed density functional theory (DFT)-based coarse-grained Monte Carlo (CGMC) modelling to simulate the geopolymerization and to determine the molecular interaction energies controlling this process, and stated that silica content was critical in determining the molecular mechanisms occurring during geopolymerization. Zhang et al [7] tried to use semi-empirical AM1 calculations to understand the molecular mechanism of geopolymerization. However, Provis et al [8] disagreed this work about the proposed states of alumina and silicate species. Recently, Kupwade-Patil et al [9] used DFT, molecular mechanics and molecular dynamics to calculate the interaction energy of N-A-S-H and potassium-alumino-silicate-hydrate

* Corresponding author.
** Corresponding author.
E-mail addresses: fengrao@umich.mx (F. Rao), shaoxian@uaslp.mx (S. Song).

http://dx.doi.org/10.1016/j.cemconcomp.2017.01.014
0958-9465/

(K-A-S-H) geopolymer structures at different temperatures.

The amorphous geopolymer structure was initially proposed as polysialate (-Si-O-Al-O-), polysialate-siloxo (Si-O-Al-O-Si-O) and polysialate-disiloxo (Si-O-Al-O-Si-O-Si-O) structures when the Si/Al ratio is 1, 2 and 3, respectively [10]. However, it is inevitable to encounter geopolymers formed at a Si/Al ratio higher than 3 due to broad raw aluminosilicates with high Si content are involved and silicates are employed as alkaline activator [11-12]. Recently, geopolymerization has been suggested as potential technology to consolidate mine tailings and oil sands tailings [4]; which are mainly unpredictable aluminosilicate minerals covering a great range of Si/Al ratios. Further, Ahmari and Zhang [13] have used copper mine tailings to produce eco-friendly bricks for construction, which contains 64.8 wt% SiO_2 and 7.08 wt% Al_2O_3 (Si/Al ratio is around 8:1). And in literature, different Si/Al ratios have been reported to reach the maximum compressive strength of synthesized geopolymers. For instance, Duxson et al [14] reported a maximum strength at Si/Al ratio of 1.9 from metakaolin based geopolymers, however Silva et al [15] stated that of 1.7 from metakaolin/sodium silicate/sodium hydroxide geopolymer. And Rowles and O' Connor [16] even reported the maximum strength was 64 ± 3 MPa at a Si/Al/Na ratio of 2.5:1:1.3 in the synthesis of a metakaolin based geopolymer with sodium silicate as activator. This controversy is acceptable because different studies were differed in other synthesizing conditions such as alkali types, curing time and temperature, etc. However, the reaction nature of silicate precursor on N-A-S-H gel formation and geopolymer's strength was not consistent in literature either. Many researchers reported that the structural stability of geopolymers increased with the addition of silicates, due to the formation of long chain silicate oligomers and Al-O-Si complexes in the geopolymers [17-18]. While some studies stated that the addition of soluble silicates could not induce fundamental changes in the structure of geopolymers [11, 19-20]. A very high silicate concentration promotes the formation of Si-rich gels with a high percentage of bridge bonds that results in a more amorphous geopolymer with lower strength [21], and excess silicate could hinder water evaporation, thus impede geopolymer structure formation [22].

We attempted to synthesize metakaolin-based geopolymers with silica fume as silica corrector to change the Si/Al ratio, to characterize the reactions and microstructures and to simulate the energy status of geopolymers at various Si/Al ratios, so as to elucidate the impact of Si and Al contents in the formation of geopolymers. It might provide some guidance for the development of geopolymer products with good durability or targeted property from mine tailings, oil sands tailings and other industrial waste, as well as to understand the chemical nature of geopolymerization at extended Si/Al ratios.

2. Experimental

2.1. Materials

Kaolinite from Hubei Chemicals in China was used to prepare metakaolin through calcination at 800 °C in air for 5 h. Table 1 gives the chemical composition of metakaolin measured by X-ray Fluorescence (XRF). The mass ratios of SiO_2 and Al_2O_3 are close to those in pure metakaolin. Sodium hydroxide (NaOH, ACS reagent grade) was used as alkali activator. Silica fume (SiO_2>98%) purchased from Jinfeng Materials, China, was used as silica corrector to change Si/Al ratios. It is measured the particle size at 50% of cumulative undersize of 2.8 μm from a Shimadzu SALD-1100 laser diffraction analyzer.

Table 1
Chemical composition of metakaolin.

Component	SiO_2	Al_2O_3	K_2O	Fe_2O_3	TiO_2	MgO
wt%	52.8	43.7	1.2	0.6	0.5	0.2

2.2. Geopolymer synthesis

In the preparation of geopolymers at Si/Al ratios of 1:1, 1.5:1, 2:1, 3:1, 4:1 and 5:1, 0.5 mol metakaolin, 5.5 mol H_2O, 1 mol NaOH were used, while silica fume (silica corrector) of 0, 0.5, 1, 2, 3 and 4 mol was used, respectively. In all the six syntheses, the molar ratios of Na_2O/Al_2O_3 and Na_2O/H_2O were 1:1 and 1:12, the ratio of solid/liquid (S/L) was 1.12:1 g/ml. In a typical synthesis of Si/Al ratio at 2:1, 1 mol NaOH and 1 mol silica fume were first dissolved in

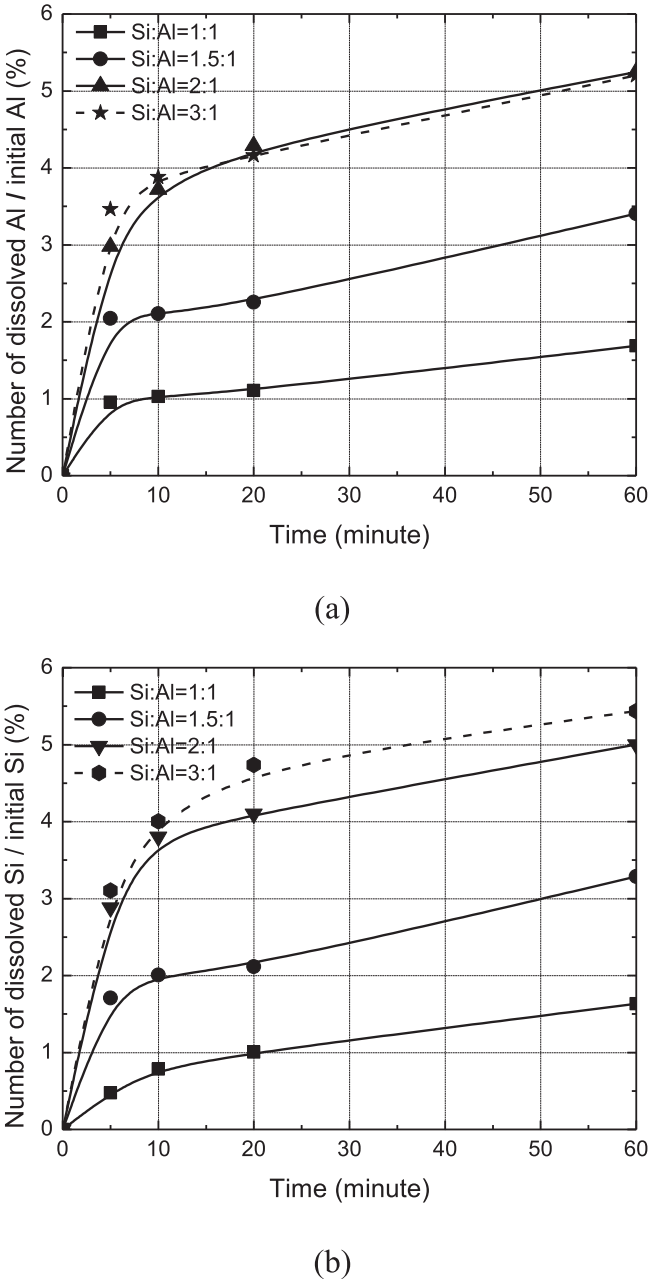

Fig. 1. Dissolution rates of Al (a) and Si (b) compounds from metakaolin.

5.5 mol (99 mL) H_2O to prepare alkaline activator. Then, the activator was mixed with 0.5 mol (111 g) metakaolin ($2SiO_2Al_2O_3$) for 5 min. After that, the mixture was poured into a cubic steel mold (50 mm × 50 mm × 50 mm). The mold was vibrated on a vibration table for 3 min to liberate the bubbles. Then, it was sealed for the curing process, in which it was first cured at 60 °C for 6 h and continued at room temperature for 7 days.

2.3. Characterization of Al, Si dissolution, N-A-S-H gel and geopolymer

The Al and Si dissolution, N-A-S-H gel and geopolymer of extended Si/Al ratios were characterized, in order to understand the chemical reactions in geopolymerizations. First, using the same dosages of metakaolin, silica fume (SiO_2), NaOH and H_2O as those used in geopolymer syntheses, the dissolved Si and Al concentrations were measured in separated tests. The alkaline activator (with silica fume) and metakaolin were mixed and agitated for a particular reaction time, namely 5, 10, 20 or 60 min, respectively. Then, 1.9 L water was added into the mixture and the suspension was agitated for 30 s. After that, the slurry was further diluted to avoid undesirable precipitation [23], filtered and analyzed for dissolved Al and Si compounds by atomic absorption spectroscopy (AAS). The dissolved Si concentrations were abstained from the measured concentrations minus added silica fume concentrations, while the dissolved Al concentrations were the measured ones. By using the same synthesizing conditions, N-A-S-H gels and geopolymers at extended Si/Al ratios were synthesized parallelly. Before curing, the N-A-S-H gels were freeze-dried and vacuum evaporated to prepare specimens for Fourier transform infrared spectroscopy (FTIR, Nexus, Thermo Nicolet, USA) measurements, in which they were milled and molded with potassium bromide (KBr). The geopolymers formed after curing were characterized by scanning electron microscopy (SEM, JEOL JSM-5610LV) and X-ray diffraction (XRD, Bruker D8) for morphology and microstructure, and mechanical tester (Hangzhou Xingo Technology, EHC-1300) for compressive strength. In the measurements of compressive strength, at least three specimens were tested and the average value was used. ^{29}Si nuclear magnetic resonance (NMR) spectra of geopolymers were obtained by using a NMR spectroscopy (Bruker AVANCE III) at 79.49 MHz. Powdered geopolymer specimens were packed into 7 mm ZrO_2 rotors. Spectra were acquired at spinning speeds of 12 kHz with peak positions referenced to an external standard of tetramethylsilane (TMS) and recorded with 1s delay time. The lack of spectral resolution for silicon in geopolymers has been overcome by adopting Gaussian peak deconvolution to separate and quantify $Q^n(mAl)$ species ($0 \le m \le n \le 4$) as previously reported [24]. NMR studies have shown that all silicon and aluminum sites are in tetrahedral coordination in geopolymers, thus $n = 4$ [25]. And the resonance of a $Q^4(mAl)$ center with the replacement of each aluminum by silicon is an approximate −5 ppm shift, with $Q^4(4Al)$, $Q^4(3Al)$, $Q^4(2Al)$, $Q^4(1Al)$, $Q^4(0Al)$ resonating at approximately −84, −89, −93, −99 and −107 ppm, respectively [26].

2.4. Modelling and simulation

Modelling and simulation were applied to geopolymer oligomers for the calculation of binding energies relative to silica atoms, and to geopolymers for the total energy. Si, Al, O and H atoms are

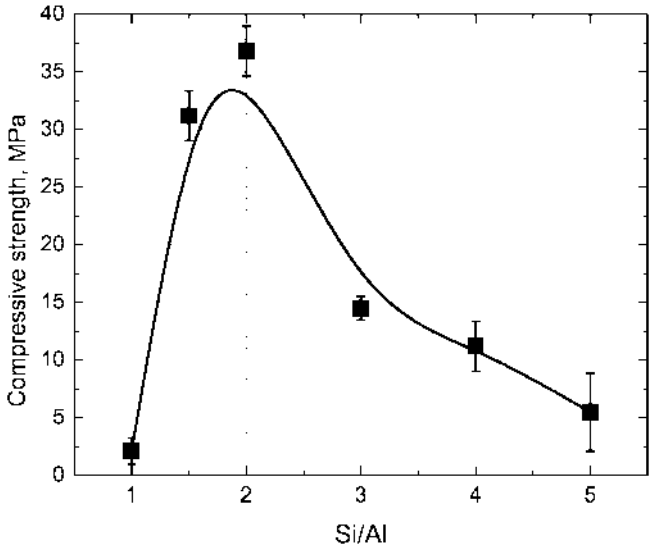

Fig. 3. Compressive strength of geopolymers as a function of Si/Al ratio.

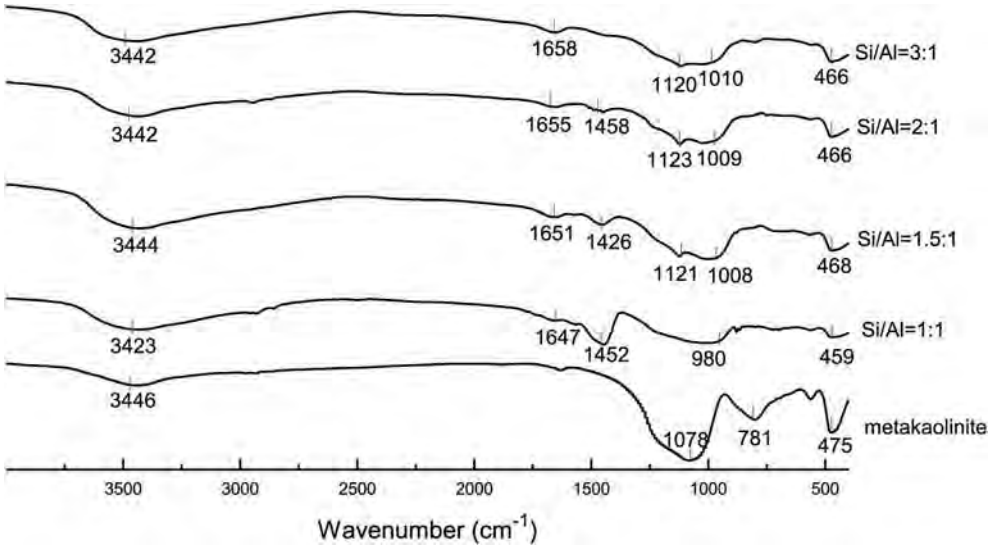

Fig. 2. FTIR spectra of the N-A-S-H gels as a function of Si/Al ratios.

modeled, and each Si or Al atom had 4 bonded neighbors (Q^4, either O or OH). The models were geometry optimized with density functional theory (DFT) calculations as reported elsewhere [27]. In energy calculation, double numerical basis sets and polarization function as adopted in $DMOL^3$ of Materials Studio were used [9]. Electrons were included in the calculation with a basis set cutoff of 0.42 nm. The geometries were assumed to converge if the energies and forces on the atoms were smaller than 0.001 kcal/mol and 0.5 kcal/mol/Å, respectively. The binding energy relative to Si atoms was calculated as following:

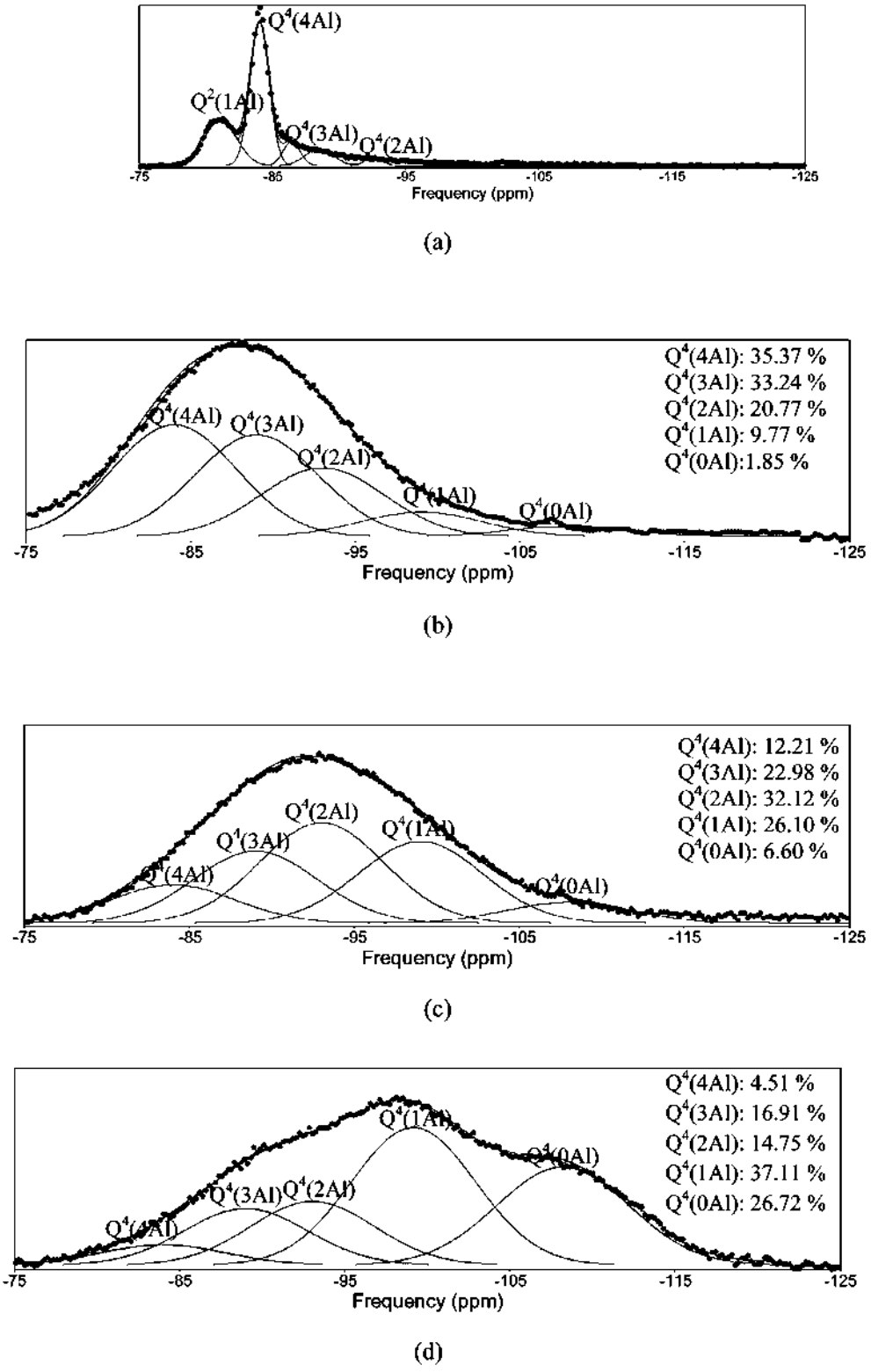

Fig. 4. ^{29}Si NMR spectra (dotted line) and their deconvolutions (solid line) of geopolymers synthesized at Si/Al ratios of 1:1 (a), 1.5:1 (b), 2:1 (c) and 4:1 (d).

$$E_{si} = E_{oligomer-Si} + E_{atomSi} - E_{oligomer}$$

where $E_{oligomer}$ was the total energy of the oligomer, $E_{oligomer\text{-}Si}$ was the total energy of the oligomer when one Si atom was removed, E_{atomSi} was the intrinsic energy of a single Si atom and E_{Si} was the binding energy relative to one Si atom. The geopolymer structure in a pure cube with the periodic boundary condition of a density 1.04 g/cm^3 was built from the modeled geopolymer oligomers through the Amorphous Cell module in Materials Studio software. The MD simulations were performed with the NPT ensemble (constant number of particles, constant pressure 0.1 MPa and temperature 298 K) for 200Ps to equilibrate the system, then with the NVT ensemble (constant number of particles, constant volume and temperature 298 K) for 1 ns? The Coulomb force was calculated using the Ewald summation scheme [28]. A time step of 1fs and a cut-off distance of 1.5 nm were adopted in simulation.

3. Results and discussions

3.1. Al, Si dissolution and N-A-S-H gel formation

In geopolymerizations, Al and Si dissolution is critical because it is the first stage that releases aluminate and silicate monomers by alkali attack on raw aluminosilicates. Fig. 1 gives the dissolution rates of Al and Si compounds at various Si/Al ratios of reaction time from 5 to 60 min. The dissolution rates of Al increases sharply in the first 5 min, and then increased slightly (Fig. 1a). At 60 min of reaction time, the number of dissolved Al/initial Al is less than 6% and the highest concentration of dissolved Al compounds is around 26 mmol/L, which is much lower than the solubility of $Al_2O_4^{2-}$ (0.72 mol/L) [29]. It corresponds well with the reported phenomenon of geopolymerization process that 1) the dissolving and polymerizing reactions take place simultaneously; 2) a long time is required for the dissolution and diffusion of aluminate and silicate monomers from raw aluminosilicates [11]. For a particular reaction time (e.g., 20 min), the dissolution rate of Al increases as increasing Si/Al ratio from 1:1 to 2:1, and then keeps a constant as increasing this ratio to 3:1. As the used alkali is a constant, this increase indicates that soluble silicates accelerate the polymerization of aluminate monomers, so as to the dissolution of Al from raw aluminosilicate (metakaolin) [30], however the acceleration of polymerization or condensation reach a balance at Si/Al = 2:1.

As noted in Fig. 1 (b), the dissolution rate of Si is in consistent with that of Al at Si/Al ratios of 1:1, 1.5:1, and 2:1, suggesting the simultaneity of alkaline dissolution of Si and Al from metakaolin. However, for initial 5 min of Si/Al ratios of 1:1, and 1.5:1, the dissolution rates of Si are lower than those of Al. The initial stage of dissolving aluminosilicate minerals in alkaline solution displays preferential release of aluminum, because the Al-O bonds are weaker than Si-O bonds, and dissolved Al species adsorb on metakaolin reducing the dissolution of Si species [31]. But this effect is weakened with increasing the reaction time because the polymerization of Si-O-Al monomers and oligomers consuming the dissolved Al compounds. For Si/Al ratio of 3:1, the dissolution rates of Si at a particular time are higher than those of Si/Al ratio of 2:1, which might be resulted from the interference of high concentration of soluble silicates (2 mol/L). The Al and Si dissolution at Si/Al ratios of 1:1, 1.5:1, 2:1 and 3:1 suggests that soluble silicate promotes Al dissolution, but reaches a balance with polymerization at Si/Al ratio of 2:1.

Fig. 2 presents the FTIR spectra of N-A-S-H gels formed at various Si/Al ratios. The absorption peaks around 3440 cm^{-1} and 1651 cm^{-1} are OH^- stretching vibrations and H-OH bonds, corresponding to structure hydroxyl (OH^-) and adsorbed water in the gels, respectively [32]. In metakaolin, these two peaks indicate the calcination of kaolinite is not complete, and a low content of free water is adsorbed during measurements. The peak around 1440 cm^{-1} is due to the asymmetric stretching mode of O-C-O bonds in CO_3^{2-} groups [33]. It appears in N-A-S-H gels but not in metakaolin, indicating that carbonation takes place on N-A-S-H gels during syntheses. The peaks at 781 cm^{-1} and 475 cm^{-1} in metakaolin spectrum are attributed to amorphous Al-O stretching vibration and O-Si-O vibration in kaolinite [34]. The intensity of these two peaks reduces in the spectra of N-A-S-H gels, indicating the reaction of metakaolin into N-A-S-H gels. The band around 1000 cm^{-1} is the overlaps of bonds of Si-O-Si (1123 cm^{-1}) in silicate derivatives [34], Si-O-Al (1078 cm^{-1}) in residual metakaolin and Si-O-T (T is tetrahedral Si or Al) asymmetric stretching band (980 cm^{-1}) in N-A-S-H gels [30]. The peak of Si-O-Al vibration in metakaolin at 1078 cm^{-1} shifts to a lower wavenumber of 980 cm^{-1} in N-A-S-H gels, because the Si-O-T linkages are of high non-bridging oxygen and Al substitutions [35]. The intensity of Si-O-T

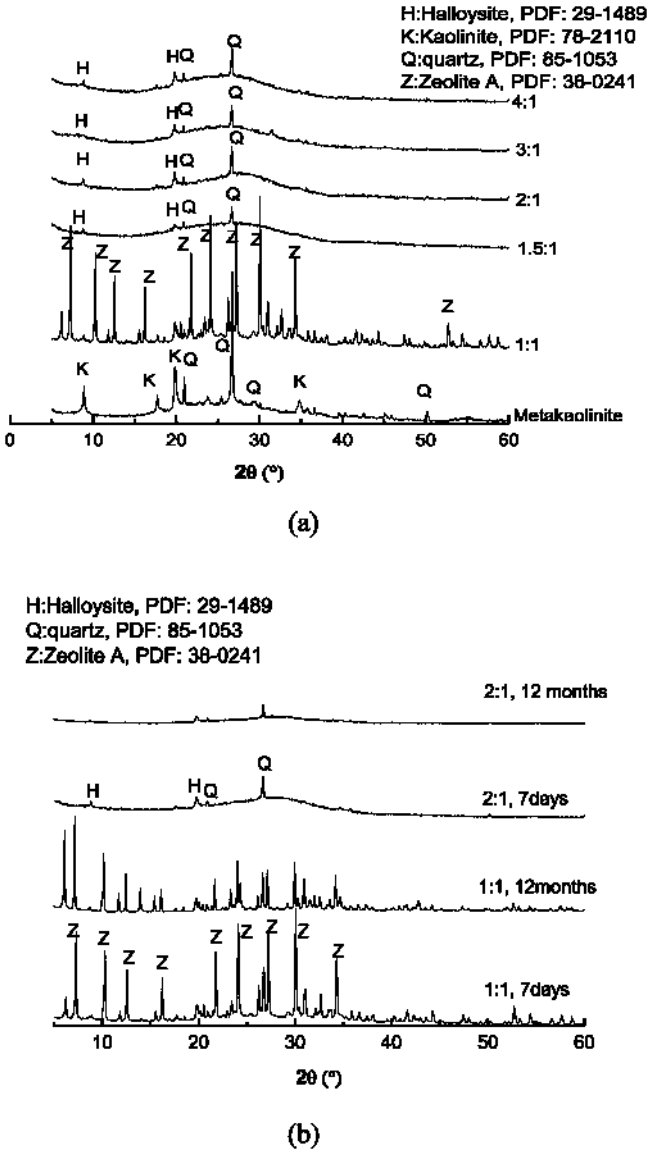

Fig. 5. XRD patterns of geopolymers synthesized at various Si/Al ratios (a) and after 12 months curing.

peak of Si/Al ratios 1.5:1 and 2:1 is higher than that of 1:1 and 3:1, suggesting more geopolymeric linkages are formed. It is in good agreement with the dissolution results of Al (Fig. 1a), and alumina dissolution is decisive in the formation of N-A-S-H gels when silicate is employed as alkaline activator.

3.2. Mechanical property and microstructure of geopolymers

Fig. 3 presents the compressive strength of geopolymers as a function of Si/Al ratios. The compressive strength increases sharply from 2.1 MPa to 31.2 MPa as changing the Si/Al ratios from 1:1 (no silicate) to 1.5:1 (0.5 mol/L silicate), indicating that soluble silicate promotes the formation of geopolymer at low concentrations. And the compressive strength increases to the maximum (36.8 MPa) with raising the Si/Al ratio to 2:1. However, with increasing the Si/Al ratios continually to 3:1, 4:1 and 5:1, the compressive strength decreases to 14.5, 11.2 and 5.5 MPa, respectively. It is in a good agreement with the study that excessive soluble silicate weakens geopolymers' strength [21].

Fig. 4 gives the ^{29}Si NMR spectra and their deconvolution of geopolymers synthesized at Si/Al ratios of 1:1, 1.5:1, 2:1 and 4:1, respectively, as well as the deconvoluted fractions of silicon tetrahedron sites present as $Q^4(4Al)$, $Q^4(3Al)$, $Q^4(2Al)$, $Q^4(1Al)$ and $Q^4(0Al)$. The dotted NMR spectrum of Si/Al ratio 1:1 (Fig. 4a) possesses a sharp peak, indicating high contents of crystalline phase are formed, which are zeolite nuclei as evidenced in the XRD measurements (Fig. 5). However, the NMR spectra of Si/Al ratios 1.5:1, 2:1 and 4:1 (Fig. 4b, c and 4d) show broad band, suggesting the amorphous structure in these geopolymers. As increasing the Si/Al ratios, peak and/or band in NMR spectra shift to right side (lower frequency), indicating less aluminum tetrahedrons are coordinated to silicon tetrahedrons. In the deconvoluted fractions, $Q^4(4Al)$ is the main compound in geopolymer of Si/Al ratio 1:1, in which a trace amount of $Q^4(3Al)$ and $Q^4(2Al)$ compounds are present. Interestingly, $Q^2(1Al)$ is found due to the high concentration of aluminate monomers. As increasing the Si/Al ratios from 1.5:1 to 2:1 and 4:1, the fractions of $Q^4(4Al)$ and $Q^4(3Al)$ decrease, while the fractions of $Q^4(1Al)$ and $Q^4(0Al)$ increase, but the fraction of $Q^4(2Al)$ shows the maximum at Si/Al ratio of 2:1. Together with mechanical properties of geopolymers at various Si/Al ratios, geopolymers with high compressive strength possess high fractions (>80%) of $Q^4(3Al)$, $Q^4(2Al)$ and $Q^4(1Al)$, which might be N-A-S-H gels, and low fractions of $Q^4(4Al)$ and $Q^4(0Al)$, which might be zeolite nuclei and silicate derivatives, respectively.

The XRD patterns of metakaolin and geopolymers synthesized at various Si/Al ratios (Fig. 5a) evidence the evolution of aluminosilicates obtained in NMR measurements. The metakaolin shows semi-crystalline to amorphous pattern with some kaolinite peaks, implying the calcination of kaolinite was not complete. The geopolymers synthesized at Si/Al ratios from 1.5:1 to 4:1 shows featureless amorphous XRD patterns with one hump centered at approximately 27–29° 2θ, which is in a good agreement with the

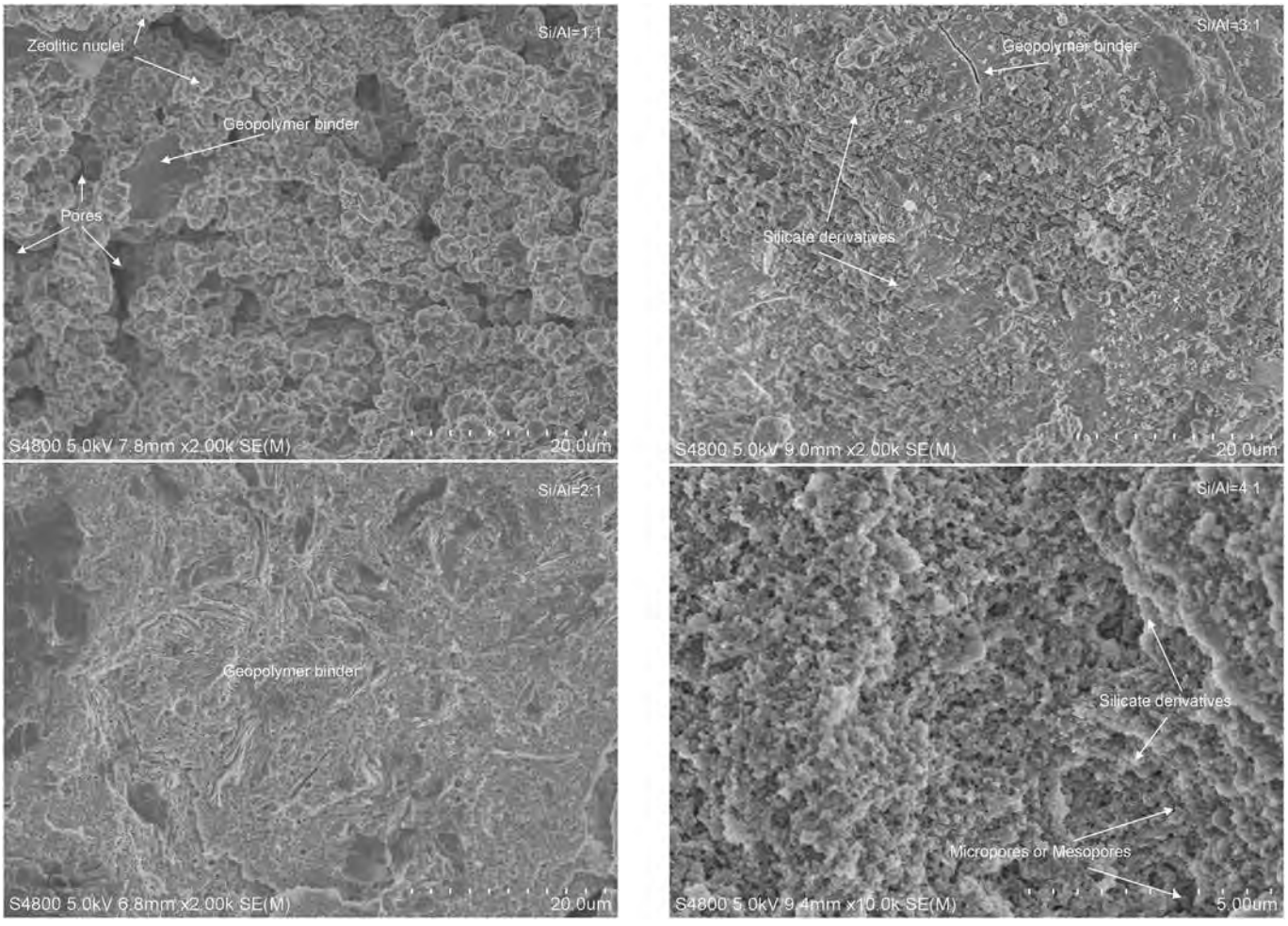

Fig. 6. SEM images of geopolymers synthesized at various Si/Al ratios.

Table 2
Binding energy relative to one Si atom and total energy of geopolymers.

Si/Al ratio	Binding energy relative to one Si atom	Total energy of geopolymers
1:1	0.66 Ha	−23701.47 kcal/mol
2:1	0.79 Ha	−21456.38 kcal/mol
3:1	0.79 Ha	−20686.83 kcal/mol
4:1	0.77 Ha	−20786.16 kcal/mol
5:1	0.76 Ha	−19935.66 kcal/mol

reported XRD patterns of geopolymers [19]. However, the geopolymer synthesized at Si/Al ratio of 1:1 presents characteristic peaks of zeolite A [3], indicating a high content of crystalline zeolitic nuclei was formed in it.

Fig. 5b shows the XRD patterns of geopolymers synthesized at Si/Al ratios of 1:1 and 2:1 after curing at room temperature for 12 months. The geopolymers give analogous XRD patterns after 12 months, namely zeolite A is identified in geopolymer of Si/Al ratio of 1:1 and quartz still exists in the 2:1 Si/Al ratio geopolymer. However, the intensities of XRD peaks become lower, which might be due to the geopolymerization reaction. Together with the NMR spectra, it can be summarized for the evolution of aluminosilicates in synthesizing geopolymers at various Si/Al ratios as following. 1) At Si/Al ratio of 1:1, relatively high concentration of aluminate monomers are dissolved by alkali, thus zeolitic nuclei of high aluminum (Q^4(4Al), Q^2(1Al)) are formed, but porous zeolite products are not formed because of the low reaction temperature and high solid concentration. 2) At Si/Al ratio around 2:1, the concentrations of aluminate and silicate monomers are proper to develop N-A-S-H gels in the microstructural forms of Q^4(3Al) and Q^4(2Al). 3) At high Si/Al ratios (e.g., 4:1), dissolved aluminate monomers are insufficient thus species of low aluminum (Q^4(1Al)) and nesosilicates or silicic acid (Q^4(0Al)) are mainly formed.

Fig. 6 gives the SEM images of geopolymers synthesized at various Si/Al ratios. At Si/Al ratio of 1:1, a little geopolymer binder and a number of zeolitic nuclei are observed. And most of these nuclei are not dispersed in the geopolymer binders, thus macrospores are formed. It is in a good agreement with the NMR result and XRD pattern that geopolymers synthesized at Si/Al ratio of 1:1 possess high contents of crystalline phase. At Si/Al ratio of 2:1, a homogeneous geopolymer binder is formed. At Si/Al ratio of 3:1, derivatives of soluble silicate (e.g., nesosilicates and silicic acid) are observed on the geopolymer binder. At Si/Al ratio of 4:1, the geopolymer binder is not found, and plenty of micropores or mesopores are formed. Together with the compressive strengths at various Si/Al ratios (Fig. 3), it can be noted that the formation of geopolymer binder is the main effect in controlling geopolymers' strength.

3.3. Simulation

Table 2 gives the binding energy relative to one Si atom and the total energy of kaolinite-based geopolymers at various Si/Al ratios, based on the optimized structures of oligomers and molecular dynamic orientation of geopolymers. The geopolymers of Si/Al ratios 2:1 and 3:1 have higher binding energies to one Si atom compared to geopolymers at Si/Al ratios of 1:1, 4:1 and 5:1, verifying geopolymers with high compressive strength could be formed at Si/Al ratios of 2:1 and 3:1. However, the total energy of geopolymers decreases with increasing the Si/Al ratios from 1:1 to 5:1, suggesting that geopolymers at Si/Al ratio of 1:1 have the most stable molecular orientation. Obviously, this energy is not in agreement with the mechanical properties of geopolymers.

4. Conclusion

Geopolymerization is an integrated process involved dissolution, N-A-S-H gel formation and condensation. Through studying the micro-structures of metakaolin geopolymers and the geopolymerization reactions of various Si/Al ratios, it is found that

1) soluble silicates promotes the dissolution of metakaolin at Si/Al ratios less than 2:1;
2) the dissolution of Al becomes decisive in the formation of N-A-S-H gels when silicate is used as alkaline activator;
3) high contents of crystalline zeolitic nuclei (Q^4(4Al)) are formed at Si/Al ratio of 1:1, and high contents of silicate derivatives are formed at Si/Al ratios higher than 3:1;
4) mechanical strength of geopolymers is dependent on the formation of N-A-S-H gel, rather than the formation of zeolitic nuclei or silicate derivatives, neither the total energy of geopolymers.

Acknowledgement

The financial supports for this work from the Consejo Nacional de Ciencia y Tecnología (CONACyT) of Mexico under the grant No. 270186 and from the National Natural Science Foundation of China under the project No. 51474167 are gratefully acknowledged. Q. Wan would like to thank the CONACYT for offering him the scholarship under the grant NO. 635638 during his PhD studying.

References

[1] J. Davidovits, Geopolymer Chemistry and Applications, Institut Géopolymère, Saint-Quentin, France, 2008.
[2] F. Pacheco-Torgal, J.A. Labrincha, C. Leonelli, A. Palomo, P. Chindaprasirt (Eds.), Handbook of Alkali-activated Cements, Mortars and Concretes, WoodHead Publishing, Cambridge, UK, 2015.
[3] P. Duxson, A. Fernandez -Jimenez, J.L. Provis, G.C. Lukey, A. Palomo, J.S.J. van Deventer, Geopolymer technology: the current state of the art, J. Mater. Sci. 42 (2007a) 2917–2933.
[4] F. Rao, Q. Liu, Geopolymerization and its potential application in mine tailings consolidation: a review, Min. Process. Extr. Metall. Rev. 36 (2015) 399–409.
[5] Z. Zhang, H. Zhu, C. Zhou, H. Wang, Geopolymer from kaolin in China: an overview, Appl. Clay Sci. 119 (2016) 31–41.
[6] C.E. White, J.L. Provis, T. Proffen, J.S.J. van Deventer, Molecular mechanisms responsible for the structural changes occurring during geopolymerization: multiscale simulation, AlChE J. 58 (2012) 2241–2253.
[7] Y. Zhang, Y. Jia, W. Sun, Z. Li, Study of ion cluster reorientation process of geopolymerisation reaction using semi-empirical AM1 calculations, Cem. Concr. Res. 39 (2009) 1174–1179.
[8] J.L. Provis, C.E. White, J.S.J. van Deventer, Discussion of Y. Zhang et al., Study of ion cluster reorientation process of geopolymerisation reaction using semi-empirical AM1 calculations, Cem. Concr. Res. 39 (12) (2009) 1174–1179. Cem. Concr. Res. 40 (2010) 827–828.
[9] K. Kupwade-Patil, F. Soto, A. Kunjumon, E.N. Allouche, D.S. Mainardi, Multi-scale modeling and experimental investigations of geopolymeric gels at elevated temperatures, Comput. Struct. 122 (2013) 164–177.
[10] J. Davidovits, The need to create a new technical language for the transfer of basic scientific information. Transfer and Exploitation of Scientific and Technical Information Luxembrourg, Commission of the European Communities, 1982, p. 7716.
[11] D. Khale, R. Chaudhary, Mechanism of geopolymerization and factors influencing its development: a review, J. Mater. Sci. 42 (2007) 729–746.
[12] Y. Zhang, W. Sun, Z. Li, Composition design and microstructural characterization of calcined kaolin-based geopolymer cement, Appl. Clay Sci. 47 (2010)

271–275.
[13] S. Ahmari, L. Zhang, Production of eco-friendly bricks from copper mine tailings through geopolymerization, Constr. Build. Mater 29 (2012) 323–331.
[14] P. Duxson, S.W. Mallicoat, G.C. Lukey, W.M. Kriven, J.S.J. van Deventer, The effect of alkali and Si/Al ratio on the development of mechanical properties of metakaolinite-based geopolymers, Colloids Surf. A 292 (2007b) 8–20.
[15] P.D. Silva, K. Sagoe-Crenstil, V. Sirivivatnanon, Kinetics of geopolymerization: role of Al_2O_3 and SiO_2, Cem. Concr. Res. 37 (2007) 512–518.
[16] M. Rowles, B. ÓConnor, Chemical optimization of the compressive strength of aluminosilicate geopolymers synthesized by sodium silicate activation of metakaolinite, J. Mater. Chem. 13 (2003) 1161–1165.
[17] A.V. McCormick, A.T. Bell, C.J. Radke, Multinuclear NMR investigation of the formation of aluminosilicate anions, J. Phys. Chem. 93 (1989) 1741–1744.
[18] W.K.W. Lee, J.S.J. van Deventer, Structural reorganisation of class F fly ash in alkaline silicate solutions, Colloids Surf. A 211 (2002) 49–66.
[19] P. Duxson, J.L. Provis, G.C. Lukey, F. Separovic, J.S.J. van Deventer, ^{29}Si NMR study of structural ordering in aluminosilicate geopolymer gels, Langmuir 21 (2005) 3028–3036.
[20] J.L. Provis, G.C. Lukey, J.S.J. van Deventer, Do geopolymer actually contain nanocrystalline zeolites? a reexamination of existing results, Chem. Mater 17 (2005) 3075–3085.
[21] M. Criado, A. Fernández-Jiménez, A. Palomo, Alkali activation of fly ash: effect of the SiO_2/Na_2O ratio Part I: FTIR study, Microporous Mesoporous Mater 106 (2007) 180–191.
[22] T.W. Cheng, J.P. Chiu, Fire-resistant geopolymer produced by granulated blast furnace slag, Min. Eng. 16 (2003) 205–210.
[23] V. Nikolic, M. Komljenovic, Z. Bascarevic, N. Marjanovic, Z. Miladinovic, R. Petrovic, The influence of fly ash characteristics and reaction conditions on strength and structure of geopolymers, Constr. Build. Mater 94 (2015) 361–370.
[24] S.K. Lee, J.F. Stebbins, The degree of aluminum avoidance in aluminosilicate glasses, Am. Min. 84 (1999) 937–945.
[25] H. Rahier, B. Van Mele, M. Biesemans, J. Wastiels, X. Wu, Low-temperature synthesized aluminosilicate glasses, J. Mater. Sci. 31 (1996) 71–79.
[26] G. Engelhardt, D. Michel, High-resolution Solid-state NMR of Silicates and Zeolites, Wiley, New York, 1987, pp. 77–135.
[27] C.E. White, J.L. Provis, T. Proffen, J.S.J. van Deventer, Quantitative mechanistic modeling of silica solubility and precipitation during the initial period of zeolite synthesis, J. Phys. Chem. C 115 (2011) 9879–9888.
[28] D. Spagnoli, B. Gilbert, G.A. Waychunas, J.F. Banfield, Prediction of the effects of size and morphology on the structure of water around hematite nanoparticles, Geochim. Cosmochim. Acta 73 (2009) 4023–4033.
[29] R.V. Lundquist, Solubility Characteristics of Sodium Aluminate, University of Michigan Library, American, 1964.
[30] A. Hajimohammadi, J.L. Provis, J.S.J. van Deventer, Effect of alumina release rate on the mechanism of geopolymer gel formation, Chem. Mater 22 (2010) 5199–5208.
[31] E. Oelkers, S.R. Gislason, The mechanism, rates and consequences of basaltic glass dissolution: I. An experimental study of the dissolution rates of basaltic glass as a function of aqueous Al, Si and oxalic acid concentration at 25°C and pH 3 and 11, Geochim. Cosmochim. Acta 65 (2001) 3671–3681.
[32] S.A. Bernal, J.L. Provis, V. Rose, R. Mejía de Gutierrez, Evolution of binder structure in sodium silicate-activated slag-metakaolin blends, Cem. Concr. Comp. 33 (2011) 46–54.
[33] T. Yang, X. Yao, Z. Zhang, H. Zhu, Effects of NaOH solution concentration and reaction time on metakaolin geopolymerization, J. Nanjing Univ. Technol. 35 (2013) 21–25 (in Chinese).
[34] N.Y. Mostafa, S.A.S. El-Hemaly, E.I. Al-Wakeel, S.A. El-Korashy, P.W. Brown, Characterization and evaluation of the pozzolanic activity of Egyptian industrial by-products I: silica fume and dealuminated kaolin, Cem. Concr. Res. 31 (2001) 467–474.
[35] A. Hajimohammadi, J.L. Provis, J.S.J. van Deventer, One-part geopolymer mixes from geothermal silica and sodium aluminate, Ind. Eng. Chem. Res. 47 (2008) 9396–9405.

Cement and Concrete Composites 80 (2017) 115–122

Contents lists available at ScienceDirect

Cement and Concrete Composites

journal homepage: www.elsevier.com/locate/cemconcomp

Combination formation in the reinforcement of metakaolin geopolymers with quartz sand

Qian Wan [a, b], Feng Rao [a, *], Shaoxian Song [b, **], Diana F. Cholico-González [a], Noemí L. Ortiz [a]

[a] CONACYT Instituto de Investigación en Metalurgia y Materiales, Universidad Michoacana de San Nicolás de Hidalgo, Ed. "U", Ciudad Universitaria, Morelia, Michoacán, 58030, Mexico
[b] School of Resources and Environmental Engineering, Wuhan University of Technology, Luoshi Road 122, Wuhan, Hubei, 430070, China

ARTICLE INFO

Article history:
Received 27 June 2016
Received in revised form
17 February 2017
Accepted 15 March 2017
Available online 18 March 2017

Keywords:
Metakaolin geopolymer
Quartz sand
Mine tailings
Combination in micro-structure

ABSTRACT

Although quartz sand is widely used as filler material in construction, a few studies investigated the incorporation of quartz sand in geopolymers. To study the incorporation of quartz sand in the reinforcement of metakaolin geopolymer not only fills this gap, but also gives a clue on using non-calcinated aluminosilicates (e.g., mine tailings) in the synthesis of geopolymers. In the presence of sodium silicate, metakaolin geopolymers were synthesized with quartz sand of various size ranges as filler material. XRD, FTIR, SEM and NMR characterizations on the geopolymers indicate the dissolution, precipitation, and the formation of combination on quartz particles that associates them into the geopolymeric gel, so as to reinforce the mechanical strength of geopolymers. The compressive strength of metakaolin geopolymers with only silicate, silicate plus quartz sand and silicate plus rutile sand is 31.2, 52.2 and 41.5 MPa, respectively. In geopolymer with silicate and quartz sand, a decreasing Si/Al ratio as increasing distance from the quartz particle is observed through an energy dispersive X-ray (EDX) mapping. The SEM images and NMR spectra suggest that the formed combination is of several micrometers with main species of polysialates (-Si-O-) such as $Q^4(2Al)$, $Q^4(1Al)$.

1. Introduction

Geopolymers are aluminosilicate concrete materials with three-dimensional (3D) amorphous micro-structure, which are synthesized through activating aluminosilicate minerals or industrial by-products with alkaline solutions [1]. Silicate is usually used in the synthesis of geopolymers to form chain silicate oligomers and Al-O-Si complexes in geopolymeric gels [2–4]. In some studies, silicate was prepared by dissolving amorphous silica (e.g., silica fume) into alkaline such as sodium hydroxide solutions [5]. Besides, semi-soluble or insoluble silica materials have been employed as additives in the synthesis of geopolymers. It is generally accepted that silica additives with higher activity promote the formation of geopolymeric gel. For example, Hajimohammadi et al. [6] compared the geopolymers synthesized with geothermal silica (low activity) and sodium silicate (high activity), in which the results show a more homogenous geopolymeric gel binder with sodium silicate. Autef et al. [7] synthesized geopolymer with varied ratios of quartz (low activity) to amorphous silica (high activity), which demonstrated that an increase of amorphous silica led to a higher polycondensation rate, while quartz sand was a non-alterable raw material. But some particular roles played by non-alterable (inert) particles in the formation of geopolymeric gel have been disclosed in recent years. For example, Rees et al. [8] stated that high surface area Al_2O_3 nanoparticles play the nucleation role in geopolymeric gel formation, which greatly increases its formation rate. And the enhancement of geopolymer's mechanical properties by adding filler materials has been reported. Phair et al. [9,10] used micro-sized ZrO_2 particles as inert filler materials in the synthesis of fly ash geopolymers, in which the inclusion of 3% by weight of zirconia increases compressive strength of the geopolymers by 13 MPa. They hypothesized the formation of insoluble sodium polysialate complexes on zirconia surface, incorporating the zirconia particles into the geopolymeric gel. Silty clay was studied as filler materials of high amount in the synthesis of fly ash geopolymers [11]. Compressive strength of the clay-fly ash

* Corresponding author.
** Corresponding author.
E-mail addresses: fengrao@umich.mx (F. Rao), shaoxian@uaslp.mx (S. Song).

http://dx.doi.org/10.1016/j.cemconcomp.2017.03.005
0958-9465/

geopolymer is 14 MPa when the ratio of fly ash to clay is 0.3. However, the interactions between filler materials and geopolymeric gel still require research on the micro-structures of geopolymers synthesized with selected filler materials, even though it is a mature technology by using them in construction with Portland cement.

Recently, mine tailings, which are vast industrial wastes rich in aluminosilicate materials after dressing ores, have been studied in the synthesis of geopolymers [12]. Geopolymerization of mine tailings not only consolidates tailing mud that accelerates recycling of water and prevents failure of tailing dams, but also offers the clues of novel applications of geopolymers, such as substrate materials in fixed-film wastewater-treatment process [13]. However, the large quantity of inert silicate minerals produced in mine tailings impedes the geopolymerization reactions. Previous research either added calcined materials (e.g., fly ash) in the synthesis of copper mine tailings geopolymer [14], or applied calcination at 950 °C for 2 h in the synthesis of tungsten mine tailings geopolymer [15]. Obviously, these treatments in the synthesis of geopolymers from mine tailings lose the original advantage of geopolymers of green concrete materials with low CO_2 production.

The present study attempts to incorporate quartz sand, which is a common inert silicate mineral in mine tailings, as filler material in the formation of metakaolin geopolymers. Silica fume is used to form silicate and maintain Si/Al ratio in the syntheses. We hypothesize the formation of "combination" gel on quartz particle surface in the presence of silicate in alkaline solution. This investigation improves the understandings of geopolymer gel formation, micro-structures of filler materials in geopolymeric gel, and synthesis of geopolymers with mine tailings or other inert industrial wastes.

2. Experimental

2.1. Materials

Kaolinite from Hubei province, China was used to prepare metakaolin through calcination at 800 °C for 5 h, of which the chemical composition was measured by X-ray Fluorescence (XRF) and given in Table 1. Sodium hydroxide (NaOH, ACS reagent grade) was used as alkali in the synthesis. Quartz sand collected from Michoacan, Mexico was used as silica filler additive. The quartz sand was milled and classified into 6 size ranges of >180 μm, 180–105 μm, 105–75 μm, 75–32 μm, 32–12 μm and <12 μm. Rutile sand (TiO_2>98%) collected from Hainan, China of size range 75–48 μm was used a comparing filler additive. Silica fume (SiO_2>98%) from Jinfeng Materials, China, was used as soluble silica additive to maintain Si/Al ratio in the syntheses. As studied previously, the silica fume reacts completely with sodium hydroxide into silicate [16].

2.2. Methods

2.2.1. Synthesis of geopolymers

Table 2 gives the parameters for synthesizing metakaolin geopolymers with quartz sand of various size ranges, rutile sand, and without filler materials but silica fume to adjust the Si/Al ratio. All syntheses were conducted by keeping Na_2O/Al_2O_3 and Na_2O/H_2O ratios of 1:1 and 1:12. The curing was kept at 60 °C for 6 h and then at room temperature (RT) for 7 days. The specimens No. 1–6 were synthesized with additives of 5 mol/L silica fume and 5 mol/L quartz sand with size ranges of 240–180 μm (No. 1), 180–105 μm (No. 2), 105–75 μm (No. 3), 75–32 μm (No. 4), 32–12 μm (No. 5) and 12–6 μm (No. 6). The specimens No. 7–12 were synthesized with additive of only quartz sand at 10 mol/L, corresponding to the 6 size ranges of descending order. The specimens No. 13–14 were synthesized with only silica fume additive of 10 mol/L and 5 mol/L, respectively. The specimen No. 15 was synthesized with rutile sand (75–48 μm) and silica fume additives of both 5 mol/L. In the typical synthesis of No. 1, 1 mol (222 g) metakaolin, 2 mol (80 g) NaOH, 0.2 L water, 1 mol (60 g) quartz sand (240–180 μm) and 1 mol (60 g) silica fume were mixed and stirred for 15 min. Then, the slurry was shaken for 10 min in a vibration table to remove the air bubbles. After that, the mixture was transferred to cubic steel molds (50 mm × 50 mm × 50 mm), which were sealed for the curing process.

Table 1
Chemical composition of metakaolin.

Components	SiO_2	Al_2O_3	K_2O	Fe_2O_3	TiO_2	MgO
wt%	52.8	43.7	1.2	0.6	0.5	0.2

Table 2
Synthesizing parameters of geopolymer specimens.

Specimen No.	Additives (mol/L)			Si/Al	Na/Al	Na_2O/H_2O
	Quartz	Silica fume	Rutile			
1–6	5	5	0	2:1	1:1	1:12
7–12	10	0	0	2:1	1:1	1:12
13	0	10	0	2:1	1:1	1:12
14	0	5	0	1.5:1	1:1	1:12
15	0	5	5	1.5:1	1:1	1:12

2.2.2. Characterization of geopolymers

The cubic products of geopolymers were characterized for their compressive strength with an EHC-1300 mechanical tester from Xingao Technology, China. The X-ray patterns were obtained by using the Brucker D8 X-ray diffraction (XRD) meter. The geopolymers were studied using a Fourier-transform infrared (FTIR) spectroscopy (Nexus, Thermo Nicolet, USA). Transmittance spectra were gathered over a wave number range of 400–4000 cm^{-1} with a resolution of 2 cm^{-1}. The morphology of geopolymer specimens were observed by a scanning electron microscope (SEM, JEOL JSM-5610LV), in which energy dispersive X-ray (EDX) mapping of Si, O, and Al were conducted to investigate the distribution of these elements in geopolymeric gel. ^{29}Si magic-angle spinning nuclear magnetic resonance (MAS NMR) spectra of geopolymers were obtained by using a NMR spectroscopy at 79.49 MHz. Powdered geopolymer specimens were packed into 7 mm ZrO_2 rotors. Spectra were acquired at spinning speeds of 12 kHz with peak positions referenced to an external standard of tetramethylsilane (TMS) and recorded with 1 s delay time.

3. Results and discussion

3.1. Reinforcement of metakaolin geopolymer by quartz fillers

Fig. 1 shows the SEM images of metakaolin geopolymers synthesized with additives of only quartz sand of 10 mol/L (No. 12), quartz sand and silica fume of both 5 mol/L (No. 6), rutile sand and silica fume of both 5 mol/L (No. 15), and only silica fume of 10 mol/L and 5 mol/L (No. 13 and 14), as well as the compressive strength data. As increasing the dosage of silica fume additive (No. 12, No. 6, No. 13), more silicate is generated, the morphology of geopolymers shows an increasing degree of homogeneity. The geopolymer synthesized without silica fume shows a porous structure and a much lower compressive strength than others. It corresponds well

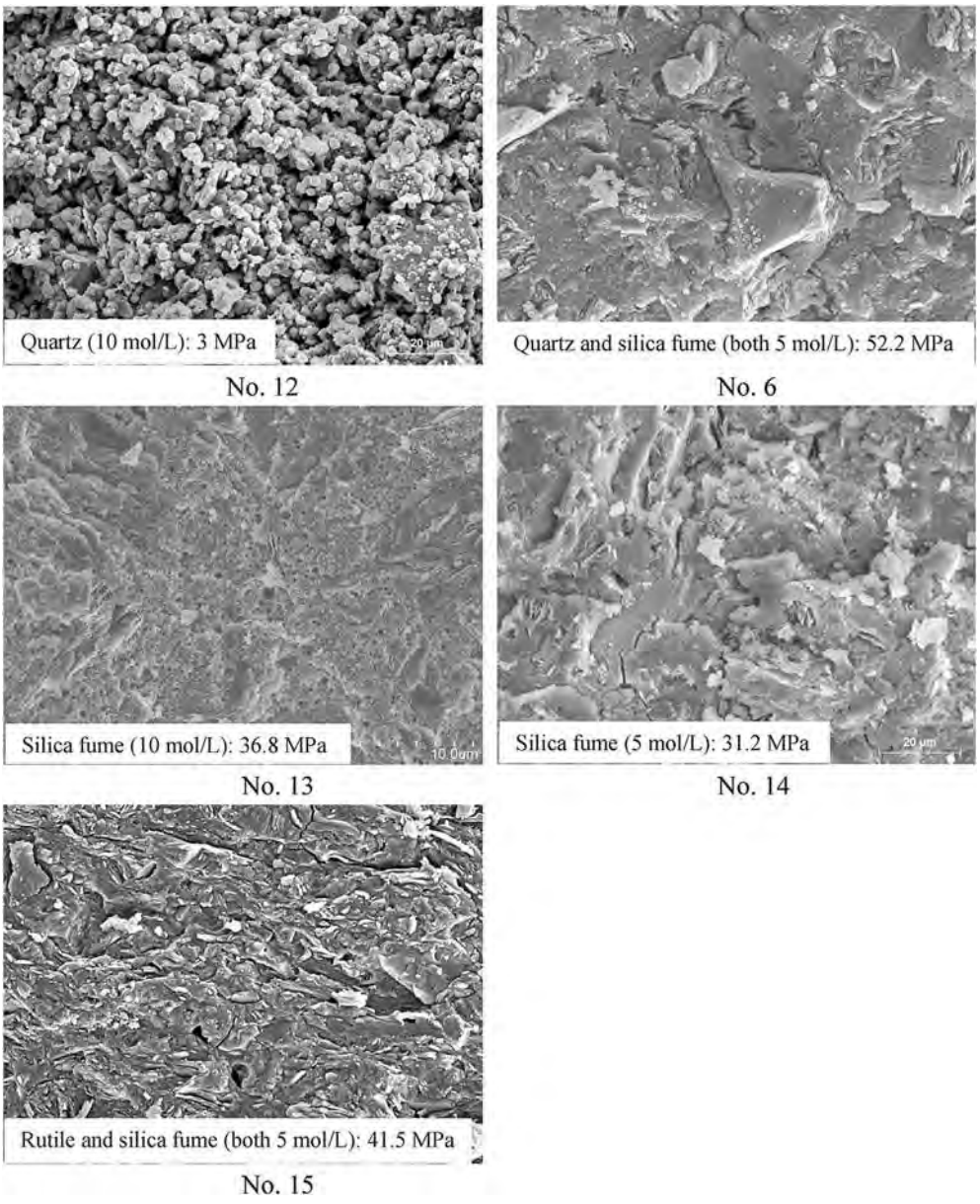

Fig. 1. SEM images and compressive strength data of metakaolin geopolymers synthesized with various additive regimes.

with the report that silicate promotes the formation of silicate oligomers and geopolymeric gel, which results in homogenous structures and increases mechanical properties of geopolymer products to some extent [17]. However, the compressive strength of geopolymer synthesized with additives of both quartz sand and silica fume (No. 6) is much higher than the geopolymers (No. 13) synthesized without quartz sand, even though more homogenous structure is produce in geopolymer No. 13. It indicates the quartz sand reinforces mechanical strength of geopolymer, which functions as inert filler material.

Some studies state that excessive soluble silicate forms "Si-" bridge bonds and hinders water evaporation in the syntheses of geopolymers, which develops amorphous structure and lowers the compressive strength of fly ash and slag geopolymers [18,19]. Therefore, geopolymer with only 5 mol/L silica fume additive (No. 14) has been synthesized for a comparison. Compared with the geopolymer No. 6, the geopolymer synthesized with equal soluble silicate shows similar homogeneous structure but a decreased compressive strength by 21 MPa. This result excludes the possibility that excessive silicate leads the reduction of compressive strength from geopolymers No. 6 to No. 13. In addition, compared with another filler material, namely rutile sand (No. 15), the geopolymer (No. 6) synthesized with quartz sand as filler material shows a resembling homogeneous structure, but a higher compressive strength by 10.7 MPa.

3.2. Combination associates quartz fillers in geopolymer gel

It has been reported that quartz sand as filler materials interacts with Portland cement, decreases the large pores in concrete, and strengths concrete paste [20]. However, a few studies investigated on the microstructural aspect of the interaction between quartz sand and geopolymeric gel. Thus FTIR measurements and SEM image analysis are employed to study the combination formation of quartz fillers in geopolymer gel. Fig. 2 shows the FTIR spectra of geopolymers synthesized with quartz and silica fume (No. 6), only

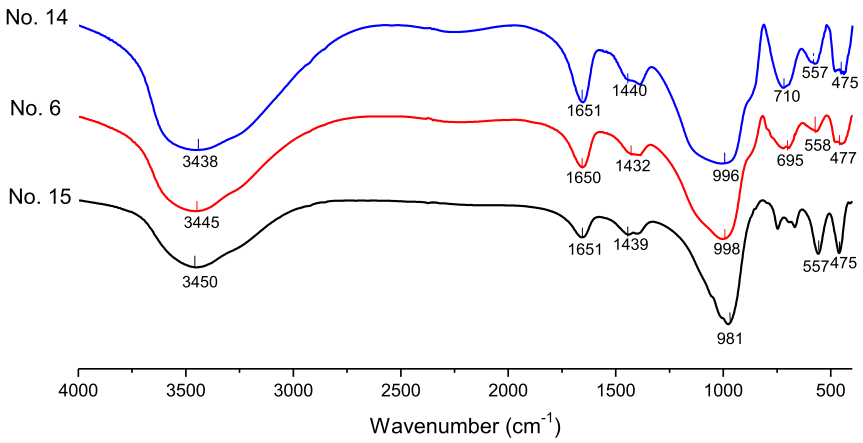

Fig. 2. FTIR spectra of geopolymers synthesized with quartz and silica fume (No. 6), only silica fume (No.14) and rutile plus silica fume (No. 15).

silica fume (No.14) and rutile plus silica fume (No. 15). The absorption peaks at 3440 cm^{-1}, 1651 cm^{-1} and 1440 cm^{-1} are OH^- stretching vibrations, H-OH bonds of free water [3] and asymmetric stretching of O-C-O bonds in CO_3^{2-} groups [21], corresponding to adsorbed H_2O and carbonation during the curing of geopolymers. They are identical peaks in both spectra of geopolymers with quartz and silica fume (No. 6) and with only silica fume (No. 14). However, the peak at 695 cm^{-1} that represents the bond of quartz only appears in geopolymer with quartz and silica fume, indicating the insolubility of quartz particles during geopolymerization. The peaks at 557 cm^{-1} and 475 cm^{-1} correspond to zeolite framework [22,23] in the geopolymer structure, which are of higher transmittance in geopolymer with only silica fume (No. 14). It suggests that more zeolite frameworks are formed during the reactions in geopolymer No. 14. The band at 980 cm^{-1} represents the Si-O-T bonds (T is tetrahedral Si or Al) in geopolymeric gel, which shifted left in the spectrum of geopolymer with quartz and silica fume compared with the spectrum of geopolymer with only with silica fume, indicating more Si-O-Si bonds have formed by adding quartz sand in geopolymerization [24]. It suggests that quartz sand might be partly dissolved to form "Si-" combinations with geopolymeric gel that incorporates the quartz particles. In addition, the spectrum of geopolymer synthesized with rutile sand and silica fume (No. 15) shows similar peaks as the geopolymer with quartz sand and silica fume (No. 6), because rutile sand and quartz sand are of similar characteristic peaks in FTIR spectra. While, its broad band at 980 cm^{-1} might be a result of the overlying of Ti-O bonds and Si-O-T vibrations.

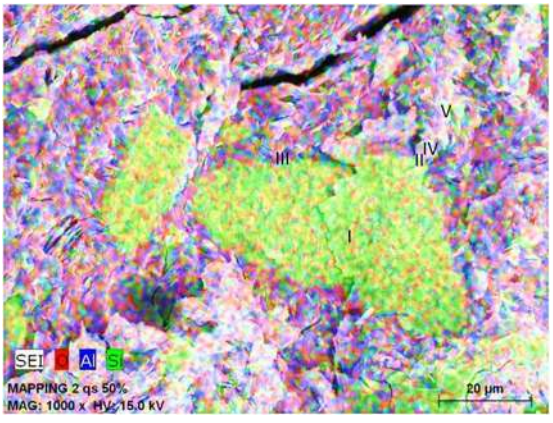

Fig. 3. Energy dispersive X-ray (EDX) mapping of Si, O, and Al in geopolymer (No. 5) synthesized with quartz sand and silica fume.

The energy dispersive X-ray (EDX) mapping of Si, O, and Al was carried out in geopolymer (No. 5) synthesized with silica fume and quartz sand of 32–12 μm. As shown in Fig. 3 around quartz particle, the relative Si/Al ratios of points I, II, III, IV, and V are 12:1, 5:1, 5:1, 2:1 and 1.5:1, respectively. At point I, the Si content is much higher than Al, indicating the insolubility of quartz particle in geopolymerization reactions. At points II and III of the combination connecting quartz particles and geopolymeric gel, the Si/Al ratios decrease equally from point I. And the Si/Al ratio decreases with increasing the distance from quartz particle to pints IV and V. At point V, the Si/Al ratio is 1.5:1, which is equal to the Si/Al ratio of raw materials (metakaolin, silica fume and quartz) if assuming no dissolution of quartz particles. This result indicates the formation of a transitional combination in several micrometers that emerges the quartz particles into geopolymeric gel. In studying interactions between quartz sand and sodium silicate [25], it is reported that both reactions of quartz dissolution and precipitation of saturated silicate species such as $SiO(OH)_3^-$ and $SiO_2(OH)_2^{2-}$ take place in the formation of combination on quartz sand particle surface. So this combination is mainly composed of polysiloxo (-Si-O-). It corresponds well with the hypothesis of the formation of specific zirconia-associated, three-dimensional polysialate species in the incorporation of zirconia into fly ash geopolymers [9]. However, it is interesting to note that the metakaolin geopolymer synthesized with rutile sand as filler possesses a lower compressive strength than that with quartz sand as filler (Fig. 1). It might be resulted from the fact that the dissolution, precipitation and formation of titanium-polysiloxo combination in rutile metakaolin geopolymer are distinguished from those in quartz metakaolin geopolymer.

3.3. Size of quartz sand in combination formation

Fig. 4 presents the compressive strength data of geopolymers synthesized with silica fume and quartz sand of various size ranges (No. 1–6), with only quartz sand of various size ranges (No. 7–12), and without quartz sand. The geopolymers synthesized with quartz sand and silica fume show high compressive strengths (Fig. 4a). The maximum strength is obtained at the size range of 75–32 μm. A slight reduction in compressive strength is observed as decreasing the particle size to 32–12 μm and 12–6 μm, suggesting the reduction of reinforcement on metakaolin geopolymers by filler material of extremely fine size. And a decrease of strength by 10 MPa is observed as increasing the particle size from 75 to 32 μm to 180–105 μm, further by 31 MPa as increasing the particle size to

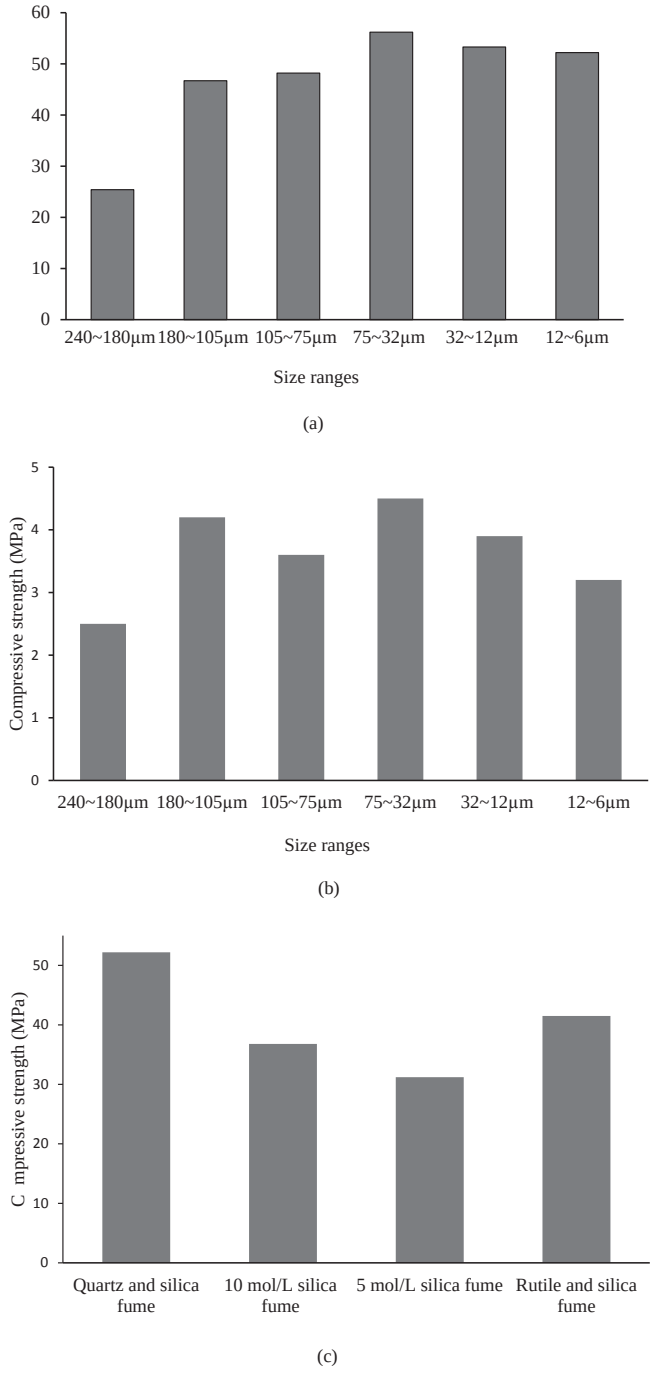

Fig. 4. Compressive strength data of geopolymers synthesized with silica fume and quartz sand (a), with only quartz sand (b) and without quartz sand (c).

240–180 μm. It suggests that quartz particles of big size are difficult to be combined into geopolymeric gel. The geopolymers (No. 7–12) synthesized without silica fume lost the homogeneous geopolymeric gel structure (Fig. 1), resulting in porous products of strength lower than 5 MPa (Fig. 4b). As summarized and compared in Fig. 4c, the geopolymer synthesized with silica fume and quartz sand of optimal size range possesses a much higher compressive strength (>10 MPa) than those without quartz sand or with rutile sand.

The combination should be positively correlated with the surface area of quartz particles, because they are formed by dissolution

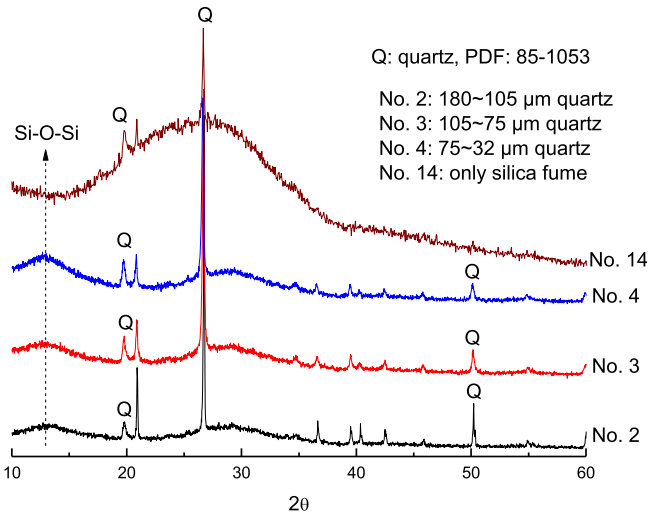

Fig. 5. XRD spectra of geopolymers No. 2, 3, 4 and 14.

and precipitation of hydrolyzed silica species only on the surface of particles. The smaller is the particle size, the more combination forms. Fig. 5 shows the XRD patterns of geopolymers (No. 2, 3 and 4) synthesized with silica fume and quartz sand of size ranges 180–105 μm, 105–75 μm, and 75–32 μm, respectively, and of geopolymer (No. 14) with only silica fume. The four spectra show the amorphous structure of geopolymers with trace peak of quartz, which is more noticeable in the spectra of geopolymers with quartz sand. It confirms the insolubility of quartz sand in geopolymerization reactions. It is interesting to note that the peak intensity of amorphous Si-O-Si chains in geopolymeric gel at 2θ of 13° [26] increases as decreasing the quartz particle size, indicating the formation of more Si-O-Si chains in the combination as decreasing particle size.

The short-range ordering and molecular structure of geopolymers have been investigated with great success using NMR spectroscopy [27]. The lack of spectral resolution for silicon in geopolymers has been overcome by adopting Gaussian peak deconvolution to separate and quantify $Q^n(mAl)$ species ($0 \leq m \leq n \leq 4$) [28]. It is reported from other NMR studies that all silicon and aluminum sites are in tetrahedral coordination in geopolymers, thus $n = 4$ [29]. And the resonance of a $Q^4(mAl)$ center with the replacement of each aluminum by silicon is an approximate −5 ppm shift, with $Q^4(4Al)$, $Q^4(3Al)$, $Q^4(2Al)$, $Q^4(1Al)$, $Q^4(0Al)$ resonating at approximately −84, −89, −93, −99 and −107 pmm, respectively [30]. Fig. 6 shows the ^{29}Si NMR spectra and their deconvolution of geopolymers (No. 2, 3, and 4) synthesized with silica fume and quartz sand of various size ranges 180–105 μm, 105–75 μm, and 75–32 μm, respectively, and of geopolymer (No. 14) with only silica fume. The spectra of geopolymers synthesized with silica fume and quartz show typical broad resonance centered at −85 to −93 ppm, which is in accordance with previous studies [27]. The peak at −107 ppm in the spectra of geopolymers (No. 2, 3, and 4) with quartz sand represents the residual quartz particles, of which the intensity increases as increasing the particles size. It verifies the dissolution and formation of combination is positively correlated with the surface area of quartz particles. The lager is the particle size, the smaller is the specific surface area, the more residual quartz remains. The spectrum of the geopolymer (No. 14) synthesized with only silica fume is different from those with quartz sand and silica fume, which shows very low intensity at the peak of quartz and two sharp peaks at −84 and −90 ppm. It suggests the main micro-structures in

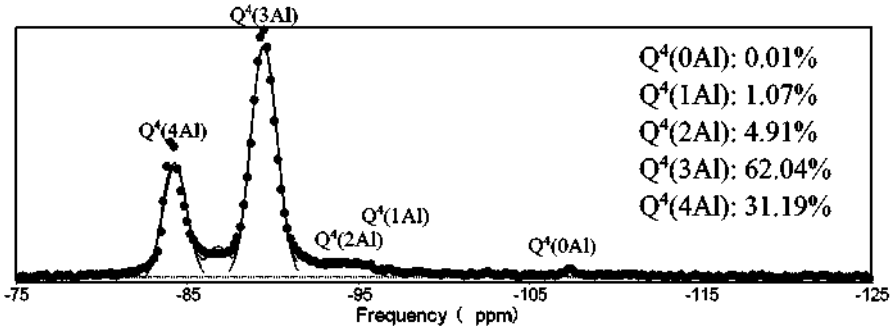

No. 14

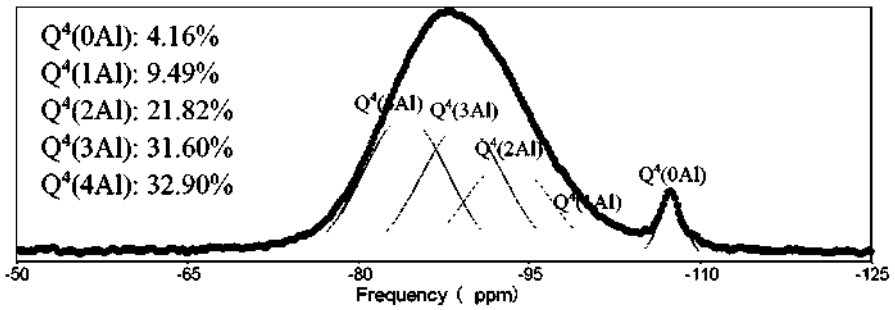

No. 4

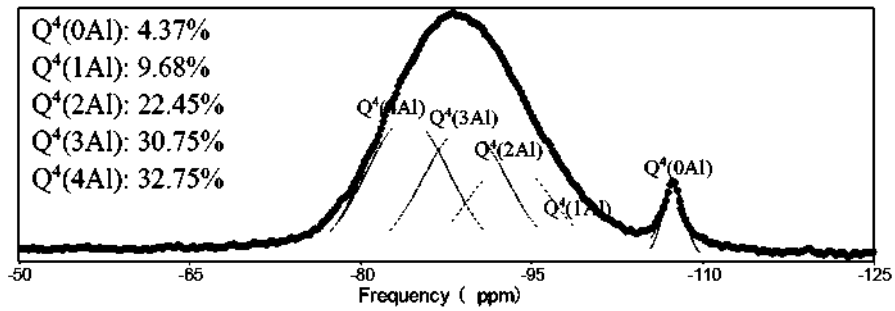

No. 3

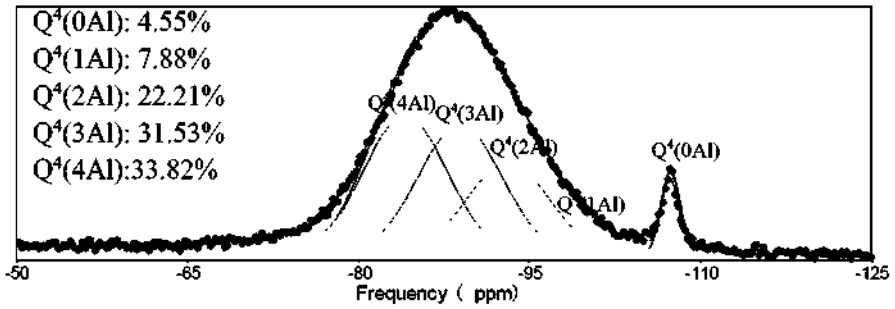

No. 2

Fig. 6. ^{29}Si NMR spectra (left side) and their deconvolution (right size) of geopolymers synthesized with silica fume and quartz sand of various size ranges, and of geopolymer with only silica fume.

geopolymer No. 14 is zeolite framework [31], showing good agreement with the FTIR results (Fig. 2).

Deconvolution of ^{29}Si NMR spectra gives the fractions of silicon tetrahedron sites present as $Q^4(4Al)$, $Q^4(3Al)$, $Q^4(2Al)$, $Q^4(1Al)$ and

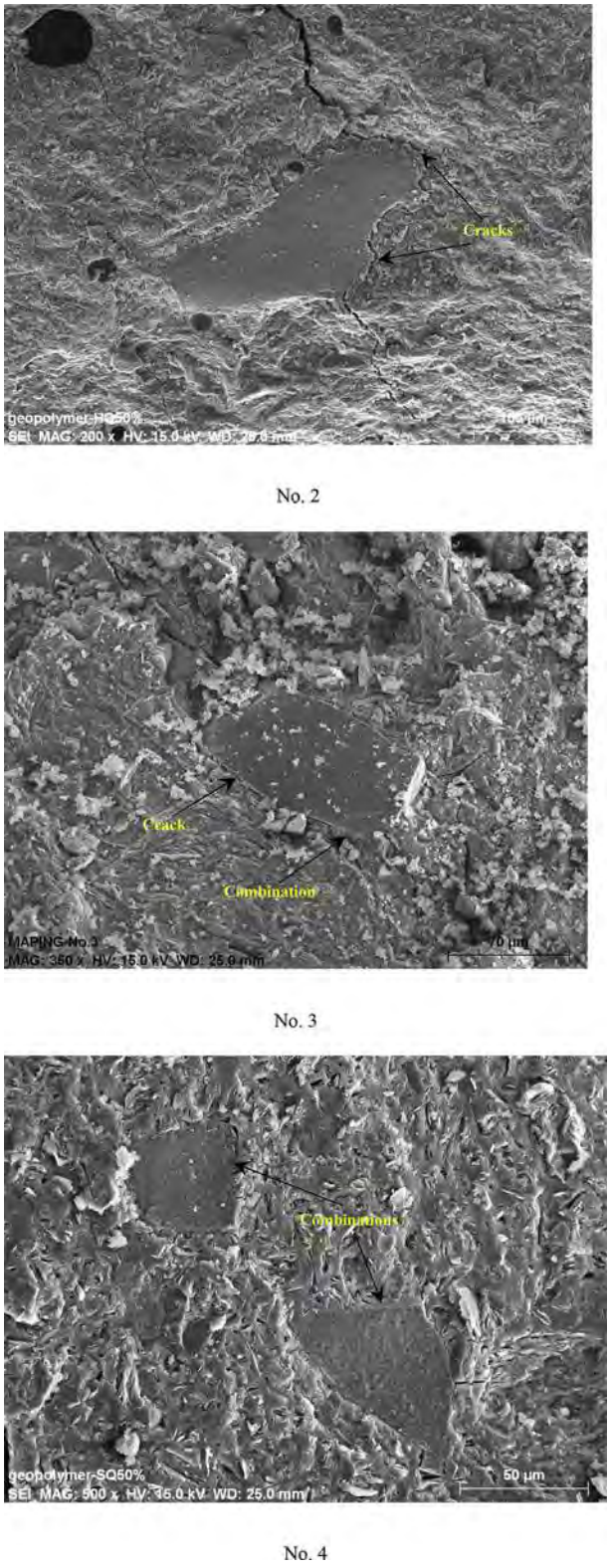

Fig. 7. SEM images of metakaolin geopolymers with silica fume and quartz sand of various size ranges.

$Q^4(0Al)$. In the geopolymer (No. 14) with only silica fume, $Q^4(0Al)$ is not observed, which obeys Loewenstein's Rule in geopolymeric gel that every aluminum ion forms $Al(OSi)_4$ [27]. The fraction $Q^4(4Al)$ is equal of 30% in the four geopolymers, indicating the $Q^4(4Al)$ sites are resulted from geopolymeric gel and not affected by the formation of combinations on quartz particles. Interestingly, the fraction $Q^4(3Al)$ is higher in geopolymer (No. 14) with only silica fume than in geopolymers (No. 2, 3 and 4) with quartz sand and silica fume, but the fractions $Q^4(2Al)$ and $Q^4(1Al)$ behave the opposite. It suggests the lack of paring aluminum tetrahedrons or the excess of silicon tetrahedrons in geopolymers with quartz sand. In comparison with geopolymer No. 14, the addition of quartz sand is the only difference in synthesizing parameters of geopolymer No. 2, 3 and 4. Therefore, incorporation of quartz sand into metakaolin geopolymers affects the ratio of silicon to aluminum tetrahedrons by either production of silicate species or competition of alkalis with metakaolin in the dissolution of quartz particles. As the particle size of quartz sand decreases in geopolymers 2, 3 and 4, more surface of quartz is involved in the dissolution, thus a higher ratio of silicon to aluminum tetrahedrons is produced and higher fractions of $Q^4(2Al)$ and $Q^4(1Al)$ are observed in the deconvolution of NMR spectra.

Fig. 7 presents the SEM images of metakaolin geopolymers with silica fume and quartz sand of size ranges in 180–105 μm (No. 2), 105–75 μm (No. 3), and 75–32 μm (No. 4). Cracks are easily observed in the geopolymer with quartz sand of 180–105 μm. While both crack and combination are observed as decreasing the size range of quartz sand to 105–75 μm. However, combination is mainly observed around quartz particles in the size range of 75–32 μm. It is in a good agreement with the previous results that more combination is formed around quartz particles of smaller size range, because they are of higher surface area.

4. Conclusion

1) In the presence of soluble silicate, incorporation of quartz sand reinforces the mechanical strength of metakaolin geopolymers. The maximum compressive strength of 56.2 MPa was obtained at quartz sand particles of 75–32 μm.
2) Energy dispersive X-ray (EDX) mapping in SEM images indicates the formation of combination by several micrometers around quartz particles, which associates them to the geopolymeric gel as filler materials in metakaolin geopolymers. The left shift of Si-O-T band in FTIR spectra of the geopolymers verifies the Si-O-Si bonds in combination, while the peak at 695 cm^{-1} indicates the insolubility of quartz sand. The XRD and NMR spectra of metakaolin geopolymers with quartz sand confirm both the residual quartz sand particles and the dissolution and precipitation of combination on quartz particle surfaces.
3) In metakaolin geopolymers synthesized with quartz sand of various size ranges, the smaller is the particle size, the higher is the particle surface involved in the formation of combination, thus higher fractions of $Q^4(2Al)$ and $Q^4(1Al)$ are observed in their micro-structures.

Acknowledgement

The financial supports for this work from the Consejo Nacional de Ciencia y Tecnología (CONACyT) of Mexico under the grant No. 270186 and from the National Natural Science Foundation of China under the project No. 51474167 are gratefully acknowledged. Q. Wan would like to thank the CONACyT for offering him the scholarship under the grant NO. 635638 during his PhD studying.

References

[1] J.L. Provis, J.S.J. van Deventer (Eds.), Geopolymers Structure, Processing, Properties and Industrial Applications, Woodhead Publishing Limited, Oxford, UK, 2009.

[2] M. Rowles, B. ÓConnor, Chemical optimisation of the compressive strength of aluminosilicate geopolymers synthesized by sodium silicate activation of metakaolinite, J. Mater. Chem. 13 (2003) 1161–1165.
[3] S.A. Bernal, J.L. Provis, V. Rose, R. Mejía de Gutierrez, Evolution of binder structure in sodium silicate-activated slag-metakaolin blends, Cem. Concr. Comp. 33 (2011) 46–54.
[4] W.K.W. Lee, J.S.J. van Deventer, Structural reorganisation of class F fly ash in alkaline silicate solutions, Colloids Surf. A Physicochem Eng. Asp. 211 (2002) 49–66.
[5] S.A. Bernal, E.D. Rodríguez, R. Mejía de Gutierrez, J.L. Provis, S. Delvasto, Activation of metakaolin/slag blends using alkaline solutions based on chemically modified silica fume and rice husk ash, Waste Biomass Valori 3 (2012) 99–108.
[6] A. Hajimohammadi, J.L. Provis, J.S.J. van Deventer, The effect of silica availability on the mechanism of geopolymerization, Cem. Concr. Comp. 41 (2011) 210–216.
[7] A. Autef, E. Joussein, G. Gasgnier, S. Rossignol, Role of the silica source on the geopolymerization rate, J. Non-Cryst. Solids 358 (2012) 2886–2893.
[8] C.A. Rees, J.L. Provis, G.C. Lukey, J.S.J. van Deventer, The mechanism of geopolymer gel formation investigated through seeded nucleation, Colloids Surf. A Physicochem. Eng. Asp. 318 (2008) 97–105.
[9] J.W. Phair, J.S.J. van Deventer, J.D. Smith, Mechanism of polysialation in the incorporation of zirconia into fly ash-based geopolymers, Ind. Eng. Chem. Res. 39 (2000) 2925–2934.
[10] J.W. Phair, J.S.J. van Deventer, J.D. Smith, Interaction of sodium silicate with zirconia and its consequences for polysialation, Colloids Surf. A Physicochem. Eng. Asp 182 (2001) 143–159.
[11] P. Sukmak, S. Horpibulsuk, S. Shen, Strength development in clay-fly ash geopolymer, Constr. Build. Mater. 40 (2013) 566–574.
[12] F. Rao, Q. Liu, Geopolymerization and its potential application in mine tailings consolidation: a review, Min. Process. Extr. Metall. Rev. 36 (2015) 399–409.
[13] I. Silva, J. Castro-Gomes, A. Albuquerque, Mineral waste geopolymeric artificial aggregates as alternative materials for wastewater-treatment processes: study of structural stability and pH variation in water, J. Mater. Civ. Eng. 24 (2012) 623–628.
[14] L. Zhang, S. Ahmari, J. Zhang, Synthesis and characterization of fly ash modified mine tailings-based geopolymers, Constr. Build. Mater. 25 (2011) 3773–3781.
[15] F. Pacheco-Torgal, J. Castro-Gomes, S. Jalali, Investigations about the effect of aggregates on strength and microstructure of geopolymeric mine waste mud binders, Cem. Concr. Res. 37 (2007) 933–941.
[16] Q. Wan, F. Rao, S. Song, R.E. García, R.M. Estrella, C.L. Patiño, Y. Zhang, Geopolymerization reaction, microstructure and simulation of metakaolin-based geopolymers at extended Si/Al ratios, Cem. Concr. Comp. 79 (2017) 45–52.
[17] A.V. McCormick, A.T. Bell, C.J. Radke, Multinuclear NMR investigation of the formation of aluminosilicate anions, J. Phys. Chem. 93 (1989) 1741–1744.
[18] M. Criado, A. Fernández-Jiménez, A. Palomo, Alkali activation of fly ash: effect of the SiO_2/Na_2O ratio: Part I: FTIR study, Microporous Mesoporous Mater. 106 (2007) 180–191.
[19] T.W. Cheng, J.P. Chiu, Fire-resistant geopolymer produced by granulated blast furnace slag, Min. Eng. 16 (2003) 205–210.
[20] H. Moosber-Bustnes, B. Lagerblad, E. Forssberg, The function of fillers in concrete, Mat. Struct. 37 (2004) 74–81.
[21] T. Yang, X. Yao, Z. Zhang, H. Zhu, Effects of NaOH solution concentration and reaction time on metakaolin geopolymerization, J. Nanjing Univ. Technol. 35 (2013) 21–25 (in Chinese).
[22] Z. Fu, D. Yin, D. Yin, Q. Li, L. Zhang, Y. Zhang, Synthesis, characterization and catalytic properties of titanium and boron co-substituted silicalite zeolites, Microporous Mesoporous Mater. 29 (1999) 351–359.
[23] N.Y. Mostafa, S.A.S. El-Hemaly, E.I. Al-Wakeel, S.A. El-Korashy, P.W. Brown, Characterization and evaluation of the pozzolanic activity of Egyptian activity of Egyptian industrial by-products I: silica fume and dealuminated kaolin, Cem. Concr. Res. 31 (2001) 467–474.
[24] A. Hajimohammadi, J.L. Provis, J.S.J. van Deventer, One-part geopolymer mixes from geothermal silica and sodium aluminate, Ind. Eng. Chem. Res. 47 (2008) 9396–9405.
[25] S. Lucas, M.T. Tognonvi, J.L. Gelet, J. Soro, S. Rossignol, Interactions between silica sand and sodium silicate solution during consolidation process, J. Non-Cryst. Solids 357 (2011) 1310–1318.
[26] T. Bakharev, Geopolymeric materials prepared using class F fly ash and elevated temperature curing, Cem. Concr. Res. 35 (2005) 1224–1232.
[27] T. Duxson, J.L. Provis, G.C. Lukey, F. Separovic, J.S.J. van Deventer, ^{29}Si NMR study of structural ordering in aluminosilicate geopolymer gels, Langmuir 21 (2005) 3028–3036.
[28] S.K. Lee, J.F. Stebbins, The degree of aluminum avoidance in aluminosilicate glasses, Am. Min. 84 (1999) 937–945.
[29] H. Rahier, B. Van Mele, M. Biesemans, J. Wastiels, X. Wu, Low-temperature synthesized aluminosilicate glasses, J. Mater. Sci. 31 (1996) 71–79.
[30] G. Engelhardt, D. Michel, High-resolution Solid-state NMR of Silicates and Zeolites, Wiley, New York, 1987, pp. 77–135.
[31] M.R. Rowles, J.V. Hanna, K.J. Pike, M.E. Smith, B.H. ÓConnor, ^{29}Si, ^{27}Al, ^{1}H, and ^{23}Na MAS NMR study of the bonding character in aluminosilicate inorganic polymers, Appl. Magn. Reson. 32 (2007) 663–689.

Journal of Non-Crystalline Solids 460 (2017) 74–80

Contents lists available at ScienceDirect

Journal of Non-Crystalline Solids

journal homepage: www.elsevier.com/locate/jnoncrysol

Reexamining calcination of kaolinite for the synthesis of metakaolin geopolymers - roles of dehydroxylation and recrystallization

Qian Wan [a,b], Feng Rao [a,*], Shaoxian Song [b]

[a] Instituto de Investigación en Metalurgia y Materiales, Universidad Michoacana de San Nicolás de Hidalgo, Ed. "U", Ciudad Universitaria, Morelia, Michoacán 58030, Mexico
[b] School of Resources and Environmental Engineering, Wuhan University of Technology, Luoshi Road 122, Wuhan, Hubei 430070, China

ARTICLE INFO

Article history:
Received 12 October 2016
Received in revised form 5 January 2017
Accepted 12 January 2017
Available online xxxx

Keywords:
Metakaolin geopolymer
Calcination
Dehydroxylation
Al coordination

ABSTRACT

Properties of metakaolins heated in a temperature range of 550–950 °C for 6 h are characterized by TGA and DSC for thermal analysis, NMR for Al coordination, and XRD for crystal structure. Dehydroxylation is the main reaction with heating temperature of 550–800 °C, and then recrystallization becomes important. Although recrystallization affects greatly the beginning of geopolymerization reactions even at a moderate heating temperature like 800 °C, a plateau of high compressive strength of geopolymers is obtained in the range of 650–850 °C. It is found that optimal mechanical property of geopolymers can be obtained with metakaolins of sufficient dehydroxylation and low recrystallization. In zeolite synthesis using metakaolin, the reactivity of metakaolin was at a maximum when the content of Al^{VI} was at a minimum. However, in the case of metakaolin geopolymer synthesis, joint effects of dehydroxylation and recrystallization determine the reactivity of metakaolin in geopolymerization reactions.

1. Introduction

Geopolymers are synthesized by activating aluminosilicates with highly alkaline solution. They have attracted wide attention in recent years as a potential alternative to ordinary Portland cement (OPC) of low carbon emissions [1]. Metakaolin obtained through the calcination of kaolinite is one of the most studied aluminosilicates in the preparation of geopolymers because of its consistent chemical composition and properties [2]. Calcination is applied to induce dehydration, dehydroxylation and recrystallization to kaolinite, of which the reaction rate depends on the starting kaolinite and the heating regime [3]. For heating regime, calcination temperature among 500–900 °C, mostly 600 °C, 700 °C and 800 °C are used, but the heating time are varied greatly in literature [4]. For instance, Rahier et al. [5] applied heating at 700 °C for one hour in their pioneering studies of the synthesis, structure and properties of metakaolin geopolymers. Sagoe-Crentsil and Weng [6] employed heating at 850 °C for 5 h in studying the dissolution processes, hydrolysis and condensation reactions in metakaolin geopolymer preparation. Zhang et al. [7] used heating at 700 °C for 12 h in studying the composition design and microstructure of metakaolin geopolymer. It is generally accepted that metakaolin obtained through heating possesses amorphous structure, in which the SiO_4 sheets persist but in a distorted form, while the octahedral sheets are profoundly altered, although some short-range structure is preserved [8]. In heating process, Al coordination first changes from octahedral (Al^{VI}) to pentahedral (Al^{V}) and tetrahedral (Al^{IV}), with Al^{V} and Al^{IV} developing simultaneously. Then, Al^{VI} reappears when new phases begin to crystallize, some Al^{IV} persists, but Al^{V} disappears [3]. The transition of Al coordination has been used in the elucidation of the zeolite yield in its synthesis and compressive strength of metakaolin and $Ca(OH)_2$ mixture, and it is accepted that the reactivity of metakaolin was at a maximum when the content of Al^{VI} was at a minimum [9].

In the synthesis of metakaolin geopolymers, a plenty of studies reported heating regime as a synthesizing parameter without discussing the reactivity of metakaolin [10–12]. Some studies correlated heating temperature to the structure and mechanical property of metakaolin geopolymers, and stated an optimal heating temperature. For example, Elimbi et al. [13] heated kaolinite clays at 450, 500, 550, 600, 650, 700, 750, 800 °C, and stated the optimal temperature of 700 °C for metakaolin geopolymer. A few studies discussed the reactivity of metakaolin in the formation of geopolymers. Wang [14] et al. reported that Al atoms in geopolymers were tetrahedral and octahedral (Al^{IV}, Al^{VI}) and Si atoms were tetrahedral at heating temperature of 800 °C, but at 900 °C there were recrystallized octahedral Al atoms (Al^{VI}) and tetrahedral Si atoms. And they stated that the higher degree of polymerization, bulk density, and mechanical properties of geopolymers were obtained at heating temperature of 900 °C. Kuenzel et al. [15] studied coordination of Al $^{(IV, V \text{ and } VI)}$ atoms in three types of metakaolin, and the properties of geopolymers formed from them. They stated that no clear correlation was found between the Al^{V} content in metakaolin samples and geopolymer setting time, heat output or strength development.

* Corresponding author.
E-mail address: fengrao@umich.mx (F. Rao).

http://dx.doi.org/10.1016/j.jnoncrysol.2017.01.024
0022-3093/

The present work attempts to reexamine the structural properties of metakaolins heated at various temperatures, and correlate to the geopolymerization reaction, the microstructure, morphology and mechanical properties of metakaolin geopolymers. We hypothesize that the calcination rate of metakaolins determines the geopolymerization reaction and mechanical properties of metakaolin geopolymers.

2. Experimental

2.1. Materials

Kaolinite with a particle size of 50% <4 μm was collected from Hubei province, China. It was heated at 550 °C, 600 °C, 650 °C, 700 °C, 750 °C, 800 °C, 850 °C, 900 °C and 950 °C in air for 6 h, respectively, in the preparation of metakaolin. Table 1 gives the chemical composition of metakaolin measured by X-ray Fluorescence (XRF). The mass ratios of SiO_2 and Al_2O_3 are close to those in pure metakaolin. Sodium silicate (Na_2SiO_3, ACS reagent grade) was used as alkali activator.

2.2. Metakaolin geopolymer synthesis

In the preparation of geopolymers with metakaolins heated at various temperatures, 1 mol metakaolin (222 g), 1 mol Na_2SiO_3 (122 g) and 12 mol H_2O (216 mL) were used, with the molar ratios of Na_2O/Al_2O_3 and Na_2O/H_2O were 1:1 and 1:12, and the solid/liquid (S/L) was 1.03:1 g/mL. In a typical synthesis by using metakaolin heated at a particular temperature (e.g., 700 °C), the 122 g Na_2SiO_3 was first dissolved in 216 mL water to prepare the alkaline activator solution. Then, it was mixed with 222 g metakaolin for 10 min. After that, the mixture was poured into three cubic steel molds (50 mm × 50 mm × 50 mm). The molds were vibrated on a vibration table for 3 min to liberate the bubbles. Then, they were sealed for the curing process, in which it was first cured at 60 °C for 6 h and continued at room temperature for 7 days.

2.3. Characterizations of metakaolin, geopolymerization reactions and geopolymer microstructure

Differential scanning calorimetry (DSC) and thermogravimetric analysis (TGA) were performed using a STA 449F3 DSC-TG test machine (Netzsch, Germany) to characterize the nature of kaolinite at heating rate of 10 °C/min in nitrogen atmosphere from 0 to 1100 °C. X-ray diffraction (XRD, Bruker D8) was employed to characterize the microstructure of metakaolin heated at various temperatures. ^{27}Al nuclear magnetic resonance (NMR) spectra of metakaolin and geopolymer were determined with NMR spectroscopy (Bruker AVANCE III) at 104.3 MHz. Powdered specimens were packed into 4 mm ZrO_2 rotors. Spectra were acquired at spinning speeds of 10 kHz with peak positions referenced to aluminum nitrate ($Al(NO_3)_3$) and recorded with 2 s delay time. The coordination of Al $^{(VI, V \text{ and } IV)}$ in metakaolin was obtained by applying Seasolve PeakFit™ software and Gaussian peak deconvolution as reported elsewhere [16].

Geopolymerization is an integrated process that involves dissolution of aluminosilicates, reorientation, polymerization and condensation. By using the same dosages of metakaolin and alkaline activator as those used in geopolymer syntheses, the dissolved Al concentrations were measured in separated tests. Alkaline activator and metakaolin were first mixed and agitated for 60 min. Then, 3.8 L water was added into the mixture and the suspension was agitated for 30 s. After that, the slurry was further diluted to avoid undesirable precipitation, filtered and analyzed for dissolved Al compounds by atomic absorption spectroscopy (AAS) [17]. The isothermal heat revolution in the first 48 h of geopolymerization reactions, such as dissolution, polymerization and condensation, were characterized by a C80 microcalorimeter from Setaram, France, with the external temperature maintained at 25 ± 0.001 °C. The metakaolin geopolymers were characterized with

Table 1
Chemical composition of metakaolin.

Component	SiO_2	Al_2O_3	K_2O	Fe_2O_3	TiO_2	MgO
wt%	52.8	43.7	1.2	0.6	0.5	0.2

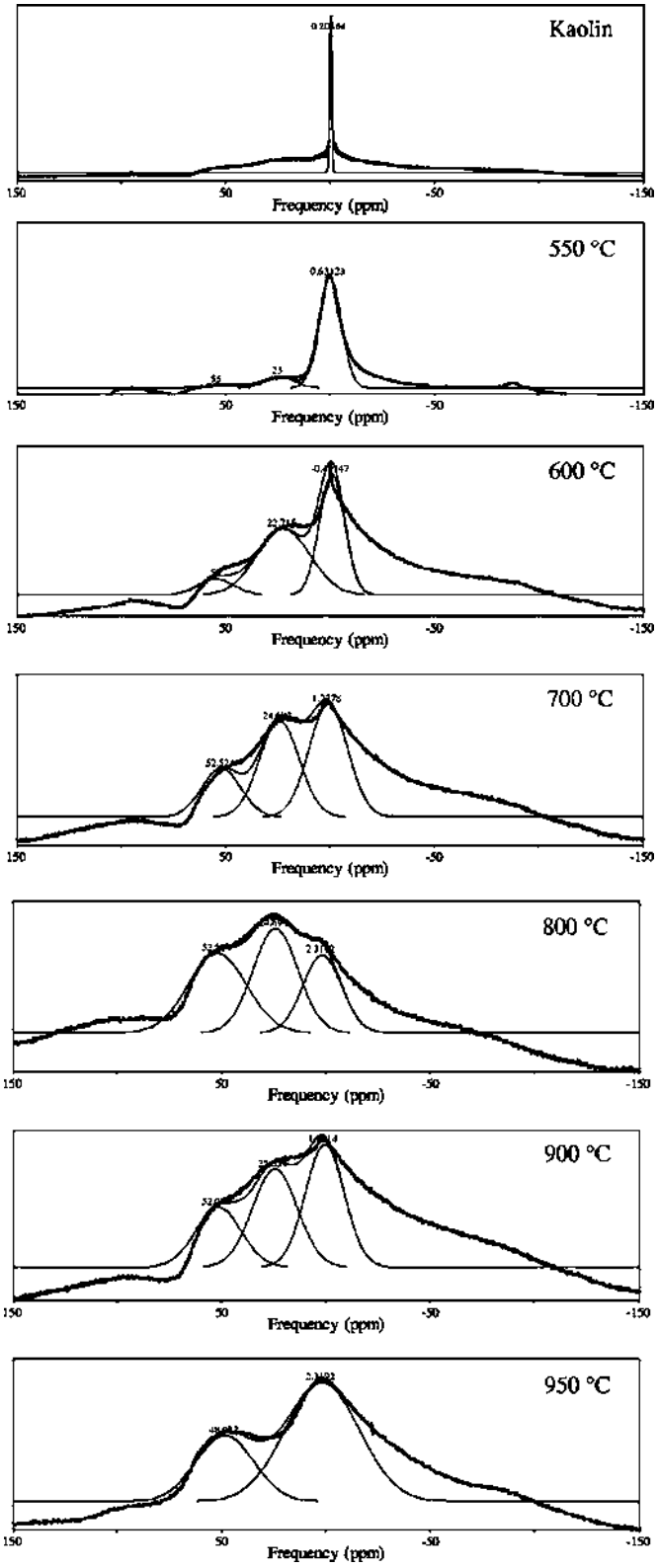

Fig. 1. ^{27}Al NMR spectra (dotted line) and their deconvolution (solid line) of metakaolin heated at various temperatures.

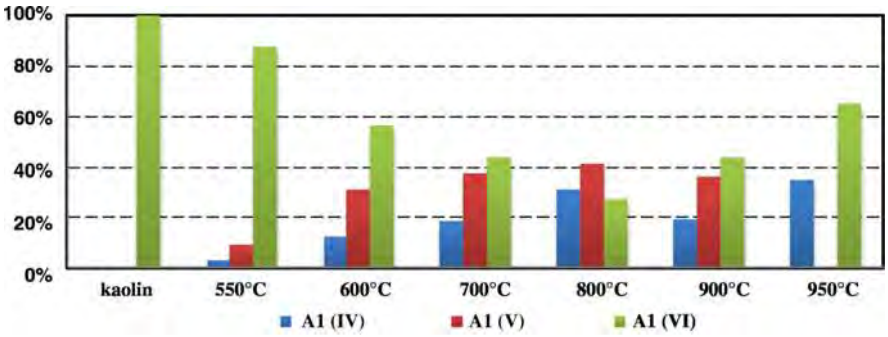

Fig. 2. Fractions of Al^{VI}, Al^{V} and Al^{IV} coordination in metakaolin heated at various temperatures.

scanning electron microscope (SEM, JSM-5610LV JEOL) for their morphology, and mechanical tester (Hangzhou Xingo Technology, EHC-1300) for compressive strength.

3. Results

Fig. 1 gives the ^{27}Al NMR spectra and their deconvolution of kaolin heated at various temperatures, as well as the fractions of aluminum coordination, namely Al^{VI}, Al^{V} and Al^{IV}, are summarized in Fig. 2. The NMR spectrum of kaolin possesses only a sharp peak, indicating high contents of crystalline phase (octahedral Al sheet). The NMR spectra of metakaolin heated at various temperatures show broad band and several peaks, suggesting the formation of amorphous phase and the transformation of aluminum coordination. According to reported Al coordination in phyllosilicates by NMR spectroscopy, the frequencies around 0, 25, and 55 ppm correspond to Al^{VI}, Al^{V} and Al^{IV}, respectively [18,19]. In metakaolin heated at different temperatures, these frequencies might change trivially because of the different status of tetrahedral Si linked to Al [20]. For instance, Al^{VI} is characterized at 0.2 ppm and 2.3 ppm in kaolin and metakaolin heated at 800 °C, indicating AlO_6 links to tetrahedral $Si(Q^3)$ or $Si(Q^2)$ after dehydroxylation at 800 °C. As noted in Fig. 2, only Al^{VI} is identified in kaolin at room temperature, Al^{VI}, Al^{V} and Al^{IV} are identified at heating temperatures between 550 and 900 °C, while Al^{VI} and Al^{IV} are shown at heating temperature of 950 °C. The fractions of Al^{VI} decrease as increasing heating temperature to 800 °C, with Al^{V} and Al^{IV} increase simultaneously, then the fractions of Al^{VI} re-increase as increasing heating temperature to 950 °C, simultaneously Al^{V} decreases to zero.

Fig. 3 shows the DSC and TGA curves of the kaolin sample, in which three temperature regions have been classified. In region I from 40 to 400 °C, the weight loss increases gradually (TGA), and the first endothermic peak around 100 °C in DSC curve corresponds to the dehydration of adsorbed water. In region II from 400 to 780 °C, the weight loss increases sharply, and the second endothermic peak at 500 °C in DSC curve is related to dehydroxylation of the kaolin sample. In regions III from 780 to 1100 °C, the weight loss increases slightly, and the exothermic peak at 990 °C suggests the recrystallization of metakaolin. In the upper temperature regions, dehydration and dehydroxylation may overlap, as well as dehydroxylation and recrystallization. These results correspond well with the reported thermal analysis of kaolinite [3,21], the differences on temperatures for endothermic and exothermic peaks might be resulted from the properties of kaolinite samples from different origins.

Fig. 4 presents the XRD spectra of metakaolin samples heated at temperatures from 550 to 950 °C. The spectra of 600 to 900 °C show amorphous pattern with trace crystalline peak of quartz, implying the amorphous structure of metakaolin. At 550 °C, the spectrum shows amorphous structure with crystalline peaks of kaolinite and quartz, suggesting the incompletion of dehydroxylation. At 950 °C, the spectrum shows amorphous structure with crystalline peaks of spinel-type γAl_2O_3 and mullite, indicating recrystallization of the metakaolin. These results are in a good agreement with the NMR results and thermal

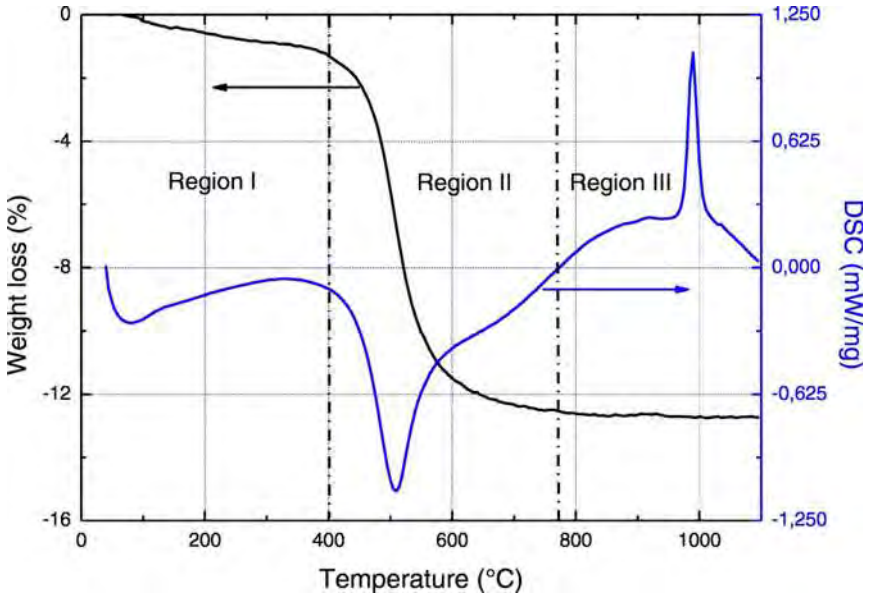

Fig. 3. Thermal analysis curves of the kaolin sample.

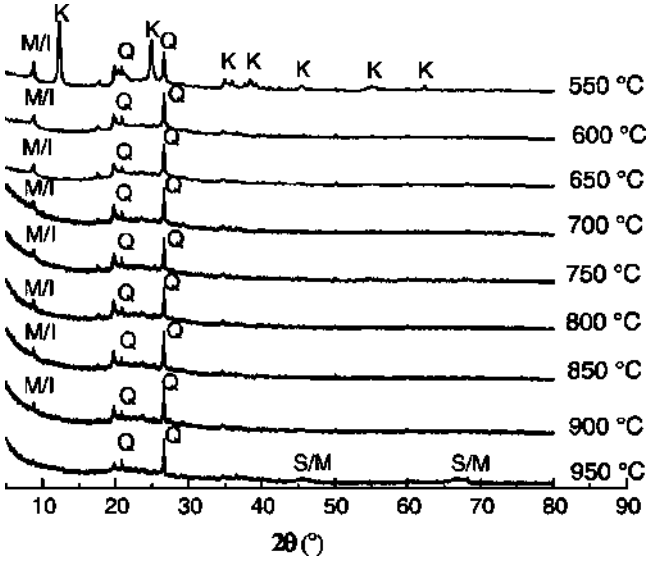

Fig. 4. XRD patterns of metakaolin heated at 550–950 °C (K: kaolinite PDF: 78-2110; M/I: mica/illite PDF: 46-0741; Q: quartz PDF: 79-1906; S/M: spinel-type γAl_2O_3/mullite PDF: 87-0345).

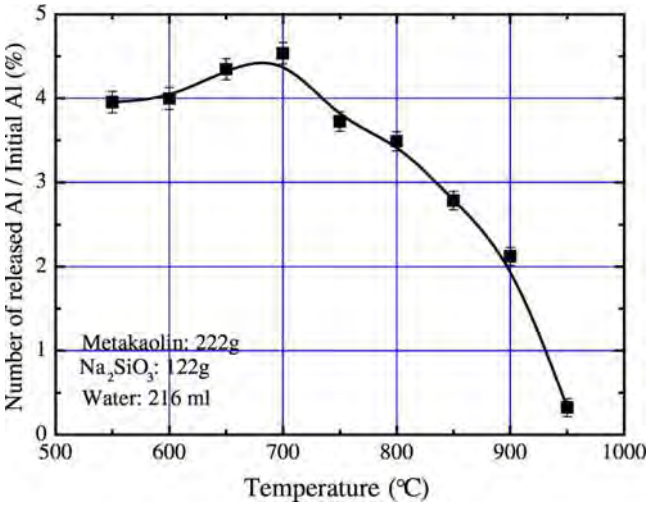

Fig. 5. Dissolution rates of Al compounds with metakaolin heated at various temperatures.

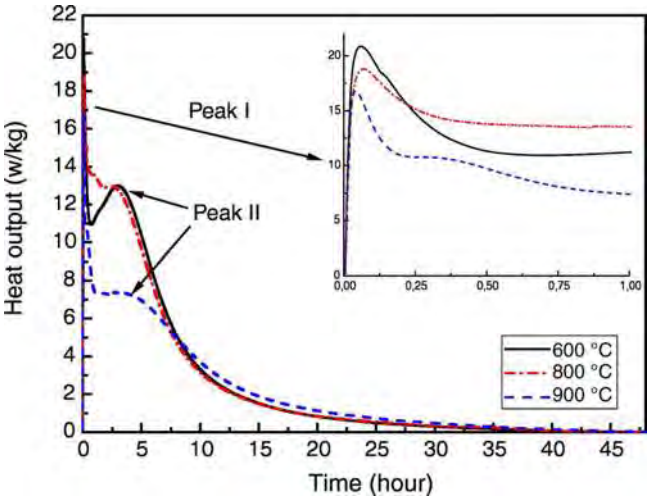

Fig. 6. Heat evolution of geopolymerization reactions with metakaolin heated at various temperatures.

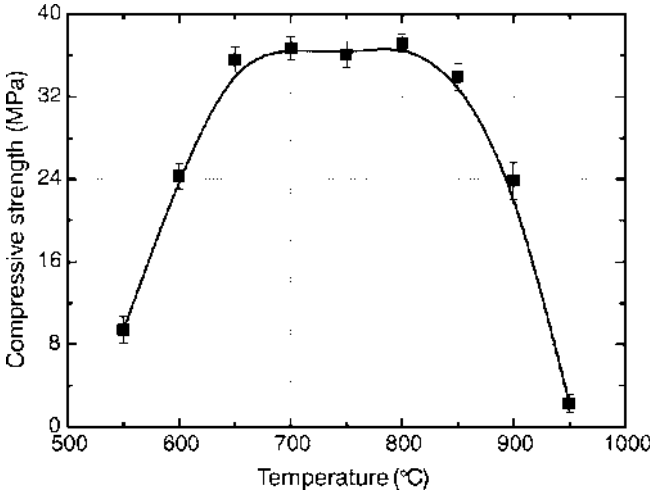

Fig. 7. Compressive strength of geopolymer synthesized with metakaolin samples heated from 550 °C to 950 °C.

analysis that different degrees of dehydroxylation and recrystallization take place through calcination with temperatures from 550 to 950 °C.

In geopolymerization, Al and Si dissolution is critical because it is the first stage that releases aluminate and silicate monomers by alkali attack on raw aluminosilicates, followed by polymerization of the monomers and condensation into three-dimensional aluminosilicate network [22]. In order to characterize dissolution rates of metakaolin heated at various temperatures, the rates of Al release at 60 min with the same amounts of metakaolin, sodium silicate and water has been measured in separated tests, of which the results are present in Fig. 5. With metakaolin heated from 550 to 700 °C, the rates of Al release are high and increases slightly. Then, the rates of Al release decrease sharply as increasing heating temperature from 700 to 950 °C.

Heat revolution of geopolymerization reactions with metakaolin heated at 600, 800 and 900 °C in the first 48 h has been studied and present in Fig. 6. The exothermic peak I, which is sharp and appears immediately after mixing, implies the wetting of metakaolin particles and

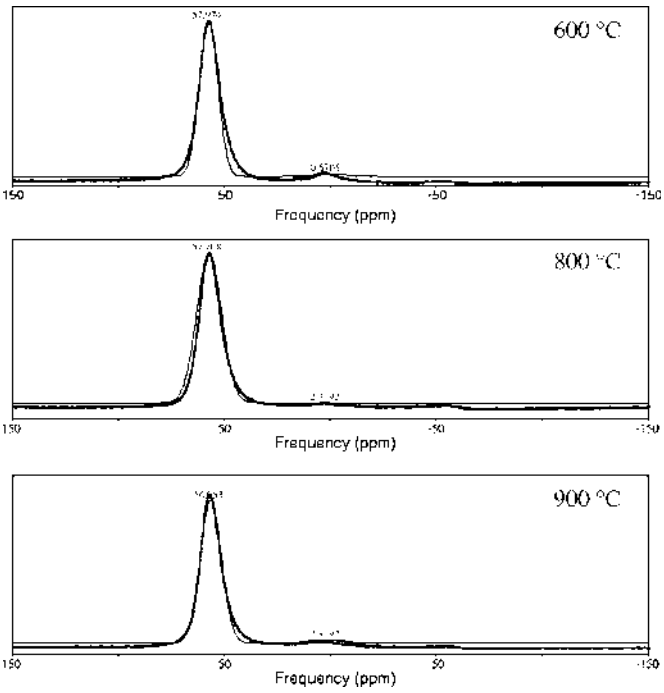

Fig. 8. ^{27}Al NMR spectra of geopolymers synthesized with metakaolins heated at various temperatures.

dissolution reactions [15]. The time required for this process is <15 min. For peak I, the heat output of geopolymerization decreases as increasing calcination temperatures, indicating calcination reduces wettability of metakaolin. The exothermic peak II, which takes place around 3 h, indicates reactions of continue dissolution and polymerization that oligomers combine to form geopolymer network. The heat output of geopolymerization in this process is equal of both metakaolins heated at 600 and 800 °C, which is much higher than that at 900 °C. It suggests that the intensity of dissolution and polymerization reactions with metakaolin heated at 900 °C is much lower than those at 600 and 800 °C [23].

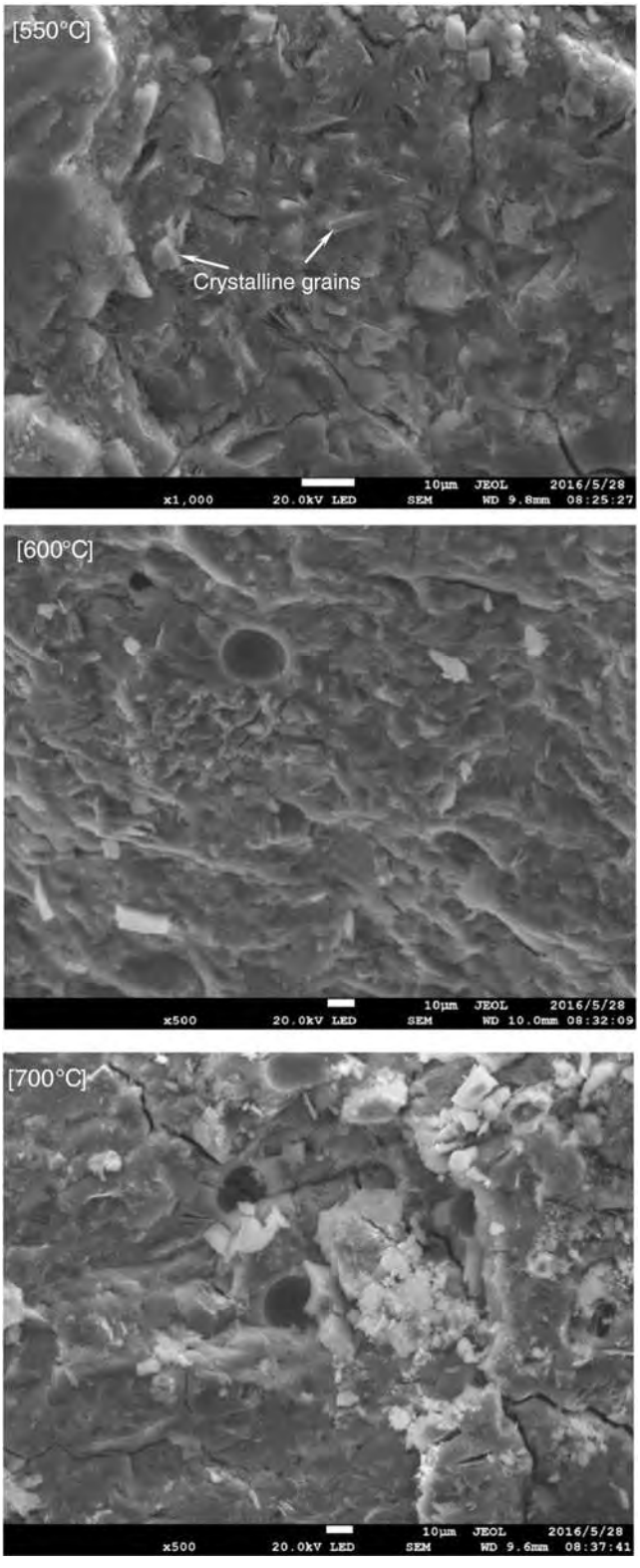

Fig. 9. SEM images of geopolymer synthesized with metakaolin heated at various temperatures.

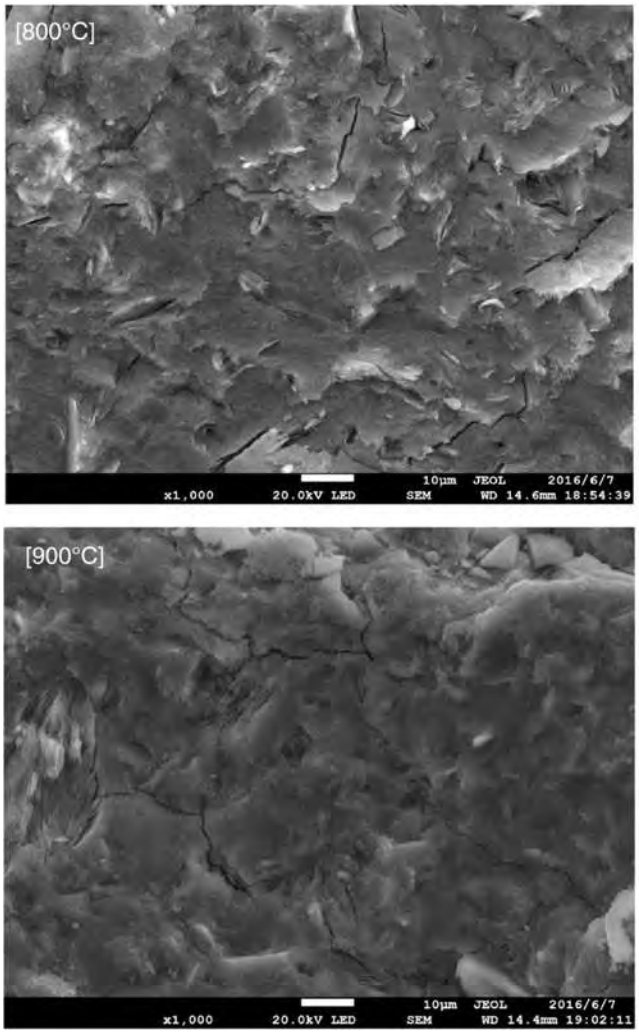

Fig. 9 (*continued*).

Fig. 7 gives the compressive strength of geopolymers with metakaolin heated at various temperatures. The compressive strength increases sharply from 9.4 to 35.6 MPa as changing the metakaolin calcination temperature from 550 to 650 °C. Then, the compressive strength keeps a plateau (>30 MPa) as increasing metakaolin calcination temperature from 650 to 850 °C. However, with increasing the metakaolin calcination temperature continually to 900 and 950 °C, the compressive strength reduces to 23.8 and 2.2 MPa, respectively.

Fig. 8 shows the ^{27}Al NMR spectra and their deconvolution of geopolymers synthesized with metakaolins heated at 600, 800 and 900 °C. The spectra possess a dominant sharp peak at frequency around 57 ppm, which represents Al^{IV} and implies the formation of geopolymer gel in the geopolymers [24]. Except for the main product peak of geopolymer gel, the small peak suggests residual Al^{VI} in the geopolymers. The location of this peak is at frequency of 0.57 ppm for 600 °C and 2.32 ppm for 800 and 900 °C, which differentiates that Al^{VI} in the precursor metakaolins are of residual kaolinite and of recrystallization, respectively. Interestingly, the Al^{V}, which appears in raw metakaolins, is transformed into Al^{IV} in the geopolymerization reactions [4].

Fig. 9 shows the SEM images of geopolymers synthesized with metakaolin heated at various temperatures. In geopolymer with metakaolin heated at 550 °C, a part of crystalline grains appears, indicating residual kaolinite in the geopolymer. However, the crystalline grains become less and disappear as increasing the calcination temperature of metakaolin. And the geopolymers with metakaolin heated at 800 and 900 °C show extremely homogeneous geopolymer binder in microstructure.

4. Discussion

Kaolinite goes through dehydroxylation and/or recrystallization in typical calcination regimes in the syntheses of metakaolin geopolymers. The octahedral Al sheets are destroyed, and then transformed to a spinel-type phase or Si-containing γAl_2O_3 together with amorphous silica, after that, mullite and cristobalite are recrystallized on further heating [3,9]. With calcination time of 6 h and changing calcination temperature, the results of thermal analysis, NMR measurements and XRD patterns show a good agreement on the calcination rate of the metakaolin samples. As increasing the calcination temperature from 550 to 800 °C, endothermic dehydroxylation takes place mainly; fraction of Al^{VI} decreases constantly; kaolinite only appears in the XRD spectrum of 550 °C. While as increasing it from 800 to 950 °C, the kaolinite samples pass through both dehydroxylation and recrystallization (exothermic); fraction of Al^{VI} increases again; spinel-type γAl_2O_3 and mullite appears in the XRD spectrum of 950 °C. The calcination rate of metakaolin determines the geopolymerization reactions and mechanical property of geopolymers when other parameters are the same in the syntheses of geopolymers.

For the beginning of geopolymerization reaction, metakaolin heated at 600 °C possesses higher reaction rate than that at 800 °C, as indicated from the higher heat output in the first 15 min and higher Al dissolution rate in the first hour. This result is opposite of the fact that metakaolin heated at 600 °C has lower calcination rate (dehydroxylation) than that heated at 800 °C. However, recrystallization becomes important at 800 °C as this temperature is in region III and the overlap of dehydroxylation and recrystallization in the calcination process (Fig. 3), even though it is not the main reaction. Thus recrystallization is highly detrimental to beginning geopolymerization reaction. And if the recrystallization degree is high enough (e.g., metakaolin heated at 900 °C), this effect lasts for more hours. However, geopolymerization is an integrated process involving dissolution, polymerization, condensation and consolidation, of which these reactions overlap and last as long as months. The long reaction time gives the possibility to form geopolymers with optimal mechanical property, even though the beginning of geopolymerization reactions might be different [25]. Thus a plateau of high compressive strength is obtained in the range of heating temperature from 650 to 850 °C, but Al dissolution turns to decrease at 700 °C. And it is consistent with reported studies that diverse heating regimes were supposed to be optimal and applied. The statement [13] of only one temperature as the optimal heating temperature of metakaolin in the synthesis of geopolymers is dubious.

Sufficient degree of dehydroxylation and low recrystallization might be the two boundary conditions in the formation of geopolymers with high compressive strength. In this study, with heating temperature lower than 650 °C, the reduction of compressive strength is resulted from insufficient dehydroxylation. With heating temperature higher than 850 °C, the reduction of compressive strength is due to recrystallization in metakaolins. It is different from zeolite formation that metakaolin was found to have maximum reactivity when it had minimum Al^{VI} [9,26], because zeolite formation is a short time reaction compared to geopolymerization. Furthermore, the fractions of Al coordination, which has been used as criteria of metakaolin reactivity in zeolite formation and mechanical property of metakaolin and $Ca(OH)_2$ mixture, is not a convenient criteria of metakaolin in the synthesis of geopolymer. For example, the fractions of Al^{VI}, Al^{V} and Al^{VI} of metakaolin heated at 700 °C are almost equal to those of metakaolin heated at 900 °C (Fig. 2), but the compressive strength of geopolymers synthesized by these metakaolins are greatly different (Fig. 7). In metakaolin heated at 900 °C, recrystallization increases the fraction of Al^{VI} and decreases the fractions of Al^{V} and Al^{IV} to make them equal to those of metakaolin heated at 700 °C. And it is understandable that controversial statements have been present in studies when using Al coordination as criteria of metakaolin reactivity in the synthesis of geopolymers. In addition, microstructure of geopolymers studied by NMR and SEM measurements show some characteristics of metakaolin heated at various temperatures, but not reveal the detrimental recrystallization effect in geopolymerization.

5. Conclusion

1) Dehydroxylation and recrystallization take place in heating kaolinite at moderate temperature (550–800 °C) and high temperature (850–950 °C), respectively. And the fractions of Al^{VI} coordination in the metakaolins decrease first and then increase due to recrystallization in this heating regime.

2) Recrystallization plays a great detrimental role in the dissolution in geopolymerization reaction. Thus the rate of beginning geopolymerization reaction with metakaolin heated at 600 °C is higher than that heated at 800 °C. But a plateau of high compressive strength of geopolymers is obtained with metakaolins of heating temperature in the range of 650–850 °C, because the long geopolymerization reaction time makes the different geopolymers gain the final and optimal mechanical property.

3) The joint effects of dehydroxylation and recrystallization determine the reactivity of metakaolins in geopolymerization reactions and mechanical properties of geopolymers, rather than the only Al^{VI} content.

Acknowledgement

The financial supports for this work from the Consejo Nacional de Ciencia y Tecnología (CONACyT) of Mexico under the grant no. 270186 and from the National Natural Science Foundation of China under the project no. 51474167 are gratefully acknowledged. Q. Wan would like to thank the CONACyT for offering him the scholarship under the grant no. 635638 during his PhD studying.

References

[1] F. Rao, Q. Liu, Geopolymerization and its potential application in mine tailings consolidation: a review, Miner. Process. Ext. Metall. 36 (2015) 399–409.
[2] Z. Zhang, H. Zhu, C. Zhou, H. Wang, Geopolymer from kaolin in China: an overview, Appl. Clay Sci. 119 (2016) 31–41.
[3] L. Heller-Kallai, Thermally modified clay minerals, in: F. Bergaya, G. Lagaly (Eds.), Handbook of Clay Science, second ed.Elsevier, Amsterdam, 2013.
[4] P. Duxson, A. Fernández-Jiménez, J.L. Provis, A. Palomo, J.S.J. van Deventer, Geopolymer technology: the current state of the art, J. Mater. Sci. 42 (2007) 2917–2933.
[5] H. Rahier, B. Mele, M. Biesemans, J. Wastiels, X. Wu, Low-temperature synthesized aluminosilicate glasses, J. Mater. Sci. 31 (1996) 71–79.
[6] K. Sagoe-Crentsil, L. Weng, Dissolution processes, hydrolysis and condensation reactions during geopolymer synthesis: part II. High Si/Al ratio systems, J. Mater. Sci. 42 (2007) 3007–3014.
[7] Y. Zhang, W. Sun, Z. Li, Composition design and microstructural characterization of calcined kaolin-based geopolymer cement, Appl. Clay Sci. 47 (2010) 271–275.
[8] C.E. White, J.L. Provis, T. Proffen, J.S.J. van Deventer, The effects of temperature on the local structure of metakaolin-based geopolymer binder: a neutron pair distribution function investigation, J. Am. Ceram. Soc. 93 (2010) 3486–3492.
[9] J. Rocha, J. Klinowski, ^{29}Si and ^{27}Al magic-angle-spinning NMR studies of the thermal transformation of kaolinite, Phys. Chem. Miner. 17 (1990) 179–186.
[10] P. Rovnaník, Effect of curing temperature on the development of hard structure of metakaolin-based geopolymer, Constr. Build. Mater. 24 (2010) 1176–1183.
[11] H. Wang, H. Li, F. Yan, Synthesis and mechanical properties of metakaolinite-based geopolymer, Colloids Surf. A 268 (2005) 1–6.

[12] P. Duxson, S.W. Mallicoat, G.C. Lukey, J.S.J. van Deventer, The effect of alkali and Si/Al ratio on the development of mechanical properties of metakaolin-based geopolymers, Colloids Surf. A Physicochem. Eng. Asp. 292 (2007) 8–20.
[13] A. Elimbi, H.K. Tchakoute, D. Njopwouo, Effects of calcination temperature of kaolinite clays on the properties of geopolymer cements, Constr. Build. Mater. 25 (2011) 2805–2812.
[14] M. Wang, D. Jia, P. He, Y. Zhou, Influence of calcination temperature of kaolin on the structure and properties of final geopolymer, Mater. Lett. 64 (2010) 2551–2554.
[15] C. Kuenzel, T.P. Neville, S. Donatello, L. Vandeperre, A.R. Boccaccini, C.R. Cheeseman, Influence of metakaolin characteristics on the mechanical properties of geopolymers, Appl. Clay Sci. 83 (2013) 308–314.
[16] D. Massiot, F. Fayon, M. Capron, I. King, S. Le Calve, B. Alonso, J.O. Durand, B. Bujoli, Z. Gan, G. Hoatson, Modelling one and two-dimensional solid-state NMR spectra, Magn. Reson. Chem. 40 (2002) 70–76.
[17] V. Nikolic, M. Komljenovic, Z. Bascarevic, N. Marjanovic, Z. Miladinovic, R. Petrovic, The influence of fly ash characteristics and reaction conditions on strength and structure of geopolymers, Constr. Build. Mater. 94 (2015) 361–370.
[18] J. Sanz, J.M. Serratosa, Silicon-29 and aluminum-27 high-resolution MAS-NMR spectra of phyllosilicates, J. Am. Ceram. Soc. 106 (17) (1984) 4790–4793.
[19] D. Massiot, P. Dion, J.F. Alcover, F. Bergaya, ^{27}Al and ^{29}Si MAS NMR study of kaolinite thermal decomposition by controlled rate thermal-analysis, J. Am. Ceram. Soc. 78 (1995) 2940–2944.
[20] E. Prudhomme, P. Michaud, E. Joussein, A. Smith, C. Peyratout, I. Sobrados, J. Sanz, S. Rossignol, Geomaterial foams: role assignment of raw materials in the network formation, J. Sol-Gel Sci. Technol. 61 (2012) 436–448.
[21] W. Smykatz-Kloss, The determination of the degree of (dis-) order of kaolinites by means of differential thermal analysis, Chem. Erde 33 (1974) 358–364.
[22] A. Hajimohammadi, J.L. Provis, J.S.J. van Deventer, Effect of alumina release rate on the mechanism of geopolymer gel formation, Chem. Mater. 22 (18) (2010) 5199–5208.
[23] Z. Zhang, H. Wang, J.L. Provis, F. Bullen, A. Reid, Y. Zhu, Quantitative kinetic and structural analysis of geopolymers. Part 1. The activation of metakaolin with sodium hydroxide, Thermochim. Acta 539 (2012) 23–33.
[24] S.J. Lyu, Y.H. Hsiao, T.T. Wang, T.W. Cheng, T.H. Ueng, Microstructure of geopolymer accounting for associated mechanical characteristics under various stress states, Cem. Concr. Res. 54 (2013) 199–207.
[25] P. Sukmak, S. Horpibulsuk, S. Shen, Strength development in clay–fly ash geopolymer, Constr. Build. Mater. 40 (2013) 566–574.
[26] S. Chandrasekhar, Influence of metakaolinization temperature on the formation of zeolite 4A from kaolin, Clay Miner. 31 (1996) 253–261.

Applied Clay Science 146 (2017) 223–229

Contents lists available at ScienceDirect

Applied Clay Science

journal homepage: www.elsevier.com/locate/clay

Research paper

Geothermal clay-based geopolymer binders: Synthesis and microstructural characterization

Qian Wan[a,b], Feng Rao[a,b,*], Shaoxian Song[a,**], Carlos Alberto León-Patiño[b]

[a] School of Resources and Environmental Engineering, Wuhan University of Technology, Luoshi Road 122, Wuhan, Hubei 430070, China
[b] CONACYT Instituto de Investigación en Metalurgia y Materiales, Universidad Michoacana de San Nicolás de Hidalgo, Ed. "U", Ciudad Universitaria, Morelia, Michoacán 58030, Mexico

ARTICLE INFO

Keywords:
Kaolinite
Cristobalite
Geothermal clay
Geopolymer
Microstructure

ABSTRACT

Geothermal clay rich in kaolinite was first prepared into geopolymer binders. Preparation conditions of calcination on geothermal clay, Na_2SiO_3 and NaOH combination in alkaline activator, and water content were studied. Thermal nature of the geothermal clay was characterized by TG-DSC and XRD measurements, which shows characteristics of kaolinite and cristobalite during calcination. Mechanical property, morphology and microstructure of the geothermal clay-based geopolymers were characterized by compressive strength measurements, SEM observation and NMR spectra analysis. With optimal synthesizing parameters, geothermal clay-based geopolymer possessed a compressive strength of 19.5 MPa, as well as a homogeneous geopolymeric gel with high percentages of $Q^4(2Al)$ and $Q^4(1Al)$. As geothermal clay is supposed to be of intermediate dissolution reactivity in geopolymerization, this synthesis might extend the kinds of raw aluminosilicates in geopolymer formation.

1. Introduction

Geopolymer, a three-dimensional amorphous binder material, has attracted extensive attention due to the potential properties in replacement of ordinary Porland cement (OPC), but of low CO_2 emission in the synthesis process (Davidovits, 1989; Duxson et al., 2007). Chemical reactions in synthesizing geopolymers, namely geopolymerization, are integrated processes involved the dissolution of raw materials in highly alkaline solution to form silicate and aluminate monomers, reorientation and polymerization of these monomers into oligomers and network, and the condensation of the network (Rao and Liu, 2015). In geopolymerization, the dissolution of monomers plays an important role because it forms the precursors for polymerization and condensation. Generally, calcination in the pre-treatment or to choose by-products after calcination is employed to obtain raw materials with high reactivity for the dissolution of monomers. For instance, metakaolin obtained through heating kaolinite in the temperature range among 500–900 °C was studied as exemplary material in geopolymer synthesis (Rahier et al., 1996). Calcination forms an amorphous structure to the kaolinite, in which the SiO_4 sheets persist but in a distorted form, while the octahedral aluminum sheets are profoundly altered, although some short-range structure is preserved (Wan et al., 2017). Similarly, ore-dressing tailings of bauxite heated at 800 °C for 1 h has been synthesized into geopolymer of 40 MPa in compressive strength (Ye et al., 2014). Fly ash, which is the other most extensively studied raw material for synthesizing geopolymers, is the by-products of coal combustion (van Jaarsveld et al., 2002). Granulated blast furnace slag, which is the by-products of iron smelting, is also used as raw aluminosilicate in geopolymerization. In addition, mechanical activation has been used to enhance the dissolution activity of raw aluminosilicates. Temuujin et al. (2009) reported that grinding fly ash in a vibration mill with a milling media to powder ratio of 10 led to an 80% increase in compressive strength of the produced geopolymers when compared with geopolymers synthesized directly from raw material. Obviously, calcination and mechanical activation are the opposite of low CO_2 emission, which is the important advantage of geopolymer synthesis.

Therefore, in pursuing the commercialization of geopolymer as environmental friendly construction material, raw aluminosilicates from industrial waste without pre-treatment are studied extensively. For example, kaolinite, albite and silty clay were used as fine aggregates in the preparation of fly ash-based geopolymers (Xu and van Deventer, 2002; Sukmak et al., 2013). And Ahmari et al. (2012) used waste concrete powder as additive in the synthesis of fly ash-based geopolymer, of which the maximum compressive strength was 35 MPa. Another waste named red mud that produced in alumina refining process was synthesized into geopolymers using rice husk ash (full in SiO_2) and

* Corresponding author at: CONACYT Instituto de Investigación en Metalurgia y Materiales, Universidad Michoacana de San Nicolás de Hidalgo, Ed. "U", Ciudad Universitaria, Morelia, Michoacán 58030, Mexico.
** Corresponding author.
E-mail addresses: fengrao@umich.mx (F. Rao), shaoxian@uaslp.mx (S. Song).

http://dx.doi.org/10.1016/j.clay.2017.05.047
Received 17 January 2017; Received in revised form 30 May 2017; Accepted 31 May 2017

NaOH as alkaline activator (He et al., 2013). However, these syntheses rely on the limited industrial by-products (e.g., fly ash), which would be an obstacle in large-scale applications in some countries. Furthermore, oil sands tailings and many mine tailings that contain aluminosilicate minerals as their main constituents have been proposed as raw materials in the syntheses of geopolymers (Rao and Liu, 2015). Zhang et al. (2011) pioneered the preparation of copper mine tailings-based geopolymer bricks, but compression was applied in the bricks formation. Thus to synthesize geopolymers directly from industrial waste is interesting area that can be studied further for selecting the proper raw aluminosilicate.

Clay minerals related to geothermal activity, which is named geothermal clay in this study, are abundant aluminosilicates in geothermal fields. Their properties are not only affected by temperature but also by several factors such as rock and fluid chemistry, time, fluid/rock ratio, the nature of the precursor material or the mechanism of the crystal growth (Mas et al., 2006). Geothermal clay is usual industrial waste after drilling wells in geothermal energy exploitation. Many studies reported the geological characteristics of geothermal clay (Mas et al., 2006), but no application of geothermal clay has been found so far. However, geothermal silica from geothermal power plants, which is an analogous by-product to geothermal clay, is employed as additive in OPC and geopolymer syntheses. For example, Gómez-Zamorano and Escalante-García (2010) prepared Portland cement pastes substituted with 0%, 5%, 10% and 15% of geothermal silica in mass and cured at 10, 20, 40 and 60 °C for up to 540 days. According to calcium hydroxide contents analysis, they found that the geothermal silica showed a strong pozzolanic behavior. Hajimohammadi et al. (2011) used geothermal silica to mix with solid sodium aluminate and sodium silicate solution in the preparation of geopolymers at SiO_2/Al_2O_3 ratio of 3. In the present study, geothermal clay is studied as raw aluminosilicate in preparing geopolymers, of which the microstructure is characterized. We hypothesize that the clay endured geothermal activity possesses higher reactivity in the dissolution of silicate and aluminate monomers than usual clay. This study might enrich the types of raw aluminosilicates for the synthesis of geopolymers and give a further understanding on geopolymerization reactions.

2. Experimental

2.1. Materials

Geothermal clay rock was collected from the Los Azufres geothermal field, Mexico at the depth of 250 m where the temperature exceeds 150 °C. It was measured the particle size at 50% and 85% of cumulative undersize of 26.9 μm and 36.3 μm, respectively from a Shimadzu SALD-1100 laser diffraction analyzer. Table 1 gave the chemical analysis of the whole geothermal clay rock measured by X-ray fluorescence (XRF, PANalytical Axios), in which SiO_2 and Al_2O_3 are the main components with Si/Al ratio around 3.5. Fig. 1 showed the X-ray diffraction (XRD, Bruker D8) pattern and scanning electron microscopy (SEM, JEOL JSM-5610LV) image of the geothermal clay. The quantitative analysis of XRD pattern gave 47.44% kaolinite, 49.85% cristobalite in mass, and trace amount of tridymite and quartz in the geothermal clay. The SEM image showed kaolinite and cristobalite particles in micrometers, exhibiting platy and granular shapes, respectively. Although other clay minerals (e.g., montmorillonite or illite) were not identified in the XRD pattern of the geothermal clay, they were presumably included according to the components of Table 1.

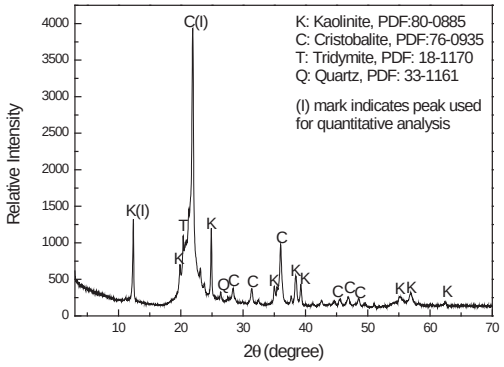

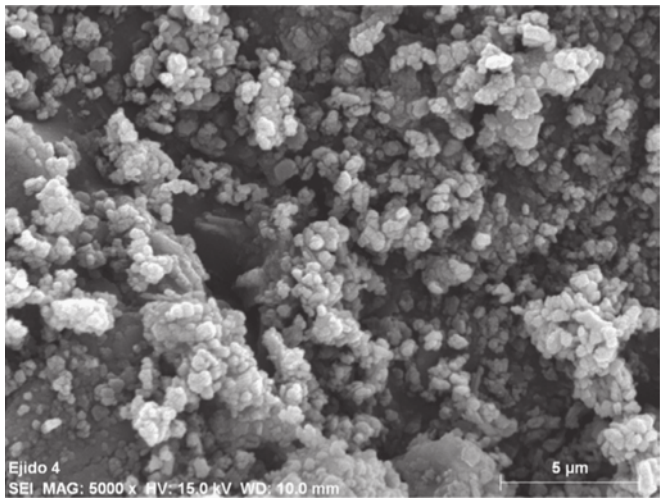

Fig. 1. XRD pattern and SEM image of the geothermal clay.

Sodium hydroxide (NaOH) and sodium silicate (Na_2SiO_3) of analytical reagents of the American Chemical Society (ACS) reagent grade were purchased from Sinopharm Chemical Reagent, China and used as alkaline activator in the synthesis of geopolymers.

2.2. Geopolymer synthesis

In a typical synthesis, alkaline solution was first prepared and then mixed with the geothermal clay. The mixture was poured into a cubic steel mold (50 mm × 50 mm × 50 mm) and vibrated on a vibration table for 3 min to liberate the air bubbles. After that, the mold was sealed for the curing process, in which it was first cured at 60 °C for 6 h and continued at room temperature for 7 days. Table 2 gave the preparing regimes of geothermal clay-based geopolymers, of which the variables were the calcination of geothermal clay, the alkaline activator combination and the water dosage. For preparations No. 1–8, geothermal clay sample (222 g) without and with calcination at 200, 400, 450, 500, 550, 600 and 800 °C were used as raw aluminosilicates. The calcination was performed in a muffle stove with heating rate of 15 °C/min. Once the calcination temperature reached the required value, the alumina crucibles with geothermal clay were heated for 6 h more. After that, the samples were left in the furnace to cool down. The alkaline activator solutions were synthesized consistently with 0.5 mol Na_2SiO_3, 0.5 mol NaOH and 9 mol H_2O, making the solid to liquid and Na/Al

Table 1
Chemical analysis of the whole geothermal clay rock.

Components	SiO_2	Al_2O_3	SO_3	K_2O	Na_2O	MgO	Fe_2O_3	CaO	TiO_2	ZrO_2	LOI
Mass %	71.30	17.11	1.80	0.37	0.07	0.03	0.08	0.03	0.055	0.02	9.089

Table 2
Preparation regime of geothermal clay-based geopolymers.

No.	Calcination (°C)	Alkaline activator		Na/Al	Si/Al	H_2O (mol)
		Na_2SiO_3 (mol)	NaOH (mol)			
Variable in heating temperature						
1–8	0–800	0.5	0.5	2.01	4.2	9
Variable in alkaline activator						
9	800		1	2.68	4.9	9
10	800	1	0	1.34	3.5	9
11	800	0.5	0	1.34	4.2	9
12	800	0.5	0.25	1.68	4.2	9
13	800	0.5	0.5	2.01	4.2	9
14	800	0.5	1	2.68	4.2	9
Variable in water dosage						
15	800	0.5	0.5	2.01	4.2	10
16	800	0.5	0.5	2.01	4.2	11
17	800	0.5	0.5	2.01	4.2	12

ratios in geopolymers as 1.37 and 2.01, respectively. For preparations No. 9–14, raw aluminosilicates were of geothermal clay (222 g) heated at 800 °C, while the alkaline activator solutions were different in the Na_2SiO_3 to NaOH ratios. For preparations No. 15–17, geothermal clay samples (222 g) were heated at 800 °C and alkaline activator solutions were of 0.5 mol Na_2SiO_3 and 0.5 mol NaOH. The variable was the water dosage, of which 10 mol, 11 mol and 12 mol were used respectively.

2.3. Characterization of the geothermal clay and geopolymers

Differential scanning calorimetry (DSC) and thermogravimetric (TG) analysis were performed using a STA 449F3 TG-DSC test machine (Netzsch, Germany) to characterize thermal nature of the geothermal clay at heating rate of 10 °C/min in nitrogen from 40 to 1100 °C. The XRD patterns were obtained with a Bruker D8 diffractometer using monochromatic Cu-Kα_1 radiation (λ = 1.5406 Å). Quantification of different phases was carried out using the computer program MAUD 1.8, which is based on the Rietveld method combined with a Fourier analysis (Celik, 2010). The specimens of geopolymer were characterized by SEM and XRD for microstructures and morphology, and mechanical tester (Hangzhou Xingo Technology, EHC-1300) for compressive strength. In the measurements of compressive strength, three specimens were tested and the average value was used. ^{29}Si nuclear magnetic resonance (NMR) spectra of geopolymers were obtained by using a NMR spectroscopy (Bruker AVANCE III) at 79.49 MHz. Powdered geopolymer specimens were packed into 7 mm in diameter ZrO_2 rotors. Spectra were acquired at spinning speeds of 12 kHz with peak positions referenced to an external standard of tetramethylsilane (TMS) and recorded with 1 s delay time.

3. Results and discussion

3.1. Heat-treated geothermal clay

The thermal analysis of the geothermal clay was performed to elucidate its reactivity in geopolymerization. Fig. 2 presented the TG-DSC curves of the geothermal clay sample, which gave the collective thermal nature of its main components, namely kaolinite and cristobalite (Fig. 1). First, they are analogous to the TG-DSC curves of kaolinite (Wan et al., 2017). The endothermic peaks at around 100 and 550 °C in the DSC curve might be attributed to the moisture or absorbed water in hydrous clay minerals (e.g., illite and montmorillonite) (Liu et al., 2010) and dehydroxylation in kaolinite, corresponding to gradual and sharp mass losses in the TG curve, respectively. The "exothermic" peak at 1010 °C, which showed in status of less endothermic because of the interference from cristobalite, suggests the recrystallization of

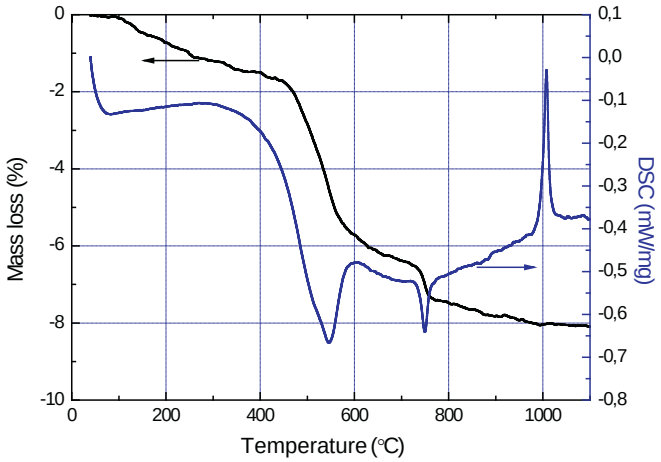

Fig. 2. Thermal analysis curves of the geothermal clay sample.

metakaolin, corresponding to a slightly mass loss. Secondly, cristobalite, which is a high-temperature polymorph of silica, confirmed its stability in mass loss (TGA) but endothermic (DSC) nature in the temperature range of 40–1100 °C (Damby et al., 2014). Thirdly, the endothermic peak at 750 °C, which corresponded to a sharp mass loss of around 1%, might be due to the gasification of aluminum sulfate (Johnson and Gallagher, 1971). As noted in Table 1, the mass percentage of SO_3 is 1.8%. Obviously, calcination at 550 °C induces the dehydroxylation of kaolinite in the geothermal clay sample and greatly increases its dissolution activity, so as to offer a high reactivity in geopolymerization.

The XRD patterns of geothermal clay heated at various temperatures (Fig. 3) were consistent with the results of thermal analysis. In the XRD patterns of 200 and 400 °C, kaolinite, cristobalite and trace amount of tridymite were observed, corresponding to that of geothermal clay without calcination (Fig. 1). However, in the XRD patterns of 600 and 800 °C, kaolinite was not observed. And it is interesting to note that the trace amount of tridymite was not observed at heating temperatures of 600 and 800 °C.

3.2. Geopolymer and microstructure

Fig. 4 presented the compressive strength of geopolymers synthesized with geothermal clay samples heated at various temperatures. Of geothermal clay without calcination, geopolymer was hardly formed, of which possessed a low compressive strength around 1 MPa. It verifies the hypothesis that geothermal clay possesses higher dissolution activity than normal clays because it is able to form geopolymer without

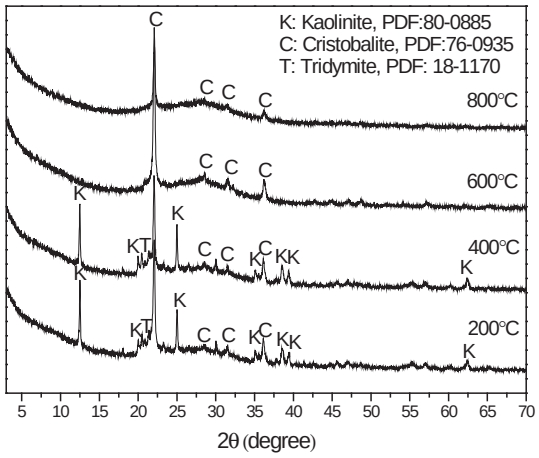

Fig. 3. XRD patterns of geotherm clay samples heated at various temperatures.

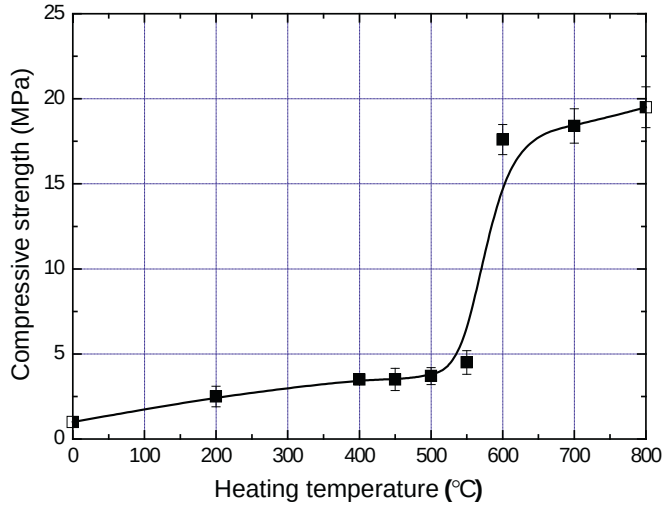

Fig. 4. Compressive strength of geopolymers synthesized with geothermal clay samples heated at various temperatures (No. 1–8).

calcination. With heating temperatures of 200–550 °C, the compressive strength of geopolymers increased slightly to 4.5 MPa. However, as increasing the heating temperature continually (600–800 °C), compressive strength of geopolymers increased sharply to more than triple times and then kept a plateau. The sharp increase in the compressive strength of geopolymers as changing heating temperature from 550 to 600 °C is in good agreement with the thermal analysis of the geothermal clay, in which 550 °C is a critical temperature for inducing dehydroxylation of kaolinite.

The microstructure of geopolymers corresponds well with the increase in compressive strength. In studying microstructure of geopolymers, short-range ordering and molecular structure have been investigated with great success using NMR spectroscopy (Duxson et al., 2005). The lack of spectral resolution for silicon in geopolymers has been overcome by adopting Gaussian peak deconvolution to separate and quantify $Q^n(mAl)$ species ($0 \le m \le n \le 4$, m, n = integer) (Lee and Stebbins, 1999). It has been reported that all silicon and aluminum sites are in tetrahedral coordination in geopolymers, thus $n = 4$ (Rahier et al., 1996). And the resonance of a $Q^4(mAl)$ center with the replacement of each aluminum by silicon is an approximate -5 ppm chemical shift, with $Q^4(4Al)$, $Q^4(3Al)$, $Q^4(2Al)$, $Q^4(1Al)$, $Q^4(0Al)$ resonating at approximately -84, -89, -93, -99 and -108 ppm, respectively (Engelhardt and Michel, 1987). Fig. 5 showed the ^{29}Si NMR spectra and their deconvolution of geopolymers synthesized with geothermal clay heated at various temperatures. At heating temperature of 500 °C, the spectrum of geopolymer showed sharp peaks, indicating high contents of crystalline phase in it. While the spectra of geopolymers synthesized with geothermal clay heated at 600 and 800 °C showed broad band, suggesting the formation of amorphous geopolymeric gel. Because Si/Al ratio in the precursors is 4.2 (Table 2), $Q^4(2Al)$ and $Q^4(1Al)$ should be mainly formed in the geopolymeric gel. Thus in the spectra of 600 and 800 °C, the percentages of $Q^4(2Al)$ and $Q^4(1Al)$ were of 62% and 57%,

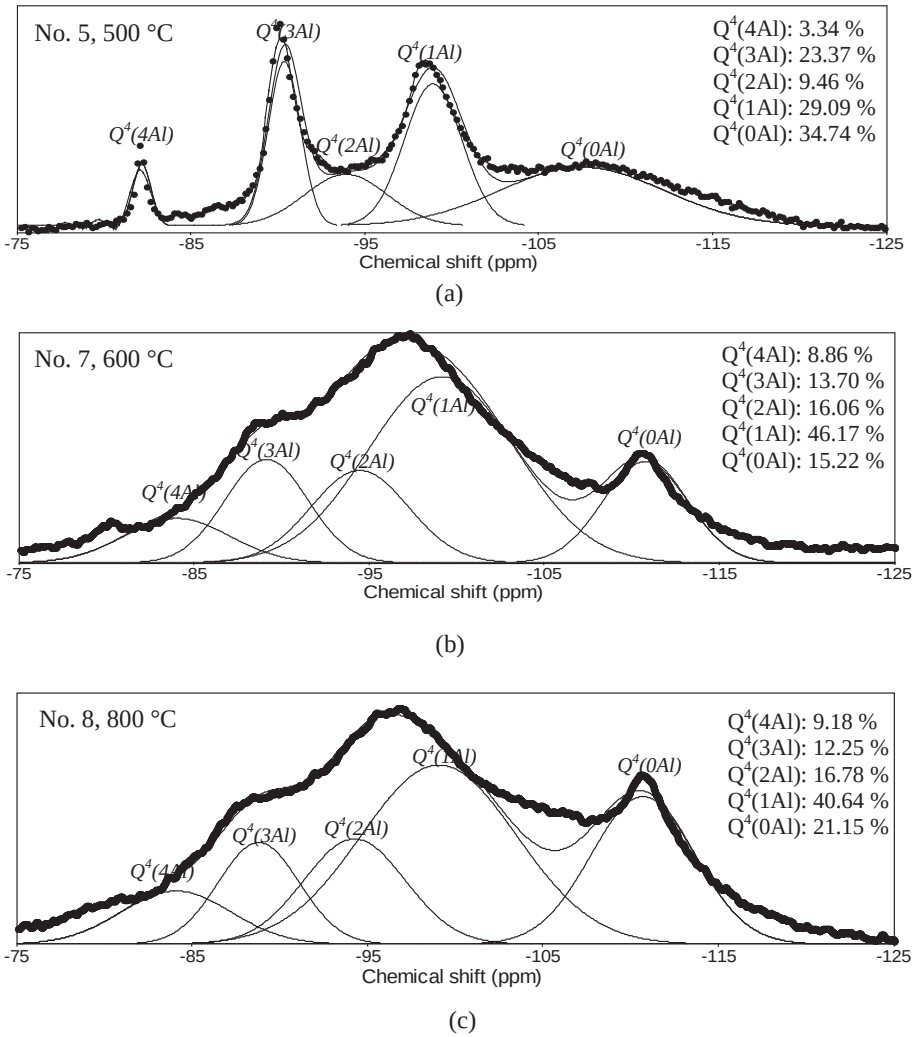

Fig. 5. ^{29}Si NMR spectra and their deconvolution of geopolymers synthesized with geothermal clay heated at 500 (a), 600 (b) and 800 °C (c).

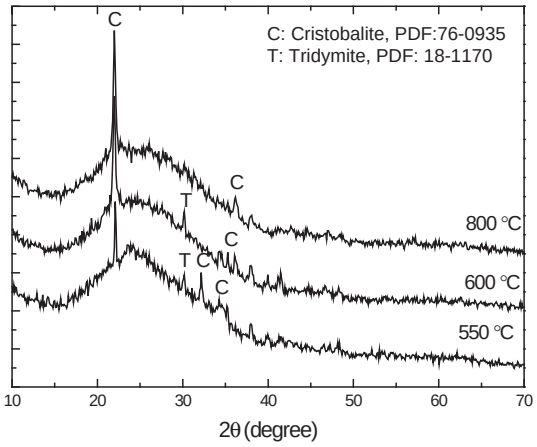

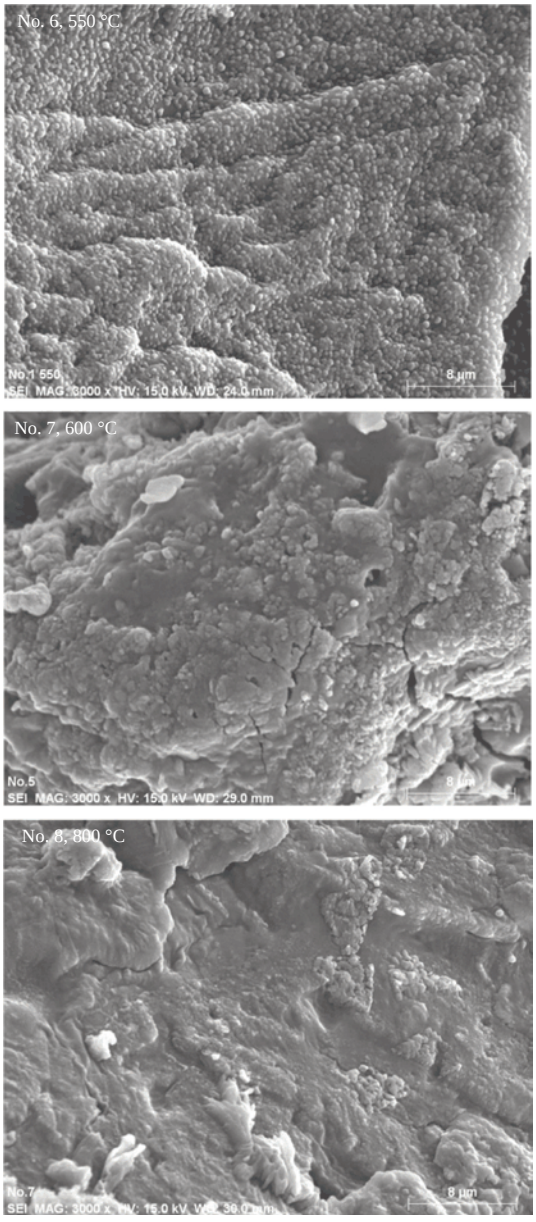

Fig. 6. XRD patterns and SEM images of geopolymers synthesized with geothermal clay heated at various temperatures.

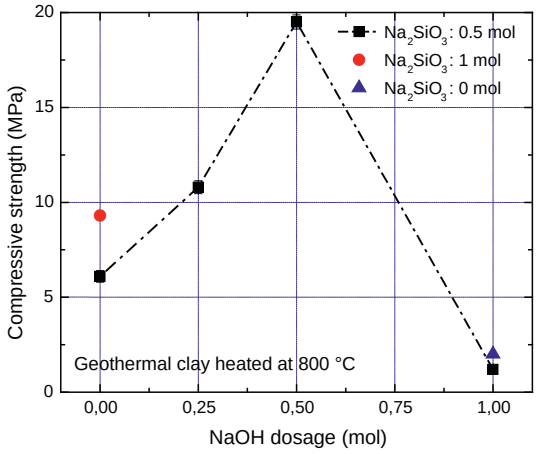

Fig. 7. Compressive strength of geopolymers activated with various combinations of Na_2SiO_3 and NaOH (No. 9–14).

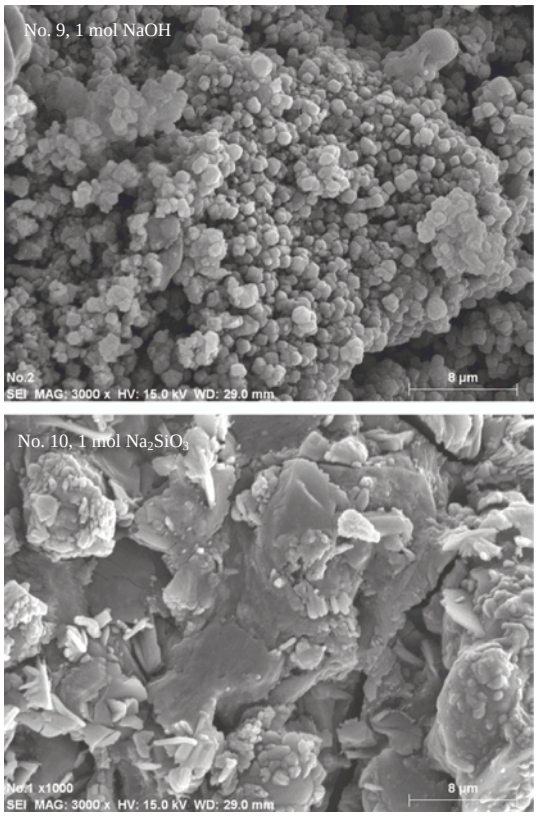

Fig. 8. SEM images of the geopolymers activated with only 1 mol NaOH or Na_2SiO_3.

respectively, but they were of 38% in the spectrum of 500 °C. It verifies the formation of high contents of geopolymeric gel in geopolymers synthesized with geothermal clay heated at 600 and 800 °C. In geopolymer of 500 °C, the high contents of $Q^4(4Al)$ and $Q^4(3Al)$ indicates dehydroxylation of kaolinite is incomplete (Wan et al., 2017), and the high content of $Q^4(0Al)$ might suggest the formation of sodium silicate glasses from the unreacted Na_2SiO_3 activator (Maekawa et al., 1991).

Fig. 6 gave the XRD patterns and SEM images of geopolymers synthesized with geothermal clay heated at various temperatures. With geothermal clay heated at 550, 600 and 800 °C, the XRD patterns of geopolymers showed similar amorphous phase in geopolymeric gel and undissolved silica (cristobalite and trace amount of tridymite). However, the SEM images showed different morphology. At 550 °C, a plenty of granular particles dispersed and covered on the geopolymeric gel,

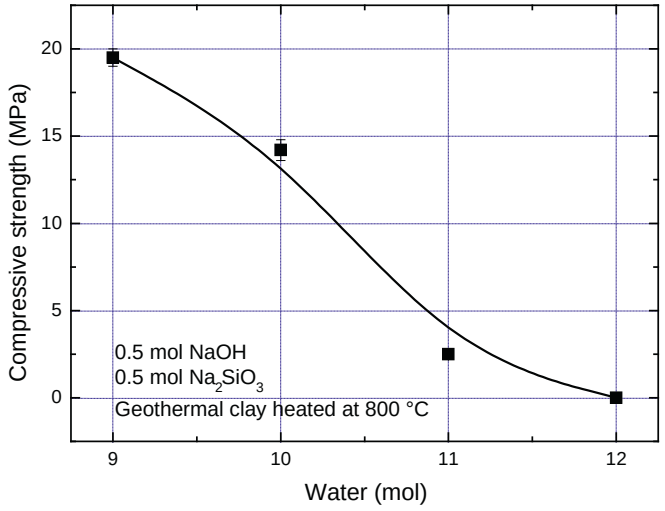

Fig. 9. Compressive strength of geopolymers synthesized at different water contents (No. 8, 15–17).

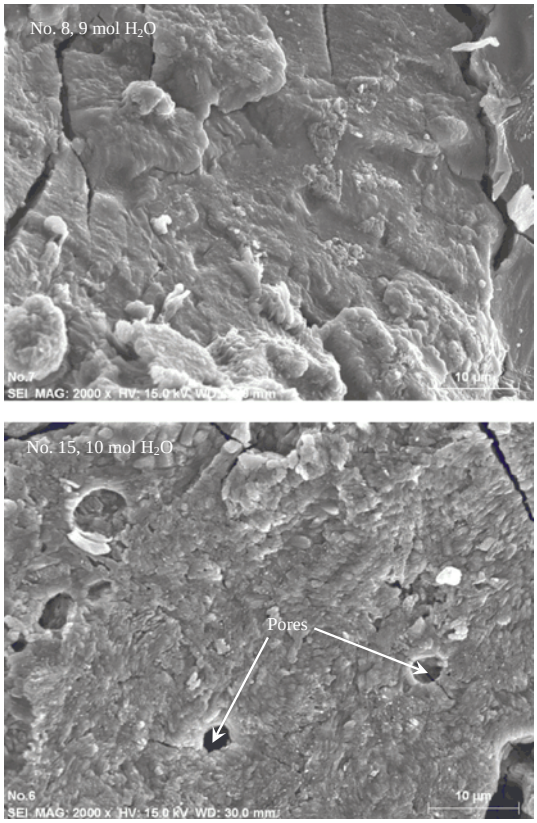

Fig. 10. SEM images of geopolymers synthesized with different water contents.

indicating insufficient dissolution and some components are not involved in the geopolymerization reaction. The geopolymers synthesized with geothermal clay heated at 600 and 800 °C showed more homogeneous binder structure with less unreacted particles, indicating higher dissolution degree of raw aluminosilicates. Based on the facts that kaolinite and cristobalite are two main components in the geothermal clay (Fig. 1) and cristobalite remains after geopolymerization (Fig. 6), it can be assert that the kaolinite (metakaolin after heating) and critobalite play the roles of geopolymeric gel formation and unreacted particles, respectively.

Fig. 7 presented the compressive strength of geopolymers synthesized with different combinations of Na_2SiO_3 and NaOH in activating geothermal clay heated at 800 °C. With only 1 mol Na_2SiO_3 or NaOH, low compressive strength of geopolymers at 9 and 2 MPa was obtained respectively, suggesting the irreplaceable role of Na_2SiO_3 and NaOH in the alkaline activator. At 0.5 mol Na_2SiO_3, the compressive strength of geopolymers increased as increasing the NaOH dosage to 0.5 mol, but reduced greatly as increasing NaOH dosage continually to 1 mol. It is consistent with the report that a high content of NaOH decreases the strength of geopolymers (Palomo et al., 1999).

Fig. 8 gave the SEM images of geopolymers synthesized with only 1 mol NaOH or Na_2SiO_3. The platy kaolinite and granular critobalite particles were observed in agglomeration at alkaline activator of 1 mol NaOH, which suggests no formation of geopolymeric gel and results in low compressive strength. With 1 mol Na_2SiO_3 as activator, geopolymeric binder was observed but with cracks, and undissolved kaolinite or critobalite particles were observed on geopolymeric gel, suggesting NaOH plays the role in the dissolution raw aluminosilicate. Compared with the geopolymer synthesized with 0.5 mol Na_2SiO_3 and 0.5 mol NaOH as activator (Fig. 6), it is found that Na_2SiO_3 and NaOH tend to play the roles of geopolymeric gel formation and aluminosilicate dissolution, respectively, in activating geothermal clay.

Compressive strength of geopolymers synthesized with different water content was presented in Fig. 9. The minimum water content for inducing sufficient mixing during synthesis was 9 mol. As increasing the water content, the compressive strength of geopolymers decreased steadily. And geopolymer could not be formed at the water content of 12 mol.

Fig. 10 gave the SEM images of geopolymers synthesized with water contents of 9 and 10 mol. A homogenous geopolymeric gel was observed at water content of 9 mol, but pores were observed at water content of 10 mol, which might be attributed to the evaporation of residual water. Thus the increase of water content is detrimental to geopolymer formation with geothermal clay, because it leads to the formation of porous structure and lowers the compressive strength. It is in good agreement with the report that excessive water hinders polycondensation in geopolymer formation and lowers the compressive strength (Zuhua et al., 2009).

4. Conclusion

1) Geothermal clay rich in kaolinite possesses higher reactivity than normal clays in geopolymerization, so that it can be synthesized into geopolymers of low compressive strength. The reactivity of geothermal clay is enhanced through calcination. Thermal analysis of the geothermal clay shows analogous behavior as that of kaolinite, but it is affected by the endothermic nature of critobalite.
2) At a heating temperature > 550 °C, the compressive strength and microstructure of geothermal clay-based geopolymers are remarkably improved, in which a homogeneous geopolymeric gel with high percentages of $Q^4(2Al)$ and $Q^4(1Al)$ is formed.
3) In activating geothermal clay to synthesize geopolymers, Na_2SiO_3 and NaOH tend to play the roles of geopolymeric gel formation and aluminosilicate dissolution, respectively. High water content leads to porous structure and low compressive strength in geothermal clay-based geopolymers

Acknowledgement

The financial supports for this work from the National Natural Science Foundation of China under the project No. 51474167 and from the Consejo Nacional de Ciencia y Tecnología (CONACyT) of Mexico under the grant No. 270186 are gratefully acknowledged. Q. Wan would like to thank the CONACyT for offering him the scholarship under the grant NO. 635638 during his PhD studying.

References

Ahmari, S., Ren, X., Toufigh, V., Zhang, L., 2012. Production of geopolymeric binder from blended waste concrete powder and fly ash. Constr. Build. Mater. 35, 718–729.

Celik, H., 2010. Technological characterization and industrial application of two Turkish clays for the ceramic industry. Appl. Clay Sci. 50, 245–254.

Damby, D.E., Llewellin, E.W., Horwell, C.J., Williamson, B.J., Najorka, J., Cressey, G., Carpenter, M., 2014. The α–β phase transition in volcanic cristobalite. J. Appl. Crystallogr. 47 (4), 1205–1215.

Davidovits, J., 1989. Geopolymers and geopolymeric materials. J. Therm. Anal. 35 (2), 429–441.

Duxson, P., Provis, J.L., Lukey, G.C., Separovic, F., van Deventer, J.S.J., 2005. ^{29}Si NMR study of structural ordering in aluminosilicate geopolymer gels. Langmuir 21 (7), 3028–3036.

Duxson, P., Fernández-Jiménez, A., Provis, J.L., Lukey, G.C., Palomo, A., van Deventer, J.S.J., 2007. Geopolymer technology: the current state of the art. J. Mater. Sci. 42 (9), 2917–2933.

Engelhardt, G., Michel, D., 1987. High-resolution Solid-state NMR of Silicates and Zeolites. Wiley, New York.

Gómez-Zamorano, L., Escalante-García, J., 2010. Effect of curing temperature on the nonevaporable water in portland cement blended with geothermal silica waste. Cement. Concrete. Comp. 32, 603–610.

Hajimohammadi, A., Provis, J.L., van Deventer, J.S.J., 2011. The effect of silica availability on the mechanism of geopolymerisation. Cem. Concr. Res. 41, 210–216.

He, J., Jie, Y., Zhang, J., Yu, Y., Zhang, G., 2013. Synthesis and characterization of red mud and rice husk ash-based geopolymer composites. Cement. Concrete. Comp. 37, 108–118.

van Jaarsveld, J.G.S., van Deventer, J.S.J., Lukey, G.C., 2002. The effect of composition and temperature on the properties of fly ash-and kaolinite-based geopolymers. Chem. Eng. J. 89 (1), 63–73.

Johnson, D.W., Gallagher, P.K., 1971. Kinetics of the decomposition of freeze-dried aluminum sulfate and ammonium aluminum sulfate. J. Am. Ceram. Soc. 54 (9), 461–465.

Lee, S.K., Stebbins, J.F., 1999. The degree of aluminum avoidance in aluminosilicate glasses. Am. Mineral. 84 (5–6), 937–945.

Liu, G., Wu, S., van de Ven, M., Molenaar, A., Besamusca, J., 2010. Characterization of organic surfactant on montmorillonite nanoclay to be used in bitumen. J. Mater. Civ. Eng. 22, 794–799.

Maekawa, H., Maekawa, T., Kawamura, K., Yokokawa, T., 1991. The structural groups of alkali silicate glasses determined from ^{29}Si Mas-NMR. J. Non-cryst. Solid. 127, 53–64.

Mas, A., Guisseau, D., Patrier, M.P., Beaufort, D., Genter, A., Sanjuan, B., Girard, J.P., 2006. Clay minerals related to the hydrothermal activity of the Bouillante geothermal field (Guadeloupe). J. Volcanol. Geotherm. Res. 158, 380–400.

Palomo, A., Grutzeck, M.W., Blanco, M.T., 1999. Alkali-activated fly ashes: a cement for the future. Cement. Concrete. Res. 29 (8), 1323–1329.

Rahier, H., van Mele, B., Biesemans, M., Wastiels, J., Wu, X., 1996. Low-temperature synthesized aluminosilicate glasses. J. Mater. Sci. 31 (1), 71–79.

Rao, F., Liu, Q., 2015. Geopolymerization and its potential application in mine tailings consolidation: a review. Miner. Process. Extr. Metall. Rev. 36 (6), 399–409.

Sukmak, P., Horpibulsuk, S., Shen, S., 2013. Strength development in clay-fly ash geopolymer. Constr. Build. Mater. 40, 566–574.

Temuujin, J., Williams, R.P., van Riessen, A., 2009. Effect of mechanical activation of fly ash on the properties of geopolymer cured at ambient temperature. J. Mater. Process. Technol. 209, 5276–5280.

Wan, Q., Rao, F., Song, S., 2017. Reexamining calcination of kaolinite for the synthesis of metakaolin geopolymers-roles of dehydroxylation and recrystallization. J. Non-cryst. Solid. 460, 74–80.

Xu, H., van Deventer, J.S.J., 2002. Geopolymerisation of multiple minerals. Miner. Eng. 15, 1131–1139.

Ye, J., Zhang, W., Shi, D., 2014. Effect of elevated temperature on the properties of geopolymer synthesized from calcined ore-dressing tailing of bauxite and ground-granulated blast furnace slag. Constr. Build. Mater. 69, 41–48.

Zhang, L., Ahmari, S., Zhang, J., 2011. Synthesis and characterization of fly ash modified mine tailings-based geopolymers. Constr. Build. Mater. 25 (9), 3773–3781.

Zuhua, Z., Xiao, Y., Huajun, Z., Yue, C., 2009. Role of water in the synthesis of calcined kaolin-based geopolymer. Appl. Clay Sci. 43 (2), 218–223.

Computational Materials Science 132 (2017) 74–80

Contents lists available at ScienceDirect

Computational Materials Science

journal homepage: www.elsevier.com/locate/commatsci

Variation of interlayer binding energy of muscovite in its swelling

Feifei Jia [a], Bingqiao Yang [b], Qian Wan [c], Shaoxian Song [a,*]

[a] School of Resources and Environmental Engineering, Wuhan University of Technology, Luoshi Road 122, Wuhan, Hubei 430070, China
[b] School of Resource and Civil Engineering, Wuhan Institute of Technology, Xiongchu Avenue 693, Wuhan, Hubei 430073, China
[c] Instituto de Investigación en Metalurgia y Materiales, Universidad Michoacana de San Nicolás de Hidalgo, Ed. "U", Ciudad Universitaria, Morelia, Michoacán 58030, Mexico

ARTICLE INFO

Article history:
Received 13 October 2016
Received in revised form 16 February 2017
Accepted 17 February 2017
Available online 3 March 2017

Keywords:
Interlayer binding energy
Muscovite
Molecular dynamics simulation

ABSTRACT

The interlayer binding energy of natural muscovite after thermal and ionic exchange treatments has been investigated using X-ray diffraction, molecular dynamics simulation and one-dimensional Patterson function. The results showed that the interlayer binding energy was reduced to less than 1/30th of its strength subsequent to thermal and ionic exchange treatments. The decrease of the binding strength after thermal treatment might be due to the modification of atomic positions within the layer and a slight increase of interlayer spacing. A dramatic decrease of the binding strength from 110.05 kJ/mol to 19.09 kJ/mol was observed after the $LiNO_3$ treatment. The mechanism might be explained by a combination of an increase of interlayer spacing and Li^+ immersion into the layers. In addition, interlayer spacing was increased to 3 nm when octadecyl trimethyl ammonium ion (OTA^+) intercalation was used, resulting in the interlayer binding energy approaching 0 kJ/mol.

1. Introduction

Muscovite is a 2:1 layered silicate. Several layers together form a particle. The layers are built of an octahedral sheet, sandwiched between two Si-O sheets [1]. The Si-O tetrahedral sheet is connected at the vertices with the oxygen atoms to form a coplanar hexagonal lattice. A hydroxyl group at the center of each hexagon gives rise to a triangular lattice providing the bottom face of the $AlO_4(OH)_2$ octahedron. An inverted Si-O tetrahedral sheet is then attached to the top face of these octahedrons to complete the muscovite layer [2]. The binding between the muscovite layers has electrostatic and van der Waals interactions [3]. The origin of the ionic binding is from the substitution of Si^{4+} and Al^{3+} in the layers by low-charge cations that gives the silicate layers a negative charge and attracts K^+ in the interlayers to balance the negative charge [4]. It has been reported that the binding energy between the adjacent layers of 6.02×10^{23} muscovite molecules is 134 kJ [5], which tightens the interlayer strongly. Therefore, cleaving natural muscovite into individual layers is difficult.

The exfoliation of muscovite could be realized through applying strong external forces or modifying the interlayer structure. Mechanical forces, for example grinding [6], are important external forces. Ultrasonic treatment has been used to separate adjacent layers. Caseri et al. indicated that the specific surface area of muscovite determined by methylene blue (MB) adsorption was increased from 3.4 m^2/g to more than 100 m^2/g after ultrasound cleavage of muscovite in a $LiNO_3$ solution [7]. Another method is to heat muscovite up to 800 °C, followed by adding it immediately to a saturated Na_2CO_3 or $NaHCO_3$ solution and neutralizing the mixture by HCl [8]. It is believed that in the presence of acid, CO_3^{2-} or HCO_3^- penetrates into the interlayers. The muscovite layers are then separated by the pressure of the evolved CO_2. Commercially, this method can produce muscovite particles with a thickness of about 130 nm, corresponding to approximate 130 silicate layers. However, the methods fail in producing nanoscale particles because the binding strength is intimately related to the ability of muscovite exfoliation and the quality of resulting particles.

In our previous paper, we presented a novel method for the exfoliation of natural muscovite into monolayers. It consists of swelling the interlayers through thermal treatment followed by ionic exchange to reduce the interlayer binding strength, and then exfoliation with ultrasound [9,10]. The key to achieve the exfoliation is to modify the bonds in the interlayer structure. Therefore, it is of great significance to understand the variations of interlayer binding energy when the natural muscovite is swollen, in order to optimize the thermal and ionic exchange treatments.

In this study, we attempted to investigate the variations of interlayer binding energy in muscovite using the molecular dynamics (MD) simulation, X-ray diffraction (XRD) and the one-dimensional (1D) Patterson function. The MD simulation was used to obtain muscovite structure after each treatment, while XRD was

* Corresponding author.
E-mail address: shaoxian@uaslp.mx (S. Song).

http://dx.doi.org/10.1016/j.commatsci.2017.02.023
0927-0256/

used to determine the basal spacing of muscovite. The peaks in the 1D Patterson function represent the interatomic distance vectors, which provide a good description of the distance between atom planes. The interlayer spacing and atomic positions after the thermal and ionic exchange treatments were then calculated and the binding energy was obtained. The objective was to obtain a better understanding of the exfoliation mechanisms of natural muscovite.

2. Methods

2.1. Determination of interlayer binding energy

The interlayer binding energy (IBE) is defined as the energy difference between a single crystal and one which has been cleaved, exposing two open surfaces [5,11], as shown in Eq. (1):

$$IBE = E_{layer1} + E_{layer2} - E_{total} \quad (1)$$

where E_{layer1} and E_{layer2} are energies of two layers, while E_{total} is the energy of the crystal before being separated. The lattice energy E consists of the attraction terms caused by the Coulomb and van der Waals interactions and nonelectrostatic repulsion term. The value of the Coulomb energy can be readily calculated from Eq. (2) [12]

$$U = -\frac{e^2}{2}\sum_{j=1}^{N}\sum_{i=1}^{\infty}\frac{k\cdot z_i z_j}{r_{ij}}\times 10^7 \quad (2)$$

where U is the Coulomb energy, kJ; k is the factor to convert the unit of U, 9.0×10^9 N·m^2/C^2; N is the number of atoms in the unit cell; Z is the valence of the ion; r is the interionic distance, Å; and e is electrical charge, 1.6×10^{-19} C; 10^7 is 10^{-3} divided by 10^{-10} because the unit of U and r is in kJ and Å, respectively. The Lennard-Jones expression is most commonly used to approximate the van der Waals interactions and nonelectrostatic repulsion, as shown in Eq. (3) [13]

$$V_{LJ} = \varepsilon\left[\left(\frac{r_m}{r}\right)^{12} - 2\left(\frac{r_m}{r}\right)^{6}\right] \quad (3)$$

where ε is the depth of the potential well, kJ/mol; r is the distance between the atoms, Å; and r_m is the distance at which the potential reaches its minimum, Å. The atomic positional parameters are the prerequisites in calculating the IBE according to Eqs. (1)–(3). Accordingly, in this work, these parameters can be obtained through a combination of molecular dynamics (MD) simulation, XRD and 1D Patterson function, followed by computing IBE with the above equations using the software of *Materials Studio* (MD) *6.0*.

2.2. Muscovite swelling

The natural muscovite sample (termed M) used in this work for swelling tests was collected from Liaoning Science Co., Ltd, China. The XRD pattern shown in Fig. 1 indicated that the main composition of the sample was monoclinic muscovite 2M1, without any other impurities being determined. The inductively coupled plasma atomic emission spectroscopic and thermogravimetric analysis showed that the chemical formula of one muscovite molecule in the natural sample was $(K_{0.81}Na_{0.09})(Mg_{0.05}Fe_{0.17})(Si_{3.04}Al_{2.65}Rb_{0.01}Ti_{0.01})O_{10}(OH)_{1.5}$. Therefore, one mole natural muscovite has 6.02×10^{23} of the above muscovite molecules.

The muscovite swelling tests were carried out in three steps: (1) the muscovite powder (M) was roasted at 750 °C to obtain the calcinated product (M750); (2) the M750 was further treated in molten lithium nitrate ($LiNO_3$) at 300 °C to exchange all K^+, yielding a product of Li-M750; (3) the Li-M750 was finally treated in the saturated octadecyl trimethyl ammonium chloride (OTAC) solution to insert large molecules into the interlayers to obtain the product

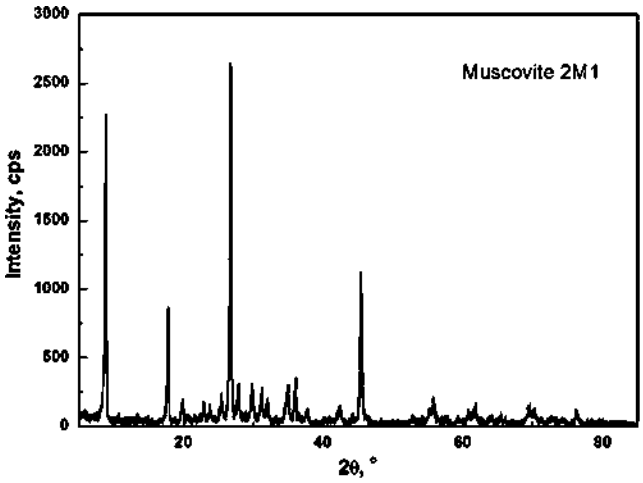

Fig. 1. The XRD pattern of the natural muscovite sample.

OTA-M750. The details of the experimental method were described in our previous publication [10].

The chemical reagents used in this work were all of analytical grade, purchased from Sinopharm Chemical Reagent Co., Ltd, China. Ultrapure Milli-Q water was used throughout.

2.3. Measurements

The elemental analysis of muscovite was performed using the PerkinElmer Optima4300DV ICP.

Mineral phase and structure changes before and after treatments were determined using a Bruker D8 Advance X-ray diffractometer with Cu K_α radiation. The diffraction patterns, ranging from 5° to 80° (2θ), were collected with a step-scanning speed of 10°/min, while small-angle diffraction patterns from 1° to 10° (2θ) were collected with a step-scanning speed of 1°/min.

FT-IR measurements were conducted using a Thermo Scientific Nicolet 6700 FT-IR spectrometer, with the pellets being prepared by pressing a mixture of 1–2 mg of the sample and 200–300 mg of dried KBr.

2.4. Molecular dynamics simulation

Muscovite has a monoclinic space group *C2/c* [14]. The original muscovite model was based on the structure defined in Guggenheim's work [15]. The lattice parameters were $a = 0.52$ nm, $b = 0.9021$ nm, $c = 2.007$ nm, and $\beta = 95.71°$ and the atom positional coordinates are shown in Table 1, where no atom substitution is listed. The perfect structure model of muscovite was built with software *Materials Studio 6.0* by importing the space group, lattice parameters and atom positional coordinates. It is common that substitution occurs in the natural sample; therefore, based on the chemical formula obtained in this study, two tetravalent Si atoms and one trivalent Al atom were substituted by two Al atoms and one divalent Fe atom, respectively. After that, the energy of the structure was minimized by the Discover Module using the *Materials Studio 6.0* software. The lattice parameters ($a = 0.5217$ nm, $b = 0.9185$ nm, $c = 2.022$ nm, $\beta = 95.75°$) and atom positions of dehydroxylated muscovite (Li-M750) were given by Gridi-Bennadji et al. [16] (shown in Table 1), according to which the structure of dehydroxylated muscovite was built with *Materials Studio 6.0*. The same Al/Si and Fe/Al substitutions took place in the dehydroxylated muscovite as in the original. In the interaction simulation of $LiNO_3$ into dehydroxylated muscovite, a dehydroxylated muscovite model was cut parallel to the (*0 1 0*) direction to

Table 1
Atom positional coordinates of muscovite.

Atom	Perfect muscovite			Dehydroxylated muscovite		
	x	*y*	*z*	*x*	*y*	*z*
K	0	0.0982	0.25	0	0.1001	0.25
Al	0.2511	0.0836	0.0001	0.2751	0.0958	0.0041
Si	0.4648	0.9294	0.13565	0.4746	0.9328	0.1313
Si	0.4517	0.2584	0.13545	0.4486	0.2569	0.1407
O	0.4170	0.0926	0.1683	0.4139	0.0827	0.1684
O	0.251	0.8112	0.1582	0.2569	0.8219	0.1536
O	0.251	0.3705	0.1690	0.2408	0.3767	0.1700
O	0.4579	0.9438	0.0536	0.5037	0.9581	0.0510
O	0.3858	0.2528	0.0537	0.3615	0.2494	0.0603
OH	0.4565	0.5636	0.0503	0.0	0.0	0.0

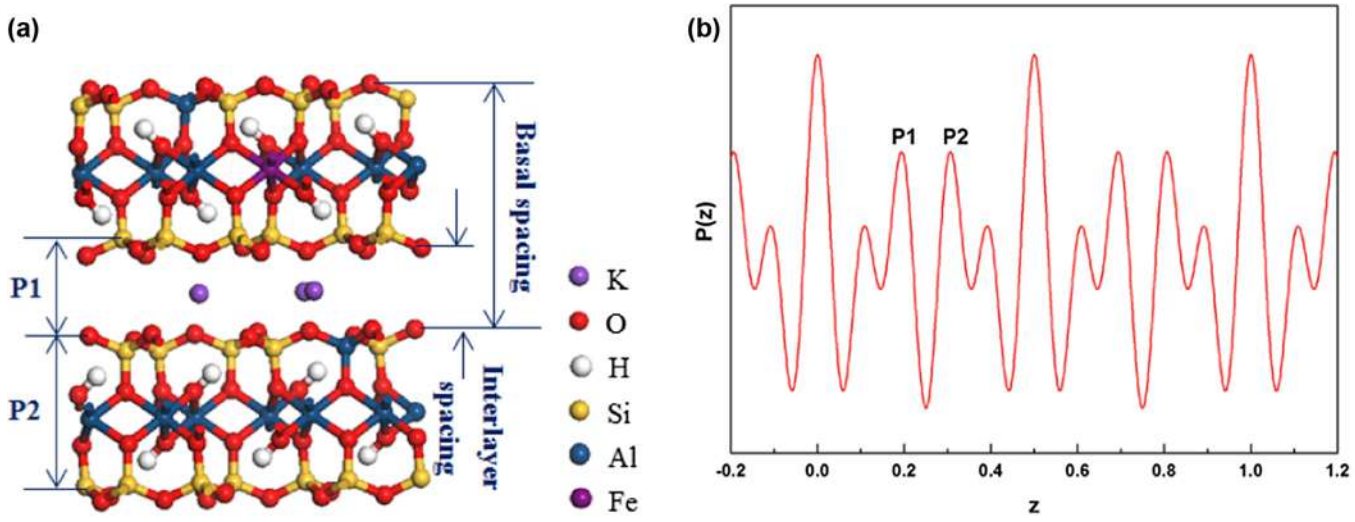

Fig. 2. Structure model along the c-axis viewed in the *yz* plane (the third Si atom in the first Si row and the fifth Si atom in the third Si row were substituted by two Al atoms, the fourth Al atom in the first Al row was substituted by one Fe atom) (a) and the plot of the 1D Patterson function (b) of the original muscovite. Interlayer spacing is the distance between surface O plane in one layer and the nearest O plane in the other layer, while basal spacing is the thickness of one layer and the interlayer spacing, as shown in (a).

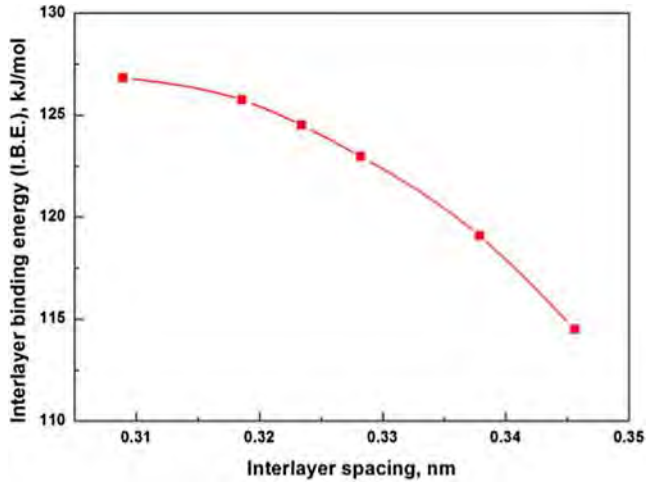

Fig. 3. Interlayer binding energy of the original muscovite as a function of the interlayer spacing.

create the edge structures while keeping the crystal stoichiometry unchanged. Subsequently, 100 $LiNO_3$ molecules were added into the dehydroxylated muscovite system. Periodic boundary conditions were applied in three dimensions and the reactions of $LiNO_3$ into dehydroxylated muscovite were simulated using *Materials Studio 6.0*. The Universal Force Field (UFF) was used in the simulation due to a good compromise between accuracy and availability of the parameters for all atoms in the molecular models [17–19]. The simulation was performed at constant numbers of particles, pressure and temperature (NPT) ensemble of 573 K and 101 kPa. The total simulation time was 40 ns. The simulated muscovite structure was subjected to MD simulations with OTAC. Initially, a configuration of five OTAC molecules was constructed and added to two hundred fifty H_2O molecules with SPC/E model to make the OTAC solution. Subsequently, the interaction between the Li-M750 and OTAC solution was then simulated using MD, employing NPT ensemble at 353 K and 101 kPa for a duration of 160 ns. Finally, the modified muscovite model was extracted for further calculation.

The interlayer binding energy of muscovite in each process was calculated according to Eq. (1) applying the UFF, where the Coulomb and van der Waals interactions were calculated according to Eqs. (2) and (3), respectively.

3. Results and discussion

3.1. The IBE of original muscovite

The structure model of the original muscovite (M) after substitutions is displayed in Fig. 2(a). It was observed that two tetrava-

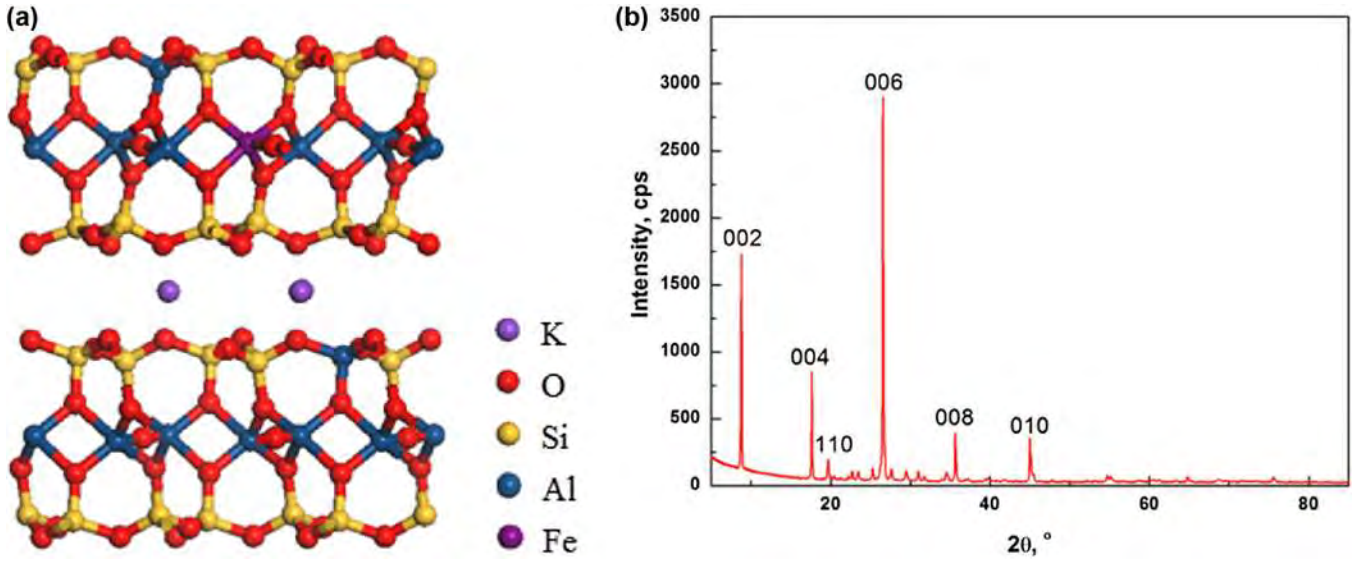

Fig. 4. Structure model (a) and the XRD pattern (b) of muscovite after thermal treatment.

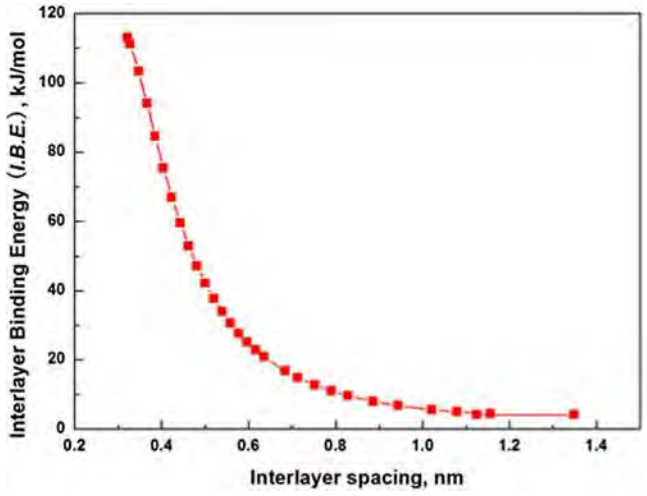

Fig. 5. Interlayer binding energy of muscovite after thermal treatment as a function of interlayer spacing.

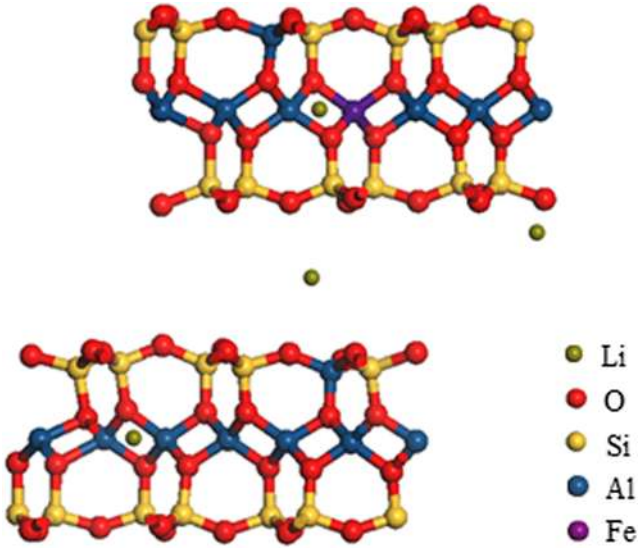

Fig. 6. Structure model of muscovite after $LiNO_3$ treatment.

lent Si atoms and one trivalent Al atom were substituted by two Al atoms and one Fe atom, respectively. The coordinates of the hydroxyl in the octahedron were unsymmetrically arranged. Fig. 2(b) shows the 1D Patterson function plot of M. According to the structure of muscovite, P1 is attributed to the O-Si vector between the surface O and Si in the neighboring aluminosilicate layer, while P2 represents the O-Si vector between the surface O and Si on the other side of the same aluminosilicate layer (Fig. 2(a)). The value of P1 + P2 is equal to the basal spacing *d*. For sample M, the basal spacing was 0.992 nm, as calculated by Bragg's law according to the XRD pattern (Fig. 1). z in Fig. 2(b) is the fractional coordinate on the *c*-axis. P1 is at 0.193 (z_1), P2 is at 0.307 (z_2), reading from Fig. 2(b), and the basal spacing of M was d = 0.992 nm, so P1 and P2 equaled 0.383 nm ($[z_1/(z_1 + z_2)] \times d$) and 0.609 nm ($[z_2/(z_1 + z_2)] \times d$), respectively. The distance between the surface O and its closest Si in the same layer was around 0.064 nm (Fig. 2(a)). Then the interlayer spacing was 0.319 nm, which was the difference between P1 and the nearest O-Si vector distance.

Fig. 3 presents the variation in the IBE of the original muscovite (Fig. 2(a)) as a function of the increase in the layer separation with the distance varying between 0.309 and 0.348 nm. As shown in this figure, the IBE of muscovite with an interlayer spacing of 0.319 nm was around 126 kJ/mol, which was slightly lower than that reported by Giese (134 kJ/mol) [5], which might be due to the substitutions of Si and Al atoms or small rearrangements of the structure in the optimization [20].

3.2. IBE variation due to thermal treatment

The structure model of muscovite after thermal treatment at 750 °C is shown in Fig. 4(a), where the disappearance of -OH and slight modification of the atom positions in the layers were clearly observed. In addition, the coordination of Al was changed from 6- to 5-fold, which agrees well with the dehydroxylation of muscovite in the thermal treatment proposed by Udagawa et al. [21]:

$$2(OH) \Rightarrow H_2O(\uparrow) + O,$$

where two hydroxyl groups were transferred into a water molecule with one residual oxygen atom undersaturated with respect to the

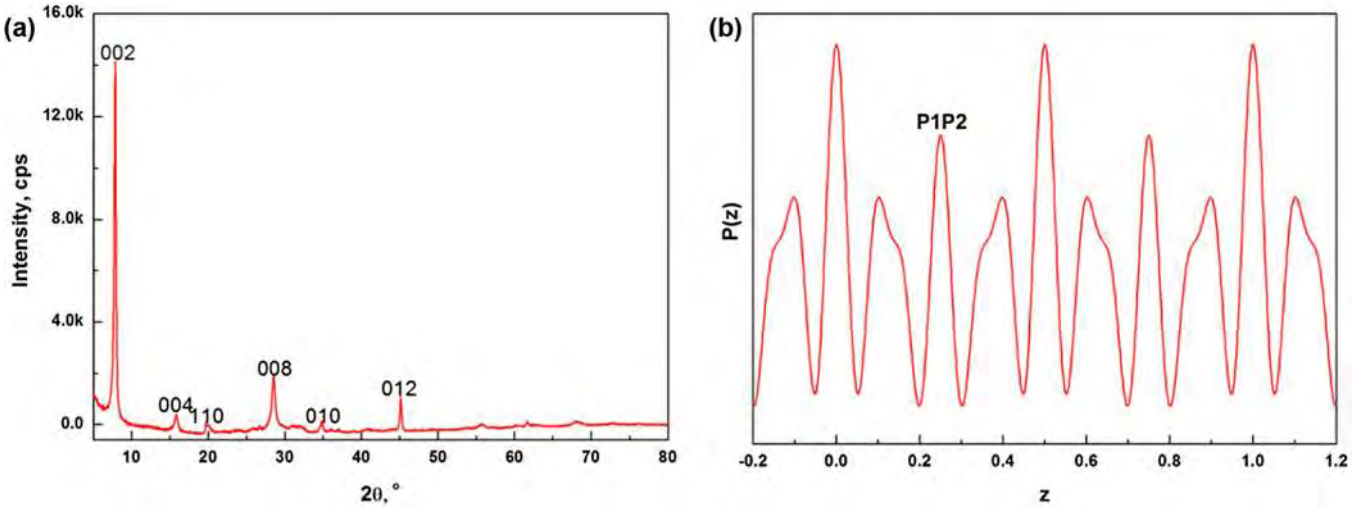

Fig. 7. The XRD pattern (a) and 1D Patterson function plot along the c-axis (b) of Li-M750.

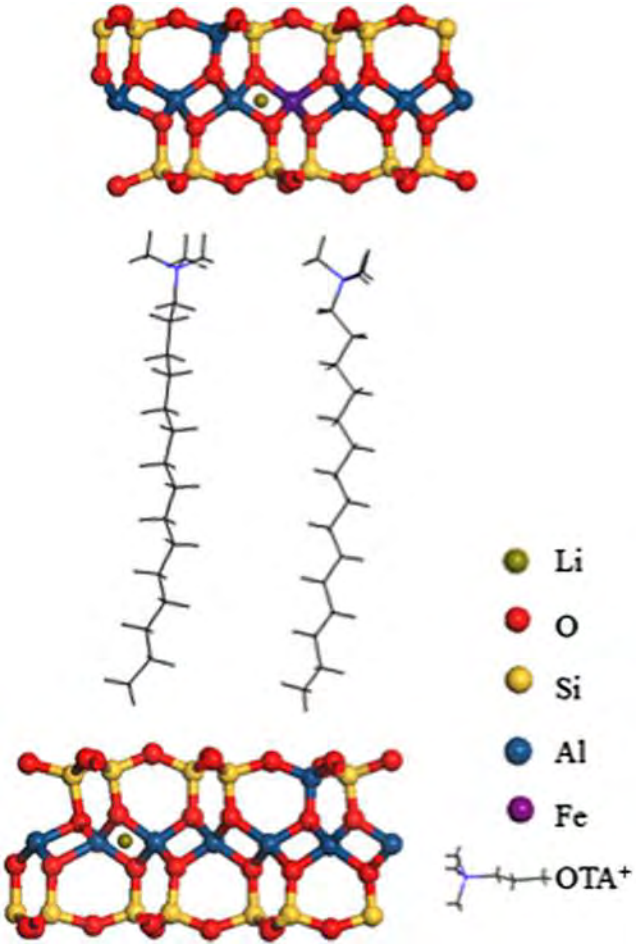

Fig. 8. Structure model of muscovite after OTAC treatment.

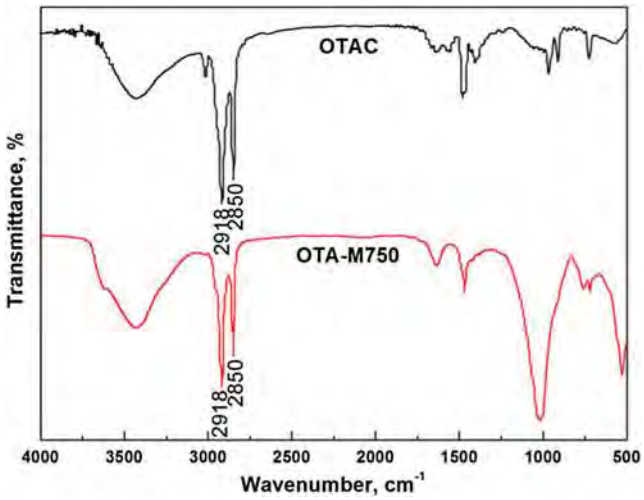

Fig. 9. Middle-infrared spectra of OTAC and OTA-M750.

positive charge. In order to compensate, Al atoms moved closer to the residual oxygen, resulting in distortion of the octahedral layer and rearrangement of its adjacent tetrahedral layer [22]. The basal spacing of muscovite after thermal treatment was 1.004 nm according to the XRD pattern (Fig. 4(b)), indicating a 0.012 nm increase due to thermal treatment. The dehydroxylated muscovite model shown in Fig. 4(a) indicated an increase of 26% and 74% for the layer and the interlayer, respectively. This observation was consistent with previous research that the interlayer separation increase accounted for about 80% of the total enlargement, while the increase of the layer accounted for the rest [15]. Therefore, the thickness of the layer and the interlayer spacing were approximately 0.676 nm and 0.328 nm, respectively.

Fig. 5 shows the IBE of the dehydroxylated muscovite as a function of the interlayer spacing. It demonstrates that the resulting IBE was around 110.05 kJ/mol when the interlayer spacing was 0.328 nm, indicative of a 15.61 kJ/mol decrease in the interlayer binding strength after dehydroxylation. However, Fig. 3 indicates that the IBE was around 123.02 kJ/mol when the interlayer spacing was 0.328 nm without atom position modification. This further suggests that the decrease of the IBE was likely due to not only the increase of the interlayer spacing, but also the modification of the atom positions.

3.3. IBE variation due to Li^+ treatment

The dehydroxylated muscovite structure subsequent to $LiNO_3$ treatment is shown Fig. 6, which indicates that all the K^+ were sub-

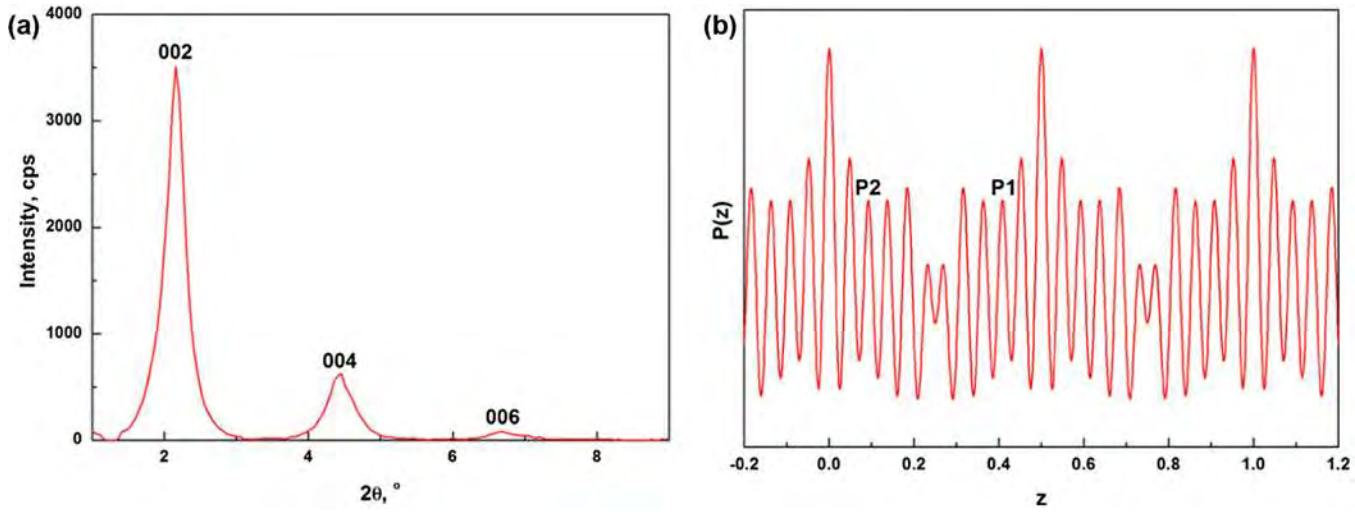

Fig. 10. The XRD pattern (a) and 1D Patterson function plot along the c-axis (b) of OTA-M750.

stituted by Li^+, with some of latter being immersed into the vacancies of the layer. In addition, the distance between the adjacent layers was obviously enlarged.

Fig. 7(a) reveals that all the (*00l*) peaks shifted left once the Li^+ substitution occurred, suggesting an increase of the basal spacing compared with the muscovite after thermal treatment. Peak (*002*) at $2\theta = 7.8°$ corresponds to 1.136 nm basal spacing. It is worth mention that the peak position of (*110*) did not vary, which indicates that the main variation of the muscovite structure in the $LiNO_3$ treatment occurs along the *c* direction instead of the *a*, *b* direction. This is in good agreement with previous work where the muscovite had almost the same (*hk0*) patterns before and after $LiNO_3$ treatment [23]. Thus, the above evidence indicates that the exchange of K^+ by Li^+ increased the basal spacing of muscovite, but did not change the skeleton structure of the aluminosilicate layer.

Fig. 7(b) shows the 1D Patterson map of the Li-M750 derived from the XRD data. P1 and P2 overlapped at z = 0.250 and the basal spacing of the Li-M750 was calculated as 1.136 nm. Therefore, both P1 and P2 referred to 0.568 nm for the Li-M750. After a 40 ns MD simulation of the reaction between $LiNO_3$ and dehydroxylated muscovite, the basal spacing of muscovite was around 1.136 nm. The distance of the nearest O-Si vector was approximately 0.06 nm, and the interlayer spacing was then about 0.508 nm.

The calculated IBE of the structure in Fig. 6 with an interlayer spacing of 0.508 nm was 19.09 kJ/mol. The IBE for talc and pyrophyllite with only the van der Waals force in the interlayer was 17.50 kJ/mol and 27.33 kJ/mol, respectively [24]. This meant that $LiNO_3$ treatment reduced the interlayer binding strength of muscovite to a very low level. If only interlayer spacing enlargement from 0.328 nm to 0.508 nm occurred in the $LiNO_3$ treatment, IBE would be calculated around at 40.10 kJ/mol according to Fig. 5. However, an additional reduction of binding strength (21.01 kJ/mol) was observed, which might be due to the phenomenon that the immersion of Li^+ into the vacancies of the layer (Fig. 6) caused the charge parameterization of the atoms in the layer, especially the Al atoms, and therefore the attraction between layers was reduced. In conclusion, a combination of an increase in interlayer spacing and the immersion of Li^+ into the layers reduced the interlayer energy of muscovite.

3.4. IBE variation due to OTAC intercalation

The structure of muscovite after OTAC treatment is shown in Fig. 8. It was evident that Li^+ in the interlayer was replaced by ordered OTA^+, resulting in an increase in interlayer spacing. The order of OTA^+ in muscovite interlayer was further confirmed by the results from FT-IR measurements, as shown in Fig. 9. The bands of CH_2 asymmetric and symmetric stretching vibration modes of an alkyl chain in OTA-M750 were observed at 2918 cm^{-1} and 2850 cm^{-1}, respectively, exactly the same with the ordered alkyl chain [25,26], indicating the similar order of OTA^+ in OTA-M750 as that in crystalline OTAC.

The significance for the space group *C*2/*c* is the lack of odd (*00l*) diffraction peaks. In addition, Fig. 10(a) shows a linear relationship of the *d* values of the three peaks derived from OTA-M750 ($d_{Peak1} = 2d_{Peak2} = 3d_{Peak3}$). Therefore, the three peaks were (*002*), (*004*) and (*006*), respectively. According to Bragg's equation, the basal spacing calculated from the diffraction peak (*002*) was 3.77 nm, which was significantly greater than that of 1.136 nm of Li-M750 due to the intercalation with OTA^+. Fig. 10(b) shows that P2 is at z = 0.092, whereas P1 moves rightward to z = 0.408, corresponding to a thickness of 3.08 nm and 0.69 nm for P1 and P2, respectively. This indicated an increase of interlayer spacing of muscovite to approximately 3 nm. Fig. 5 demonstrates that the interlayer binding strength of dehydroxylated muscovite was lower than 4.19 kJ/mol when the interlayer spacing exceeded 1.1 nm. Therefore, when the interlayer spacing increased to approximately 3 nm, the attraction between adjacent layers will be significantly less than 4.19 kJ/mol even approaching 0 kJ/mol.

The interlayer energy of muscovite after OTAC intercalation approached 0 kJ/mol in MD, meaning that the binding energy between muscovite layers approached 0 kJ/mol. In the case of the real muscovite sample in the exfoliation, it had many more layers compared to the crystal structure in MD, therefore the interlayer energy of the real muscovite sample was far from zero. This meant that an external force was needed to exfoliate the muscovite sample. Even so, it is true that the interlayer energy of swollen muscovite after OTA^+ intercalation was decreased to less than 1/30th of that of untreated muscovite sample. This explained the easy rupture and cleavage of muscovite into thin particles after treatments.

4. Conclusions

(1) Distortion of the octahedral layer, rearrangement of the adjacent tetrahedral layer and a slight increase of the interlayer spacing due to dehydroxylation were observed when

thermal treatment was applied, giving rise to a decrease of the interlayer binding strength from 125.66 kJ/mol to 110.05 kJ/mol.

(2) The immersion of Li^+ into the layers and the increase of interlayer spacing decreased the binding energy of muscovite to a very low range (19.09 kJ/mol), which was verified by the molecular dynamics simulation and XRD measurements.

(3) The interlayer spacing of muscovite was significantly increased to approximately 3 nm in the OTA^+ intercalation, which almost eliminated the attraction between the adjacent layers.

Acknowledgements

The financial support for this work from the National Natural Science Foundation of China – China under project no. 51474167 is gratefully acknowledged. The authors express gratitude to the College of Materials Science and Engineering, Anhui University of Science and Technology, for its assistance with the MD simulations.

References

[1] F. Bergaya, B.K.G. Theng, G. Lagaly, Handbook of Clay Science, Elsevier, 2006.
[2] H.C. Gupta, M.M. Sinha, C.C.S. Rawat, B.B. Tripathi, Phys. Stat. Sol. 185B (1994) 117–121.
[3] A. Bailey, H. Daniels, J. Chem. Phys. 77 (1973) 501–515.
[4] K. Tamura, S. Yokoyama, C.S. Pascua, H. Yamada, Mater. Chem. 20 (2008) 2242–2246.
[5] R.F. Giese, Nature Phys. Sci. 248 (1974) 580–581.
[6] E. Papirer, A. Eckhardt, F. Muller, J. Mater. Sci. 25 (1990) 5109–5117.
[7] W.R. Caseri, R.A. Shelden, U.W. Suter, Colloid Polym. Sci. 270 (1992) 392–398.
[8] J.J. Bardet, 1951. US Pat 2549880.
[9] F. Jia, S. Song, RSC Adv. 5 (2015) 52882–52887.
[10] F. Jia, J. Su, S. Song, Colloids Surf. A: Physicochem. Eng. Asp. 471 (2015) 19–25.
[11] K. Kupwade-Patil, F. Soto, A. Kunjumon, E.N. Allouche, D.S. Mainardi, Comput. Struct. 122 (2013) 164–177.
[12] J. Sherman, Chem. Rev. 11 (1932) 93–170.
[13] J.E. Lennard-Jones, Proc. R. Soc. Lond. A 106 (738) (1924) 463–477.
[14] J.J. Liang, F.C. Hawthorne, Can. Mineral. 34 (1996) 115–122.
[15] S. Guggenheim, Y. Chang, A.F. Koster van Groos, Am. Mineral. 72 (1987) 537–550.
[16] F. Gridi-Bennadji, B. Beneu, J.P. Laval, P. Blanchart, Appl. Clay Sci. 38 (2008) 259–267.
[17] R. Toth, A. Coslanich, M. Ferrone, M. Fermeglia, S. Pricl, S. Miertus, E. Chiellini, Polymer 45 (2004) 8075–8083.
[18] F. Gardebien, J.L. Bredas, R. Lazzaroni, J. Phys. Chem. B 109 (25) (2005) 12287–12296.
[19] M. Pospisil, A. Kalendova, P. Capkova, J. Simonik, M. Valaskova, J. Colloid Interface Sci. 277 (1) (2004) 154–161.
[20] R.F. Giese, Clays Clay Miner. 23 (2) (1975) 165–166.
[21] S. Udagawa, K. Urabe, H. Hasu, Jpn. Assoc. Miner. Petrol Econ. Geol. 69 (1974) 281–389.
[22] I. Vassanyi, A. Szabo, Mater. Sci. Forum 133–136 (1993) 655–658.
[23] X. Yu, L. Zhao, X. Gao, X. Zhang, N. Wu, J. Solid State Chem. 179 (2006) 1569–1574.
[24] R.F. Giese, Zeitschrift fur Kristallographie-Crystall. Mater. 141(1–6) (1975) 138–144.
[25] N.V. Venkataraman, S. Vasudevan, J. Phys. Chem. B 105 (2001) 7639–7650.
[26] S. Barman, N.V. Venkataraman, S. Vasudevan, R. Seshadri, J. Phys. Chem. B 107 (2003) 1875–1883.